On the role of stochastic effects in bacterial growth and sociobiology

Karl Wienand

München 2017

On the role of stochastic effects in bacterial growth and sociobiology

Karl Wienand

A dissertation submitted
to the Faculty of Physics
of the Ludwig–Maximilians–Universität
München
for the degree of
DOCTOR RERUM NATURALIUM

Munich, 22.11.2017

First referee: Prof. Dr. Erwin Frey
Second referee: Prof. Dr. Mauro Mobilia
Date of the oral examination: 16.1.2018

It doesn't make a difference how beautiful your guess is,
it doesn't matter how smart it is who made the guess, or what their name is,
if it disagrees with experiment, it's wrong.

—R. P. Feynman

Zusammenfassung

Wachstum, soziale Interaktion und stochastische Schwankungen prägen, neben natürlicher Selektion, das Leben von Bakterien. Populationen verbreiten sich durch Wachstum, und ihre interne Dynamik wird von sozialen Interaktionen gesteuert, während Stochastizität den Prozess durchzieht—sei es in Form demographischer Schwankungen, als unvorhersehbare Umweltveränderungen oder als Variationen im Prozess der Populationsbildung.

Meine Dissertation konzentriert sich darauf, wie das Zusammenwirken dieser Faktoren das evolutionäre Schicksal bakterieller Populationen bestimmt und wie man mit Hilfe der Mathematik ihre jeweiligen Rollen entwirren kann. Teil I der Arbeit handelt von der Entwicklung präziser mathematischer Modelle zur Beschreibung des Wachstums und der sozialen Dynamik einer konkreten bakteriellen Population; Teil II behandelt die Verkettung von umweltbedingtem Zufall und demographischen Schwankungen in einer rein theoretischen Population.

Die Ergebnisse meiner Forschung zeigen, dass Umwelt und soziale Kräfte die Evolution einer Population bestimmen. Gleichzeitig hebt diese Arbeit hervor, wie wichtig es ist, biologische Spezifizitäten zu identifizieren und miteinzubeziehen, wenn es um die Modellierung spezifischer bakterieller Systeme geht.

Teil I: Stochastizität und soziale Interaktionen in bakteriellem Wachstum
mit Matthias Lechner, Felix Becker, Heinrich Jung und Erwin Frey
In diesem Teil der Arbeit haben wir bakterielles Wachstum in einer Kombination von Theorie und Experiment in Angriff genommen.

Das erste Projekt, *Genetic drift during exponential growth*, analysiert die Entwicklung kleiner, gemischter Populationen, deren Bakterien weder um Ressourcen kämpfen, noch soziale Interaktionen haben. Damit werden Wachstum und stochastische Schwankungen als einzige Einflüsse auf die Population isoliert. Wir wenden ein Urnenmodell an und beweisen, dass Wachstum die genetische Vielfalt der Population schützt und die Wirkung demographischer Schwankungen „einfrieren“ lässt.

Im Folgeprojekt, *Public-good-mediated social interactions during competitive bacterial growth*, ziehen wir eine Population in Betracht, in der Bakterien ein öffentliches Gut austauschen, und analysieren die Wirkung solcher Interaktionen auf Wachstum und Ökologie. Anstatt den traditionellen spieltheoretischen Standpunkt einzunehmen, quantifizieren wir die Kernaspekte der Interaktion in Experimenten und fassen sie in einem theoretischen Modell zusammen. Das Modell sagt vorher, dass eine höhere Produktion öffentliches Gutes nur zeitlich begrenzt für die Population von Vorteil ist. Die Dauer und das Mass dieses Vorteils, sowie seine Konsequenzen auf die Überlebenschance der Kooperation in der Population, hängen von der spezifischen Biochemie des öffentliches Gutes, insbesondere von seiner Akkumulation, ab.

Teil II: Zusammenwirkung von Umwelt- und Demographiebedingtem Zufall
mit Mauro Mobilia und Erwin Frey
In diesem Projekt analysieren wir auf rein theoretischer Ebene die Zusammenwirkung verschiedener Rauschquellen. Wir erarbeiten ein Modell, in dem Ressourcen zufällig zwischen Überfluss und Mangel wechseln, was die Wachstumdynamik steuert, und damit die Größe demographischer Schwankungen. Unser wichtigstes Ergebnis ist die Entwicklung eines Ansatzes, um die nichtlineare Kombination von internem und extrinsichem Rauschen zu behandeln. Mit Hilfe dieses Ansatzes entdecken wir, dass die Verteilung von Populationsgrößen verschiedene Formen annimmt, die von der Frequenz der Umweltveränderung bestimmt werden. Insbesondere eine häufig wechselnde Umwelt erzeugt einen stabilen Zustand, der sich im Rahmen der deterministischen Dynamik sonst nicht ergibt. Wir ermitteln auch die Fixierungseigenschaften der Population, vor allem die Überlebenschancen eines durch Selektion benachteiligen Bakterienstammes. Mit einer effektiven Theorie wenden wir unseren Ansatz auch auf den Austausch eines öffentlichen Gutes an.

Unsere Ergebnisse zeigen eine komplexe Zusammenwirkung von internen und extrinsischen Rauschquellen, Wachstum und sozialen Interaktionen, die die Evolution prägt. Im konkreten Fall der Evolution von Kooperation unterstützen diese Wirkungen das Überleben von Kooperatoren, zumindest für einen beschränkten Zeitraum.

Summary

Growth, social interactions, and stochastic fluctuations shape the course of bacterial life, alongside natural selection. Populations propagate through growth, and social interactions guide the internal dynamics, while stochasticity always runs through the process—be it via demographic fluctuations, unpredictable environmental changes, or variability in how populations form. My thesis focuses on how these evolutionary factors intertwine to determine the fate of bacterial populations, using mathematical tools to unravel their roles. Part I of the thesis deals with the development of rigorous mathematical models to describe the growth and social dynamics of a real bacterial population; Part II addresses the combination of environmental noise and demographic fluctuations (with and without social interactions) in a theoretical population. The results of my research show that environmental and social forces shape the evolution of a population. At the same time, this work highlights the importance of identifying and including biological details to accurately model specific bacterial systems.

Part I: Stochasticity and social interactions in bacterial growth
with Matthias Lechner, Felix Becker, Heinrich Jung, and Erwin Frey
In this part of the research, we approach bacterial growth using a combination of theory and experiments.

During a first research project, *Genetic drift during exponential growth*, we analyzed the development of small, mixed populations in which bacteria neither competed nor had social interactions. In this setting, the population is only subject to growth and stochastic fluctuations. Using an urn model, we proved that growth maintains genetic diversity in the population, freezing the effect of demographic fluctuations (see Chapter 1).

In the subsequent project, *Public-good-mediated social interactions during competitive bacterial growth*, we considered a population in which bacteria exchanged a public good, and studied the effects of such social interaction on growth and ecology. Instead of taking the traditional game-theoretical viewpoint, we quantified the interaction features experimentally, and condensed them in a theoretical model. This model predicts that producing more public good benefits a population only for limited times. How advantageous production is, the duration of the advantage, and the consequences on the survival of the cooperative trait in the population depend on the specific biochemistry of the public good itself—particularly its accumulation (see Chapter 2).

Part II: Combined effects of environmental and demographic noise
with Mauro Mobilia and Erwin Frey
In this project, we theoretically investigated the combined action of different noise sources. We formulated a model in which available resources switched stochastically between abundance and scarcity, driving changes in population size, which in turn tuned the amplitude of demographic fluctuations. Our central result is the development of an approach to treat the highly nonlinear combination of intrinsic and extrinsic noise. Using this approach, we found that the distribution of population sizes assumes different forms, depending on the rate of the environmental switching. In particular, frequently-changing environments give rise to a stable state, absent from the deterministic dynamics. We also described the fixation properties of the population, particularly the survival probability of a selectively disfavored strain. Using an effective theory, we also applied the approach to a public good interaction (see Chapter 3).

The results show an intricate interplay between intrinsic and extrinsic noise sources, growth, and social interactions, which shapes evolution. In the concrete example of the evolution of cooperation, we fond that these effects tend to aid the survival of cooperators, at least for some time.

Overview of the projects

1. Genetic drift during exponential growth

Project description This project analyzes the relation between exponential growth, typical of bacteria, and demographic fluctuations. A mixed population's composition evolves as a random walk, guided by inherently stochastic birth and death events—an effect known as *genetic drift*. Because strain extinction is irreversible, all but one strain eventually go extinct. Genetic drift, then, inexorably leads to loss of diversity in mixed populations.

We considered mixed populations consisting of two strains of *Pseudomonas putida*, starting from small, stochastic number of cells of each type. With appropriate choice of growth medium, and by considering only the exponential phase, we ensured that strains would have no social interaction, selective differences, or significant competition for resources. Therefore, growth and genetic drift alone acted on the population composition. Mathematically, we modeled the process as a Pólya urn: the urn contains marbles of two colors; at each step, one is extracted at random, then placed back, alongside another one of the same color. Using this model, we simulated the development of the distribution of population compositions, and compared the final outcome to that of experiments.

We found that growth progressively slows genetic drift by weakening demographic fluctuations. Eventually, fluctuations become inconsequential, and genetic drift stops completely. The distribution of population compositions, we observed, rapidly "freezes" to a steady state, that persists for the rest of growth. As a result, growth maintains long-term genetic diversity in the population.

This project contributes two main results to the thesis. First, it singles out the tension between growth and genetic drift, two of the evolutionary factors at the center of the work. Second, developing this approach established a path to rigorously translate measurements on bacterial systems into mathematical models, which is the thread running across the first part of my thesis.

Related publications This project resulted in the publication of the paper "Non-Selective Evolution of Growing Populations", *PLoS ONE* **10**(8), e0134300 (2015), reprinted at the end of Chapter 1 (from page 13).

Contributors This research was realized in collaboration with the lab of Prof. Dr. Heinrich Jung at the LMU department of microbiology. In the publication, I *share first author contribution*, together with Matthias Lechner (Frey group), with whom I developed the theoretical analysis, and Felix Becker (Jung group), who carried out the experiments. *Other authors* are Heinrich Jung and Erwin Frey.

2. Public-good-mediated social interactions during competitive bacterial growth

Project description In this project, we focused on the interaction between the growth of a bacterial population and the social dynamics within it. The production and exchange of public goods is a well-known example of bacterial social interaction, the subject of many studies in biology and game theory. The effect of public goods has ramifications on both growth and competition among populations.

As opposed to the previous project, here we considered a setting in which bacteria compete for limited resources. Most importantly, we introduced an interaction between individuals: one strain pays a metabolic cost (thus growing slower) to provide a public good that promotes growth of all individuals. We considered two strains of *Pseudomonas putida* as a model system: one is a constitutive public good producer, the other a non-producer. Then we studied the growth of an ensemble of populations, starting from stochastic initial mixtures of the two strains.

Instead of forcing a game-theoretical framework upon our system, we experimentally quantified the interaction parameters and translated them into a mathematical model. The social dynamics shared some general features with public good games, but the specific biochemistry of the molecule involved (in particular the fact that it accumulates) differentiated this system from traditional formulations. Numerically solving the equations of our model with stochastic initial conditions, we predicted the development of an ensemble of populations, and validated the results experimentally.

We showed that, at early stages of growth, producer-rich populations have more public good and grow faster, causing the overall fraction of producers across the ensemble to increase. The accumulation of the public good in the medium, combined with its saturating benefit, eventually erase this advantage, decreasing the producer fraction. These aspects of the public good not only play a part in the dynamics, but they are also necessary for the model to accurately replicate the experimental results.

To the broader goals of the thesis, this project addressed directly the combination of growth dynamics and social interactions in a real bacterial population. The cornerstone of our approach was rigorous mathematical modeling of the social interaction. Thanks to it, we identified the key features of the public good, and their impact on growth and on the internal evolution of the population.

Related publications This project resulted in the publication of the paper "Interactions mediated by a public good transiently increase cooperativity in growing Pseudomonas putida metapopulations", *Sci Rep* **8**, 4093 (2018), reprinted at the end of Chapter 2 (from page 46)

Contributors This research was realized in collaboration with the lab of Prof. Dr. Heinrich Jung at the LMU department of microbiology. In the publications, I *share first author contribution* with Felix Becker (Jung group), who carried out the experiments. *Other authors* are Matthias Lechner (Frey group), Erwin Frey, and Heinrich Jung.

3. Evolution in stochastic environments

Project description In this project we analyzed how randomly changing environments interact with the intrinsic stochasticity and social dynamics of a population. Unpredictable conditions are the norm rather than the exception for bacteria, and play extremely important roles in evolution. An individual's fitness, for example, may depend on environmental conditions; but sudden changes in the environment can also lead to sharp declines in population size.

We considered a population composed of two strains (one of which with a slight selective advantage), competing for limited resources that switched randomly between a state of abundance and one of scarcity. Abundant resources lead to larger populations, scarce resources to smaller ones. Because the population size tunes the amplitude of demographic fluctuations, our model couples the environmental noise to the internal one of the population.

We studied the intertwined effects of environmental and demographic noise on population size and fixation probabilities by analytical and simulation means, considering two social scenarios. In the *pure competition* scenario, strains simply competed for the finite resources. In the *public good* scenario, the slow strain provided a public good, which enhanced growth.

Our results showed that the environmental and demographic noise interact in a complex, but predictable manner. In particular, we showed that the distribution of population sizes undergoes noise-induced transitions, driven by the changing environment. Explicitly combining the effects of the two noise sources, we described the steady state distribution of population sizes. Additionally, we leveraged time scale separations to describe the fixation properties of the system. Thereby we found that the selectively disadvantaged strain survives with remarkably higher probability in this case than it would in a constant environment. We also developed an effective approach, allowing us to extend some results of the pure competition scenario to the more complex public good case.

This part of the thesis delves deeper in the mathematical details of the model, moving away from the description of a specific biological system. As a result, it becomes possible to analyze in great detail the combined action of demographic fluctuations, growth, and social interactions, even with the additional stochasticity from the environment.

Related publications The results of this project are collected in the paper "Evolution of a Fluctuating Population in a Randomly Switching Environment", *Phys Rev Lett* **119**, 158301 (2017), reprinted at the end of Chapter 3 (from page 81), as well as in the manuscript "Eco-Evolutionary Dynamics of a Population with Randomly Switching Carrying Capacity", currently submitted for publication, whose most recent version is reprinted from page 99.

Contributors This research was realized in collaboration with Prof. Mauro Mobilia of the University of Leeds. I appear as first author in both of the related publications. *Other authors* are Erwin Frey and Mauro Mobilia.

Contents

Introduction

Evolution is more than a cut-throat, individualistic competition between isolated players. In fact, a number of factors enter the process beside sheer Darwinian selection. For example, because natural populations evolve by single, stochastic births and deaths, the fitness of a single does not guarantee long survival or plentiful offspring: it merely increases its likelihood. Survival is a game of chance, and fitness can only nudge probabilities around. The environment plays a fundamental role too, setting the boundary conditions for the population. The types and amounts of resources, space, and predators, for example, can favor some individuals over others and determine the strength of selection. Finally, single individuals, as well as entire communities, can improve their survival chances through social interactions. A bee is much more likely to survive as part of a hive, a lion is more successful as member of a pride, people live better in cities than isolated in the wild. But sociality is not a prerogative of humans and animals. Far from being a collection of singles, a bacterial colony presents convoluted social networks.

Background and motivation

Bacterial cooperation Cooperation constitutes an intriguing example of such social interaction. A cooperating organism makes an investment in terms of energy or resources to provide a benefit to its entire community [1–6], for example better access to oxygen [7], nutrients [8], or protection from antibiotics [9]. One of the best-known examples is siderophore production in *Pseudomonas* [10–15]. These bacteria often live in environments where iron is not readily available. In these conditions, they secrete a molecule called *pyoverdine*, which binds to this useful element in the environment. By absorbing pyoverdine-iron complexes, bacteria obtain iron and enhance their growth. Since pyoverdine is released outside the cell, however, producers let any member of the population take advantage of it.

Synthesizing pyoverdine diverts resources away from replication [10–12]: producers pay for their cooperation by growing slower. At the same time, if the benefit truly goes to the entire community, it makes producers vulnerable to exploitation: a non-producing neighbor still reaps the benefit while saving the cost. As a result, individuals face the so-called "Dilemma of Cooperation": renounce some payoff for the common good or act in one's own interest? Acting selfishly and exploiting the labor of producing bacteria gives a clear selective advantage, therefore evolutionary theory dictates that producers should eventually die out.

Yet, cooperative behaviors run through the entire tree of life: from human communities to microbes. How they emerged and spread is one of the most challenging questions in evolutionary biology. Countless studies addressed it using game theory [4, 16–19], as well as experiments [11, 20, 21] and evolutionary arguments [1, 5, 22, 23]. These researches identified several mechanisms that promote cooperation, from the structure of populations [20, 24] to the punishment of those who do not cooperate [25, 26].

Changing environments Unpredictable environments are the rule rather than the exception in nature. This is especially the case for bacteria: their small habitats offer little inertia to physical and chemical changes, so temperature, pH, and water content can fluctuate widely within short times [27, 28]. Even relatively sheltered bacteria, such as those living inside of animals (including humans) experience ever-changing amounts of nutrients, plus their host continually douses them in hormones and other chemicals. Some of these factors change fairly regularly—for example because of daily habits and natural circadian rhythms—but the overall result is unpredictable.

When environmental conditions change, selection may favor different traits [29–34]. But the way conditions vary—abruptly or gradually, predictably or stochastically, frequently or rarely—also affects bacterial evolution [35, 36]. Finally, catastrophic downturns in environmental conditions can lead to sharp, abrupt declines in population size, also known as *population bottlenecks*. The gene pool that results from the bottleneck can

deviate a lot from the one that entered it: very fit individuals, for example, could have died out by chance, or rare mutations could end up over-represented. This is the gene pool of the population when it grows again, so bottlenecks play a very important role in evolution [37–43]. Altogether, changing environments impact a population well beyond their selective effect.

Environmental conditions, social interaction, growth, selection, and stochastic effects all tightly intertwine in affecting evolution. Social interactions, and particularly cooperation, can strengthen communities, resulting in a population-level selection on top of the traditional individual-level one [44–49]. Growth and population dynamics can change which strains are selectively favored [50] and the outcome of social interactions, especially in combination with demographic fluctuations [51–56]. The presence or absence of resources in the environment can determine population sizes, which in turn directly tune the weight of selection and demographic fluctuations [37, 57, 58]. The smaller the population, in fact, the more each single stochastic birth or death affects the population, reducing the role of selection. *Pseudomonas* populations provide a prime example of all these factors coming together: their public good works by tweaking the environmental conditions (in this case, iron availability) and promoting growth, while always subject to stochastic effects, like demographic fluctuations.

Goals and significance of this thesis

Understanding bacterial growth, sociobiology, and ecology is an important and useful task for several reasons. First, bacteria reproduce extremely quickly. This allows to observe within days or months long-term evolutionary processes, that occur over decades if not millennia in animals. Investigating bacteria, then, we can peer into the mechanisms of evolution. Secondly, bacterial communities, such as the human microbiome, are increasingly recognized as an important part of our lives. The more is known about the bacteria we host, the more we can understand their impact. Finally, understanding how bacterial communities grow and evolve can help develop alternative therapies to antibiotics, countering the current spread of resistant bacterial strain.

My research addresses the following overarching question:

How do stochastic effects, population growth, and social interactions intertwine to determine the evolutionary fate of a bacterial population?

To address it, I investigated the action of several combinations of these factors in real bacterial populations as well as purely theoretical models. Part I of the thesis focuses on studies of real bacterial populations, combining theoretical modeling and experiments. The research in Chapter 1 isolates the tension between growth and demographic fluctuations. Chapter 2 concerns the rigorous quantification of a social interaction mediated by a public good in an ensemble of *Pseudomonas* populations, examining its relation with population dynamics. Part II (comprising the sole Chapter 3), instead, explores the interplay between demographic fluctuations, social interactions, and environmental noise from a theoretical standpoint.

Part I

Stochasticity and social interactions in bacterial growth

Chapter 1

Genetic drift during exponential growth

Chapter abstract Non-selective effects play an important role in evolution. Stochastic fluctuations due to individual birth and death events, for example, cause random changes in population composition, called *genetic drift*. In the long run, a population subject to genetic drift will always *fixate*, that is, all but one of its component strains will go extinct. As a result, the population becomes homogeneous: genetic diversity is lost. Although this is a well-studied phenomenon in populations of constant size, the effects of genetic drift in growing populations remain unclear. Studying the growth of a mixed population composed of two selectively neutral strain, one can examine directly the tension between individual-based growth and genetic drift. In this chapter, I present results indicating that growth counteracts genetic drift, even stopping it altogether. This has important evolutionary consequences: by arresting drift, growth preserves genetic diversity. Using the mathematical theory of Pólya urns and experiments, it can be demonstrated that growth "freezes" this effect, maintaining long-term genetic diversity. Furthermore, it was possible to predict the steady-state distribution of compositions of an ensemble of growing populations, and confirmed this prediction with experiments.

Contribution to the overarching question The work presented in this chapter directly addresses how growth and stochastic fluctuations combine in a real bacterial population. The analysis is rooted in a rigorous mathematical description of a bacterial system, establishing an approach that will be useful in Chapter 2 as well. This allows for otherwise impossible insights in the dynamics, without losing touch with experimental reality.

1.1 Background

1.1.1 Genetic drift

Directed selection is probably the best-known factor in evolution, but not the only one. All modern understandings of the evolutionary process place a significant weight also on non-selective effects. One of the most common and perhaps most important is *genetic drift*: the change in gene frequency in a population caused by demographic fluctuations.

Growing bacterial populations are always finite, and evolve by discrete replication and death events of individual cells, which are stochastic by nature. Consider a population of size N composed of N_A genetically identical individuals, call it strain A, and of $N_B = N - N_A$ individuals of strain B. The fraction $x = N_A/N$ of A-individuals in the population increases slightly every time one reproduces (or a B dies), and decreases every time one dies (or B reproduces). These discrete, stochastic birth and death events thus determine a random walk for the fraction x between 0 and 1; if no mutations are present (thus individuals cannot switch between strains), the boundaries are absorbing. As a result, they constitute the only stable states for x. In other words, genetic drift leads to *fixation* of one strain—the population is homogeneous and only composed of individuals of that strain. Importantly, neither strain is inherently favored by drift, which simply pushes for fixation, regardless of which individuals survive. In this sense, genetic drift is *non-selective*, in stark contrast with directed (or Darwinian) selection forces that favor the survival of a specific strain.

If the population has constant size and no selection acting on it, drift alone determines its fate. The probability $P(x;t)$ that a fraction x of the population is of strain A at time t obeys then the following diffusion equation [57, 59]

$$\frac{\partial}{\partial t}P(x,t) = \frac{1}{2N}\frac{\partial^2}{\partial x^2}\left[x(1-x)P(x,t)\right] . \tag{1.1}$$

Under these conditions, the probability of having x not at the boundaries (that is, coexistence of the strains) decreases exponentially in time. This result was obtained theoretically by Kimura [59] and verified in a number of experiments (see, for example, Figure 1.2 [60]). The distribution takes approximately a U-shape; in the long run, only the peaks at $x = 0$ and $x = 1$ remain. The height of each peak reflects the fixation probability of the corresponding strain.

The diffusion constant in eq. (1.1) is proportional to the inverse of population size N, indicating that fluctuations become more important the smaller the population. Intuitively, if each strain was represented by just one individual, a single death event would suffice for fixation. The more individuals in the population, then, the less each stochastic birth and death changes their relative abundance.

1.1.2 The Pólya urn model

Kimura's solution only holds for constant population size. In some cases, one can use an effective population size approach to describe the fixation properties of the system [61]. However, exponential growth is not one of these. Elementarily described, bacterial reproduction proceeds as follows: one individual is selected at random for reproduction, and an exact copy of it is added to the population. If, instead of cells in a population we consider marbles in an urn, the problem is equivalent to the classic *Pólya urn model* [62]. This is a popular model across disciplines, from auto-catalytic chemical reactions [63, 64], to how opinions can emerge and self-organize in stock markets [65].

In its most basic formulation, presented by Eggenberger and Pólya [62], (see [64] for a more recent review), sketched in Figure 1.3, this model describes an urn containing N marbles of two colors, for example N_A yellow and N_B blue ones. At each step, we draw a marble at random, then place it back, alongside another one of the same color. The urn thus grows in size at each step. Each marble is equally likely to be drawn, therefore the probability of extracting a marble of a certain color is equal to the relative abundance of marbles of that color in the urn, for example,

$$Prob\{\text{extract yellow}\} = \frac{N_A}{N_A + N_B} . \tag{1.2}$$

Every extraction adds a marble to the extracted color to the urn, thus increasing the chance of drawing further marbles of that same color in the future. Therefore, the Pólya urn is a *self-reinforcing* (or *auto-catalytic*) *process* [63, 64]. One could intuitively expect this positive feedback to amplify each small initial fluctuation. As more and more marbles of the same color are drawn, it becomes more and more likely to extract that color, and eventually the urn would come arbitrarily close to being homogeneous. In biological terms, this corresponds to

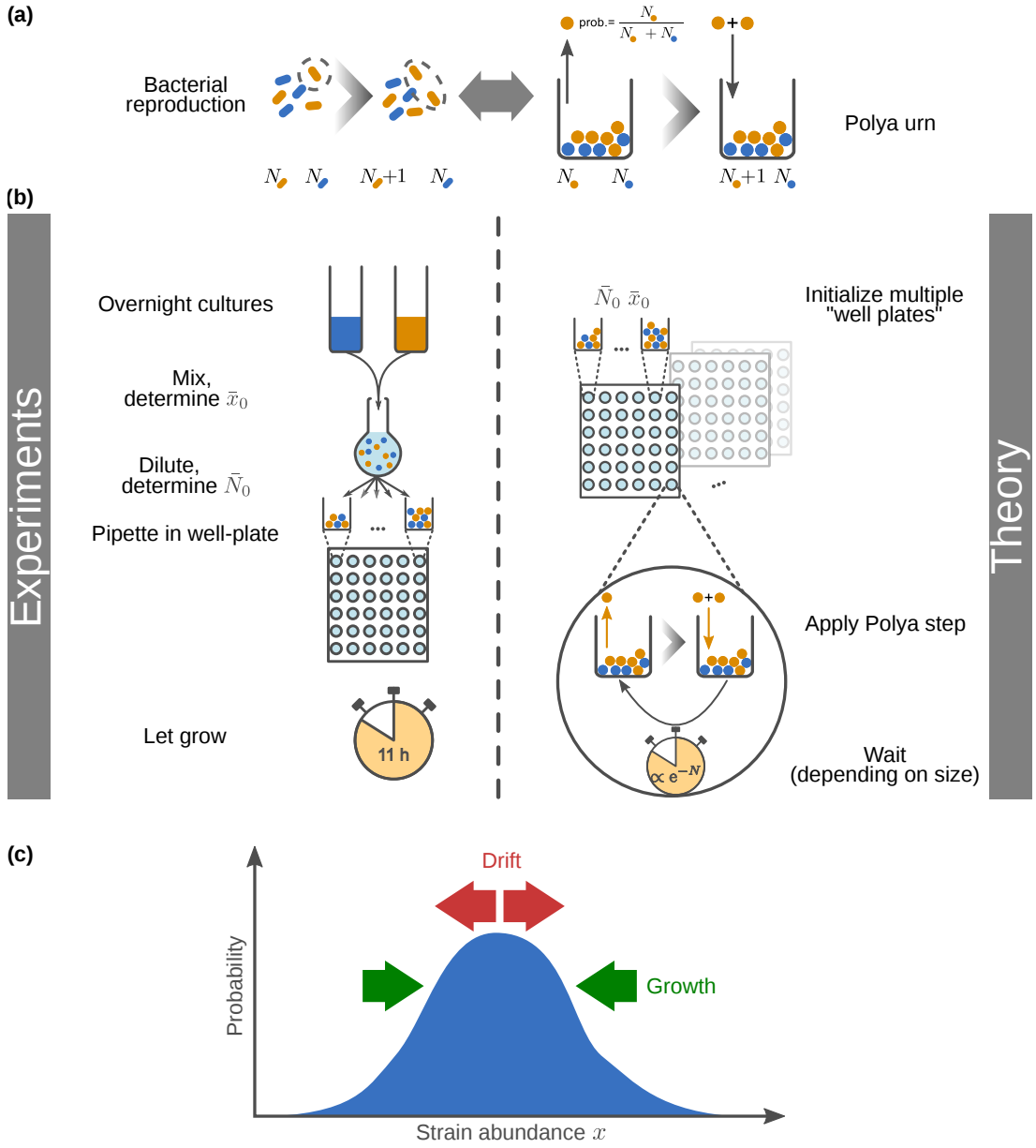

Figure 1.1: *Graphical abstract of the project.* **(a)** How non-selective bacterial reproduction resembles a Pólya urn. In both cases, each iteration adds to the population an identical copy of an individual and all individuals are equally likely to be picked for reproduction. **(b)** Sketch of the experimental and theoretical procedures. On the experimental side (left), separate cultures of the two strains are mixed, diluted, and used to inoculate the wells of a well-plate. The proportions of the mixture determine the average population composition $\bar{x}_0$, the dilution factor determines the average population size $\bar{N}_0$. Once inoculated, the populations grow exponentially for 11 hours. On the theoretical side (right), well plates are initialized with Poisson-distributed numbers of individuals of each strain, with averages $\bar{N}_0\bar{x}_0$ and $\bar{N}_0(1-\bar{x}_0)$. The populations then grow in Pólya-urn steps, separated by exponentially-distributed waiting times. **(c)** Cartoon of the competing forces of genetic drift and population growth on the compositions distribution. Drift pushes to broaden it, growth to keep it constant.

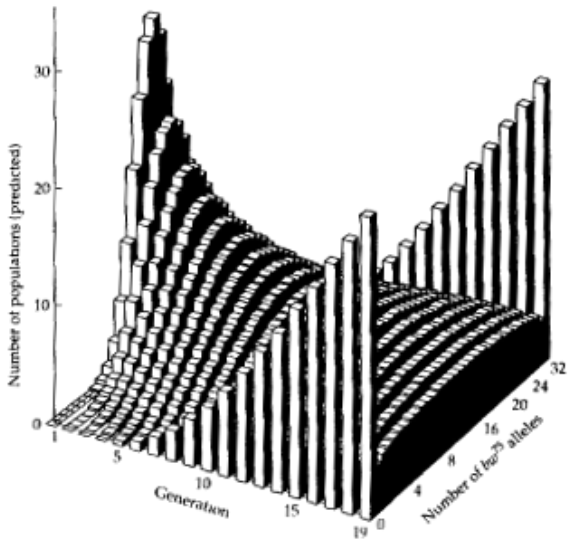

Figure 1.2: *Genetic drift leads to fixation in a fixed-size population* (from Ref. [60]). With the passing generations (left to right), the distribution of population compositions progressively broadens. As more and more populations fixate, the bulk of the distribution fades and the peaks at the boundaries rise. The results agree with Kimura's theoretical solution.

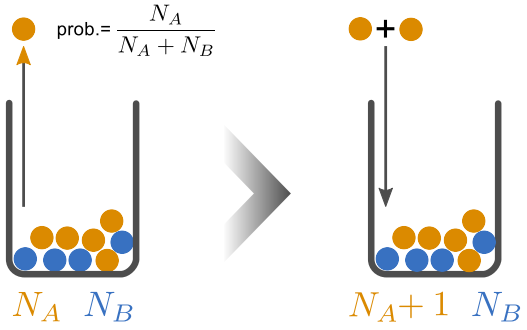

Figure 1.3: *Cartoon a Pólya urn step.* A marble is drawn from the urn and placed back, together with an exact copy of itself. Each marble has equal probability of being extracted, so the probability of picking, for example, a yellow one is equal to the relative abundance of yellow marbles. The urn increases in size at each step.

an almost-fixated population, analogous to the result of genetic drift. At the same time, however, the increasing number of marbles decreases the impact of individual fluctuations. Each added marble changes the proportions in the urn less than the previous one.

Furthermore, the probability of extracting a specific sequence of marbles only depends on how many yellow and blue marbles the sequence contains. Iterating the extraction process, the probability of extracting a specific sequence $\mathcal{S}$ of ΔN marbles, ΔA of which yellow (starting from an urn of N_A yellow and N_B marbles) can be easily computed to be

$$P(\mathcal{S}|N_A, N_B) = \frac{\Gamma(N_A + \Delta A)}{\Gamma(N_A)} \frac{\Gamma(N_B + \Delta N - \Delta A)}{\Gamma(N_B)} \frac{\Gamma(N_A + N_B)}{\Gamma(N_A + N_B + \Delta N)}\,, \tag{1.3}$$

where $\Gamma(n) = (n-1)!$ is the Euler Gamma function. Equivalently, all paths with the same starting and ending points have are equally probable. The Pólya urn is therefore also called an *exchangeable process* [64].

Moreover, it has been proven that the sequence of marble proportions x in the urn converges with probability 1 to some limit value x^*. This value, however, is a random variable [63, 64]. In other words, starting a Pólya process multiple times with the same number of marbles and the same composition x, it will converge every time to some limit composition x^* but, in general, to a different one every time. In the limit case of starting with $N_A = N_B = 1$, for example, the urn is equally likely to end anywhere between 0 and 1 (extremes excluded) [64, 65].

To find the limit distribution, consider extracting a large number ΔN of marbles. Of these, ΔA will be yellow. Clearly, there are $\binom{\Delta N}{\Delta A}$ equivalent paths for this result, and their probability is given by equation 1.3. Using the definition of the Beta function $B(m, n) = \Gamma(m)\Gamma(n)/\Gamma(m+n)$, the probability of the urn ending up with $N_A + \Delta A$ yellow marbles is finally

$$p(N_A + \Delta A|N_A, N_B, \Delta N) = \binom{\Delta N}{\Delta A} \frac{B(N_A + \Delta A, N_B + \Delta N - \Delta A)}{B(N_A, N_B)}\,. \tag{1.4}$$

This distribution is called beta-binomial distribution [63].

1.2 Growth "freezes" genetic drift

To isolate growth and genetic drift in our system, we needed to eliminate all interactions between cells, as well as any selection. To this end, we cultivated mixed bacterial populations in a medium that granted both strains the same growth rate; we also limited our analysis to the exponential growth phase, when death events and competition for resources are negligible. The other main feature of our system was the small initial populations, resulting in a high variability in initial conditions.

This relatively uncomplicated biological setting allowed for a very rigorous mathematical description, which was key to our work. The core of our approach, in fact, was the close cross-talk between theoretical and experimental side.

Research question: *How does exponential growth affect genetic drift?*

As reported in the publication (reprinted in Section 1.3), we addressed the question using analytical calculations and stochastic simulations, validated by experiments. The model, in addition allowed us to peer into parts of the dynamics unaccessible to experiment. Thus we proved that:

Exponential growth stops genetic drift and maintains genetic diversity in the population.

1.2.1 Theoretical model for stochastic, non-selective growth

We considered a large number of populations (about 10^4), grouped in "virtual well-plates" of 120 each, corresponding to many replicates of the experimental setting. Each well was initialized with a random number A_0 of individuals of strain A, and B_0 of strain B. A_0 was Poisson-distributed with mean $\bar{N}_0\bar{x}_0$ (B_0 was chosen analogously, with mean $\bar{N}_0(1-\bar{x}_0)$). This procedure generates populations of average size $\bar{N}_0$ and with an average fraction of A-individuals $\bar{x}_0$, replicating the experimental conditions.

We modeled growth as iterations of the Pólya urn, with every reproduction event corresponding to an extraction event for the urn. We also set the waiting times between urn extractions to be random and sampled

from an exponential distribution with parameter N. With this procedure, also called *Poissonization* [66, 67], the total urn size grows stochastically, with average $\langle N \rangle \propto \mathrm{e}^t$. As a result, the number N_A of individuals of type A evolves following the master equation

$$\frac{d}{dt}P(N_A,t) = (N_A-1)P(N_A-1,t) - N_A P(N_A,t)\,, \tag{1.5}$$

and analogously for the number N_B of B-individuals.

We simulated the evolution of several "virtual well plates" at once by solving eq. (1.5) using the Gillespie algorithm [68, 69]. After growth, we computed the distribution of the fraction x of A-individuals in simulations and compared it directly to the results of the experiments, see Figure 1.4.

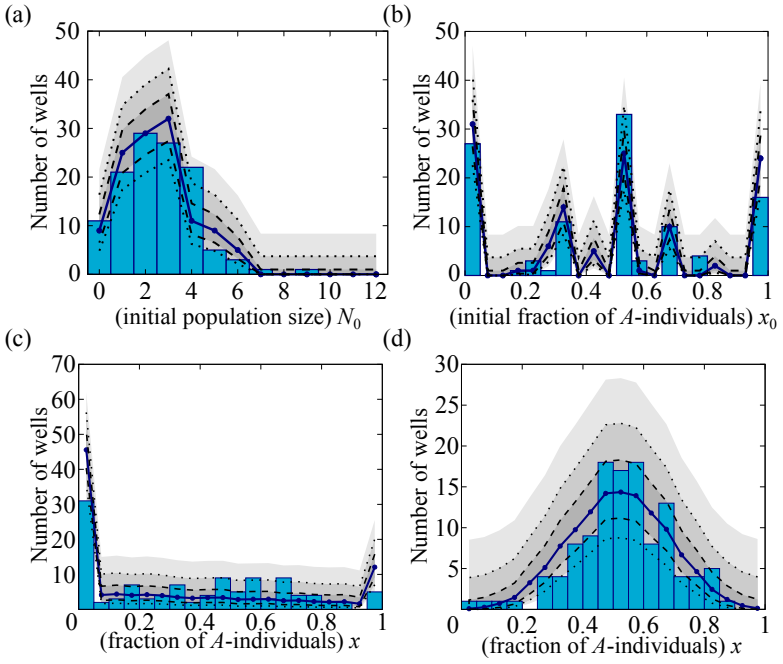

Figure 1.4: *Comparison between experimental and theoretical results* Solid lines represent the average histogram obtained following the theoretical procedure for multiple sets of 120 populations; shaded areas indicate the 68%, 95%, and 99% confidence intervals around these results; blue bars are the result of one experimental run with 120 wells. Theoretical results agree well with their experimental counterparts. **(a)** Initial size N_0 (average $\bar{N}_0 = 2.55$); **(b)** Initial composition (average $\bar{x}_0 = 0.45$); **(c)** Final composition (initial parameters $\bar{N}_0 = 2.9$, $\bar{x}_0 = 0.32$) **(d)** Final composition (initial parameters $\bar{N}_0 = 14.5$, $\bar{x}_0 = 0.52$). Adapted from Ref [70].

1.2.2 Saturating behavior of distribution moments

Our simulations show that the distribution of population compositions $x = N_A/(N_A+N_B)$ effectively "freezes" to a steady state. Figure 1.5 and the Supplementary Video show that the distribution initially broadens but, within a few generations, it reaches a stable steady state. Demographic fluctuations, which initially had a major impact on the distribution, rapidly lose importance. Moreover, we notice that the number of fixated populations (black bins at the boundaries of the plot) never increases in time. The only fixations ever present are from populations that started fixated. So the decreasing amplitude of fluctuations is stronger than the self-reinforcing positive feedback.

Quantitatively speaking, we showed that mean, variance, and skewness of the distribution of x saturate in time. We proved this using the generating function

$$F(a;t) = \sum_{N_A} a^{N_A} P(N_A;t)\,, \tag{1.6}$$

From the master equation (1.5), we obtain that $F(a;t)$ obeys

$$\frac{d}{dt}F(a;t) = (a^2-a)\frac{\partial F(a;t)}{\partial a}\,. \tag{1.7}$$

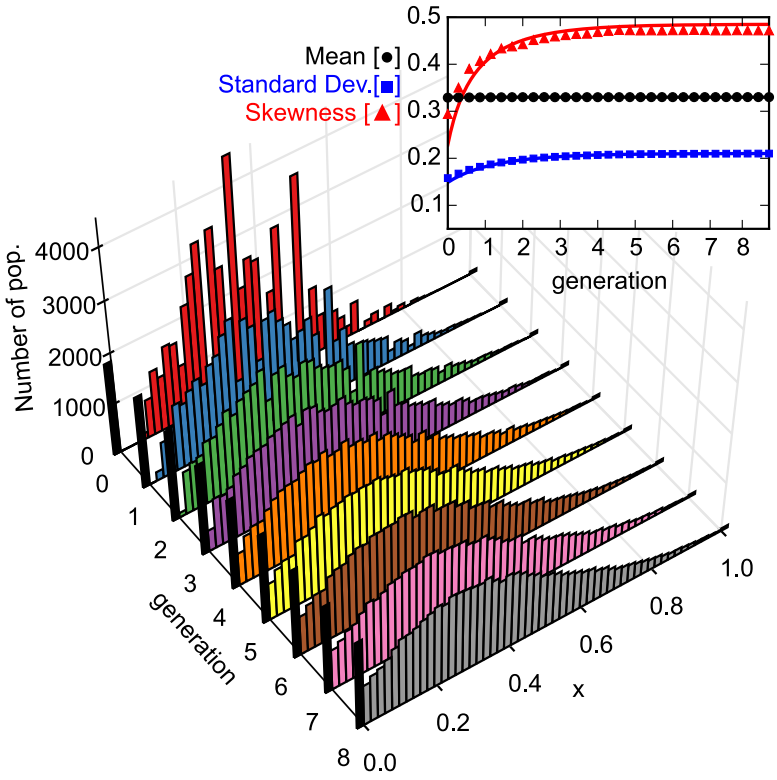

Figure 1.5: *Time series for the simulated distribution of the population composition* x (parameter values $\bar{N}_0 = 10$, $\bar{x}_0 = 0.33$). The distribution initially broadens, then freezes to a steady state. The fraction of fixated populations (black bins) remains constant during the process, as expected for a Pólya urn, and in contrast to expectations from genetic drift (see Figure 1.2). The inset shows the time course of mean, standard deviation and skewness of the distribution (symbols denote numerical simulations, solid lines theoretical predictions). The mean x remains constant throughout the evolution; standard deviation and skewness saturate to limit values, confirming the freezing of the distribution. (reprinted from Ref. [70])

By solving this equation we can obtain the time evolution for the first three moments of $P(N_A; t)$ (and analogously for $P(N_B; t)$). It is then a matter of algebra to compute, for example, mean and variance of x. Specifically, we obtained that $\langle x \rangle \equiv \bar{x}_0$: the average composition of populations is constant—as expected in the absence of selection. The variance, instead changes in time: to leading order in N_A, N_B,

$$\mathrm{Var}(x) = \frac{2 - e^{-t}}{\bar{N}_0} \bar{x}_0 (1 - \bar{x}_0) \,, \tag{1.8}$$

so $\mathrm{Var}(x)$ grows to a limit value. This reflects the initial broadening of the distribution, due to genetic drift, followed by the freezing to a steady state. Similarly, we observe an increase in skewness (see the Supplementary Information to the publication), which reflects the self-reinforcing nature of the Pólya process, also followed by saturation, confirming the distribution freezing.

1.2.3 Limit values of distribution

In the previous section, the general master equation (1.5) allowed us to compute approximate values for mean and variance of the distribution of x. However, exploiting the properties of Pólya urns and beta-binomial distributions, we can also derive the *exact* steady-state distribution of x, as well as the long-time limits of its mean and average. Thus we can confirm and complement the approximate results of the previous section.

First, we can infer the probability $P(\Delta A | A_0, B_0, \Delta N)$ of adding ΔA new A-individuals, given that the population grows by ΔN overall (from initial conditions A_0, B_0). This is given by the beta-binomial distribution in equation (1.4). Consequently, we can compute the probability $P(x)$ that the fraction of A individuals is exactly

x as

$$P(x) = \sum_{A_0,B_0} P(A_0)P(B_0)P(\Delta A = x(A_0 + B_0 + \Delta N)|A_0, B_0, \Delta N)\,. \tag{1.9}$$

Though this sum lacks a closed analytical form, it can be performed numerically.

Leveraging the properties of beta-binomial distributions, we also obtained exact, closed-form expressions for the average and variance of x. Specifically, we calculated that $\langle x\rangle \equiv \bar{x}_0$ and, in the limit $\Delta N \to \infty$,

$$\mathrm{Var}(x) \to \bar{x}_0(1-\bar{x}_0)\frac{2}{\bar{N}_0}, \tag{1.10}$$

(to leading order in $\bar{N}_0$), which also correspond to the $t \to \infty$ limits of the quantities obtained in the previous section.

1.2.4 Consequences and outlook

Our research indicates that growth counteracts the effect of demographic fluctuations within each population, maintaining strain coexistence. This behavior radically departs from the known results at constant population size (see, for example, Refs. [57–59]), but also in some growing populations, such as colony range expansion experiments [71]. In this setting, in fact, competition for limited space reduces the effects of growth, tipping the balance back towards genetic drift.

Moreover, the results of this chapter show that, by leading to broad distributions of x, growth ensures genetic variability between populations. In particular, this means that a non-selective growth phase could lead to an ensemble of large populations with the typical compositional variability of small ones. Such high variability between populations is a key component of population-level competition [44, 46]. Therefore, non-selective growth phases could play an important role in cyclic metapopulations. In this scenario, in fact, small initial sizes and high variability have profound and far-reaching consequences on evolution, see Refs. [53–56], as well as Chapter 2.

1.3 Publication reprint

Non-selective evolution of growing populations

by

K. Wienand,*[1] M. Lechner,*[1], F. Becker,*[2] H. Jung,[2] and E. Frey[1]

* Contributed equally to this work
[1]Department of Physics, Arnold Sommerfeld Center for Theoretical Physics and Center for NanoScience, Ludwig-Maximilians-Universität München, Theresienstraße 37, 80333 München, Germany,
[2] Department of Biology 1, Microbiology, Ludwig- Maximilians-Universität, Grosshaderner Straße 2-4 82152, Martinsried, Germany

reprinted from

***PLoS ONE* 10(8), e0134300 (2015),**
doi: 10.1371/journal.pone.0134300.

PLOS ONE

RESEARCH ARTICLE

Non-Selective Evolution of Growing Populations

Karl Wienand[1☯], Matthias Lechner[1☯], Felix Becker[2☯], Heinrich Jung[2], Erwin Frey[1]*

1 Arnold-Sommerfeld-Center for Theoretical Physics and Center for NanoScience, Physics Department, Ludwig-Maximilians-Universität, Munich, Germany, **2** Department of Biology 1, Microbiology, Ludwig-Maximilians-Universität, Martinsried, Germany

☯ These authors contributed equally to this work.
* frey@lmu.de

Citation: Wienand K, Lechner M, Becker F, Jung H, Frey E (2015) Non-Selective Evolution of Growing Populations. PLoS ONE 10(8): e0134300. doi:10.1371/journal.pone.0134300

Editor: Matjaz Perc, University of Maribor, SLOVENIA

Received: May 8, 2015

Accepted: July 7, 2015

Published: August 14, 2015

Data Availability Statement: All relevant data are within the paper and its Supporting Information files.

Funding: EF was funded by the Deutsche Forschungsgemeinschaft, Priority Programme 1617 "Phenotypic heterogeneity and sociobiology of bacterial populations", grant FR 850/11-1 and the German Excellence Initiative via the programme "Nanosystems Initiative Munich" (NIM). HJ was funded by the Deutsche Forschungsgemeinschaft, Priority Programme 1617 "Phenotypic heterogeneity and sociobiology of bacterial populations", grant JU 333/5-1 (http://www.spp1617.org/). KW was supported by the Elitenetzwerk Bayern. The funders had no role in study design, data collection and

Abstract

Non-selective effects, like genetic drift, are an important factor in modern conceptions of evolution, and have been extensively studied for constant population sizes (Kimura, 1955; Otto and Whitlock, 1997). Here, we consider non-selective evolution in the case of growing populations that are of small size and have varying trait compositions (e.g. after a population bottleneck). We find that, in these conditions, populations never fixate to a trait, but tend to a random limit composition, and that the distribution of compositions "freezes" to a steady state. This final state is crucially influenced by the initial conditions. We obtain these findings from a combined theoretical and experimental approach, using multiple mixed subpopulations of two Pseudomonas putida strains in non-selective growth conditions (Matthijs et al, 2009) as model system. The experimental results for the population dynamics match the theoretical predictions based on the Pólya urn model (Eggenberger and Pólya, 1923) for all analyzed parameter regimes. In summary, we show that exponential growth stops genetic drift. This result contrasts with previous theoretical analyses of non-selective evolution (e.g. genetic drift), which investigated how traits spread and eventually take over populations (fixate) (Kimura, 1955; Otto and Whitlock, 1997). Moreover, our work highlights how deeply growth influences non-selective evolution, and how it plays a key role in maintaining genetic variability. Consequently, it is of particular importance in life-cycles models (Melbinger et al, 2010; Cremer et al, 2011; Cremer et al, 2012) of periodically shrinking and expanding populations.

Introduction

Stochastic effects play an important role in population dynamics [8–11], particularly when competition between individuals is non-selective. Most previous theoretical analyses have studied how a non-selectively evolving trait can spread and eventually replace all other variants (fixate) under conditions in which the population size remains constant [2, 12, 13]. However, both natural and laboratory populations frequently experience exponential growth. Here we show that genetic diversity in growing populations is maintained despite demographic noise,

analysis, decision to publish, or preparation of the manuscript.

Competing Interests: The authors have declared that no competing interests exist.

and reaches a stationary but random limit. We used a well-controlled model system in which well-mixed co-cultures of a wild-type *Pseudomonas putida* strain and an isogenic mutant were grown under non-selective conditions. Multiple subpopulations were generated, each containing a random number of individuals of each strain. Depending on the average initial population size and the strain ratio, we observed distinct stationary probability distributions for their genetic composition. Moreover, we showed that the dynamics of growing populations can be mapped to Pólya urn models [4], permitting the observed maintenance of genetic diversity to be understood as the random limit property of a fair game between individual strains. Generalizing the Pólya urn model to include the effects of random initial sampling and exponential growth allowed us to predict the evolution of the composition distribution. Using numerical and analytical methods we found that the distribution broadens at first but quickly "freezes" to a stationary distribution, which agrees with the experimental findings. Our results provide new insights into the role of demographic noise in growing populations.

Results and Discussion

Evolutionary dynamics is driven by the complex interplay between selective and non-selective (or neutral) effects. The paradigm of non-selective evolution originates from the seminal work of Kimura [1], in which he solved the Wright-Fisher model, thus showing that non-selective effects—and specifically genetic drift—can have a determinant role in evolution. His results sparked an ongoing debate about the nature and potency of randomness as a fundamental evolutionary force [13–15]. For very small populations genetic drift is generally considered an important factor [13], as the theory successfully predicts the outcomes of neutral evolution experiments [9, 16].

In most theoretical analyses, constant (or effectively constant) population sizes are assumed, and the role of population growth is neglected. Bacterial populations, however, often undergo rapid growth—especially when they are small. For example, as few as 10 individuals of some highly virulent pathogens (e.g. enterohemorrhagic *Escherichia coli* or *Shigella dysenteriae*) suffice to initiate a deadly infection in a human host [17, 18]. Another case of small, growing populations are water-borne bacteria that feed on phytoplankton products. Due to nutrient limitation in open water, these bacteria typically live in small populations in close proximity to the planktonic organism [19]. During spring blooms, the phytoplankton releases more organic material, boosting the bacterial growth rate [19–21]. In nature, such small populations often form by adventitious dispersal from a larger reservoir population [22]. A typical example is the spreading of pathogens from host to host. This random "sampling" from a reservoir yields small populations whose genetic compositions differ from that of the reservoir (a phenomenon known as the *founder effect* [23]). Recent studies also showed that the combination of population growth and stochastic fluctuations can have a major impact on the evolution [5–7, 24] and genetics [25] of small populations.

To probe how population growth shapes genetic diversity, we used a well-characterized microbial model system, namely the soil bacterium *Pseudomonas putida* KT2440 [3, 29, 27]. The wild-type strain KT2440 produces pyoverdine, an iron-scavenging molecule that supports growth when iron becomes scarce in the environment. Here we consider co-cultures of two genetically distinct strains: the wild-type, pyoverdine-producing strain KT2440 (strain *A*) and the mutant non-producer strain 3E2 (strain *B*). We set up conditions of non-selective competition between these strains by using an iron-replete medium (casamino acids, supplemented with 200 μM $FeCl_3$). In this medium, production of pyoverdine is effectively repressed [27], such that both strains have the same growth rate and neither has an advantage (see S2 Table). Producer (KT2440 wild type) and non-producer (3E2) strains were first mixed and diluted to

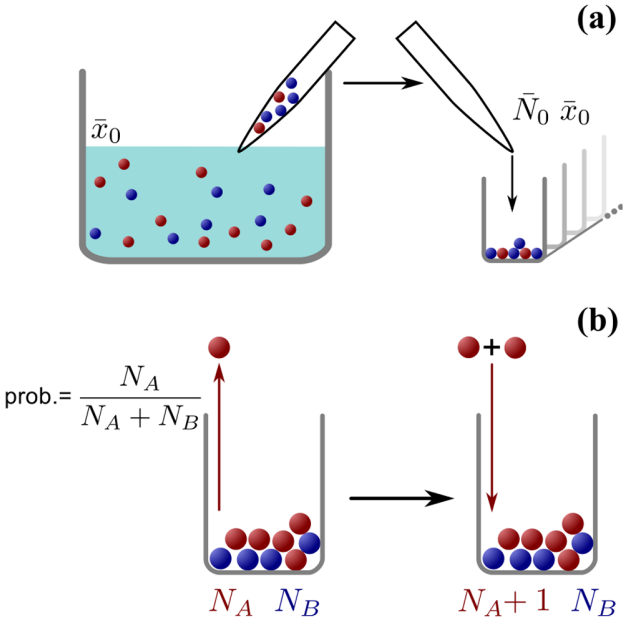

Fig 1. Schematic depiction of urn sampling and growth. (a) Schematic illustration of the random initial conditions. An infinite reservoir contains a diluted mixture of bacteria, a fraction $\bar{x}_0$ of which are of strain *A*. We draw small volumes of liquid from the reservoir containing small, random numbers of individuals, which conform to a Poisson distribution with mean (determined by the dilution of the reservoir population). A certain fraction of this initial population is of strain *A*. The mean value of this fraction is equal to $\bar{x}_0$. We use these individuals to initiate populations in the wells of a microtiter plate, so that each population starts with a random size N_0 and a random fraction of A-individuals x_0. **(b)** Illustration of the Pólya urn model. If a bacterial population is represented as an urn, each individual as a marble and each bacterial strain as a color, this urn model captures the essentials of bacterial reproduction in our populations. At each iteration, a marble is drawn at random and returned to the urn, together with another one of the same color. The probability of extracting a marble of either color is determined solely by its relative abundance, making the process non-selective (since no strain has inherent advantages, see S2 Table). The rate of growth in population size can be rendered exponential (see S2 Fig) by letting the waiting time between successive iterations be exponentially distributed (also known as Poissonization).

doi:10.1371/journal.pone.0134300.g001

yield Poisson dilution conditions. Then we initiated a large number of subpopulations from this reservoir by pipetting aliquots of the cell suspension into the wells of a 96-well plate, thereby generating a large ensemble of subpopulations with a random distribution of initial cell number N_0 and producer fraction x_0 (Fig 1). Use of shaken liquid cultures ensured homogeneous well-mixed conditions for all cells in the same well (access to nutrients, oxygen, etc.), and exponential growth was observed in all cases (see S2 Fig).

This experimental setting is well described within the mathematical framework of a *Pólya urn model*. Consider each bacterium in the population as a marble in an urn, and its genotype as the color of the marble (e.g. red for strain *A*, and blue for strain *B*). Population growth results from single reproduction events in which an individual randomly divides. This is mathematically equivalent to a stochastic event in which a marble is chosen at random from the urn and put back, together with another one of the same color. This random process, introduced by Eggenberger and Pólya [4], exhibits several important properties [28–31]. It is *self-reinforcing*: each time a marble is extracted, another one of the same color is added, increasing the likelihood of extracting a marble of that color again. In the context of bacterial populations, this means that every birth event for one strain makes it more likely that further birth events of that same strain will occur in the future. Note, however, that *fixation*, i.e., complete loss of one type

of marble from the population, cannot occur, simply because in the Pólya urn model marbles are neither removed nor do they change their color. This fully reflects the experimental conditions: During exponential growth, rates of cell death are negligible, and within the observation time mutations will be extremely rare, given the population sizes considered. The bacteria in each well reproduce randomly at a per-capita (average) rate μ. To translate this to the urn model, drawing of a marble is assumed to be a stochastic Poisson process, with a "per-marble" rate μ (a procedure known as *Poissonization* or *embedding* [32, 33]). Mathematically, the growth process in then described by a Master Equation: The time evolution for the probability $P(N_A, t)$ of finding N_A individuals of strain A at time t reads

$$\frac{\mathrm{d}}{\mathrm{d}t}P(N_A;t) = (N_A - 1)P(N_A - 1;t) - N_A P(N_A;t)\,, \tag{1}$$

where we have set the growth rate to $\mu = 1$ in order to fix the time scale (for an introduction to the mathematical concepts see, e.g., [34]); the corresponding Master equation for individuals of strain B is of identical form. To study the composition of the populations, we use the more convenient quantities $N = N_A + N_B$ (total size) and $x = N_A/N$ (fraction of individuals of strain A).

To start the experiment, we inoculated the wells of 96-well-plates by drawing small volumes of diluted liquid bacterial culture from a large reservoir (Fig 1(a)). Each volume contains a random number of bacteria whose mean value is controlled by the dilution of the reservoir. The fraction of bacteria of strain A (wild type) in that volume is also random, with its mean value $\bar{x}_0$ given by the fraction of strain A in the reservoir. In the mathematical formulation, this setup corresponds to stochastic initial conditions for the Pólya urn model: the initial population size N_0 for each well is given by a Poisson distribution with mean $\bar{N}_0$, and each individual is assigned to strain A or B with probability $\bar{x}_0$ and $1 - \bar{x}_0$), respectively. This procedure is also equivalent to treating the initial numbers of A- and B-individuals as independent, Poisson-distributed random variables with mean values $\bar{N}_0\bar{x}_0$ and $\bar{N}_0(1 - \bar{x}_0)$), respectively [6].

Fig 2 shows a time series of the histogram for the composition x of all subpopulations considered, as obtained from a stochastic simulation of the Master Eq (1) for a given random initial condition (with $\bar{N}_0 = 10$ and $\bar{x}_0 = 0.33$). Surprisingly, the distribution first broadens, but then quickly "freezes" to a steady state (see S1 Video). This is genuinely different from Kimura"s result for populations with constant size [1] (or similar results with effectively constant size [2]) where the balance between stochastic birth and death events leads to genetic drift, and thereby eventually to the extinction of one of the two strains. In contrast, for a growing population, death events are negligible, and therefore there is no fixation of the population during growth. Instead, fixation arises as a direct consequence of the initial sampling process, as can be seen from the heights of the black bins in the histogram (at $x = 0$ and $x = 1$), which remain constant over time (Fig 2). During growth, the composition of each subpopulation, instead of drifting to fixation at either $x = 0$ or $x = 1$, reaches a stationary limit value x^*, where it remains thereafter [35]. This limit value is random: starting several subpopulations (urns) from the exact same initial composition of strain A and B (blue and red marbles), each reaches a limit, but in general these limits differ from one another. Once all of the subpopulations in an ensemble reach their limit, the distribution of the population composition freezes to a steady state, which is equal to the probability distribution of x^*. Similar random limit properties appear in other fields, with *lock-in* in economics as the best-known example [30].

The inset in Fig 2 shows approximate solutions for the time evolution of mean, standard deviation, and skewness of the composition x, which we obtained by analytically solving the Master Eq (1) (see S2 Text). The analytical results agree well with their numerical counterparts. In particular, the mean value remains constant over time, as it must for a non-selective process.

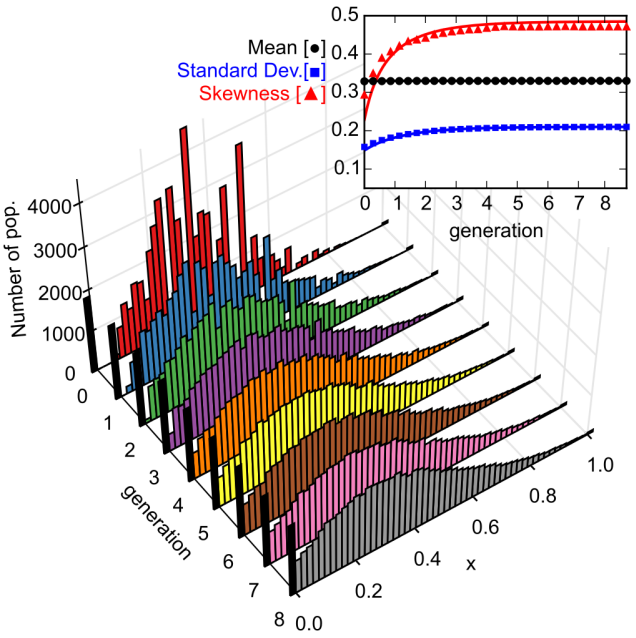

Fig 2. Time series for the simulated distribution of the population composition *x*. The distribution initially broadens, then freezes to a steady state (see S1 Video). The fraction of populations that have $x = 0$ or $x = 1$ (indicated by the black bins) remains constant during the time evolution, as expected for a Pólya urn process, and in contrast to expectations from genetic drift (see S1 Table). In each well the population follows a stochastic path and reaches a (random) limit composition, and the distribution freezes only when all populations reached their limit. The parameter values used in the simulation are $\bar{N}_0 = 10$ and $\bar{x}_0 = 0.33$ The inset shows the mean, standard deviation and skewness as a function of the number of generations, with symbols denoting numerical simulations, and the solid lines corresponding to the theoretical prediction of Eq (2) (and also those in S2 Text). Analytical and numerical values agree. The mean $\langle x \rangle$ remains constant throughout the evolution, as expected for a non-selective process; standard deviation and skewness saturate to limit values, confirming the freezing of the distribution.

doi:10.1371/journal.pone.0134300.g002

For the time evolution of the variance, which is a measure for the spread of a distribution, we obtain to leading order in population size

$$\mathrm{Var}_{\mathrm{poi}}[x](t) = \frac{2 - \mathrm{e}^{-t}}{\bar{N}_0} \bar{x}_0 (1 - \bar{x}_0) \,. \tag{2}$$

The broadening and freezing of the distribution is reflected in the exponential decay term of the variance. Note that the skewness increases as well, because growth is self-reinforcing (see inset in Fig 2). To further test the validity of the stochastic simulations, we also calculated the limit values of the average and variance after extended periods of evolution exactly, and found that they match the numerical solutions of the Master Equation perfectly (see S1 Text).

We tested these theoretical predictions using *P. putida* as a bacterial model system. We mixed the wild-type and mutant strains in order to obtain different initial fractions $\bar{x}_0$. The degree of dilution of the mixture determines the average initial cell number $\bar{N}_0$, with which we inoculated 120 wells per experiment (96-well plate format). In order to compare the experimental data with our model, we set up simulations that matched the experimental configuration by initializing $\bar{N}_0$ and $\bar{x}_0$ with the same values as measured in the experiments. We simulated the time evolution of about 10^4 populations, grouped in "virtual plates" of 120 wells each. Every virtual plate produced a histogram like the one we obtained from experiments. We then generated an average histogram of the virtual plates and used its values to compute the

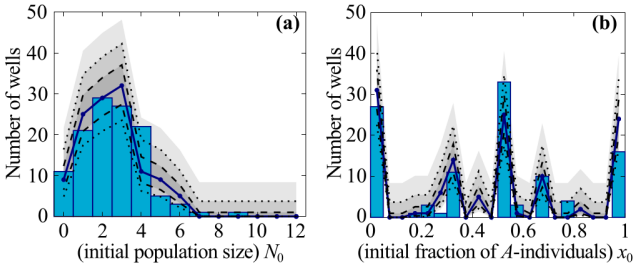

Fig 3. Initial distributions for population size N_0 and composition x_0 (parameter values $\bar{N}_0 = 2.55$, $\bar{x}_0 = 0.45$). The experimental distributions (bars) for N_0 (panel **(a)**) and x_0 (panel **(b)**) are measured from 120-well ensembles. The average $\bar{N}_0$ and $\bar{x}_0$ calculated from the measured values determine the parameters for the simulated distributions. The theoretical average distribution (solid blue line) is the average of the same distributions generated for 84 sets of 120 wells. Using that average we calculate the Wilson binomial confidence intervals (gray areas) for 68% (between dashed lines), 95% (between dotted lines) and 99.73% confidence. The measured and simulated distributions agree well within statistical error, confirming our assumption that individuals of strain *A* and *B* in the experiments start Poisson-distributed with mean $\bar{N}_0\bar{x}_0$ and $\bar{N}_0(1-\bar{x}_0)$, respectively. The ragged distribution of x_0 derives from a small-number effect, and disappears at larger values of N_0 (see main text, and also S3 Fig).

doi:10.1371/journal.pone.0134300.g003

binomial confidence intervals [36] for the count in each bin, and compared those with the experimental distribution.

Fig 3(a) shows a representative experimental histogram of the initial population sizes N_0 for strong dilution with $\bar{N}_0 = 2.55$. It is well approximated by a Poisson distribution, and agrees with the simulation results within statistical errors (blue line and shaded gray areas in Fig 3(a)). Fig 3(b) shows the probability distribution of the corresponding initial compositions x_0 of the populations, where again theoretical and experimental values agree well within statistical error. Note also that in every well the composition x_0 must be a simple fraction; this means that only a few numerical values are possible for small initial population sizes N_0. This small-number effect explains why the distribution of x_0 in Fig 3(b) is so ragged. The distribution becomes much smoother for larger initial population sizes (see S3 Fig). Taken together, these results for the distribution of initial population size and composition confirm that the inoculation of the individual wells is a stochastic sampling process with Poissonian statistics.

Next, we were interested in how the composition of the bacterial population would evolve under non-selective (neutral) growth conditions. To this end we let the 120 populations grow for an 11-hour period, during which they remained in exponential growth phase (see S2 Fig). Then we measured the population size $N(t)$ in each well by counting colony-forming units, and $x(t)$ by counting the pyoverdine-producing colonies (see Materials and Methods). Fig 4 shows the final outcome for four different initial conditions, i.e. combinations of the initial average population size $\bar{N}_0$ and composition $\bar{x}_0$. We first wanted to know what determines the number of wells that contain only individuals of either strain *A* or strain *B*, i.e. that are fixated. To this end we compared the experimentally observed values with the corresponding predictions from the numerical simulations of the Pólya urn model (Fig 4). Since both results agree within statistical error, we conclude that fixation of a population is a consequence of the initial sampling process and is not due to fixation during population growth (see also S1 Table). This is especially obvious for small average initial population size or compositions close to $x = 0$ or $x = 1$, where a large fraction of the wells contains cells of strain *A* or *B* only (Fig 4(a) and 4(d)). Next we wished to learn how the final distribution of the population composition (i.e. the random limits, x^*) depends on the initial average composition $\bar{x}_0$. For $\bar{x}_0 = 0.5$, we observed both by experiment and theoretically that the initial distribution significantly broadened (by a factor

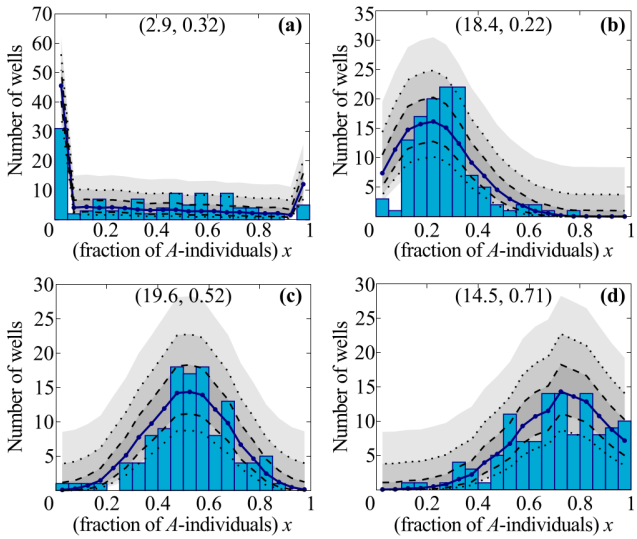

Fig 4. Steady-state distributions of population composition *x* for different initial conditions. The experimental distribution (bars) is the result of growth on 120 independent wells. We use the measured average x_0 and N_0 from the experiments to initialize the simulations of several 120-well ensembles. After growth, we compute the histogram for each of these ensembles and obtain the average theoretical distribution (blue line). Using the values from this distribution, we compute the three confidence intervals (shaded gray areas) for each bin for 68% (between dashed lines), 95% (between dotted lines) and 99.73% confidence. The two sets of data match: most experimental data agree with the first prediction confidence region, practically all with the second one. The limit distributions are clearly different from the initial ones (see S1 Fig). The importance of growth in changing the distributions depends on the initial size N_0 (see main text, and S1 Fig). Parameter values: $\bar{N}_0 = 2.9, \bar{x}_0 = 0.32$ (panel **(a)**); $\bar{N}_0 = 18.4, \bar{x}_0 = 0.22$ (panel **(b)**); $\bar{N}_0 = 19.6$, $\bar{x}_0 = 0.52$ (panel **(c)**); $\bar{N}_0 = 14.5, \bar{x}_0 = 0.71$ (panel **(d)**).

doi:10.1371/journal.pone.0134300.g004

of $\sqrt{2}$) but remained symmetrical (Fig 4(c) and S1 Fig). In contrast, starting from distributions with average values below or above 0.5 caused the final distribution to broaden and also become skewed towards smaller or larger values of *x*, respectively (Fig 4(b) and 4(d)). Moreover, we found quantitative agreement between experiment and numerical simulations within statistical errors in all analyzed parameter regimes (see blue lines and shaded areas in Fig 4): most experimental histograms fall within the first confidence interval of the prediction (darkest gray areas, between dashed lines), and almost all fall within the 99.73% confidence interval.

Taken together, our combined theoretical and experimental analysis gives a coherent picture of evolution during non-selective (exponential) growth. We have shown, experimentally and by analogy with the Pólya urn model, that for each well-mixed population the composition of the population reaches a random stationary limit, and, unlike populations with constant size, generally does not fixate. For a large ensemble of populations, this implies that the probability distribution for the population composition converges to limit distributions (Figs 2 and 4), which are nothing like Kimura"s result for constant-sized populations. Our result is also quite different from that obtained in range expansion experiments [37] or other settings featuring population growth without death on two-dimensional substrates. There, monoclonal sectoring patterns arise as a consequence of random genetic drift, which drives population differentiation along the expanding fronts of bacterial colonies, unlike our well-mixed populations that freeze to coexistence.

Our study also shows that, in a growing population with stochastic initial conditions, demographic noise has two possible sources: the initial sampling process by which subpopulations are formed, and the subsequent growth process. The initial average population size $\bar{N}_0$ sets

their relative weight (see S3 Text and S1 Fig). For very small $\bar{N}_0$, of the order of one or two individuals, the formation process already determines the final composition distribution: most populations start off fixated, many with just a single founder individual, and the composition of each well remains the same during growth. For very large $\bar{N}_0$, of the order of a few hundreds, the sampling process is again central: the composition distribution changes very little before freezing, and growth generates only a very limited amount of variation. In these two limiting regimes, neglecting stochastic effects during growth leaves the evolutionary outcome practically unchanged. In contrast, for small founder colonies such as those typically found during population bottlenecks [18, 19, 38] ($\bar{N}_0 \sim 10$), population growth is responsible for the major part of the variation observed in the final distribution.

Moreover, our results reveal that a growing population reaches a random limit composition much faster than genetic drift leads to fixation in populations of constant size. Typical fixation times for genetic drift increase logarithmically with the population size [11], while the time scale for freezing is independent of population size. This has important consequences for the role of stochastic effects when a population passes from exponential growth phase to stationary phase, in which growth rate and death rate are equal. Then, the composition of the population shows both freezing and fixation, albeit at quite distinct times because the relevant time scales differ markedly. During growth the composition distribution quickly freezes, as described above. Once the population reaches its stationary size, it slowly drifts to fixation, following Kimura-like dynamics.

We also believe that our results have a broad range of applications since growing populations are ubiquitous in nature. For example, experimental studies of *P. aeruginosa* [22, 39] have shown that typical life cycles pass through different steps with regularly occurring dispersal events being followed by the formation of new colonies. As initial colony sizes are typically small, such dispersal events coincide with *population bottlenecks* and subsequent exponential growth. During these phases of the life cycle, population dynamics is often selectively neutral and hence falls within the framework of the present work. The degree of diversity generated during these population bottlenecks has been shown to be crucial for some proposed mechanisms for the evolution of cooperation under selective pressure [5–7, 40–42]. Our analysis quantifies the ensuing degree of diversity and points to the relative importance of sampling versus growth for long-term behavior of the reservoirs. This may have important consequences for the degree of genetic diversity observed in natural populations with life-cycle structures [38].

Materials and Methods

Strains and cultivation conditions

The *P. putida* strains KT2440 (wild type) and 3E2 (mutant with defective pyoverdine synthesis) [3] were used as pyoverdine producers and non-producers, respectively. Cells were grown in casamino acid medium (CAA) containing per liter: 5 g casamino acids, 0.8445 g K_2HPO_4, 0.1404g $MgSO_4 \bullet (H_2O)$ [3]. The CAA medium was supplemented with 200 μM $FeCl_3$ (CAA-Fe) to suppress pyoverdine production (see S2 Table). Overnight cultures of the individual strains in CAA-Fe medium were adjusted to an OD_{600} of 1, diluted 10^{-2} fold, mixed to yield the desired producer fraction, and further diluted to create Poisson distribution conditions. Producer/non-producer co-cultures were started by inoculating the central 60 wells of two 96-well plates thereby adjusting the average initial cell number $\bar{N}_0$ to values between 2 and 25 cells/150 μL. Wells at the border of the plates were filled with water to minimize evaporation from central wells. For non-selective growth, co-cultures were grown in CAA-Fe medium shaking at 30°C for given periods of time. Due to the random distribution of initial cell number N_0 and producer faction x_0 in the 120 wells, each experiment was unique. An experiment was

limited to 120 wells to allow initiation of the analysis of the subpopulations in the individual wells without uncontrolled changes of growth parameters during analysis. The experiment duration was set to 11h to allow evolution to act for a significant number of generations (see S1 Table), while leaving bacteria in exponential growth phase (see S2 Fig)

Determination of growth parameters

Cell numbers N_0 and $N(t)$ were determined by counting the colony forming units (cfu) of individual wells. For this purpose 100μL aliquots of the individual wells were plated on cetrimide [43] or King's B agar (contains per liter: 20 g peptone, 10 g glycerol, 1.965 g $K_2HPO_4(3H_2O)$, 0.842 g $MgSO_4(H_2O)$ [44]. Producer fractions x_0 and $x(t)$ were determined based on the capability of cells to produce the green fluorescent pyoverdine either by direct counting of fluorescent and non-fluorescent colonies on the plates or after growth in iron-limited CAA medium. The fraction of dead cells was determined by life/dead staining with propidium iodide [45], and was always <0.02 of the total cell number under the experimental conditions.

Simulation of growing populations

We performed simulations of 10080 wells using a Gillespie algorithm [46]. The initial numbers of "cells" per well were drawn at random from a Poisson distribution with a mean value of $\bar{N}_0$ measured in the corresponding experiment. The strain assigned to every individual in each well was determined by the outcome of a Bernoulli trial (i.e., coin-flip-like process) and the probability of assignment to strain A was set to the value of $\bar{x}_0$ measured in the experiment. After initialization, wells were grouped into 84 virtual 120-well "plates", and a random waiting time was selected for each well, drawn from an exponential distribution with the population size as parameter. The Gillespie algorithm was run until the average size across all wells matched the average size measured at the end of the growth experiments, or until a specified time had elapsed (see S2 Fig).

Supporting Information

S1 Video. Time evolution of composition distribution. The distribution of compositions x first broadens due to demographic noise, but soon "freezes" to a steady state. The steady state form is maintained as long as the populations grow. Parameter values are $\bar{N}_0 = 10, \bar{x}_0 = 0.33$ (as for Fig 2).
(MP4)

S1 Text. Exact calculations for steady-state composition distribution and moments. Using the theory of Pólya urns, we calculate exactly the steady state values of: (i) the distribution of population compositions x, (ii) its mean value, and (iii) its variance.
(PDF)

S2 Text. Approximate calculations for the time evolution of the distribution moments. We use the Master equation of the growth process (Eq (1)) to determine the time evolution of variance and skewness of the composition distribution. These values are used in Eq (2) and Fig 2.
(PDF)

S1 Fig. Initial and steady state distributions, relative entropy. Panels (a),(b),(c): Initial and final distributions of x for three regimes of $\bar{N}_0$. When $\bar{N}_0$ is very small or very large (panels **(a)** and **(b)**), the evolutionary fate of the population is largely determined by the initial population sampling. Therefore, the initial distribution (red bars) and the steady-state one (green bars) look qualitatively very similar. For intermediate values of $\bar{N}_0$, however, population growth

becomes more important, and the distributions look very different. The amount of composition values the population can access through growth can be quantified looking at the "unpredictability" of the steady-state composition, once the initial one is known: the more unpredictable, the more are made accessible by growth. Mathematically, the measure for this is called *conditional entropy*: the higher the entropy, the more unpredictable the outcome. Panel **(d)** shows the conditional entropy as function of $\bar{N}_0$. Indeed, very small or very large initial populations experience little to no additional noise from growth, while in populations with intermediate values of $\bar{N}_0$ ($\bar{N}_0 \simeq 15$) growth is a major source of demographic noise. (Parameter values: $\bar{N}_0 = 2$ **(a)**, $\bar{N}_0 = 2000$ **(b)**, $\bar{N}_0 = 20$ **(c)**; $\bar{x}_0 = 0.25$ in all panels)
(TIF)

S3 Text. Comparison of initial and steady-state distributions of x, and entropy of the steady state distribution conditioned on the initial one. We use conditional entropy to analyze the impact of growth on the distribution of compositions *x*. The results are also depicted in S1(d) Fig
(PDF)

S2 Fig. Growth curve of a mixed population. The population consists of pyoverdine producer (*P. putida* KT2440) and non-producer (*P. putida* 3E2) under non-selective (iron replete) conditions. Individual precultures of the strains were mixed and diluted in iron replete medium to yield $\bar{N}_0 = 4$ (in 150 μL), and $\bar{x}_0 = 0.5$. Cells were grown aerobically at 30°C for 24 hours. The dots represent the mean $N(t)$ of three independent replications, the bars the corresponding standard deviation. After a lag phase of about 2 hours, the cells start to grow exponentially and reach the stationary phase after about 14 h of growth. For the non-selective growth experiments used to test the predictions of the Pólya urn model, cells were grown for 11.5 h to ensure exponential growth conditions.
(TIF)

S3 Fig. Additional initial conditions measurements. The experimental distributions (bars) are measured from 120-well ensembles, the average N_0 and x_0 from those sets the parameters for the simulated distributions. The theoretical average distribution (solid line) is the average of the same distributions generated for 84 sets of 120 wells. Using that average we calculate three Wilson binomial confidence intervals (gray areas). Experiments and theory agree within statistical error: the distribution of sizes (panels **(a)** and **(c)**) follows a Poisson distribution. The raggedness of the distribution of *x* for at small $\bar{N}_0$ (see panel **(b)** and Fig 3(b) in main text) is due to a small size effect: since *x* must be a simple fraction, when N_0 is small only a few values are available (see main text). This effect disappears for average initial sizes $\bar{N}_0 \simeq 10$ (see panel **(d)**). Parameter values: $\bar{N}_0 = 5.75, \bar{x}_0 = 0.43$ **(a)** and **(b)**; $\bar{N}_0 = 26.49, \bar{x}_0 = 0.45$ **(c)** and **(d)**.
(TIF)

S1 Table. Comparison between results from our experiments and those in [9]. While experiments for constant-sized populations of *Drosophila* observe significant fixations within the first tens of generations, we instead observe freezing of the probability distribution for the population composition, without any fixation.
(PDF)

S2 Table. Comparison of growth and pyoverdine production per cell of *P. putida* KT2440 and 3E2. Separate cultures of producer (*P. putida* KT2440) and non-producer (*P. putida* 3E2) were grown in iron-limiting (no addition of $FeCl_3$) and iron-replete medium (addition of 200 μM $FeCl_3$) at 30°C. The cell density was measured at 600 nm, and specific growth rates were calculated from density values of the exponential phase. The pyoverdine production was

determined by fluorescence emission measurements (excitation 400 nm, emission at 460 nm). The pyoverdine production per cell represents the ratio of pyoverdine fluorescence and optical density measured after 24 h of growth. The values in the table are averages over a minimum of five experiments, with the corresponding standard deviation. The fluorescence value for the non-producing mutant in iron-limiting medium is 0 because the culture failed to grow.
(PDF)

Acknowledgments

For fruitful discussions we thank Madeleine Opitz, Johannes Knebel, Markus Weber, Stefano Duca, Matthias Bauer, Kirsten Jung. We thank Michelle Eder (HJ lab) for excellent technical assistance. P. putida strain 3E2 was kindly provided by P. Cornelis (Vrije Universiteit Brussels, Belgium).

Author Contributions

Conceived and designed the experiments: HJ FB. Performed the experiments: HJ FB. Analyzed the data: FB HJ ML KW EF. Contributed reagents/materials/analysis tools: EF ML KW. Wrote the paper: EF HJ ML KW. Designed theoretical analysis: EF ML KW. Performed theoretical analysis: ML KW.

References

1. Kimura M (1955) Solution of a process of random genetic drift with a continuous model. PNAS. PMID: 16589632
2. Otto SP, Whitlock MC (1997) The probability of fixation in populations of changing size. Genetics 146: 723–733. PMID: 9178020
3. Matthijs S, Laus G, Meyer JM, Abbaspour-Tehrani K, Schäfer M, et al. (2009) Siderophore-mediated iron acquisition in the entomopathogenic bacterium pseudomonas entomophila l48 and its close relative pseudomonas putida KT2440. Biometals 22: 951–964. doi: 10.1007/s10534-009-9247-y PMID: 19459056
4. Eggenberger F, Pólya G (1923) Über die statistik verketteter vorgänge. ZAMM—Journal of Applied Mathematics and Mechanics / Zeitschrift für Angewandte Mathematik und Mechanik 3: 279–289.
5. Melbinger A, Cremer J, Frey E (2010) Evolutionary game theory in growing populations. Phys Rev Lett 105: 178101. doi: 10.1103/PhysRevLett.105.178101 PMID: 21231082
6. Cremer J, Melbinger A, Frey E (2011) Evolutionary and population dynamics: a coupled approach. Phys Rev E 84: 051921. doi: 10.1103/PhysRevE.84.051921
7. Cremer J, Melbinger A, Frey E (2012) Growth dynamics and the evolution of cooperation in microbial populations. Sci Rep 2: 281. doi: 10.1038/srep00281 PMID: 22355791
8. Crow JF, Kimura M (1970) An Introduction to Population Genetics. Harper and Row.
9. Hartl DL, Clark AG (1989) Principles of population genetics. Sinauer, Sunderland, MD, USA, 2nd edition.
10. Frey E, Kroy K (2005) Brownian motion: a paradigm of soft matter and biological physics. Ann Phys 14: 20–50. doi: 10.1002/andp.200410132
11. Blythe RA, McKane J (2007) Stochastic models of evolution in genetics, ecology and linguistics. J Stat Mech: 07018. doi: 10.1088/1742-5468/2007/07/P07018
12. Caballero A (1994) Developments in the prediction of effective population size. Heredity 73: 657–679. doi: 10.1038/hdy.1994.174 PMID: 7814264
13. Gillespie JH (2001) Is the population size of a species relevant to its evolution? Evolution 55: 2161–2169. doi: 10.1554/0014-3820(2001)055%5B2161:ITPSOA%5D2.0.CO;2 PMID: 11794777
14. Hahn MW (2008) Toward a selection theory of molecular evolution. Evolution 62: 255–265. doi: 10.1111/j.1558-5646.2007.00308.x PMID: 18302709
15. Hurst LD (2009) Fundamental concepts in genetics: genetics and the understanding of selection. Nat Rev Genet 10: 83–93. doi: 10.1038/nrg2506 PMID: 19119264

16. Buri P (1956) Gene frequency in small populations of mutant drosophila. Evolution 10: 367–402. doi: 10.2307/2406998
17. Center for Food Safety and Applied Nutrition Causes of Foodborne Illness: Bad Bug Book—BBB—Escherichia coli O157:H7 (EHEC). Provides basic information about Escherichia coli O157:H7.
18. Kurjak A, Chervenak FA (2006) Textbook of Perinatal Medicine. Informa UK Ltd, 2nd edition.
19. Grossart HP, Levold F, Allgaier M, Simon M, Brinkhoff T (2005) Marine diatom species harbour distinct bacterial communities. Environmental Microbiology 7: 860–873. doi: 10.1111/j.1462-2920.2005.00759.x PMID: 15892705
20. Bird DF, Kalff J (1984) Empirical relationships between bacterial abundance and chlorophyll concentration in fresh and marine waters. Can J Fish Aquat Sci 41: 1015–1023. doi: 10.1139/f84-118
21. Buchan A, LeCleir GR, Gulvik CA, González JM (2014) Master recyclers: features and functions of bacteria associated with phytoplankton blooms. Nat Rev Micro 12: 686–698. doi: 10.1038/nrmicro3326
22. Stoodley P, Sauer K, Davies DG, Costerton JW (2002) Biofilms as complex differentiated communities. Annual Review of Microbiology 56: 187–209. doi: 10.1146/annurev.micro.56.012302.160705 PMID: 12142477
23. Levin SA (1974) Dispersion and population interactions. The American Naturalist 108: 207–228. doi: 10.1086/282900
24. Sanchez A, Gore J (2013) Feedback between population and evolutionary dynamics determines the fate of social microbial populations. PLoS biology 11: e1001547. doi: 10.1371/journal.pbio.1001547 PMID: 23637571
25. Parsons TL, Quince C, Plotkin JB (2010) Some consequences of demographic stochasticity in population genetics. Genetics 185: 1345–1354. doi: 10.1534/genetics.110.115030 PMID: 20457879
26. Buckling A, Harrison F, Vos M, Brockhurst MA, Gardner A, et al. (2007) Siderophore-mediated cooperation and virulence in pseudomonas aeruginosa. FEMS Microbiol Ecol 62: 135–41. doi: 10.1111/j.1574-6941.2007.00388.x PMID: 17919300
27. Cornelis P, Matthijs S, Van Oeffelen L (2009) Iron uptake regulation in pseudomonas aeruginosa. Biometals 22: 15–22. doi: 10.1007/s10534-008-9193-0 PMID: 19130263
28. Cohen JE (1976) Irreproducible results and the breeding of pigs (or nondegenerate limit random variables in biology). BioScience 26: 391–394.
29. Schreiber SJ (2001) Urn models, replicator processes, and random genetic drift. SIAM Journal on Applied Mathematics 61: 2148–2167. doi: 10.1137/S0036139999352857
30. Sornette D (2009) Why Stock Markets Crash: Critical Events in Complex Financial Systems. Princeton University Press.
31. Pemantle R (2007) A survey of random processes with reinforcement. Probability Surveys 4: 1–79. doi: 10.1214/07-PS094
32. Athreya KB, Karlin S (1968) Embedding of urn schemes into continuous time markov branching processes and related limit theorems. The Annals of Mathematical Statistics 39: 1801–1817. doi: 10.1214/aoms/1177698013
33. Kotz S, Mahmoud H, Robert P (2000) On generalized pólya urn models. Statistics & Probability Letters 49: 163–173.
34. Allen L (2003) An Introduction to Stochastic Processes with Biology Applications. Prentice Hall.
35. Arthur WB, Ermoliev YM, Kaniovski YM (1987) Path-dependent processes and the emergence of macro-structure. European Journal of Operational Research 30: 294–303. doi: 10.1016/0377-2217(87)90074-9
36. Wilson EB (1927) Probable inference, the law of succession, and statistical inference. Journal of the American Statistical Association 22: 209–212. doi: 10.1080/01621459.1927.10502953
37. Hallatschek O, Hersen P, Ramanathan S, Nelson DR (2007) Genetic drift at expanding frontiers promotes gene segregation. PNAS 104: 19926–19930. doi: 10.1073/pnas.0710150104 PMID: 18056799
38. Hammerschmidt K, Rose CJ, Kerr B, Rainey PB (2014) Life cycles, fitness decoupling and the evolution of multicellularity. Nature 515: 75–79. doi: 10.1038/nature13884 PMID: 25373677
39. Hall-Stoodley L, Costerton JW, Stoodley P (2004) Bacterial biofilms: from the natural environment to infectious diseases. Nat Rev Microbiol 2: 95–108. doi: 10.1038/nrmicro821 PMID: 15040259
40. Chuang JS, Rivoire O, Leibler S (2009) Simpson's paradox in a synthetic microbial system. Science 323: 272–5. doi: 10.1126/science.1166739 PMID: 19131632
41. Oliveira NM, Niehus R, Foster KR (2014) Evolutionary limits to cooperation in microbial communities. PNAS 111: 17941–17946. doi: 10.1073/pnas.1412673111 PMID: 25453102
42. Melbinger A, Cremer J, Frey E The emergence of cooperation from a single cooperative mutant.

43. Brown VI, Lowbury EJL (1965) Use of an improved cetrimide agar medium and other culture methods for pseudomonas aeruginosa. J Clin Pathol 18: 752–756. doi: 10.1136/jcp.18.6.752 PMID: 4954265

44. King EO, Ward MK, Raney DE (1954) Two simple media for the demonstration of pyocyanin and fluorescin. Journal of Laboratory and Clinical Medicine 44: 301–307. PMID: 13184240

45. Suzuki T, Fujikura K, Higashiyama T, Takata K (1997) DNA staining for fluorescence and laser confocal microscopy. J Histochem Cytochem 45: 49–53. doi: 10.1177/002215549704500107 PMID: 9010468

46. Gillespie D (1976) General method for numerically simulating stochastic time evolution of coupled chemical reactions. J Comp Phys 22: 403–434.

Non-selective evolution of growing populations
Supplementary Information

Karl Wienand, Matthias Lechner, Felix Becker, Heinrich Jung, and Erwin Frey

Video: Time evolution of composition distribution.

`https://vimeo.com/108884249`

The distribution of compositions x first broadens due to demographic noise, but soon "freezes" to a steady state. The steady state form is maintained as long as the populations grow. Parameter values are $\bar{N}_0 = 10$, $\bar{x}_0 = 0.33$ (as for Fig. 2).

Exact calculations for steady-state composition distribution and moments.

Calculation of probability distribution.

Each population in the ensemble is initialized with A_0 individuals of type A and B_0 of type B. In the general case, A_0 and B_0 are independent random variables for each population with distributions $P(A_0)$ and $P(B_0)$. All populations evolve for ΔN reproduction events, of which a random amount ΔA generate new A-individuals. From the mathematical literature [35], it is well-known that ΔA follows a beta-binomial, with A_0, B_0 and ΔN as parameters. The fraction of A-individuals x, then follows the probability

$$P(x) = \sum_{A_0,B_0} P(A_0)P(B_0)P(\Delta A = x(A_0 + B_0 + \Delta N) - A_0 | A_0, B_0, \Delta N)\,, \tag{3}$$

where the sums run over all allowed values of their respective indices. $P(\Delta A = k|A_0, B_0, \Delta N)$ is the probability of ΔA being equal to k, given the values of A_0, B_0 and ΔN. The sum may easily be performed numerically. For the moments of the distribution there are, however, also closed-form analytic expressions.

Exact calculation of asymptotic moment values

Let $\langle\cdot\rangle_0$ be the average over the initial conditions, $\langle\cdot\rangle_{\Delta A}$ be an average over ΔA, and $\langle\cdot\rangle$ be an average over both quantities. From the properties of the beta-binomial distribution we know that, for a given initial condition, we have

$$\langle \Delta A \rangle_{\Delta A} = \frac{\Delta N A_0}{A_0 + B_0}\,, \tag{4}$$

$$\mathrm{Var}[\Delta A] = \frac{\Delta N A_0 B_0 (A_0 + B_0 + \Delta N)}{(A_0 + B_0)^2 (A_0 + B_0 + 1)}\,. \tag{5}$$

For the mean of $\langle x \rangle$, one obtains

$$\langle x \rangle \overset{(4)}{=} \langle x_0 \rangle_0 = \bar{x}_0\,.$$

Hence, the average composition is exactly conserved throughout the time evolution of the populations. In other words, the stochastic process is a martingale.

For the variance we obtain

$$\begin{aligned}
\mathrm{Var}[x] &= \left\langle \left(\frac{A_0 + \Delta A}{A_0 + B_0 + \Delta N} \right)^2 \right\rangle - \langle x_0 \rangle_0^2 && (6)\\
&= \left\langle \frac{A_0^2 + 2A_0 \langle \Delta A \rangle_{\Delta A} + \mathrm{Var}[\Delta A] + \langle \Delta A \rangle_{\Delta A}^2}{(A_0 + B_0 + \Delta N)^2} \right\rangle_0 - \langle x_0 \rangle_0^2 && (7)\\
&\overset{(4)}{=} \left\langle \left(\frac{A_0}{A_0 + B_0} \right)^2 + \frac{\mathrm{Var}[\Delta A]}{(A_0 + B_0 + \Delta N)^2} \right\rangle_0 - \langle x_0 \rangle_0^2 && (8)\\
&\overset{(5)}{=} \mathrm{Var}[x_0] + \left\langle \frac{\Delta N A_0 B_0}{(A_0 + B_0)^2 (A_0 + B_0 + \Delta N)^2 (A_0 + B_0 + 1)} \right\rangle_0 && (9)\\
&= \mathrm{Var}[x_0] + \langle x_0(1 - x_0) \rangle_0 \left\langle \frac{1}{N_0 + 1} \frac{\Delta N}{N_0 + \Delta N} \right\rangle_0 . && (10)
\end{aligned}$$

For long times (i.e., $\Delta N \gg 1$), $\Delta N + N_0 \simeq \Delta N$ and (10) reduces to

$$\mathrm{Var}[x] \to \mathrm{Var}[x_0] + \left\langle \frac{1}{N_0 + 1} \right\rangle_0 \langle x_0(1 - x_0) \rangle_0 . \tag{11}$$

The argument up to here is completely independent of the particular choice of initial conditions. If the initial distribution is known, we may even make the value of the variance more explicit. In particular, consider the distribution we obtain from experiments: in each well, N_0 is Poisson-distributed with mean $\bar{N}_0$. Then one gets

$$\left\langle \frac{1}{N_0 + 1} \right\rangle_0 = \frac{1 - \mathrm{e}^{-\bar{N}_0}}{\bar{N}_0} . \tag{12}$$

Within each well of (random) size N_0 there is an initial random number A_0 of A-individuals, which follows a Binomial distribution with parameters N_0 and $\bar{x}_0$. For this choice of distribution, it is possible that $N_0 = 0$, which would lead to an undetermined value of $x_0 = A_0/N_0$, and therefore also for the average $\langle x_0 \rangle$. We can solve this problem by redefining x_0:

$$x_0 := \begin{cases} \bar{x}_0 & , N_0 = 0 \\ \frac{A_0}{N_0} & , \text{otherwise} \end{cases} \tag{13}$$

so that x_0 and its average have definite values, and $\langle x_0 \rangle_0 = \bar{x}_0$. With this we can compute the second moment of x_0:

$$\langle x_0^2 \rangle_0 = \sum_{N_0=1}^{\infty} \mathrm{e}^{-\bar{N}_0} \frac{\bar{N}_0^{N_0}}{N_0!} \left\{ \sum_{A_0=0}^{N_0} \binom{N_0}{A_0} \bar{x}_0^{A_0} (1 - \bar{x}_0)^{N_0 - A_0} \frac{A_0^2}{N_0^2} \right\} + \bar{x}_0^2 \mathrm{e}^{-\bar{N}_0} . \tag{14}$$

The sum inside the braces can be solved using exponential and binomial series and yields

$$\langle x_0^2 \rangle_0 = \bar{x}_0^2 + \bar{x}_0(1 - \bar{x}_0) \mathrm{e}^{-\bar{N}_0} \sum_{N_0=1}^{\infty} \frac{\bar{N}_0^{N_0}}{N_0! N_0} . \tag{15}$$

The remaining series is an exponential integral (Ei), and therefore

$$\mathrm{Var}[x_0] = \bar{x}_0(1 - \bar{x}_0) \mathrm{e}^{-\bar{N}_0} \left[\mathrm{Ei}(\bar{N}_0) - \gamma - \ln(\bar{N}_0) \right] =: \bar{x}_0(1 - \bar{x}_0) \varphi(\bar{N}_0) , \tag{16}$$

where we defined $\varphi(\bar{N}_0) := \mathrm{e}^{-\bar{N}_0} \left[\mathrm{Ei}(\bar{N}_0) - \gamma - \ln(\bar{N}_0) \right]$. Then the variance of x reads

$$\begin{aligned}
\mathrm{Var}[x] &= \mathrm{Var}[x_0] + \frac{1 - \mathrm{e}^{-\bar{N}_0}}{\bar{N}_0} \langle x_0(1 - x_0) \rangle && (17)\\
&= \bar{x}_0(1 - \bar{x}_0) \left[\varphi(\bar{N}_0) + \frac{1 - \mathrm{e}^{-\bar{N}_0}}{\bar{N}_0} \left(1 - \varphi(\bar{N}_0) \right) \right] . && (18)
\end{aligned}$$

For large $\bar{N}_0$, through an asymptotic expansion [47],

$$\mathrm{Ei} \simeq \frac{1}{\bar{N}_0}\mathrm{e}^{\bar{N}_0}\sum_{m=0}^{\bar{N}_0-1} m!\bar{N}_0^{-m} - \frac{1}{3}\sqrt{\frac{2\pi}{\bar{N}_0}}\,, \tag{19}$$

$\varphi(\bar{N}_0)$ can be approximated by

$$\varphi(\bar{N}_0) \simeq \frac{1}{\bar{N}_0}\sum_{m=0}^{\bar{N}_0-1} m!\bar{N}_0^{-m} - \mathrm{e}^{-\bar{N}_0}\left[\frac{1}{3}\sqrt{\frac{2\pi}{\bar{N}_0}} - \gamma - \ln(\bar{N}_0)\right]. \tag{20}$$

To leading order in $\bar{N}_0$, then, the variance of x becomes

$$\mathrm{Var}[x] = \bar{x}_0(1-\bar{x}_0)\frac{2}{\bar{N}_0}\,,$$

in perfect agreement with our approximate results based on Master equations (Eq. (2) in main text, see also below).

Approximate calculations for the time evolution of the distribution moments

Using the Master Equation for the number of individuals of each strain (1), we are able to obtain the time evolution of the first three moments of the distribution of x. Equation (1) is sometimes called "Simple Growth Equation" and can be exactly solved (see, for example, [38]) using generating functions like

$$F(a,t) := \sum_{N_A} a^{N_A}\, P(N_A,t). \tag{21}$$

To approximate the time evolution of the first three moments of x, however, we do not need the full solution, but only the first three moments of N_A and N_B. To this end, we insert the Master Equation (Eq. (1) in main text) in the definition of the generating function to get the time derivative for $F(a,t)$:

$$\frac{d}{dt}F(a,t) = \left(-a+a^2\right)\partial_a F(a,t). \tag{22}$$

To obtain the time evolution of the nth moment, we apply the nth derivative with respect to a on both sides of equation (22), and solve for the corresponding moment. For the first three moments, the solution is

$$\langle N_A\rangle = \mathrm{e}^t K_1\,, \tag{23}$$
$$\langle N_A^2\rangle = \mathrm{e}^t(\mathrm{e}^t-1)K_1 + \mathrm{e}^{2t}K_2\,, \tag{24}$$
$$\langle N_A^3\rangle = \mathrm{e}^t\left(-3\mathrm{e}^t+2\mathrm{e}^{2t}+1\right)K_1 + 3\mathrm{e}^{2t}\left(\mathrm{e}^t-1\right)K_2 + \mathrm{e}^{3t}K_3\,. \tag{25}$$

K_1, K_2, K_3 are integration constants, which depend on the initial conditions. We consider the case of Poisson initial conditions. This means that the initial number of A is Poisson-distributed with mean value $\bar{N}_{A,0}$,

$$\langle N_A(t=0)\rangle \stackrel{!}{=} \bar{N}_{A,0}\,, \tag{26}$$

and, since for the Poisson distribution the variance equals the mean, we get

$$\operatorname{Var} N_A(t=0) \stackrel{!}{=} \bar{N}_{A,0}\,. \tag{27}$$

Employing these conditions in the solutions of the differential equations we found in Eq. (23) and (24), we get

$$\begin{aligned} \langle N_A \rangle &= \mathrm{e}^t \bar{N}_{A,0}\,, & (28)\\ \operatorname{Var} N_A &= \mathrm{e}^t(2\mathrm{e}^t - 1)\bar{N}_{A,0}. & (29) \end{aligned}$$

By the known properties of the Poisson distribution, the skewness of our initial distribution equals to $1/\sqrt{\bar{N}_{A,0}}$. Using Eqs. (25), (28), and the definition of the skewness, we obtain the general time evolution of the skewness

$$v(N_A) = \frac{\bar{N}_{A,0}\left(6e^{2t} - 6e^t + 1\right)e^t}{\left(\bar{N}_{A,0}\left(2e^t - 1\right)e^t\right)^{3/2}}\,. \tag{30}$$

For N_B, the calculations are analogous. Note also that all calculations were exact so far.

With the moments of N_A and N_B we can find the (approximate) time evolution of variance and skewness of $x = N_A/(N_A + N_B)$. For the mean of x we have already seen in the exact calculation (see Eq. (6)) that it does not change with time, and hence its time evolution is already known.

To calculate the time evolution of the variance of x, we consider x as a function of N_A and N_B:

$$x(N_A, N_B) = \frac{N_A}{N_A + N_B}. \tag{31}$$

Using the time independence of the mean ($\langle x(N_A, N_B)\rangle = x(\langle N_A\rangle, \langle N_B\rangle)$), a bivariate Taylor expansion around $(\langle N_A\rangle, \langle N_B\rangle)$, and the time evolution of the moments, Eqs. (28) and (30), we get for the variance of x:

$$\begin{aligned} \operatorname{Var} x &= \langle [x(N_A, N_B) - \langle x(N_A, N_B)\rangle]^2\rangle & (32)\\ &= \left\langle [x(N_A, N_B) - x(\langle N_A\rangle, \langle N_B\rangle)]^2 \right\rangle & (33)\\ &= \langle [x'_{N_A}(\langle N_A\rangle, \langle N_B\rangle)(N_A - \langle N_A\rangle) + & (34)\\ &\quad + x'_{N_B}(\langle N_A\rangle, \langle N_B\rangle)(N_B - \langle N_B\rangle) + \mathcal{O}\left(N_A^{-2}, N_B^{-2}\right)]^2\rangle & (35)\\ &= \frac{\langle N_B\rangle^2}{\langle N\rangle^4}\operatorname{Var} N_A + \frac{\langle N_A\rangle^2}{\langle N\rangle^4}\operatorname{Var} N_B + \mathcal{O}\left(N_A^{-2}, N_B^{-2}\right) & (36)\\ &= \frac{(2 - \mathrm{e}^{-t})}{N_0^4} N_{B,0} N_{A,0}\left(N_{A,0} + N_{B,0}\right) + \mathcal{O}\left(N_A^{-2}, N_B^{-2}\right) & (37)\\ &= \frac{2 - \mathrm{e}^{-t}}{\bar{N}_0}\bar{x}_0(1 - \bar{x}_0) & (38)\\ &\xrightarrow[t\to\infty]{} \frac{2}{\bar{N}_0}\bar{x}_0(1 - \bar{x}_0) & (39) \end{aligned}$$

From this we obtained Eq. (2) in main text. For infinite times the approximate result for the variance matches the exact one of Eq. (11).

The skewness of the x distribution is calculated analogously:

$$v(x) = \left\langle \left(\frac{x(N_A, N_B) - x(\langle N_A \rangle, \langle N_B \rangle)}{\sqrt{\mathrm{Var}\, x}} \right)^3 \right\rangle \tag{40}$$

$$= \frac{x_0 e^{-2t} \left(12 x_0^2 e^{2t} - 12 x_0^2 e^t + 2 x_0^2\right)}{N_0^2 \left(\frac{x_0}{N_0} \left(-2x_0 e^t + x_0 + 2e^t - 1\right) e^{-t}\right)^{1.5}}$$

$$+ \frac{x_0 e^{-2t} \left(-18 x_0 e^{2t} + 18 x_0 e^t - 3x_0 + 6e^{2t} - 6e^t + 1\right)}{N_0^2 \left(\frac{x_0}{N_0} \left(-2x_0 e^t + x_0 + 2e^t - 1\right) e^{-t}\right)^{1.5}} + \mathcal{O}\left(N_A^{-2}, N_B^{-2}\right) . \tag{41}$$

Comparison of initial and steady-state distributions of x, and entropy of the steady state distribution conditioned on the initial one.

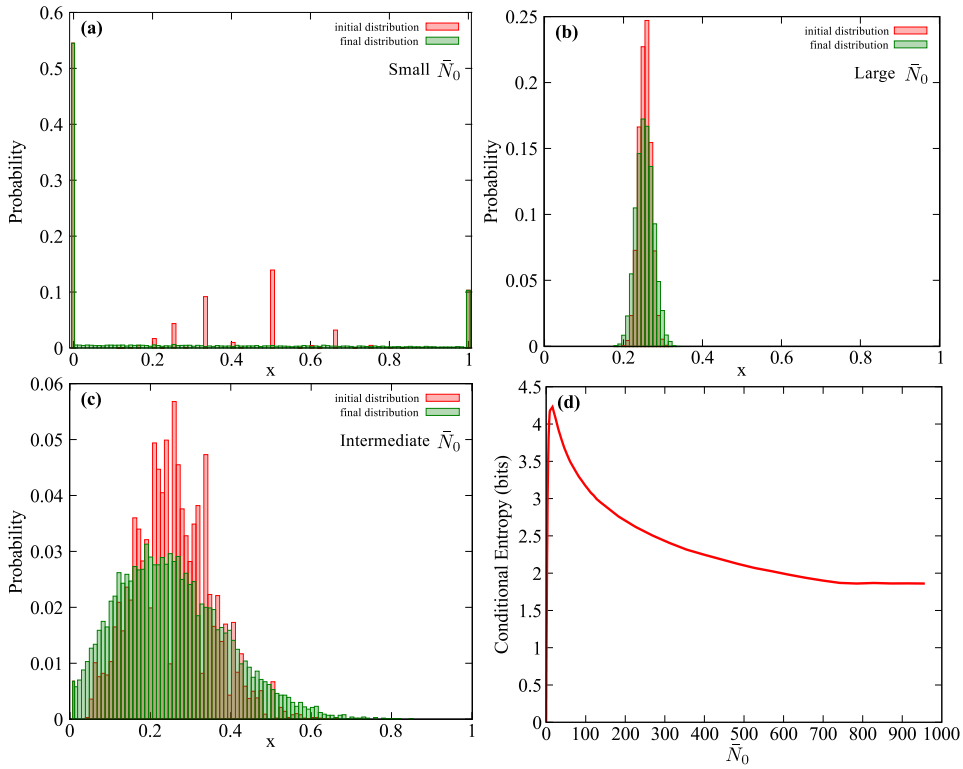

Figure 5: **Initial and steady state distributions, relative entropy. Panels (a),(b),(c)**: Initial and final distributions of x for three regimes of $\bar{N}_0$. When $\bar{N}_0$ is very small or very large (panels **(a)** and **(b)**), the evolutionary fate of the population is largely determined by the initial population sampling. Therefore, the initial distribution (red bars) and the steady-state one (green bars) look qualitatively very similar. For intermediate values of $\bar{N}_0$, however, population growth becomes more important, and the distributions look very different. The amount of composition values the population can access through growth can be quantified looking at the "unpredictability" of the steady-state composition, once the initial one is known: the more unpredictable, the more are made accessible by growth. Mathematically, the measure for this is called *conditional entropy*: the higher the entropy, the more unpredictable the outcome. Panel **(d)** shows the conditional entropy as function of $\bar{N}_0$. Indeed, very small or very large initial populations experience little to no additional noise from growth, while in populations with intermediate values of $\bar{N}_0$ ($\bar{N}_0 \simeq 15$) growth is a major source of demographic noise. (Parameter values: $\bar{N}_0 = 2$ **(a)**, $\bar{N}_0 = 2000$ **(b)**, $\bar{N}_0 = 20$ **(c)**; $\bar{x}_0 = 0.25$ in all panels)

We simulate an ensemble of populations starting from Poisson initial conditions, and track their time evolution until the x distribution freezes. Once it freezes, we can build a joint histogram of initial and final compositions, which approximates the joint distribution $P_{\text{joint}}(x_0, x_f)$. From P_{joint} we can obtain the initial and final distributions as its marginal distributions, integrating over all values of x_f and x_0, respectively. The joint information (Shannon) entropy is defined as [48]

$$H_{\text{joint}}(x_0, x_f) = -\int_0^1 \mathrm{d}x_0 \mathrm{d}x_f P_{\text{joint}}(x_0, x_f) \log(P_{\text{joint}}(x_0, x_f)) \,. \tag{42}$$

The marginal entropies $H(x_0)$ and $H(x_f)$ are defined, analogously, through integrals only of $P(x_0)$ over x_0, and $P(x_f)$ over x_f, respectively. The conditional entropy of the final distribution given the initial is defined as

$$H(x_f|x_0) = H_{\text{joint}}(x_0, x_f) - H(x_0) \,. \tag{43}$$

It measures the amount of information necessary to describe the final distribution, once all information about the distribution of x_0 is known. Therefore, $H(x_f|x_0)$ provides a measure of how entropic (or "noisy") growth itself is [49]—or, in other words, how many different final compositions are possible given the initial condition. Figure 5**(d)** shows $H(x_f|x_0)$ from repeated simulations, all with the same initial distribution form, the same $\bar{x}_0$, but different $\bar{N}_0$. For very small $\bar{N}_0$ (of the order of one or two individuals) the group formation almost completely determines the fate of populations: most populations start fixated, many with just a single founder individual, and the composition of each well remains the same during growth. The path followed by x in each population during time is a straight line, as the compositions stay constant. Therefore, x for different populations follow in time paths that do not cross or "mix". Growth produces very little demographic noise, and its conditional entropy tends to zero. For very large $\bar{N}_0$ (of the order of a few hundreds), the group sampling is again central to determine the final distribution. Very large populations, in fact, all start with similar compositions (according to the Law of Large Numbers), and their compositions are difficult to change, as each individual event has little impact. The composition distribution changes very little before freezing; time evolution paths of different populations "mix" very little. Entropy in this regime saturates for increasing initial sizes, and is rather low. Between the small size regime (where paths do not "mix") and the large size regime (where size limits "mixing"), we find a window where populations are small enough to significantly change their composition, but also large enough to not start fixated. This is the region where the conditional entropy peaks, and growth is the most important in determining the final distribution.

Intuitively, the difference in variance between initial and final distribution could provide an alternative measure of the noise introduced by growth. However, of all x distributions between 0 and 1 with fixed $\bar{x}_0$, the one with maximal variance is the one for which x is only 0 or 1, i.e., when all populations start off fixated. In this case, the compositions never change during growth and the variance stays constant. Moreover, independently on the choice of initial distribution, the difference between initial and steady-state variance decreases for increasing $\bar{N}_0$ (see Eq.(11)). Therefore, all considerations on noise sources based on variance would indicate that growth matters more when initial populations are smaller, in contrast with our observations.

	Drosophila	*P.Putida*
# of populations	107	120
Initial pop. size	16	~ 10
Max. # of generations	19	16
Pop. size	Constant	Growing
Outcome	Increasing number of fixations	No fixation, freezing

Table 1: **Comparison between results from our experiments and those in [9].**While experiments for constant-sized populations of *Drosophila* observe significant fixations within the first tens of generations, we instead observe freezing of the probability distribution for the population composition, without any fixation.

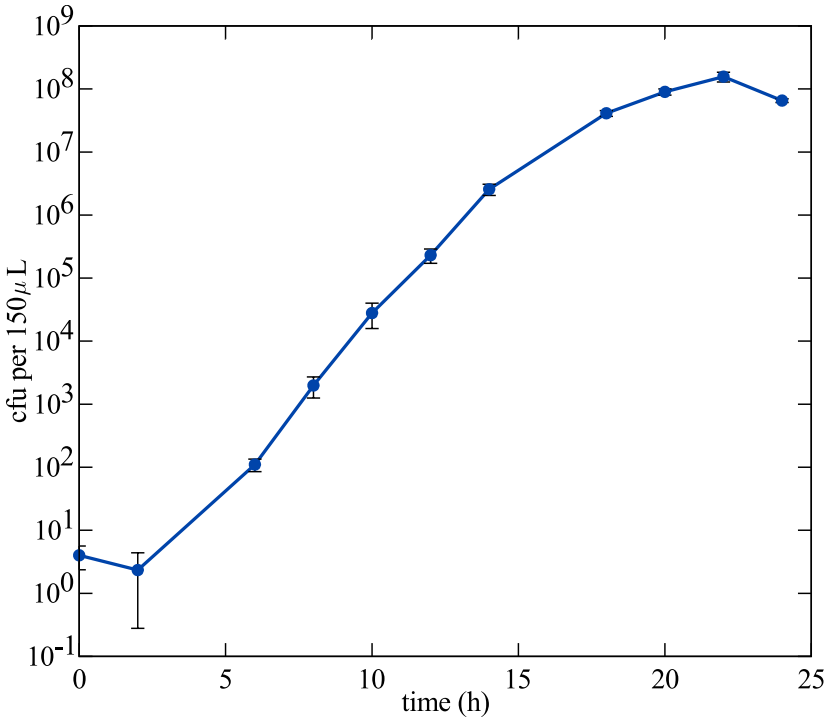

Figure 6: **Growth curve of a mixed population.** The population consists of pyoverdine producer (*P. putida* KT2440) and non-producer (*P. putida* 3E2) under non-selective (iron replete) conditions. Individual precultures of the strains were mixed and diluted in iron replete medium to yield $\bar{N}_0 = 4$ (in 150 μL), and $\bar{x}_0 = 0.5$. Cells were grown aerobically at 30°C for 24 hours. The dots represent the mean $N(t)$ of three independent replications, the bars the corresponding standard deviation. After a lag phase of about 2 hours, the cells start to grow exponentially and reach the stationary phase after about 14 h of growth. For the non-selective growth experiments used to test the predictions of the Pólya urn model, cells were grown for 11.5 h to ensure exponential growth conditions.

	Specific growth rate (h^{-1})		**Fluorescence per cell (a.u.)**	
Iron conc. (μM)	*KT2440*	*3E2*	*KT2440*	*3E2*
0	0.058±0.006	*no growth*	244.00 ± 21.3	0 ± 0
200	0.152±0.026	0.146±0.017	1.56 ± 0.27	0.93 ± 0.10

Table 2: **Comparison of growth and pyoverdine production per cell of *P. putida* KT2440 and 3E2.** Separate cultures of producer (*P. putida* KT2440) and non-producer (*P. putida* 3E2) were grown in iron-limiting (no addition of $FeCl_3$) and iron-replete medium (addition of 200 μM $FeCl_3$) at 30°C. The cell density was measured at 600 nm, and specific growth rates were calculated from density values of the exponential phase. The pyoverdine production was determined by fluorescence emission measurements (excitation 400 nm, emission at 460 nm). The pyoverdine production per cell represents the ratio of pyoverdine fluorescence and optical density measured after 24 h of growth. The values in the table are averages over a minimum of five experiments, with the corresponding standard deviation. The fluorescence value for the non-producing mutant in iron-limiting medium is 0 because the culture failed to grow.

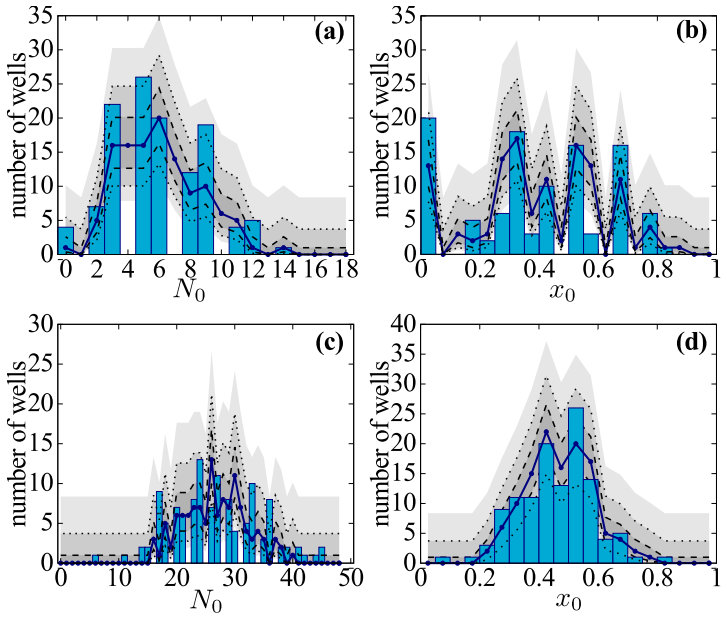

Figure 7: **Additional initial conditions measurements.** The experimental distributions (bars) are measured from 120-well ensembles, the average N_0 and x_0 from those sets the parameters for the simulated distributions. The theoretical average distribution (solid line) is the average of the same distributions generated for 84 sets of 120 wells. Using that average we calculate three Wilson binomial confidence intervals (gray areas). Experiments and theory agree within statistical error: the distribution of sizes (panels **(a)** and **(c)**) follows a Poisson distribution. The raggedness of the distribution of x for at small $\bar{N}_0$ (see panel **(b)** and Fig. 3**(b)** in main text) is due to a small size effect: since x must be a simple fraction, when N_0 is small only a few values are available (see main text). This effect disappears for average initial sizes $\bar{N}_0 \simeq 10$ (see panel **(d)**). Parameter values: $\bar{N}_0 = 5.75$, $\bar{x}_0 = 0.43$ **(a)** and **(b)**; $\bar{N}_0 = 26.49$, $\bar{x}_0 = 0.45$ **(c)** and **(d)**.

Chapter 2

Public-good-mediated social interactions during competitive bacterial growth

Chapter abstract The work in this chapter focuses on how growth, compositional variability, and social interactions intertwine to determine bacterial growth and evolution. The chapter considers a setting in which diverse, mixed populations grow while individuals exchange a public good. The substance—in this case, the iron-scavenging molecule pyoverdine—is synthesized by some individuals, then shared across the whole population. Theoretical approaches to this and similar social interactions typically frame them in terms of game theory and leave implicit the details of the public good biochemistry. In this chapter, I present results indicating how some of these details can be of great importance in population and evolutionary dynamics. In the specific case considered, pyoverdine accumulates in the environment, providing gradually diminishing benefits, and making the contribution of producers superfluous. Details such as this shape the experimental results but would be lost in a game-theoretical approach. The adopted systems biology standpoint, instead, directly quantifies the bacterial interaction, costs and benefits of the public good as well as how individuals interact with it. The results guide a rigorous mathematical description of the population. The predictions of this model, for sensible parameter choices, agree very well with experiments.

Contribution to overarching question This chapter addresses the combination of social interactions and growth in a bacterial population. The rigorous mathematical modeling adopted allows to peer into the specific effects of the public good, highlighting its importance.

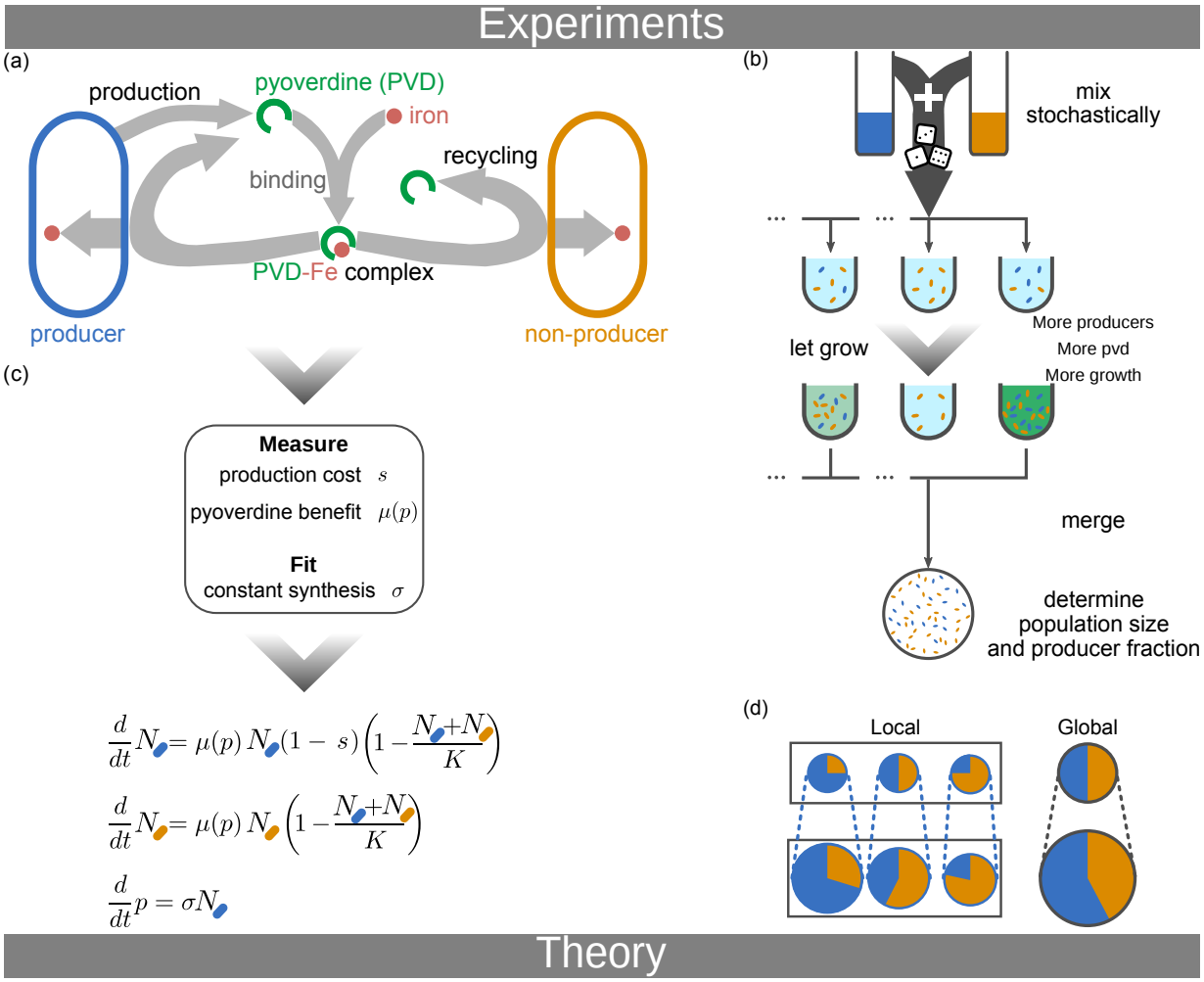

Figure 2.1: *Graphical abstract of the project.* **(a)** Sketch of the bacterial interaction: Producers secrete pyoverdine, which binds to iron in the medium. All cells (regardless of their strain) absorb the complex into their periplasm, where it is separated: iron is transported inside the cell, whereas pyoverdine is secreted back in the environment. **(b)** Sketch of the growth experiment: Pure cultures are mixed in stochastic proportions to inoculate the wells of a well-plate. This ensures that each well contains a stochastic fraction of producers. Populations containing more producers (blue) benefit from their more abundant pyoverdine and grow faster. **(c)** Road map to a model: We directly quantify the main parameters of the interaction, such as costs and benefits of pyoverdine. A single parameter (the synthesis rate of pyoverdine) is left as a fit. At given intervals, we take samples from each well and merge them in order to measure average population size and global producer fraction. **(d)** Sketch of the Simpson paradox (adapted from Ref. [51]): Producer fractions within each population (blue portions of the left pie charts) always decrease; however, as long as more producing populations grow larger (larger pies), the global producer fraction across the ensemble (right pie chart) may increase.

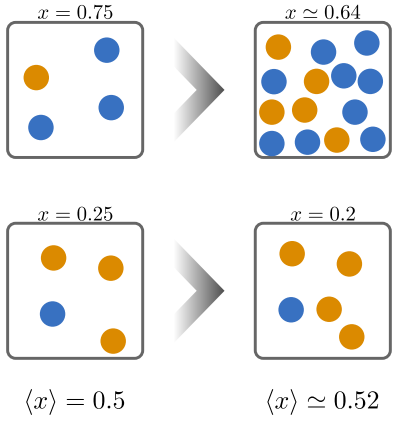

Figure 2.2: *Cartoon example of Simpson's paradox in a growing population.* Two populations start (left) with the exact same size, but different fraction of producers (blue dots). Observing again at a later time (right), although the local fraction producers decreases within each group, the *global* fraction increased from $\langle x \rangle = 0.5$ to about 0.52. This is due to the larger size of the producer-rich population (top row).

2.1 Background: Cooperation, growth, and Simpson's paradox

The emergence and establishment of cooperation is a central problem in evolutionary theory, as outlined in the Introduction. On the one hand, cooperative behaviors, such as the production of public goods, benefit the population as a whole, for example accelerating growth. On the other hand, producers of a public good suffer a disadvantage. In the case of bacteria, they pay a metabolic cost to produce the public good, thus growing slower. So, in deterministic populations of constant size, producers go extinct, unless some further mechanism fosters their survival [4, 18].

Growth radically changes the situation, especially if we consider an ensemble of several populations (also called a *metapopulation*). Within each population, producers grow on average slower than non-producers, because of the metabolic cost of producing the public good. For each population i, let $N_{f,i}$ be the number of non-producers (or free-riders) and $N_{c,i}$ the number of producers (or cooperators), who pay a metabolic cost s to provide the public good, which increases the population global growth rate according to some function $g(N_{c,i}) \geq 0$. In the deterministic limit, $N_{c,i}$ and $N_{f,i}$ then obey the differential equations:

$$\dot{N}_{c,i} = g(N_{c,i})N_{c,i}(1-s) \tag{2.1}$$
$$\dot{N}_{f,i} = g(N_{c,i})N_{f,i}\,. \tag{2.2}$$

With the simple change of variables $N_{c,i} + N_{f,i} = N_i$, $N_{c,i}/N_i = x_i$, we get

$$\dot{N}_i = g(x_i)(1-sx_i) \tag{2.3}$$
$$\dot{x}_i = -sx_i(1-x_i)g(x_i)\,. \tag{2.4}$$

Clearly, the local fraction of producers x_i within each population always decreases, reflecting the selective disadvantage of producers.

However, populations with higher x_i also grow faster, because they benefit from more abundant public goods. This introduces a population-level competition, which contrasts the selection between strains [44–48]. In this context, the *global* fraction of producers across the whole metapopulation is an interesting observable. This quantity expresses what fraction of the total individuals in the metapopulation are producers. It is defined as

$$\langle x \rangle = \frac{\sum_i N_{c,i}}{\sum_i N_{c,i} + N_{f,i}} = \frac{\sum_i x_i N_i}{\sum_i N_i}\,, \tag{2.5}$$

where the sum runs over all the populations in the ensemble. Interestingly, although the local producer fraction always decreases, the global one $\langle x \rangle$ does not have to.

This phenomenon has been connected with the Simpson's paradox [51–55, 72, 73]: a trend appearing in samples of different size may disappear or reverse when combining the samples [72, 74]. In our case, the trend of decreasing producer fractions that appears when sampling populations separately can be inverted by

combining them in the ensemble-wide global average $\langle x \rangle$ of eq. 2.5. It is also in principle possible to identify the conditions that lead to the apparently paradoxical result. The so-called Price equation [75, 76], for example, shows mathematically that an increase in $\langle x \rangle$ can appear when the covariance between local x and the growth rate is high enough. More recently, a combined theoretical-experimental work [51] showed how this kind of increase could lead to the establishment of cooperative behaviors across a metapopulation. Further theoretical analyses also proved that, barring some effect to sustain it (such as fixation), this increase can only be transient [53–55].

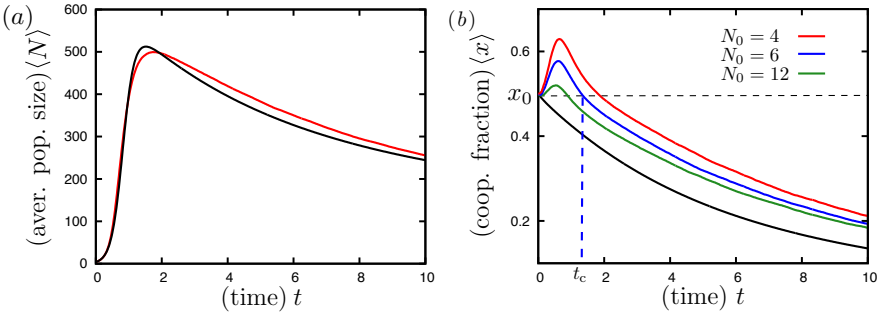

Figure 2.3: *Time course of the average population size and global producer (or cooperator) fraction* (from Ref. [54]). Black lines represent deterministic solutions, colored lines represent stochastic simulations. Panel (b), in particular, shows that the Simpson-related increase is transient, and that its amplitude decreases with initial size, if all populations start with the same composition.

This increase feeds on the variability of population compositions. If all populations started with the same size and composition, in fact, they would (deterministically speaking) have the same growth rate and the effect does not appear. For $\langle x \rangle$ to increase, populations need either start with different compositions, or with small size, as in Figure 2.3b [53]. When the variability is reduced—for example by increasing initial size, as shown in Figure 2.3b—so is the increase in $\langle x \rangle$.

2.2 Accumulating public goods shape social interactions in growing populations

Studies on public good exchange typically leave the social interaction implicit, either bundled in game-theoretical payoff structures [2–5, 16] or in inclusive fitness models [20, 23, 77–79]. This way, these approaches overlook many biological details of the interaction, which could reduce their ability to describe actual biological systems.

Research question: ***How do public good features affect social interaction and growth dynamics?***

As reported in the publication reprinted in Section 2.3, we quantitatively characterized the social interaction between bacteria and summarized it in a mathematical model, whose results agree with those of experiments. Thus, our research shows that

Public goods mediate the bacterial social interaction and facilitate growth; their specific biochemical properties shape the population dynamics

2.2.1 Experimental and theoretical approach

This project centered around using a well-defined bacterial system, which we could characterize in detail. We considered siderophore production in *Pseudomonas* [10, 11, 13, 14, 24] as our model system. To this end, we grew well-mixed *P.putida* populations composed of a constitutive public good producer strain (KP1) and a non-producing one (3E2 [10]). Because wild-type cells strictly regulate the production of pyoverdine, they can express both the non-producer and the producer phenotype, depending on the conditions. The constitutive producer mutant KP1, instead, always synthesizes pyoverdine, ensuring a well-defined interaction. The populations were initialized as stochastic mixtures of the two strains, then cultivated in shaken, nutrient-rich medium, supplemented with a molecule that binds to iron, so that cells cannot directly access it. Pyoverdine has a higher

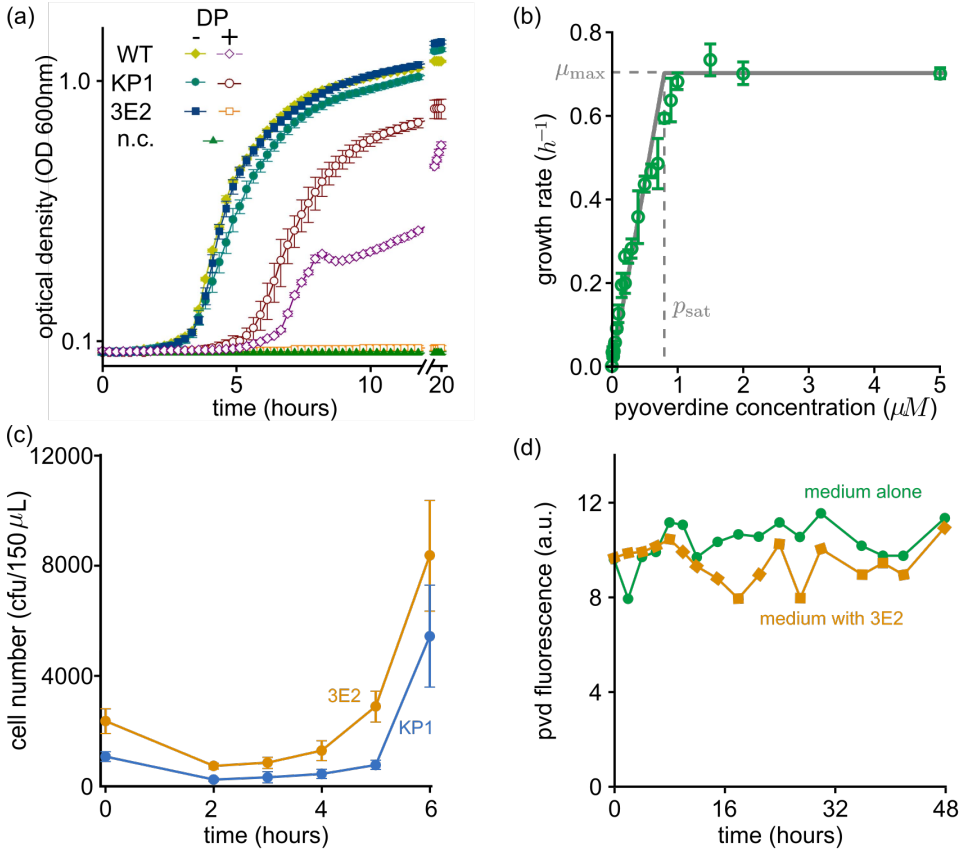

Figure 2.4: *Characterization of the social impact of pyoverdine* (PVD). **(a)** Production cost. In an environment with available iron (solid symbols), non-producer cells (strain 3E2) grow as fast as the wild-type (WT), and faster than producers. Under extreme iron limitation, PVD is needed for growth: producers (and the wild-type) grow, whereas non-producers are unable to. **(b)** Growth benefit from pyoverdine. Green dots represent the growth rate μ of non-producer cultures, with added pyoverdine. The solid gray line represents the growth rate calculated using equation (2.6) (with fitted maximal growth rate $\mu_{max} = 0.878$ and saturation concentration $p_{sat} = 0.8$. **(c)** Sharing and excludability. In mixed populations, and under extreme iron limitation, producers (KP1, blue line) and non-producers (3E2, orange line) start growth together. Since non-producers need pyoverdine to grow (see panel b), we conclude that pyoverdine is equally shared between the strains: it is non-excludable. **(d)** Durability of pyoverdine. Fluorescence of PVD in growth medium, with and without non-producer bacteria. PVD does not degrade spontaneously or through interaction with bacteria. Reprinted from Ref. [80].

binding affinity to iron, so it is able to scavenge the trapped ions, making them accessible to cells again; a population with more producer has more pyoverdine, and grows faster. All in all, with this experimental setup we obtained a well-defined bacterial system, with characterizable interaction and controlled conditions.

2.2.2 Pyoverdine acts as an accumulating public

We laid the foundation for our theoretical model by quantitatively characterizing the social interaction between producer and non-producer cells. This is also a key biological result of this research. We quantified four aspects of the public good interaction, exposed in Figure 2.4:

1. *Cost: how much synthesizing the pyoverdine slows the growth of producers*
   We measured the cost by growing producer and non-producer cells, separately, in iron-rich medium. In these conditions also non-producers could grow, while constitutive producers synthesized unnecessary pyoverdine. By comparing growth rates, we could estimate that the synthesis of pyoverdine slows down the growth of producers by 3-10%, depending on the culture conditions (see Figure 2.4a)

2. *Benefit: or how does the population-wide growth rate depend on the presence of the public good*

The benefit of pyoverdine could be measured by growing non-producers alone in iron-depleted medium, in which cells need pyoverdine to grow. We supplemented the medium with different concentrations of pyoverdine and measured the growth rate of non-producer cells. We found that the rate increases almost linearly with the concentration of added pyoverdine, then sharply levels off when the concentration approaches 1μM. Figure 2.4b shows these data, as well as the results from our theoretical modeling of the impact of pyoverdine on growth (see Section 2.2.3).

3. *Whether pyoverdine is an excludable good*
A good is dubbed *excludable* if producers are able to prevent non-producers from accessing it. To measure this property, we cultivated producers and non-producers together in iron-depleted conditions, then measured when each strain would start growing. We observed that, after an initial lag phase, both strain would initiate growth essentially at the same time, as shown in Figure 2.4c. Since pyoverdine is absolutely necessary for growth in these conditions, this means that both strains have equal access to it. In other words, *pyoverdine acts as a non-excludable good.*

4. *Whether pyoverdine is a rivalrous good*
A good is called *rivalrous* when individuals have to compete for access to limited amounts of it. *Pseudomonas* cells are known to recycle pyoverdine after use [81, 82]. This already suggests that pyoverdine should be non-rivalrous: though one cell uses it, it will soon re-secrete it, so it does not impede the access of others. In other words, cells do not compete for access to limited pyoverdine, as they do for nutrients or space. To measure this feature, we analyzed how the fluorescence of pyoverdine changed during a long time. As Figure 2.4d shows, pyoverdine is fluorescent for at least $\sim$ 48 hours (much longer than the duration of our experiments), meaning that, for all practical purposes, it does not spontaneously degrade. Moreover, a similar measurement in presence of non-producer cells showed that pyoverdine was stable in these conditions too. Therefore, while bacteria interact with pyoverdine, they do not appear to damage or degrade it.

Taken together, our measurements show that pyoverdine behaves as a proper public good (non-excludable, non-rivalrous) [16], and that its producers incur a constant cost. Moreover, due to its very long lifetime, pyoverdine accumulates in the environment once produced.

2.2.3 Modeling the interaction

We built a mathematical model of the interaction based on the experimental measurements presented in the previous section. Such model must take into account the development of the abundance of each strain, as well as the pyoverdine availability and its effect on growth. To determine how pyoverdine concentration affects growth rate, we assumed that: (i) pyoverdine molecules find and bind an iron atom as soon as they are released; (ii) cells absorb the bound pyoverdine-iron complex at a constant rate; (iii) cells try as much as possible to maintain their internal iron concentration constant; (iv) up to some saturation concentration, iron is the only factor limiting growth. From these common sense assumptions, we obtain that given a concentration p of pyoverdine, the population's growth rate μ is given by

$$\mu(p) = \mu_{\max} \min\left(\frac{p}{p_{\text{sat}}}, 1\right) . \tag{2.6}$$

p_{sat} represents the concentration at which iron availability stops being growth-limiting. Eq. (2.6) reflects the linear dependence of $\mu(p)$ on the pyoverdine concentration p we observed in experiments (see Figure 2.4b).

With this function set, we could study the deterministic equations of motion for the amount of producer cells N_c and non-producers N_f in a population, as well as the pyoverdine concentration p. Cells grow exponentially, with pyoverdine-dependent rate $\mu(p)$; producers grow slower by a factor $1-s$ because of the cost of production. When the population exhausts the resources in the environment (determined by a carrying capacity K), cells end growth by entering a dormant state. Finally, producers synthesize pyoverdine at a constant per-capita rate σ. The equations then take the form

$$\begin{aligned} \dot{N}_c &= N_c\mu(p)(1-s)\left(1-\frac{N_c+N_f}{K}\right) , \\ \dot{N}_f &= N_f\mu(p)\left(1-\frac{N_c+N_f}{K}\right) , \\ \dot{p} &= \sigma N_c . \end{aligned} \tag{2.7}$$

To better understand the dynamics, we considered the rescaled variables $n := (N_c+N_f)/K$ (how big the population is, compared to the maximal size the environment allows), $x := N_c/(N_c+N_f)$ (the fraction of producers in the population), and $v := p/p_{\rm sat}$ (how far the pyoverdine concentration is from saturation concentration). We also rescaled time by the maximal growth rate $\mu_{max} = \mu(p_{sat})$ and redefined $\mu(v) = \min(v, 1)$. Finally, we defined an *accumulation parameter* $\alpha := \sigma K/(p_{\rm sat}\mu_{\rm max})$, which expresses how fast pyoverdine accumulates, compared to population growth. High α corresponds to very fast production, rapidly leading to high pyoverdine concentration; low α means cells reproduce much faster than they synthesize pyoverdine, which limits growth for long times. Altogether the theoretical population followed these rescaled equations:

$$\begin{aligned} \dot{n} &= n\mu(v)(1-sx)(1-n)\,, \\ \dot{x} &= -s\mu(v)x(1-x)(1-n)\,, \\ \dot{v} &= \alpha n x\,. \end{aligned} \tag{2.8}$$

Experimental population started with $\sim \mathcal{O}(10^3)$ individuals and grew to a final size of $\sim \mathcal{O}(10^6)$, justifying such deterministic description.

2.2.4 Transient increase in producer fraction

To replicate the experimental conditions, we initialized a large ensemble of populations with the same size n_0 (because experimental populations were large), given by the typical ratio of initial size and final yield in experiments. Within each population, the producer fraction x_0 was stochastic, sampled from the same distribution as in experiments.

With these initial conditions, we solved equations (2.8) numerically, recording the size n and the global fraction of cooperators $\langle x\rangle$. For several choices of parameter values, $\langle x\rangle$ initially increases, peaks to a value $\langle x\rangle_{\rm max}$ before decreasing, and finally saturating to its long-term value. The observed increase, therefore, is only transient. Figure 2.5a shows such a typical trajectory of $\langle x\rangle$. As the Supplementary Video of the publication

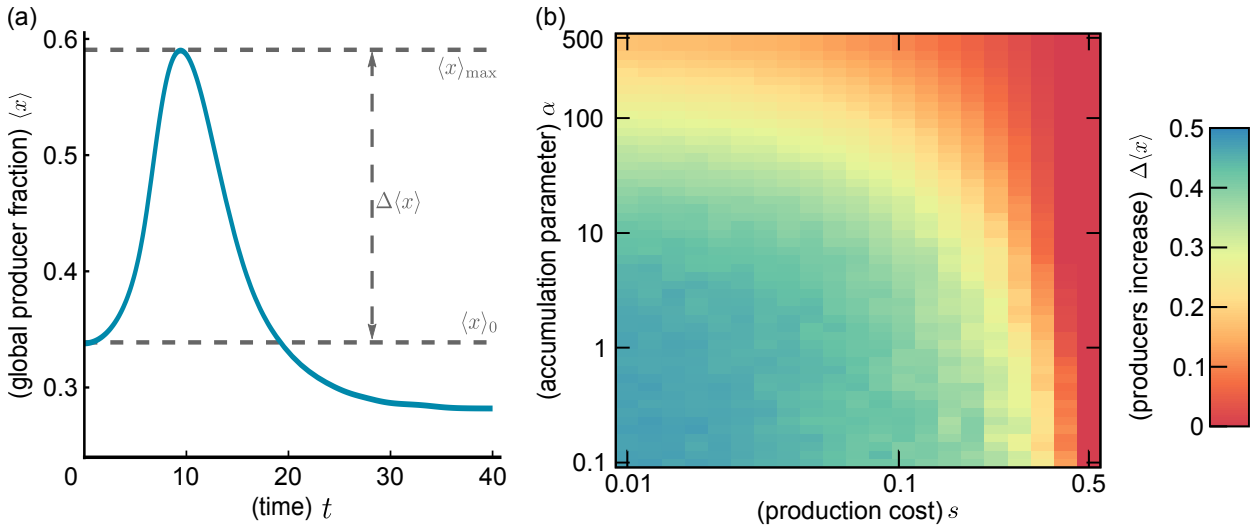

Figure 2.5: *Results on the increase in global producer fraction.* **(a)** Time course of the global producer fraction $\langle x\rangle$ in simulations (parameter values: $\alpha = 200$, $s = 0.05$, $n_0 = 10^{-3}$). Solving eqs. (2.8) numerically, we observe first an increase in the global producer fraction, which peaks at a value $\langle x\rangle_{\rm max}$, then decreases (typically below its initial value) and eventually saturates to a long-term value. **(b)** Magnitude of the maximum producer increase $\Delta\langle x\rangle$ as function of pyoverdine accumulation α and production cost s. Increasing the production cost (horizontal axis) burdens producers, thus curtailing the increase. The main advantage of producer populations is rooted in their faster growth. Higher accumulation of pyoverdine α (vertical axis), however, makes the public good benefit saturate faster, reducing the marginal benefit of pyoverdine, and also letting low-producer populations start growth sooner. Both effects contribute to reduce the amplitude of the increase.

shows, producing populations initially grow much faster. This positive correlation between producer fraction and growth rate drives the increase in global producer fraction. In time, however, pyoverdine accumulates,

meaning that populations with few producers also accrue enough of it to start growing, while in those with more producers the benefit from pyoverdine saturates. Eventually, producer-rich populations enter the dormant phase, and non-producing ones catch up with their size.

The amplitude of the increase $\Delta\langle x\rangle = \langle x\rangle_{\max} - \langle x\rangle_0$ depends on the cost s and the accumulation parameter α, as shown in Figure 2.5. Clearly, a higher s—so a heavier burden on producers—leads to less of an increase in global producer fraction. Higher accumulation parameter α also reduces $\Delta\langle x\rangle$. For $\alpha \to 0$, in fact, the pyoverdine production time scale is much slower than that of population growth. Scarce pyoverdine strictly limits growth for several generations, during which only producer-rich populations can grow appreciably. Benefit saturation also occurs very late, therefore more producing populations have a growth advantage for very long times, and lead to a high increase in producer fraction. When $\alpha \to \infty$, on the other hand, production and accumulation of pyoverdine occur faster than cell replication. A few producers thus suffice to rapidly accumulate enough public good to saturate the benefit. More producing populations only briefly have an advantage, and the resulting increase is lower. As Figure 2.6 shows, the simulation results matched experimental ones, with appropriate choices of parameters (in particular, we need to fit α to fix the global time scale and match the measured exponential growth rate).

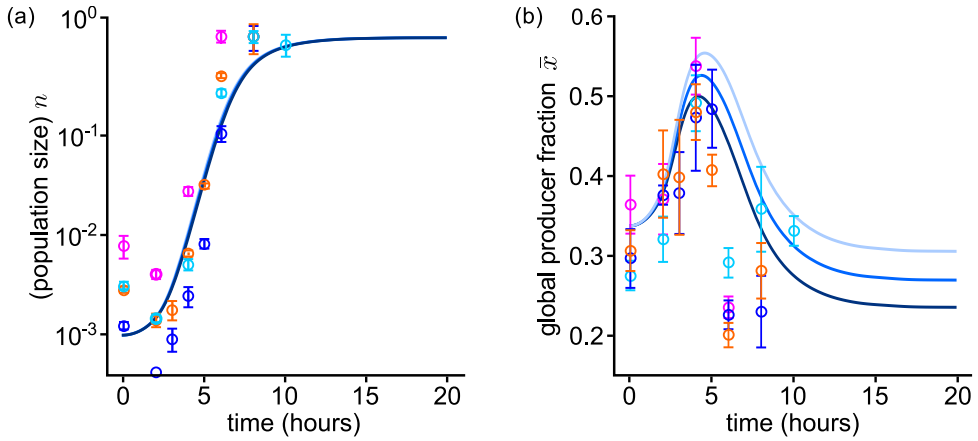

Figure 2.6: *Comparison of theory and experiments* Solid lines represent numerical solutions of equations (2.8) for different values of the production cost s (darker shades indicate higher values, $s \in \{0.03, 0.05, 0.07\}$). The accumulation parameter α is the result of a fit (here, $\alpha = 200$). Dots of different colors indicate the results of different independent experimental runs. Error bars are the standard deviations of three to five replicates of the experiment. The population size n is rescaled to the final yield (or carrying capacity). Reprinted from Ref. [80].

2.2.5 Consequences and outlook

Sociobiology studies tend to rely on preconceived notions about the interactions [11, 13, 14, 78, 79, 83, 84]. However, as the research presented in this chapter shows, biochemical details—such as public good recycling and accumulation—affects growth and long-term population dynamics.

Accumulation, in particular, has far-reaching consequences on the possibility of sustaining the observed increase in producer fraction. In fact, even if producers could "cut their losses" and stop production when some threshold concentration is reached, the benefit from more abundant pyoverdine would eventually vanish. The public good, in fact, gradually accumulates also in populations with few producers, allowing them to eventually reach the same size and pyoverdine concentrations of more producing ones. Therefore, any population-level advantage from such an accumulating public good is bound to vanish in time.

Perhaps the most interesting avenue of further research is, then, a rigorous modeling of the regulatory network, showing in detail the impact of pyoverdine and iron concentrations on synthesis, but also on cell metabolism. For this work, in fact, we employed a constitutive producer strain, but wild-type Pseudomonads (for example *P.putida* KT2440) strictly regulate production. This complex gene network involves central metabolic regulators and even genes of unknown function [10, 85]. Pyoverdine concentrations, thus, could affect growth rates beyond iron availability, potentially providing further benefits to producer strains.

2.3 Publication reprint

Interactions mediated by a public good transiently increase cooperativity in growing *Pseudomonas putida*

by

F.Becker,*[1] K. Wienand,*,[2] M. Lechner,[2] E. Frey,[2] and H. Jung[1]

* Contributed equally to this work
[1]Department of Biology 1, Microbiology, Ludwig- Maximilians-Universität, Grosshaderner Straße 2-4 82152, Martinsried, Germany,
[2]Department of Physics, Arnold Sommerfeld Center for Theoretical Physics and Center for NanoScience, Ludwig-Maximilians-Universität München, Theresienstraße 37, 80333 München, Germany

reprinted from

***Scientific Reports* 8, 4093 (2018)**,
DOI:10.1038/s41598-018-22306-9.

SCIENTIFIC REPORTS

OPEN

Interactions mediated by a public good transiently increase cooperativity in growing *Pseudomonas putida* metapopulations

Received: 21 November 2017
Accepted: 21 February 2018
Published online: 06 March 2018

Felix Becker[1], Karl Wienand[2], Matthias Lechner[2], Erwin Frey[2] & Heinrich Jung[1]

Bacterial communities have rich social lives. A well-established interaction involves the exchange of a public good in *Pseudomonas* populations, where the iron-scavenging compound pyoverdine, synthesized by some cells, is shared with the rest. Pyoverdine thus mediates interactions between producers and non-producers and can constitute a public good. This interaction is often used to test game theoretical predictions on the "social dilemma" of producers. Such an approach, however, underestimates the impact of specific properties of the public good, for example consequences of its accumulation in the environment. Here, we experimentally quantify costs and benefits of pyoverdine production in a specific environment, and build a model of population dynamics that explicitly accounts for the changing significance of accumulating pyoverdine as chemical mediator of social interactions. The model predicts that, in an ensemble of growing populations (metapopulation) with different initial producer fractions (and consequently pyoverdine contents), the global producer fraction initially increases. Because the benefit of pyoverdine declines at saturating concentrations, the increase need only be transient. Confirmed by experiments on metapopulations, our results show how a changing benefit of a public good can shape social interactions in a bacterial population.

Bacteria have complex social lives: they communicate with each other and with other organisms, form tight communities in biofilms, exhibit division of labor, compete, and cooperate[1–7]. They also produce and exchange public goods. Public goods are chemical substances that are synthesized by some individuals (known as *producers* or *cooperators*) and are then shared evenly among the whole population, including cells that did not contribute to their production[8–10]. Such social interactions can also influence population dynamics, as exemplified in the context of metapopulations[11–17]. Metapopulations consist of several subpopulations. The subpopulations may grow independently for a time, then merge into a single pool that later splits again, restarting the cycle. This ecological system, which mimics some bacterial life-cycles[18,19], also dramatically impacts the population's internal dynamics. To mathematically analyze the effects of social interactions, they can be framed in terms of game theoretical models[20–24] –for instance, the prisoner's dilemma, in the case of the exchange of public goods[25–28] –or formulated in terms of inclusive fitness models[29–31]. These approaches underestimate the impact on the social interaction of specific properties and mechanisms of action of the public good in question, mostly to simplify the mathematical description. Previous investigations have shown that, for example, phenomena like public good diffusion[32–34], interference of different public goods with each other[35], the regulatory nature of public good production[36], or its function in inter-species competition[37] may affect strain competition. The shortcomings of game-theoretical models in studying the evolution of cooperation can be overcome by systems biology modeling approaches[34,38,39].

[1]Microbiology, Department Biology 1, Ludwig-Maximilians-Universität Munich, Grosshaderner Strasse 2-4, D-82152 Martinsried, Germany. [2]Arnold-Sommerfeld-Center for Theoretical Physics and Center for Nanoscience, Ludwig-Maximilians-Universität, Theresienstrasse 37, D-80333, Munich, Germany. Felix Becker and Karl Wienand contributed equally to this work. Correspondence and requests for materials should be addressed to E.F. (email: frey@lmu.de) or H.J. (email: hjung@lmu.de)

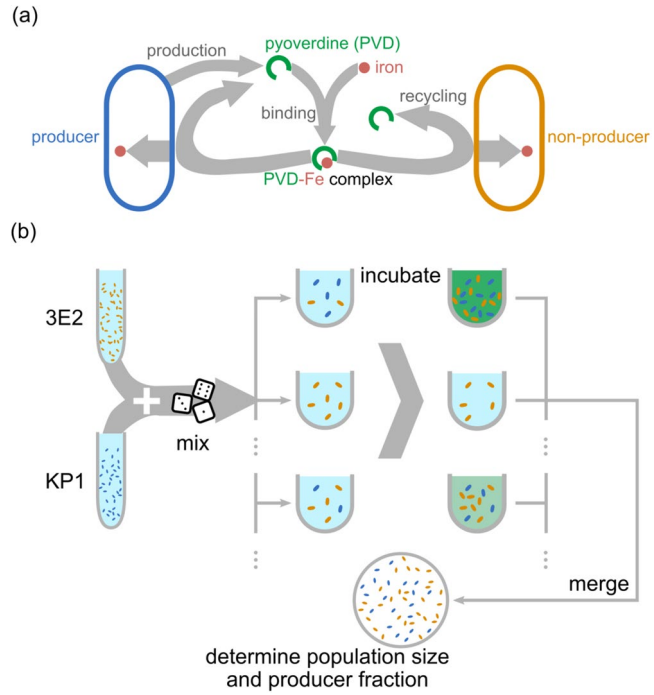

Figure 1. Outline of PVD-mediated interactions and experimental setting. (**a**) Outline of the social interaction. Producers (blue) secrete pyoverdine (PVD, green) into the environment, where it binds iron (red). The resulting Fe-PVD complex is transported into the periplasm of both producers and non-producers. Iron is reduced and incorporated into cells, while PVD is transported back into the environment to scavenge additional ferric ions[44–46]. (**b**) Metapopulation growth setting. We initiate a metapopulation by mixing producers and non-producers in random proportions and inoculating the individual populations, which grow independently. At given time points *t*, we take samples from each population, and merge them to determine the average population size and the global producer fraction of the metapopulation.

In this work, we directly quantify a social interaction mediated by a public good. Thus, we adopt a systems biology approach, rather than a more reductive game-theoretical one. We focus on the dissemination of iron-scavenging pyoverdine (PVD) in a metapopulation of fluorescent *Pseudomonas putida*, and study how its biological function determines the population dynamics.

In this well-established, native model system, cells secrete PVD into the environment to facilitate iron uptake when the metal becomes scarce[29,40–44]. PVD binds to ferric iron and is then actively transported into the periplasm. There, the iron is reduced, released and transported across the plasma membrane, while PVD is secreted back into the environment[44–46]. Figure 1 outlines the PVD-mediated interaction between producer and non-producer cells and the metapopulation set-up we use to study its effects on population dynamics.

In the following, we show, both experimentally and in computer simulations, that the global fraction of producer cells across a metapopulation increases during growth, but only transiently. This effect hinges on the specifics of PVD biochemistry, which elude a game-theoretical analysis. Thus, our study shows that the specific features of the public good considered are the key determinant of the outcome of the social interaction. Our experiments employ a well-defined system, with a constitutive producer and a non-producer strain. The simulations use a mathematical model based on quantitative measurements of PVD's costs and benefits, as well as its behavior as an accumulating public good. For appropriate values of the parameters, the theoretical results match those of experiments with *P. putida* metapopulations.

Results

Characterization of the model system. To investigate the social role of public goods, we chose the soil bacterium *P. putida* KT2440 as a model system. This is a well-defined system in which, as sketched in Fig. 1a, a single public good mediates all cell-cell interactions. *P. putida* KT2440 synthesizes a single type of siderophore – a pyoverdine (PVD) molecule[47] –and does not produce 2-heptyl-3-hydroxy-4-quinolone or other known quorum-sensing molecules that might otherwise interfere with the social interaction[48–50].

Wild-type *P. putida* KT2440 controls PVD production through a complex regulatory network. As shown in Fig. 2a, the central element of the network is the ferric uptake regulator (Fur) protein, which binds iron and, among other things, down-regulates expression of the iron starvation sigma factor *pfrI*[51–53], which in turn directs the transcription of PVD synthesis genes. As a consequence, siderophore production continually adapts to the availability of iron[47,52]. This regulation, however, obscures the costs of PVD production, as it also affects other processes. We therefore circumvented it by generating a *P. putida* strain, called KP1, which constitutively produces

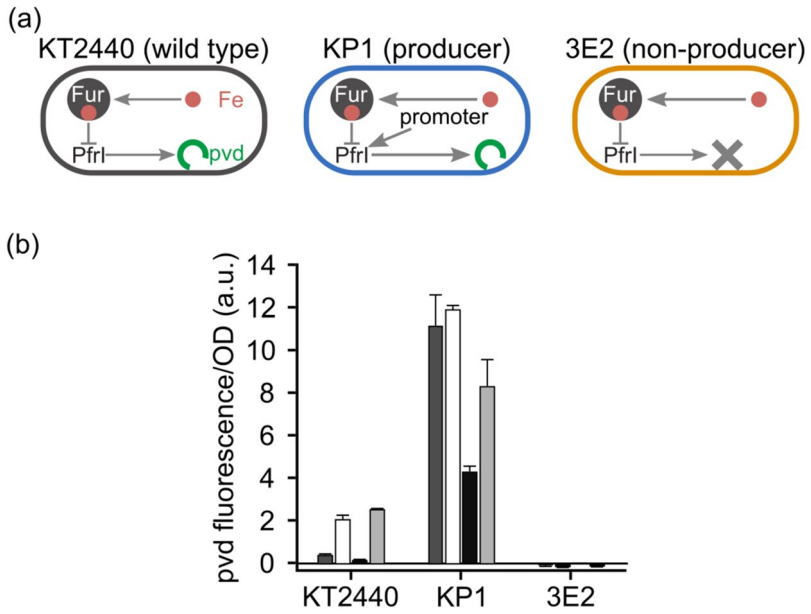

Figure 2. Characterization of the strains. (**a**) Sketch of each strain's regulatory system. In the wild-type *P. putida* KT2440 (gray), the ferric uptake regulator Fur binds iron and represses the expression of the *pfrI* gene necessary for PVD synthesis. The constitutive producer strain KP1 (blue) carries an additional copy of the *pfrI* gene controlled by a constitutive promoter. The non-producer strain 3E2 (orange) has an inactivated non-ribosomal peptide synthetase gene, which prevents PVD synthesis. (**b**) Average PVD production per cell by the wild-type and strains KP1 and 3E2 after 8 h of cultivation. The darker the columns, the more abundant is the iron in the medium. Dark gray columns represent moderate iron availability conditions (KB medium without additions); white columns represent extreme iron limitation (KB/1 mM DP); black columns represent iron-replete conditions (KB/100 μM $FeCl_3$); light gray columns represent iron-limiting conditions (KB/100 μM $FeCl_3$/1 mM DP). KP1 produces PVD under all conditions (albeit with different yields), 3E2 never produces the siderophore, and the wild-type adapts its rate of synthesis to iron availability.

PVD. KP1 carries a copy of the *pfrI* gene controlled by the constitutive promoter $P_{A1/04/03}$[54] at the *att*Tn7 site in the KT2440 genome. As the non-producer, we used strain 3E2, which carries an inactivated non-ribosomal peptide synthetase gene (pp4220) that inhibits PVD synthesis[47]. The two strains were otherwise isogenic.

We characterized producer (KP1) and non-producer (3E2) strains by measuring their average per-cell PVD production under different iron availabilities, and comparing the results with those for the wild type (strain KT2440). We cultivated all three strains, separately, in KB medium and KB supplemented with 100 μM $FeCl_3$ (for short, KB/100 μM $FeCl_3$), as well as in the same two media supplemented with the chelator dipyridyl (DP, 1 mM) to reduce iron availability. Using atom absorption spectroscopy, we determined an iron concentration in KB of about 8 μM. Figure 2b shows the average amount of PVD produced per cell after 8 h of growth (close to the end of exponential growth). The wild type partially represses production of PVD under moderate iron availability (KB, dark gray bars), and ceases synthesis altogether under high iron availability (KB/100 μM $FeCl_3$, black bars). Addition of DP reduces iron availability and stimulates PVD production in both media (Fig. 2b, white bars: KB/1 mM DP, light gray bars: KB). In contrast, KP1 produces large amounts of PVD under all tested growth conditions, and thus represents a constitutive PVD producer. The yield depends on conditions, probably because the regulated copy of *pfrI* is still present in the genome. 3E2, finally, never synthesizes PVD, regardless of the conditions, and is a true non-producer, as previously reported[47].

Quantifying the social role of pyoverdine. Having established how each strain behaves, we quantified the impact of PVD on population dynamics. Specifically, we wanted to determine the metabolic load of PVD production, its impact on growth, its stability, and how evenly it is shared with other cells.

We assessed the impact of PVD production on growth by comparing the growth rates of strains KP1 and 3E2 under iron-rich conditions (KB). As shown in Fig. 2b, neither 3E2 nor the wild-type produces substantial amounts of PVD under these conditions, and the solid symbols in Fig. 3a show that both strains grow at about the same rate. KP1, on the other hand, produces PVD and grows more slowly. The data in Supplementary Table S1 allow us to quantify this difference in growth rate. Depending on the conditions, KP1's growth rate is 3–10% lower than that of strain 3E2. For example, the difference is minimized (1.03-fold) when the medium is replaced (in a 24-well plate format) every hour, whereas the largest difference (1.10-fold) is observed in batch cultures (96-well plate format). This suggests that factors other than iron level *per se*, such as nutrients and oxygen availability, modify the metabolic impact of PVD production.

The empty symbols in Fig. 3a illustrate the growth of the strains under extreme iron limitation (KB/1 mM DP). In these conditions, PVD is indispensable for iron uptake, and only producing strains – KP1 and the wild-type – can grow at all. Less restrictive conditions (KB/100 μM $FeCl_3$ and KB/100 μM $FeCl_3$/1 mM DP) produce

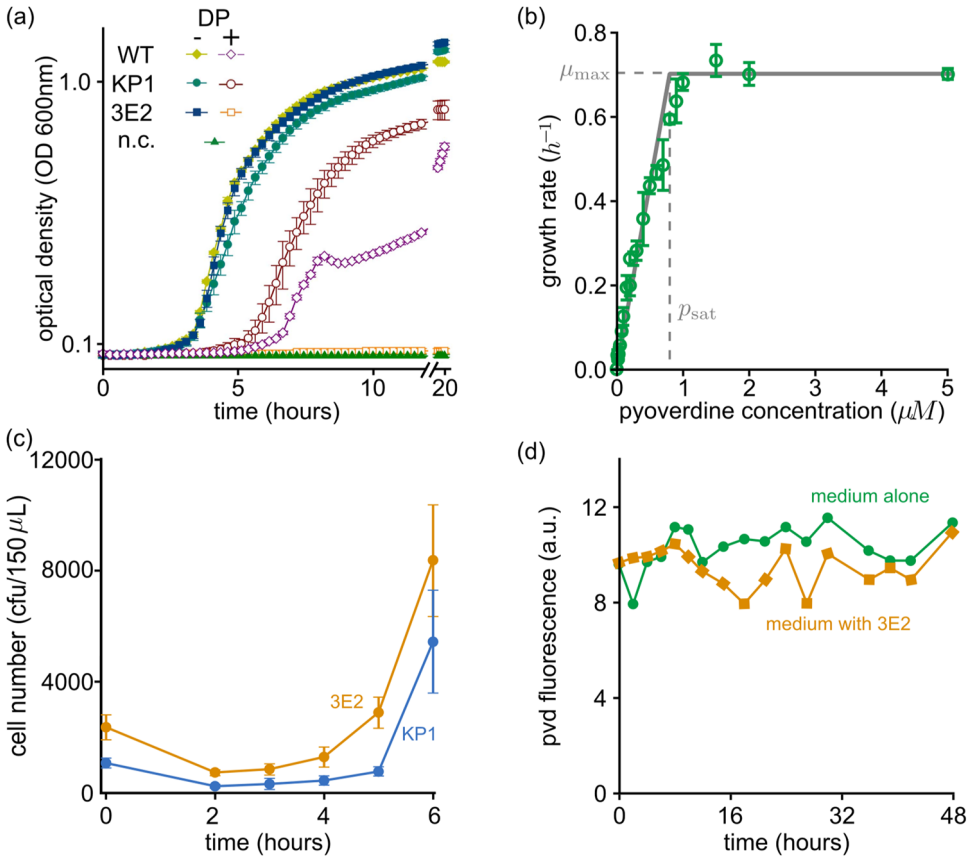

Figure 3. Characterization of the social impact of pyoverdine (PVD) in terms of costs (**a**), benefits (**b**), degree of sharing among cells (**c**) and stability (**d**). (**a**) In an environment with available iron (KB, solid symbols), non-producer cells (strain 3E2) grows as fast as the wild-type (WT), and faster than the producer (strain KP1). Under extreme iron limitation (KB /1 mM DP, empty symbols), PVD is needed for growth: KP1 and WT grow, whereas 3E2 does not (mean values and standard deviations were calculated from six measurements). (**b**) Green dots represent the growth rate μ of 3E2 cultures, measured under extreme iron limitation (KB/1 mM DP) in the presence of the indicated concentrations of added PVD (error bars are standard deviation over four replicates). The solid gray line represents the growth rate calculated using equation (2) (maximal growth rate μ_{max} and the saturation concentration p_{sat} fitted to the experimental data: $\mu_{max} = 0.878$, $p_{sat} = 0.8$). (**c**) Early growth of KP1–3E2 co-cultures (initial fraction of KP1 = 0.33) under extreme iron limitation (KB/1 mM DP). Shown are mean and SD of eight independent experiments. Since 3E2 needs PVD to grow (see panel **b**), this result indicates that PVD is shared between the strains. (**d**) Stability of PVD (2 μM) in KB medium and in the presence of the non-producer 3E2. The fluorescence emission was recorded at 460 nm (excitation 400 nm).

qualitatively similar results (see Supplementary Fig. S1). 3E2, if cultivated alone, cannot grow unless the medium is supplemented with PVD isolated from a producer culture. Figure 3b shows the maximal growth rate of 3E2 under these conditions as a function of the concentration of added PVD. For values lower than about 1 μM, the growth rate increases almost linearly with PVD concentration, then sharply levels off. Higher PVD concentrations do not further stimulate growth – which is consistent with observations of iron saturation in other bacterial systems[55,56].

This saturating behavior, we argue, stems directly from PVD's ability to bind iron and make it available to cells. Because PVD has an extremely high affinity for iron [$10^{24}\,M^{-1}$ for Fe^{3+} at pH 7[57], we can assume that each PVD molecule immediately binds an iron ion. Therefore, the PVD concentration p is equivalent to that of PVD-Fe complexes, and represents the concentration of iron accessible to cells (this may not hold if the level of PVD exceeds that of the iron available, but we expect this extreme case to arise only after the exponential growth phase in our setting, if ever). Each cell, then, incorporates iron ions at a constant rate $k \cdot p$ which is proportional to the PVD concentration p. Moreover, cells try to maintain a constant internal iron concentration Fe_{in} and reproduce at a PVD-dependent rate $\mu(p)$ when growth is limited by iron availability. If we also assume that the cell volume just before division is twice the volume $V(0)$ of a newborn cell, we find that the growth rate is proportional to p (see Supplementary Note):

$$\mu(p) = \frac{k}{Fe_{in}V(0)}p. \quad (1)$$

For PVD concentrations above 1 μM, however, some other factor limits growth. Cells cannot further increase $\mu(p)$, regardless of the PVD concentration, and the benefit of PVD saturates. In summary, there is a limit PVD concentration p_{sat} (~1 μM), below which the growth rate is proportional to the PVD concentration, following equation (1). Above p_{sat}, the growth rate is a constant μ_{max}, whose value depends on the culture conditions. In mathematical terms,

$$\mu(p) = \mu_{max} min\left(\frac{p}{p_{sat}}, 1\right) = \begin{cases} \frac{\mu_{max}}{p_{sat}} p, & if\ p < p_{sat} \\ \mu_{max}, & if\ p \geq p_{sat}. \end{cases} \quad (2)$$

The gray curve in Fig. 3b shows the function described in equation (2). Fitting the values for the parameters p_{sat} and μ_{max}, the curve closely resembles the experimental results, validating our argument.

A central question in determining the social role of PVD is whether cells share the molecule with other cells, and thus also its benefit, or keep it to themselves. In other words, to what extent is PVD a *public* good? Fig. 3c shows the early stages of growth of a mixed population of KP1 and 3E2 (initial fraction of KP1 = 0.33) under extreme iron limitation (KB/1 mM DP). After a lag phase of about 2 h, both strains begin to grow. Since 3E2 needs PVD to grow in these conditions (see above and Supplementary Fig. S1), we conclude that both strains receive the benefit at the same time, and neither has preferential access to it. In our experiments, then, PVD behaves as a truly public good. Consequently, populations that start with a higher producer fraction x_0 have more PVD available, and grow faster than populations with low x_0 values (as shown in Supplementary Figs S1 and S2).

PVD is also very stable. Figure 3d shows the fluorescence yield of PVD over 48 h in KB medium alone (green line). The value fluctuates around a constant average, indicating that PVD does not spontaneously degrade – at least not appreciably – within the time scales of our experiments. The orange line in Fig. 3d represents a similar measurement, but in the presence of non-producer cells. In this case also, fluorescence does not appreciably decay, so cells do not seem to consume PVD during the interaction. This also means that, provided producers are present, the public good accumulates in the environment once its synthesis has been triggered.

Taken together, these observations characterize the social interaction as follows: (i) Constitutive producers grow more slowly than non-producers (given equal PVD availability); (ii) PVD acts as a public good, which is homogeneously shared among cells; (iii) once produced, PVD persists: it is chemically and functionally stable, and cells recycle it rather than consuming it; (iv) the public good drives the population dynamics, since PVD is necessary for access to the iron required for growth.

Modeling social and growth dynamics. Based on the experimental results presented in the previous section, we formulated a set of equations to describe the development of a single, well-mixed population of c producers and f non-producers. The population dynamics follows a logistic growth, where the function $\mu(p)$ from equation (2) determines the per-capita growth rate. For our experimental setup, we estimate cells to incorporate only a minimal fraction of the available iron (<3%, see Supplementary Note), so the assumptions of equation (2) hold (and some other resource determines the carrying capacity K. Although KP1 synthesizes PVD at condition-dependent rates, we adopt a simplified description and model synthesis as occurring at a constant rate σ. The produced PVD does not decay but accumulates in the medium. Finally, the costs of PVD synthesis slow down the growth of producers by a factor $1 - s$ (where $s < 1$), compared to non-producers. All in all, assuming the interaction between cells and PVD is fast, the dynamics can be summarized in the following equations:

$$\begin{aligned} \frac{dc}{dt} &= c\mu(p)(1-s)\left(1 - \frac{c+f}{K}\right), \\ \frac{df}{dt} &= f\mu(p)\left(1 - \frac{c+f}{K}\right), \\ \frac{dp}{dt} &= \sigma c. \end{aligned} \quad (3)$$

This set of equations mathematically describes the experimental facts, in terms of measurable quantities. It is also different from a traditional game theoretical formulation, which would require us to somehow define a payoff function.

To better highlight the key factors of the population dynamics, we rescale the variables in equations (3). First, we measure population size in terms of the fraction of resources used up, i.e., $n := (c + f)/K$. This definition means that K determines the scale of population sizes, while n takes values between 0 and 1: as n approaches 1, the resources become depleted, and cells enter a dormant state[14]. Second, we consider the fraction $x := c/(c + f)$ of producers within each population, rather than their absolute number. Third, we measure the amount of PVD in units of the saturation concentration, $v := p/p_{sat}$ (and define $\mu(v) = min(v, 1)$). Finally, measuring time in units of the minimal doubling time $1/\mu_{max}$, equations (3) become

$$\begin{aligned} \frac{dn}{dt} &= n(1-n)(1-sx)\mu(v), \\ \frac{dx}{dt} &= -sx(1-x)(1-n)\mu(v), \\ \frac{dv}{dt} &= \alpha n x, \end{aligned} \quad (4)$$

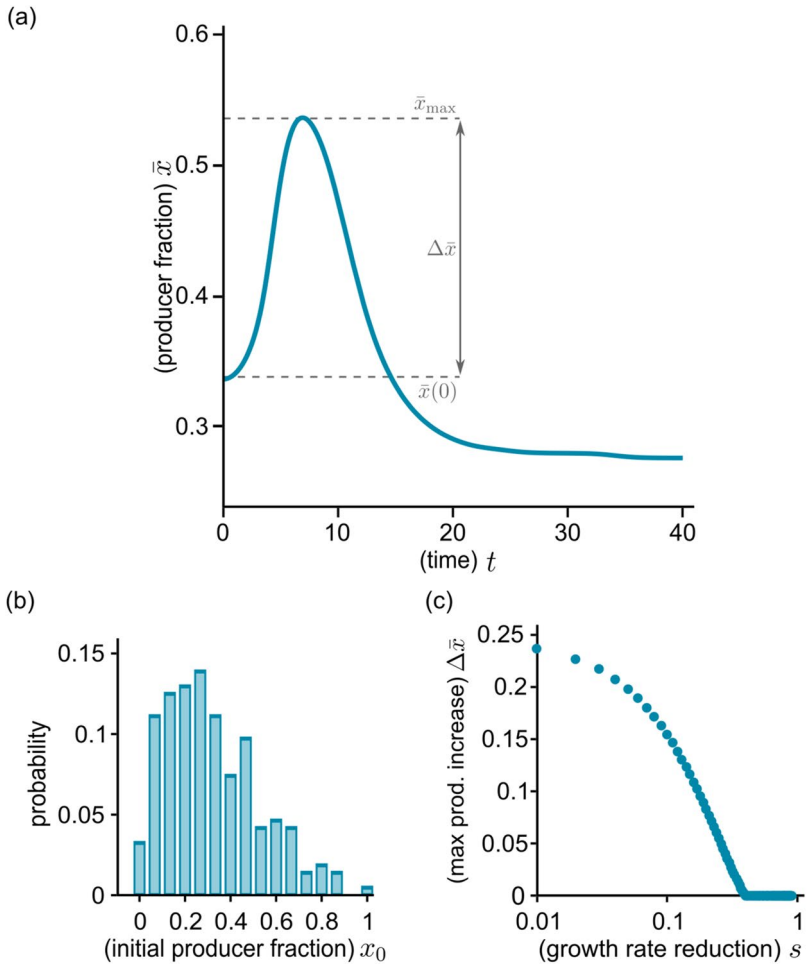

Figure 4. Simulation results for the growth of a metapopulation. The time course of the global producer fraction $\bar{x}$ (**a**) is computed by numerically solving equations (4) for a given distribution of stochastic initial compositions (**b**) (parameter values: $\alpha = 200$, $s = 0.05$, initial size $n_0 = 10^{-3}$). The producer fraction initially increases as populations with more producers begin to expand earlier (see also Supplementary Movie S1). After reaching a maximum value $\bar{x}_{\max}$, the global producer fraction decreases. (**c**) The maximal magnitude of the increase $\Delta\bar{x} = \bar{x}_{\max} - \bar{x}(0)$ decreases with stronger growth reduction s (s between 0.01 and 0.9, other parameters identical to panel (**a**)): for low s it is comparable to the initial producer fraction, while very low producer growth precludes any increase at all.

where $\alpha := \frac{\sigma K}{p_{\text{sat}}\mu_{\max}}$ is a dimensionless parameter. This parameter represents the rate at which PVD benefit saturation sets in. Keeping other factors constant, the benefit saturates sooner if production is faster (higher σ) and/or the number of total producers increases (higher K and thus larger populations). Conversely, if the saturating PVD concentration is higher (higher p_{sat}), or cell reproduction is faster (higher $\mu_{\max}$), populations can reach higher densities before the benefit saturates. Generally speaking, the lower α, the more advantageous producers are for their population. For $\alpha \to 0$ for example, the reproduction time scale is shorter than that of public good production. Therefore, the relatively scarce PVD strictly limits growth, PVD saturation occurs only after many generations, and producer-rich populations outgrow producer-poor communities for longer. At the other extreme, $\alpha \to \infty$ means that cells produce PVD much faster than they grow. In this case, a handful of producers suffices to quickly reach saturation levels of PVD. Whether they include few or many producers, all populations grow at the same rate, which negates the advantage of higher producer fractions.

We can also use equations (4) to describe a metapopulation of M independent populations. To simulate this scenario, we solve equations (4) numerically for an ensemble of stochastic initial conditions (using $M = 10^4$). We generate a stochastic distribution of initial producer fractions x_0 – depicted in Fig. 4b – as implemented in the experiments (see Fig. 5a and Materials and Methods). Because the experiments described here deal with relatively large populations (starting with around 10^3–10^4 individuals, and expanding to between 10^6 and 10^7 cells), stochasticity in the initial size is low, and we initialize all populations in the simulated ensemble with the same size $n_0 = 10^{-3}$. Once the populations are formed, the choice of s and α completely determines the population dynamics.

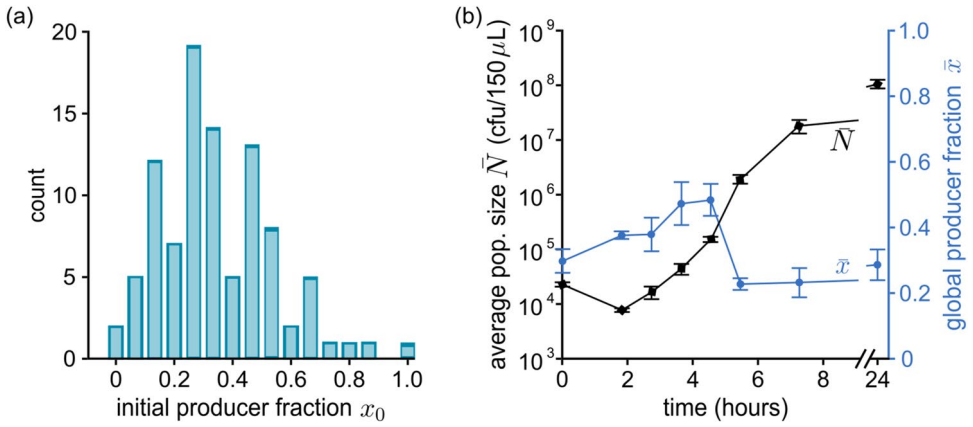

Figure 5. Experimental results for the growth of a mixed metapopulation. (**a**) Sample distribution of initial producer fractions in a 96-well plate. (**b**) Time course of the development of the total cell number $\overline{N}(t)$ and global producer fraction $\overline{x}(t)$ for a metapopulation grown under extreme iron limitation (KB/1 mM DP) in a 96-well plate shaken at 30 °C. At given time intervals, samples are taken from the wells, merged: $\overline{N}(t)$ is determined by counting cfu and $\overline{x}(t)$ is assessed based on the (green) color of colonies. Error bars are the result of three to five determinations of the respective parameter at the given time point. After a lag phase, populations begin to grow exponentially. During this phase, the global producer fraction transiently increases, dips sharply, then stabilizes to its final value.

During the simulations, we record the average size $\overline{n} = \frac{1}{M}\sum_{i=1}^{M} n_i$ and the global producer fraction $\overline{x}$ across the metapopulation

$$\overline{x} = \frac{\sum_i c_i}{\sum_i (c_i + f_i)}, \tag{5}$$

where n_i and x_i are the size and producer fraction of each population i, respectively. Note that this *global* fraction of public-good producers (i.e., the percentage of producer cells in the metapopulation) follows a different trajectory from the *local* one x_i (the fraction of producers actually present in each of the component subpopulations). Specifically, while the latter always decreases – because producers grow more slowly than non-producers – the former can, in some cases, increase.

How $\overline{x}$ changes in time within a metapopulation, according to equations (4) (with $\alpha = 200$, $s = 0.05$, $\overline{n} = 10^{-3}$ is shown in Fig. 4a, and compositions sampled from the distribution in Fig. 4b, with average $\overline{x}(0) \simeq 0.33$); Supplementary Movie S1 shows the same data, together with the evolution of the joint distribution of sizes n_i and compositions x_i. During early stages of growth, the more producers a population has, the quicker it accrues PVD, and the faster it grows. Populations with higher producer fractions rapidly increase their share in the metapopulation, driving up the global producer fraction $\overline{x}$. As time passes, populations with fewer producers also accumulate enough PVD to grow significantly (while the few with no producers never grow). Meanwhile, producer-rich populations have depleted their resources and end growth. As a result, the rate of increase of $\overline{x}$ first slows, then reaches a maximum $\overline{x}_{\max}$ and decreases again. Finally, once all populations have entered the dormant state, the global producer fraction stabilizes. Its ultimate value depends on the production cost s and, because all populations grow to the same size, it is lower or equal to the initial $\overline{x}(0)$.

The overall time course of $\overline{x}$ and $\overline{n}$ depends crucially on the choice of parameters, which reflect the features of the bacterial strains, as well as the cultivation conditions. Figure 4c, for example, shows how changing the growth reduction s affects the magnitude of the increase in global producer fraction $\Delta\overline{x} = \overline{x}_{\max} - \overline{x}(0)$ (for $\alpha = 200$ and the initial conditions shown in Fig. 4b). It is intuitively clear that a slower producer growth would yield a smaller increase. As the figure shows, we can find a region of extreme reduction ($s > 0.4$, which is unlikely to appear in natural systems), which cannot be offset by the benefit from the public good, thus producing no increase whatsoever in producer fraction. For lower values (roughly between 0.1 and 0.4), $\Delta\overline{x}$ is positive, and increases as s is lowered. Finally, for low s (below 0.1), $\Delta\overline{x}$ increases further, reaching values comparable with $\overline{x}(0)$, implying that the global producer fraction $\overline{x}$ almost doubles during growth, albeit transiently. The specific values of s at which different results occur depend on the choice of α and of the x_0 distribution. Nevertheless, the qualitative behavior of $\Delta\overline{x}$ remains the same.

The model thus provides insights into this public-good-mediated social interaction, and implies that it leads to a transient, but potentially very significant, increase in producer fraction. In the following section, we show that these predictions are in good agreement with experiments on competitive growth of mixed populations of producers and non-producers.

Comparison between experimental and theoretical results. We grew mixed populations composed of producers KP1 and non-producers 3E2 under extreme iron limitation (KB/1 mM DP), in which PVD is indispensable for iron uptake and growth (see Supplementary Fig. S1). The metapopulation consisted of a 96-well plate

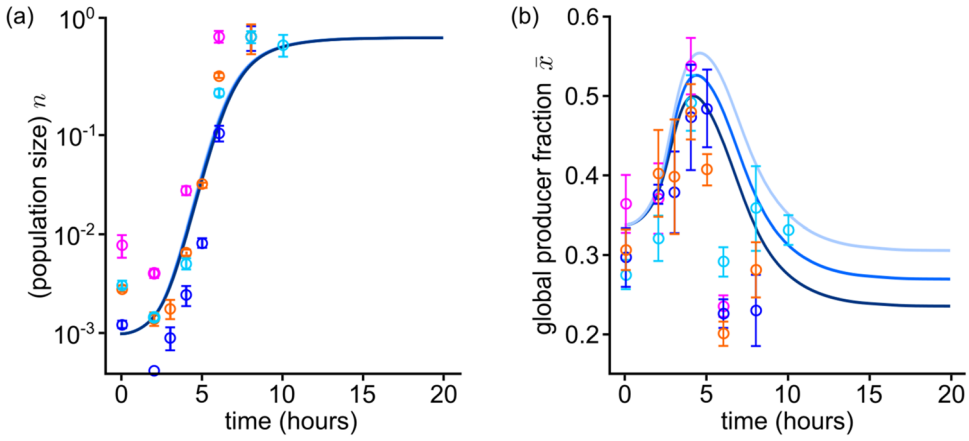

Figure 6. Comparison of simulation and experimental results for the population size (**a**) and global producer fraction (**b**) in a metapopulation. Solid lines represent numerical solutions of equations (4) for different values of the growth rate reduction s, and in (**b**) darker shades indicate higher values ($s \in \{0.03, 0.05, 0.07\}$). Dots of different colors indicate the results of different independent experimental runs. Error bars are the result of three to five determinations of the respective parameter at the given time point in one experiment. The population size n is rescaled to the final yield (or carrying capacity). The stochastic initial compositions are sampled from the distribution in Fig. 4b. For appropriate values of the parameters (determined from fitting of the growth curve in (**a**)), theoretical and experimental result agree.

(so the metapopulation size is $M = 96$), and each well was inoculated with about 10^4 cells. Producers and non-producers in each well were mixed in stochastic proportions, sampled from the distributions shown in Figs 4b and 5a, which were derived from the weighted average of three dice rolls (see Materials and Methods). These initial conditions mimic the characteristic variability of small populations. The mean initial producer fraction was $\bar{x}(0) \simeq 0.33$. As outlined in Fig. 1b, at given time points t, samples were taken from each well, merged, and their average cell number $\overline{N}(t) = \frac{1}{M}\sum_{i=1}^{M} c_i + f_i$ and mean global producer fraction $\bar{x}(t)$ were determined. Figure 5 shows the results of a representative experiment. On average, populations start growing after a lag phase of about 2 h and enter stationary phase after around 8 h. The global producer fraction $\bar{x}$ initially increases, up to a maximum $\bar{x}_{\max} \simeq 0.5$. After sharply dipping to $\bar{x}_{\min} \simeq 0.2$, it levels off to values around 0.2–0.3, and remains constant for at least 24 h. These results qualitatively agree with those obtained by solving equations (4) for an analogous metapopulation (see previous section and Fig. 4).

The only qualitative departure from the simulation results is that $\bar{x}$ drops towards the end of growth phase ($t \simeq 6$ h) in the experiments. Notably, however, this also corresponds to an acceleration in population growth. Most probably, this stems from a change in the metabolic state of cells, which is not captured by the simplified description encoded in the equations (4).

We can also directly compare theoretical and experimental results. As initial conditions for the simulations, we sample the values of x_0 from the same distribution as in the experiments, and set $\bar{n}_0 = 10^{-3}$, which we estimated by dividing the mean minimum size from experiments (taken at the end of the lag phase, so as to eliminate the slight population decay) by the final yield. To set s, we considered that KP1 grows at a rate that is between 1.03 and 1.10 times lower than that for 3E2 (as determined previously), which corresponds to a range for s of between 0.03 and 0.09. Since the rate of approach to saturation α reflects several complex processes, we opted to fit it.

The data from four separate experiments (colored dots) and simulations for three possible values of s and an appropriate saturation rate, $\alpha = 200$ (solid lines) are shown in Fig. 6. To meaningfully compare the two sets of data, we also need to fix the global time scale of simulations, which is done by fitting the slope of the exponential phase in Fig. 6a. The increase in the global producer fraction observed in simulations agrees very well with experiment (Fig. 6b): $\bar{x}$ grows to a maximum $\bar{x}_{\max} \simeq 0.5$ over similar periods, then decreases, and stabilizes to similar values.

Besides the aforementioned end-of-growth discrepancy – which seems to be due to behaviors well beyond the scope of our simplified mathematical description – experimental and theoretical results match.

Discussion

In this work, we showed that social interactions mediated by a public good result in a transient increase in the global fraction of producers in a growing bacterial metapopulation. By combining theoretical modeling and experiments, we were able to quantitatively describe an exchange interaction involving a public good in a bacterial metapopulation.

We selected as our model system the native production of the iron-chelating siderophore pyoverdine (PVD) in *P. putida* KT2440 under iron limitation[41,47]. We characterized a constitutive producer (KP1) and a non-producer strain (3E2), and determined the growth rate reduction due to producing PVD. Under the chosen conditions, PVD is essential for iron acquisition and growth. We demonstrated that populations that produce more PVD grow faster than those with less (under otherwise identical conditions), though the magnitude of the benefit

progressively diminishes as PVD accumulates, and eventually vanishes when the available iron ceases to limit growth. Based on these experimental facts, we constructed a set of differential equations that describes the growth of mixed populations of PVD producers and non-producers. Solving these equations for a large metapopulation, we found that, at first, the more producers (and thus more PVD) are present in the sub-populations, the faster they grow. This generates a positive covariance between composition and growth rate, which drives the global producer fraction up, in accordance with the Price equation[15,17,58]. As PVD accumulates, however, the benefit to cells eventually saturates, reducing the advantage enjoyed by these producer-rich populations; meanwhile, populations containing fewer producers begin to grow and ultimately catch up with the initially faster ones. Therefore, the increase in the global fraction of producers is transient, both in simulations and in experiments.

Previous experimental studies related similar phenomena to the so-called Simpson's paradox[11,12]. However, they considered an artificial bacterial system, in which both the need for the public good and its production mechanism had been designed specifically for the experiments. In contrast, we employed a native system and quantified its social interactions, particularly the function and biochemical properties of the public good. Our analysis also shows that, without mechanisms to sustain it, the Simpson-related increase can only be transient. This conclusion is also compatible with previous qualitative predictions[13–16], based on game theory models with implicit public goods. However, in contrast to our experiments, these studies predict that the producer fraction should peak at the end, instead of the mid-point of exponential growth. This indicates that simple cost-benefit considerations do not suffice to describe the social interaction. Inclusive fitness models have been used to describe an analogous scenario in wild-type *P. aeruginosa*, reaching qualitative conclusions compatible with our results[29,30]. Similarly to game-theoretical approaches, however, they remain mainly conceptual[59]. Our systems biology approach, instead, provides a simple description, with testable quantitative predictions, as well as important insights into the social interaction.

In metapopulation settings, diffusion, dispersal, and mobility affect public good interactions[30,60]. Besides these factors, our results highlight the potential role of the timing of dispersal. Some studies already pointed to dispersal timing, by considering a metapopulation that periodically splits into groups and merging these again to reform the pool. After several cycles, the metapopulation might develop stable coexistence of the strains[13–16], or even have the producers fixate[11,12]. Testing this process, however, requires Poisson dilution conditions which implicate very low initial densities of producer cells. As a consequence, large fractions of cells die under iron-limiting conditions before physiologically effective PVD concentrations are reached. Therefore, a repetitive scenario of group formation and merging is experimentally not feasible for our well mixed cultivation conditions. In principle, introduction of a non-selective growth phase may rescue such a scenario[61].

An interesting next step will be to include regulatory aspects in our system. Like many other bacteria, the wild-type *P. putida* KT2440 continually senses changes in environmental conditions, and uses this information to tune production of the public good[62–64]. By employing constitutive producer strains, we shifted the focus more on the social role of PVD itself, while replicating a potential earlier stage of evolution (if PVD production evolved before regulation). Our model also indicates that a cost-saving strategy such as down-regulation of PVD production as a consequence of PVD accumulation is not sufficient to prevent the long-term decline of the global fraction of producers, because all populations with producers eventually accumulate the same PVD concentration. So accounting for regulation, which has been shown to also impact growth[65], will also necessarily involve elaborate production curves[63] and cost-saving strategies[66]. Ultimately, adaptive production raises complex questions about how cells shape the ecological and environmental conditions in which they interact[67].

Another possible extension would be to allow privatized use of the public good. Privatized use of siderophores, in particular, has been shown to introduce fascinating social dynamics into intra- and inter-species competition[35,68–70]. Limited diffusion and private use have important social consequences[32,33]. Indeed, several studies have intensely debated under what conditions the secreted siderophores actually behave as public goods[42,71–73]. In our conditions, however, populations seem to behave as well-mixed, with negligible privatization.

Taken together, our work uses a simplified setting to highlight the determinant role of public goods in social interactions and population dynamics. For example, we showed the profound consequences of the public good's accumulation and saturating benefits, which simple game-theoretical considerations would fail to describe. Our approach could clearly be extended to investigate the fundamental principles underlying different interactions and bacterial systems. Thereby it should stimulate more mechanistic analyses of bacterial social interactions and their impact on population development.

Materials and Methods

Strains and growth conditions. *Escherichia coli* DH5α [F- φ80d *lacZ* ΔM15 Δ(*lacZYA-argF*) U169 *deoR recA1 endA1 hsd* R17(rk−, mk+) *phoA supE44* λ- *thi-1 gyrA96 relA1*] was used as the carrier for plasmids. *Pseudomonas putida* KT2440 and the derived strain 3E2 (non-producer)[47] were employed as PVD producer (wild-type) and non-producer, respectively. *E. coli* strains were grown in lysogeny broth (LB) at 37 °C, and *P. putida* strains were grown at 30 °C in King's medium B (KB)[74]. KB medium was supplemented with 100 µM $FeCl_3$ and/or 1 mM of the iron chelator 2,2′-dipyridyl (DP) where indicated. Solid media were LB or KB with 1.5% agar.

Generation of the constitutive PVD producer strain KP1. A *P. putida* strain that constitutively produces PVD was generated by placing a copy of the *pfrI* gene under the control of the constitutive promoter $P_{A1/04/03}$[54]. For this purpose, $P_{A1/04/03}$ and the *pfrI* gene were amplified by PCR from the plasmid mini*Tn*7(Gm) $P_{A1/04/03}$ecfp-a[75] and the *P. putida* genome, respectively, cloned into plasmid pUC18R6K-mini-*Tn*7T-Gm, and inserted at the *att*Tn7 site in *P. putida* KT2440 following a mini-*Tn*7 protocol for *Pseudomonas*[76]. The resulting *P. putida* strain KP1 was verified by PCR amplification of corresponding genome regions and sequencing. All oligonucleotide primers used for strain generations and verification are listed in Supplementary Table S2.

Quantitative analysis of PVD production. Pre-cultures of the respective strains were grown in iron-replete medium (KB/200 µM $FeCl_3$) at 30 °C for 18 h. The pre-cultures were used to inoculate the appropriate media for the growth of the cultures used in experiments ($N_0 = 10^7$ cells mL^{-1}). Experiments were performed in 24-well plates (2 mL culture/well). The plates were shaken at 300 rpm at 30 °C. At given time points samples were taken and the optical density at 600 nm was measured. Subsequently, cells were removed by centrifugation, and the relative PVD content was determined by measuring the fluorescence emission at 460 nm (excitation 400 nm). PVD production was analyzed under iron limitation (KB/1 mM DP; KB/100 µM $FeCl_3$/1 mM DP) and iron replete conditions (KB; KB/100 µM $FeCl_3$). Each individual experiment was performed with three parallel replicates. A minimum of three independent experiments were conducted per condition.

Growth characteristics of strains under different environmental conditions. Pre-cultures of the respective strains were grown in iron-replete medium as described above for the analysis of PVD production, and used to inoculate the appropriate media for growth of the cultures used in experiments ($N_0 = 10^7$ cells mL^{-1}). Experiments were performed in 96-well plates (150 µL culture/well). The plates were shaken at 300 rpm at 30 °C. Growth was followed by measuring the optical density at 600 nm using a microplate reader (Infinite® M200 from Tecan Trading AG). The measurement was controlled and monitored with the i-control™ Software from Tecan Trading AG (30 °C, shaking at 280 rpm, 880 s per cycle, minimum 80 cycles). Each condition was implemented in six replicates per experiment, including medium blanks. For low cell numbers (e.g., $N_0 = 10^4$ cells 150 μL^{-1}), growth was analyzed by determining colony forming units (*cfu*) over time (threefold per time point). The specific growth rate μ represents a quantitative measure of growth in the exponential phase and was calculated using the following equation: $\mu = \frac{\ln(N_{t2} - N_{t1})}{t2 - t1}$.

Quantitative assessment of the benefit of PVD. The benefit conferred by PVD was quantified under iron-limiting conditions (KB/1 mM DP) with the non-producer strain 3E2. PVD was isolated according to a previously described protocol[77] and added to the medium at concentrations of between 0 and 20 µM. Growth was monitored via optical density measurement, and the specific growth rate μ was calculated as described in the previous paragraph. Each individual experiment was performed with four parallel repeats per PVD concentration, and three independent experiments of this type were conducted per PVD concentration.

Determination of PVD sharing in mixed culture. Cells were grown in KB/1 mM DP (initial producer frequency $\overline{x}(0) \simeq 0.33$, $N_0 = 10^4$ cells/150 µL, 96-well plate format) at 30 °C. Colony forming units (*cfu*) were determined at given time points (five replicates per time point), and producer and non-producer cells were discriminated by colony color and size. Three independent experiments were performed, each yielding similar results.

Stability of PVD in KB medium with and without bacteria. Medium without cells and medium containing about 10^7 cells mL^{-1} of the non-producer were supplemented with 2 µM PVD and incubated at 30 °C for 48 h. At given time points samples were taken, and the relative PVD contents of medium and of the supernatant of medium with cells were determined by measuring the fluorescence emission of PVD at 460 nm (excitation 400 nm).

Competitive growth experiments. To analyze the impact of the initial producer frequencies x_0 on growth, strains KP1 and 3E2 were mixed in KB/1 mM DP (96-well plate, $N_0 = 10^4$ cells 150 μL^{-1}, $x_0 \in \{0, 0.1, 0.2, 0.3, 0.5, 0.75, 1.0\}$). Total cell numbers were determined at the end of the lag phase and after 8 h of shaking at 30 °C by counting *cfu*. For each condition, a minimum of three individual experiments were performed. To analyze the development of the total cell number $\overline{N}(t)$ and global producer frequency $\overline{x}(t)$ in metapopulations, a random distribution of the initial producer frequency x_0 was established by rolling three dices. The values of each triplet were weighted (lowest 2/3, middle 2/9 and highest 1/9) and rounded to yield sixteen different values from 0 to 15 that are equivalent to sixteen different initial producer frequencies x_0 ranging from 0 to 1.0 and result in an initial average global cooperator fraction $\overline{x}(0)$ of about 0.33. Cells were grown in KB/1 mM DP (96-well plate, $N_0 = 10^4$ cells 150 μL^{-1}) at 30 °C while shaking at 300 rpm. At given time points aliquots of each well were merged and $\overline{N}(t)$ was determined by counting *cfu*. The global producer frequency $\overline{x}(t)$ was obtained based on differences in the color and size of the colonies of KP1 and 3E2 on KB agar plates (minimum three replicates per time point).

Stochastic initial conditions and ensemble averages. We generate all triplets of the integers between 0 and 5 to simulate the results of a sequence of (simultaneous) throws of three dice. Since the weights in the experimental procedure are assigned based on the order of the rolled values, we order the "rolled" values within each triplet from lowest to highest. This results in a table of all possible 3-dice rolls, which we can use directly to generate the initial conditions and simulate equations (4). To speed up calculations, however, we remove duplicate triplets: for example, 113, 131, 311 are different triplets before sorting, but are the same after. Once we remove the duplicate combinations, we assign the appropriate probability to them, i.e. the number of ways to produce them before sorting divided by the total number of triplets. With a minimal combinatorics, one can compute the total number of triplets ($6^3 = 216$), and the multiplicities of triplets: those with three equal values have only one way to appear before sorting; those with two equal values have three; those with all different values have six.

To simulate the time evolution of n and x, we generate the initial composition x_0 for each triplet, using the weighted average described above. After setting n_0, α, and s, the temporal evolution of the average $\overline{x}$ and $\overline{n}$ in ensembles of populations can be computed by solving equations (4) for each of the allowed values of x_0 and weighting it using the relative probability, computed as described above.

Data Availability. The data that support the findings of this study are available from the corresponding authors upon reasonable request.

References

1. Ackermann, M. A functional perspective on phenotypic heterogeneity in microorganisms. *Nat Rev Microbiol* **13**, 497–508, https://doi.org/10.1038/nrmicro3491 (2015).
2. Germerodt, S. *et al*. Pervasive selection for cooperative cross-feeding in bacterial communities. *PLoS Comp Biol* **12**, e1004986, https://doi.org/10.1371/journal.pcbi.1004986 (2016).
3. Hawver, L. A., Jung, S. A. & Ng, W. L. Specificity and complexity in bacterial quorum-sensing systems. *FEMS Microbiol Rev* **40**, 738–752, https://doi.org/10.1093/femsre/fuw014 (2016).
4. Kolter, R. & Greenberg, E. P. Microbial sciences: the superficial life of microbes. *Nature* **441**, 300–302, https://doi.org/10.1038/441300a (2006).
5. Papenfort, K. & Bassler, B. L. Quorum sensing signal-response systems in Gram-negative bacteria. *Nat Rev Microbiol* **14**, 576–588, https://doi.org/10.1038/nrmicro.2016.89 (2016).
6. Veening, J. W., Smits, W. K. & Kuipers, O. P. Bistability, epigenetics, and bet-hedging in bacteria. *Annu Rev Microbiol* **62**, 193–210, https://doi.org/10.1146/annurev.micro.62.081307.163002 (2008).
7. Keymer, J. E., Galajda, P., Lambert, G., Liao, D. & Austin, R. H. Computation of mutual fitness by competing bacteria. *Proc Natl Acad Sci USA* **105**, 20269–20273, https://doi.org/10.1073/pnas.0810792105 (2008).
8. Rainey, P. B. & Rainey, K. Evolution of cooperation and conflict in experimental bacterial populations. *Nature* **425**, 72–74, https://doi.org/10.1038/nature01906 (2003).
9. West, S. A., Diggle, S. P., Buckling, A., Gardner, A. & Griffins, A. S. The social lives of microbes. *Annu Rev Ecol Evol Syst* **38**, 53–77, https://doi.org/10.1146/annurev.ecolsys.38.091206.095740 (2007).
10. Menon, R. & Korolev, K. S. Public good diffusion limits microbial mutualism. *Phys Rev Lett* **114**, 168102, https://doi.org/10.1103/PhysRevLett.114.168102 (2015).
11. Chuang, J. S., Rivoire, O. & Leibler, S. Simpson's paradox in a synthetic microbial system. *Science* **323**, 272–275, https://doi.org/10.1126/science.1166739 (2009).
12. Chuang, J. S., Rivoire, O. & Leibler, S. Cooperation and Hamilton's rule in a simple synthetic microbial system. *Mol Syst Biol* **6**, 398, https://doi.org/10.1038/msb.2010.57 (2010).
13. Cremer, J., Melbinger, A. & Frey, E. Evolutionary and population dynamics: a coupled approach. *Phys Rev E, Stat Nonlinear Soft Matter Phys* **84**, 051921, https://doi.org/10.1103/PhysRevE.84.051921 (2011).
14. Cremer, J., Melbinger, A. & Frey, E. Growth dynamics and the evolution of cooperation in microbial populations. *Sci Rep* **2**, 281, https://doi.org/10.1038/srep00281 (2012).
15. Melbinger, A., Cremer, J. & Frey, E. Evolutionary game theory in growing populations. *Phys Rev Lett* **105**, 178101, https://doi.org/10.1103/PhysRevLett.105.178101 (2010).
16. Melbinger, A., Cremer, J. & Frey, E. The emergence of cooperation from a single mutant during microbial life cycles. *J R Soc Interface* **12**, https://doi.org/10.1098/rsif.2015.0171 (2015).
17. Price, G. R. Extension of covariance selection mathematics. *Ann Hum Genet* **35**, 485–490 (1972).
18. Costerton, J. W. *et al*. Bacterial Biofilms in Nature and Disease. *Annu Rev Microbiol* **41**, 435–464 (1987).
19. Xavier, J. B. Social interaction in synthetic and natural microbial communities. *Mol Syst Biol* **7**, 483, https://doi.org/10.1038/msb.2011.16 (2011).
20. Frey, E. Evolutionary game theory: Theoretical concepts and applications to microbial communities. *Physica A-Stat Mech Appl* **389**, 4265–4298, https://doi.org/10.1016/j.physa.2010.02.047 (2010).
21. Gore, J., Youk, H. & van Oudenaarden, A. Snowdrift game dynamics and facultative cheating in yeast. *Nature* **459**, 253–256, https://doi.org/10.1038/nature07921 (2009).
22. Hofbauer, J. & Sigmund, K. *Evolutionary Games and Population Dynamics*. (Cambridge University Press, 1998).
23. Hofbauer, J. & Sigmund, K. Evolutionary game dynamics. *B Am Math Soc* **40**, 479–519, https://doi.org/10.1090/S0273-0979-03-00988-1 (2003).
24. Reichenbach, T., Mobilia, M. & Frey, E. Mobility promotes and jeopardizes biodiversity in rock-paper-scissors games. *Nature* **448**, 1046–1049, https://doi.org/10.1038/nature06095 (2007).
25. Axelrod, R. & Hamilton, W. D. The evolution of cooperation. *Science* **211**, 1390–1396 (1981).
26. Damore, J. A. & Gore, J. Understanding microbial cooperation. *J Theor Biol* **299**, 31–41, https://doi.org/10.1016/j.jtbi.2011.03.008 (2012).
27. Frank, S. A. *Foundations of social evolution*. (Princeton University Press, 1998).
28. Hamilton, W. D. The genetical evolution of social behaviour. I. *J Theor Biol* **7**, 1–16 (1964).
29. Griffin, A. S., West, S. A. & Buckling, A. Cooperation and competition in pathogenic bacteria. *Nature* **430**, 1024–1027, https://doi.org/10.1038/nature02744 (2004).
30. Kümmerli, R., Gardner, A., West, S. A. & Griffin, A. S. Limited dispersal, budding dispersal, and cooperation: an experimental study. *Evolution* **63**, 939–949, https://doi.org/10.1111/j.1558-5646.2008.00548.x (2009).
31. Nowak, M. A. Five rules for the evolution of cooperation. *Science* **314**, 1560–1563, https://doi.org/10.1126/science.1133755 (2006).
32. Julou, T. *et al*. Cell-cell contacts confine public goods diffusion inside *Pseudomonas aeruginosa* clonal microcolonies. *Proc Natl Acad Sci USA* **110**, 12577–12582, https://doi.org/10.1073/pnas.1301428110 (2013).
33. Kümmerli, R., Schiessl, K. T., Waldvogel, T., McNeill, K. & Ackermann, M. Habitat structure and the evolution of diffusible siderophores in bacteria. *Ecol Lett* **17**, 1536–1544, https://doi.org/10.1111/ele.12371 (2014).
34. Dobay, A., Bagheri, H. C., Messina, A., Kümmerli, R. & Rankin, D. J. Interaction effects of cell diffusion, cell density and public goods properties on the evolution of cooperation in digital microbes. *J Evol Biol* **27**, 1869–1877, https://doi.org/10.1111/jeb.12437 (2014).
35. Inglis, R. F., Biernaskie, J. M., Gardner, A. & Kümmerli, R. Presence of a loner strain maintains cooperation and diversity in well-mixed bacterial communities. *Proc Biol Sci* **283**, https://doi.org/10.1098/rspb.2015.2682 (2016).
36. MacLean, R. C., Fuentes-Hernandez, A., Greig, D., Hurst, L. D. & Gudelj, I. A mixture of "cheats" and "co-operators" can enable maximal group benefit. *PLoS Biol* **8**, e1000486, https://doi.org/10.1371/journal.pbio.1000486 (2010).
37. Niehus, R., Picot, A., Oliveira, N. M., Mitri, S. & Foster, K. R. The evolution of siderophore production as a competitive trait. *Evolution* **71**, 1443–1455, https://doi.org/10.1111/evo.13230 (2017).
38. Widder, S. *et al*. Challenges in microbial ecology: building predictive understanding of community function and dynamics. *ISME J* **10**, 2557–2568, https://doi.org/10.1038/ismej.2016.45 (2016).
39. Harcombe, W. R. *et al*. Metabolic resource allocation in individual microbes determines ecosystem interactions and spatial dynamics. *Cell Rep* **7**, 1104–1115, https://doi.org/10.1016/j.celrep.2014.03.070 (2014).
40. Buckling, A. *et al*. Siderophore-mediated cooperation and virulence in *Pseudomonas aeruginosa*. *FEMS Microbiol Ecol* **62**, 135–141, https://doi.org/10.1111/j.1574-6941.2007.00388.x (2007).
41. Kümmerli, R., Jiricny, N., Clarke, L. S., West, S. A. & Griffin, A. S. Phenotypic plasticity of a cooperative behaviour in bacteria. *J Evol Biol* **22**, 589–598, https://doi.org/10.1111/j.1420-9101.2008.01666.x (2009).

42. Zhang, X. X. & Rainey, P. B. Exploring the sociobiology of pyoverdin-producing *Pseudomonas*. *Evolution* **67**, 3161–3174, https://doi.org/10.1111/evo.12183 (2013).
43. Visca, P., Imperi, F. & Lamont, I. L. Pyoverdine siderophores: from biogenesis to biosignificance. *Trends Microbiol* **15**, 22–30 (2007).
44. Imperi, F., Tiburzi, F. & Visca, P. Molecular basis of pyoverdine siderophore recycling in *Pseudomonas aeruginosa*. *Proc Natl Acad Sci USA* **106**, 20440–20445, https://doi.org/10.1073/pnas.0908760106 (2009).
45. Gasser, V., Guillon, L., Cunrath, O. & Schalk, I. J. Cellular organization of siderophore biosynthesis in *Pseudomonas aeruginosa*: evidence for siderosomes. *J Inorg Biochem* **148**, 27–34, https://doi.org/10.1016/j.jinorgbio.2015.01.017 (2015).
46. Hannauer, M., Barda, Y., Mislin, G. L. A., Shanzer, A. & Schalk, I. J. The ferrichrome uptake pathway in *Pseudomonas aeruginosa* Involves an iron release mchanism with acylation of the siderophore and recycling of the modified desferrichrome. *J Bacteriol* **192**, 1212–1220, https://doi.org/10.1128/Jb.01539-09 (2010).
47. Matthijs, S. *et al*. Siderophore-mediated iron acquisition in the entomopathogenic bacterium *Pseudomonas entomophila* L48 and its close relative *Pseudomonas putida* KT2440. *Biometals* **22**, 951–964, https://doi.org/10.1007/s10534-009-9247-y (2009).
48. Lee, J. & Zhang, L. The hierarchy quorum sensing network in *Pseudomonas aeruginosa*. *Protein Cell* **6**, 26–41, https://doi.org/10.1007/s13238-014-0100-x (2015).
49. Martins dos Santos, V. A. P., Heim, S., Moore, E. R., Stratz, M. & Timmis, K. N. Insights into the genomic basis of niche specificity of *Pseudomonas putida* KT2440. *Environ Microbiol* **6**, 1264–1286, https://doi.org/10.1111/j.1462-2920.2004.00734.x (2004).
50. Niewerth, H., Bergander, K., Chhabra, S. R., Williams, P. & Fetzner, S. Synthesis and biotransformation of 2-alkyl-4(1H)-quinolones by recombinant *Pseudomonas putida* KT2440. *Appl Microbiol Biotechnol* **91**, 1399–1408, https://doi.org/10.1007/s00253-011-3378-0 (2011).
51. Cornelis, P., Matthijs, S. & Van Oeffelen, L. Iron uptake regulation in *Pseudomonas aeruginosa*. *Biometals* **22**, 15–22, https://doi.org/10.1007/s10534-008-9193-0 (2009).
52. Swingle, B. *et al*. Characterization of the PvdS-regulated promoter motif in *Pseudomonas syringae* pv. *tomato* DC3000 reveals regulon members and insights regarding PvdS function in other pseudomonads. *Mol Microbiol* **68**, 871–889, https://doi.org/10.1111/j.1365-2958.2008.06209.x (2008).
53. Pasqua, M. *et al*. Ferric uptake regulator Fur is conditionally essential in *Pseudomonas aeruginosa*. *J Bacteriol* **199**, https://doi.org/10.1128/JB.00472-17 (2017).
54. Lanzer, M. & Bujard, H. Promoters largely determine the efficiency of repressor action. *Proc Natl Acad Sci USA* **85**, 8973–8977 (1988).
55. Semsey, S. *et al*. Genetic regulation of fluxes: iron homeostasis of *Escherichia coli*. *Nucleic Acids Res* **34**, 4960–4967, https://doi.org/10.1093/nar/gkl627 (2006).
56. Thulasiraman, P. *et al*. Selectivity of ferric enterobactin binding and cooperativity of transport in Gram-negative bacteria. *J Bacteriol* **180**, 6689–6696 (1998).
57. Meyer, J.-M. & Abdallah, M. A. The fluorescent pigment of *Pseudomonas fluorescens:* biosynthesis, purification and physicochemical properties. *J Gen Microbiol* **107**, 319–328 (1978).
58. Price, G. R. Selection and covariance. *Nature* **227**, 520–521 (1970).
59. Ghoul, M. *et al*. Pyoverdin cheats fail to invade bacterial populations in stationary phase. *J Evol Biol* **29**, 1728–1736, https://doi.org/10.1111/jeb.12904 (2016).
60. Gelimson, A., Cremer, J. & Frey, E. Mobility, fitness collection, and the breakdown of cooperation. *Phys Rev* E **87**, https://doi.org/10.1103/PhysRevE.87.042711 (2013).
61. Wienand, K., Lechner, M., Becker, F., Jung, H. & Frey, E. Non-selective evolution of growing populations. *PLoS One* **10**, e0134300, https://doi.org/10.1371/journal.pone.0134300 (2015).
62. Dandekar, A. A., Chugani, S. & Greenberg, E. P. Bacterial quorum sensing and metabolic incentives to cooperate. *Science* **338**, 264–266, https://doi.org/10.1126/science.1227289 (2012).
63. Heilmann, S., Krishna, S. & Kerr, B. Why do bacteria regulate public goods by quorum sensing?-How the shapes of cost and benefit functions determine the form of optimal regulation. *Front Microbiol* **6**, 767, https://doi.org/10.3389/fmicb.2015.00767 (2015).
64. Smalley, N. E., An, D., Parsek, M. R., Chandler, J. R. & Dandekar, A. A. Quorum sensing protects *Pseudomonas aeruginosa* against cheating by other species in a laboratory coculture model. *J Bacteriol* **197**, 3154–3159, https://doi.org/10.1128/JB.00482-15 (2015).
65. Kiviet, D. J. *et al*. Stochasticity of metabolism and growth at the single-cell level. *Nature* **514**, 376–379, https://doi.org/10.1038/nature13582 (2014).
66. Kümmerli, R. & Brown, S. P. Molecular and regulatory properties of a public good shape the evolution of cooperation. *Proc Natl Acad Sci USA* **107**, 18921–18926, https://doi.org/10.1073/pnas.1011154107 (2010).
67. Bauer, M., Knebel, J., Lechner, M., Pickl, P. & Frey, E. Ecological feedback in quorum-sensing microbial populations can induce heterogeneous production of autoinducers. *Elife* **6**, https://doi.org/10.7554/eLife.25773 (2017).
68. Jiricny, N. *et al*. Fitness correlates with the extent of cheating in a bacterium. *J Evol Biol* **23**, 738–747, https://doi.org/10.1111/j.1420-9101.2010.01939.x (2010).
69. Lee, W., van Baalen, M. & Jansen, V. A. Siderophore production and the evolution of investment in a public good: An adaptive dynamics approach to kin selection. *J Theor Biol* **388**, 61–71, https://doi.org/10.1016/j.jtbi.2015.09.038 (2016).
70. Pande, S. *et al*. Privatization of cooperative benefits stabilizes mutualistic cross-feeding interactions in spatially structured environments. *ISME J* **10**, 1413–1423, https://doi.org/10.1038/ismej.2015.212 (2016).
71. Kümmerli, R. & Ross-Gillespie, A. Explaining the sociobiology of pyoverdin producing *Pseudomonas*: a comment on Zhang and Rainey (2013). *Evolution* **68**, 3337–3343, https://doi.org/10.1111/evo.12311 (2014).
72. Ghoul, M., West, S. A., Diggle, S. P. & Griffin, A. S. An experimental test of whether cheating is context dependent. *J Evol Biol* **27**, 551–556, https://doi.org/10.1111/jeb.12319 (2014).
73. Rainey, P. B., Desprat, N., Driscoll, W. W. & Zhang, X. X. Microbes are not bound by sociobiology: response to Kümmerli and Ross-Gillespie (2013). *Evolution* **68**, 3344–3355, https://doi.org/10.1111/evo.12508 (2014).
74. King, E. O., Ward, M. K. & Raney, D. E. Two simple media for the demonstration of pyocyanin and fluorescin. *J Lab Clin Med* **44**, 301–307 (1954).
75. Lambertsen, L., Sternberg, C. & Molin, S. Mini-Tn7 transposons for site-specific tagging of bacteria with fluorescent proteins. *Environ Microbiol* **6**, 726–732 (2004).
76. Choi, K. H. & Schweizer, H. P. mini-Tn7 insertion in bacteria with single attTn7 sites: example *Pseudomonas aeruginosa*. *Nat Prot* **1**, 153–161, https://doi.org/10.1038/nprot.2006.24 (2006).
77. Meyer, J. M. *et al*. Siderotyping of fluorescent pseudomonads: characterization of pyoverdines of *Pseudomonas fluorescens* and *Pseudomonas putida* strains from Antarctica. *Microbiology* **144**, 3119–3126, https://doi.org/10.1099/00221287-144-11-3119 (1998).

Acknowledgements

This work was supported by the Deutsche Forschungsgemeinschaft through grant SPP1617 (JU 333/5–1, 2 and FR 850/11–1, 2). We thank Michelle Eder (HJ lab) for excellent technical assistance. *P. putida* strain 3E2 was kindly provided by P. Cornelis (Vrije Universiteit Brussels, Belgium).

Author Contributions

Designed and performed the experiments: F.B., H.J.; designed and performed theoretical analysis: K.W., M.L., E.F.; analyzed the experimental and computational data: F.B., K.W., M.L., E.F., H.J. Wrote the paper: K.W., M.L., E.F., F.B., H.J.

Additional Information

Supplementary information accompanies this paper at https://doi.org/10.1038/s41598-018-22306-9.

Competing Interests: The authors declare no competing interests.

Publisher's note: Springer Nature remains neutral with regard to jurisdictional claims in published maps and institutional affiliations.

Interactions mediated by a public good transiently increase cooperativity in growing *Pseudomonas putida* metapopulations

Felix Becker,[a] Karl Wienand,[b] Matthias Lechner,[b] Erwin Frey,[b,*] Heinrich Jung[a,*]

[a]Microbiology, Department Biology 1, Ludwig-Maximilians-Universität Munich, Grosshaderner Strasse 2-4, Martinsried, Germany; [b]Arnold-Sommerfeld-Center for Theoretical Physics and Center for Nanoscience, Ludwig-Maximilians-Universität, Theresienstrasse 37, D-80333 Munich, Germany

[*]Correspondence to: Heinrich Jung, hjung@lmu.de (HJ) and Erwin Frey frey@lmu.de (EF). FB and KW contributed equally to this work.

Supplementary Information

Notes

Derivation of the growth rate $\mu(p)$

Assume a cell is born with an internal iron concentration $Fe_{\text{in}}(0)$ and a volume $V(0)$. Let p be the concentration of PVD-Fe complexes (which we take to be the same as that of PVD; see text). Each cell, then, incorporates iron ions at a constant rate kp that is proportional to the concentration of PVD. So at time t after its birth, the cell has accumulated kpt iron ions. Its internal iron concentration $Fe_{\text{in}}(t)$, then, is $Fe_{\text{in}}(0)V(0)$ (that is, the number of iron atoms at birth), plus the iron it has collected, all divided by the volume birth $V(t)$ it has reached:

$$Fe_{\text{in}}(t) = \frac{Fe_{\text{in}}(0)V(0)+kpt}{V(t)} \quad .$$

Because cells try to maintain iron concentration homeostasis, we can consider Fe_{in} to be constant. Moreover, as long as iron is the limiting factor for growth, the growth rate $\mu(p)$ depends only on the PVD concentration.

On average, cells divide at time $t_D = 1/\mu(p)$, given that growth is logistic. Moreover, at the moment of division, the cell has attained twice the volume of its future daughters: $V(t_D) = 2V(0)$. With these substitutions in the above equation, and minimal algebra, we obtain equation (2).

Estimation of iron incorporated into cells

The iron content of a bacterial cell ranges from $\sim 10^5$ to 10^6 atoms per cell[1,2]. In our experimental setup, cells reach a maximum density of 2×10^7 cells per 150 µL at the end of the exponential growth phase accumulating in total 2×10^{12} to 2×10^{13} iron atoms. We determined the iron concentration of our KB preparation by atomic absorption spectroscopy and found a concentration of ~8 µM (corresponding to $\sim 7.2\times10^{14}$ iron atoms per 150 µL KB medium). Using these numbers we calculated that ~0.28 to 2.8% of the total iron of KB is incorporated into cells by the end of the exponential growth phase.

Impact of simple regulation

Our conclusions are robust (at least qualitatively) against simple cost-saving strategies. More specifically, PVD accumulation makes it so that stopping synthesis to save costs is not sufficient to prevent the long-term decline of the global fraction of producers, as we prove in

the following.

Let the synthesis rate σ and the production cost s in equation (3) depend on the pyoverdine concentration p. As a general form of cost-saving regulation, we consider that producers cease to synthesize PVD when its concentration reaches some threshold p_c: $\sigma(p_c) = 0$. After synthesis stops, there producers incur no further cost and thus grow at the same rate as non-producers: $s(p_c) = 0$. If a population has any amount of producers (that is, if $x_0 \neq 0$), at least some PVD is produced and, because it accumulates, its concentration steadily grows until it reaches p_c. In the long run, then, all populations with $x_0 \neq 0$ end up with the same PVD concentration (namely p_c).

As in our analysis, producer-rich populations grow faster for a limited time, then less producing ones catch up. Concurrently, the producer fraction within each population declines (during production) or stays constant (when production stops). This tension engenders a "Simpson's paradox" setting much like the one we presented in the case of constitutive production. Furthermore, because all populations reach the same ultimate size, the final value of $\bar{x}$ is simply the average of the producer fraction x in each population. These values are lower than the respective x_0, because of the cost of production.

References

1 Abdul-Tehrani, H. *et al.* Ferritin mutants of *Escherichia coli* are iron deficient and growth impaired, and *fur* mutants are iron deficient. *J Bacteriol* **181**, 1415-1428 (1999).

2 Andrews, S. C., Robinson, A. K. & Rodriguez-Quinones, F. Bacterial iron homeostasis. *FEMS Microbiol Rev* **27**, 215-237 (2003).

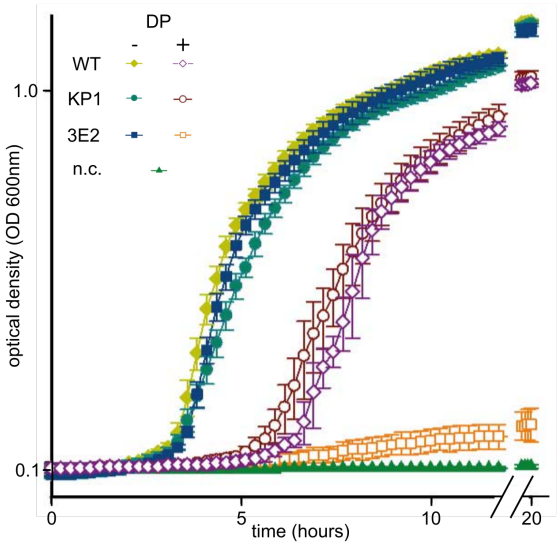

Figure S1. Growth of *P. putida* KT2440 and the derived strains KP1 and 3E2 under iron replete and limiting conditions. Cells were grown in KB supplemented with iron (KB/100 µM $FeCl_3$, full symbols) and in KB with iron chelator DP (KB/100 µM $FeCl_3$/1 mM DP, empty symbols). When iron is more available, PVD is not needed for growth, 3E2 and WT grow about at the same rate, and KP1 grows slower. Under iron limitation, producing strains (KP1 and WT) benefit from production and grow much faster than non-producing 3E2. The experiment was performed as described in the legend of Fig. 3a.

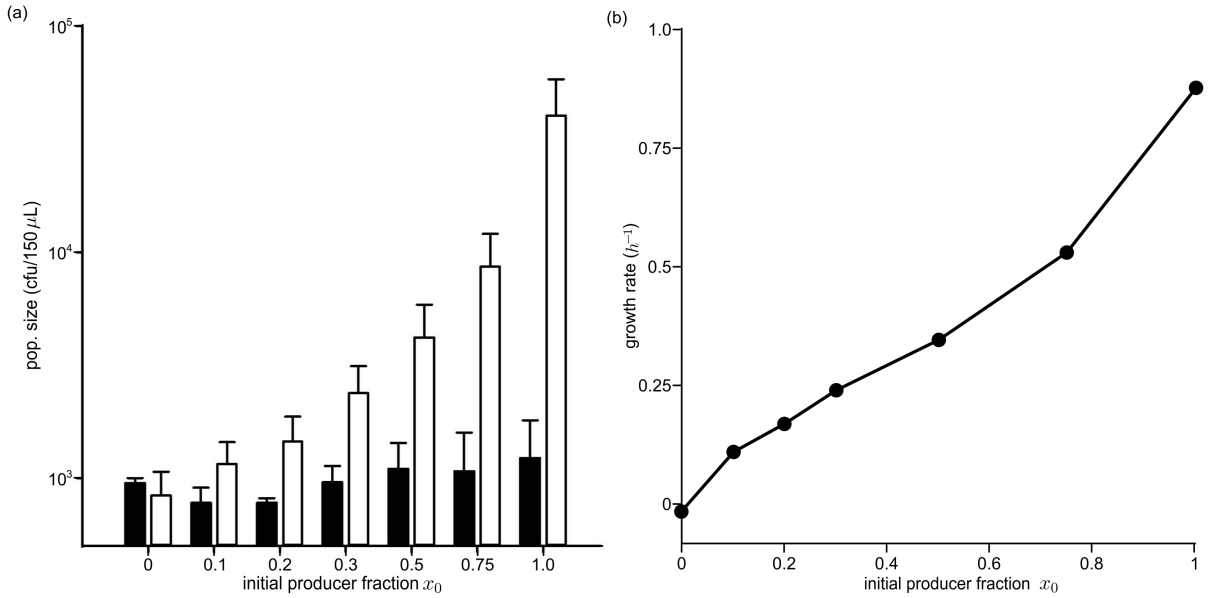

Figure S2. Impact of the initial producer fraction x_0 on the growth of mixed populations under iron limiting conditions. **(a)** Impact of the initial producer fraction x_0 on the growth yield. Strains KP1 and 3E2 were grown in mixed culture under iron-limiting conditions (KB/1 mM DP, N_0 about 10^3 cells/150 µL, 96-well plate format) with the given initial producer frequencies x_0. Total cell numbers were determined by counting *cfu* at the beginning of the experiment (black columns) and after 8 h of incubation (weight columns). For each condition, minimum three individual experiments were performed. (**b**) Impact of the initial producer fraction x_0 on the specific growth rate μ. Mixed cultures of strains KP1 and 3E2 with x_0 values between 0 (=100% 3E2) and 1 (=100% KP1) were incubated in shaking 96-well microtiter plates at 30°C ($N_0 = 10^7$ cells mL^{-1}). Growth was analyzed by measuring the optical density at 600 nm using a Tecan microplate reader. μ was determined for each condition from the exponential phase of the resulting growth curves. All growth parameters represent the means of five growth experiments. Deviations were <10% of the mean value.

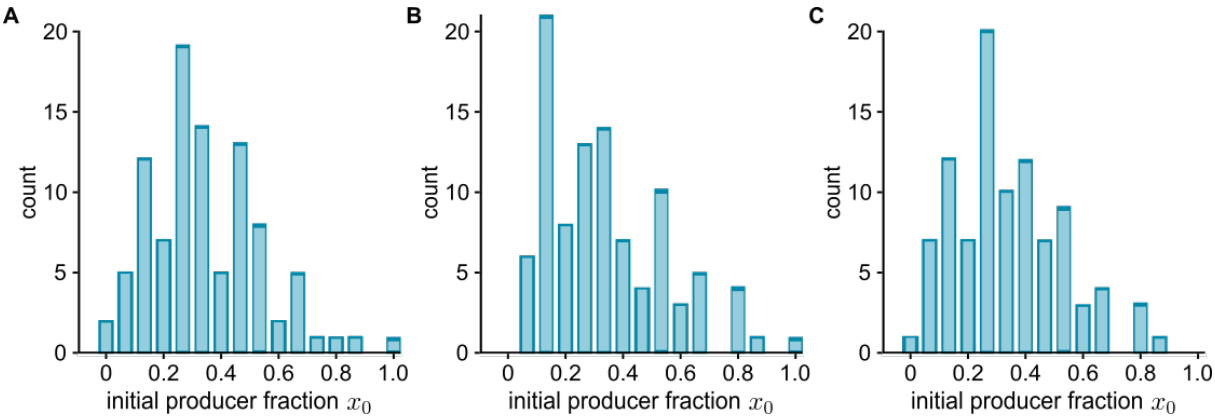

Figure S3. Distribution of initial compositions x_0 in three replicates of the experiment. Although specific values differ, the overall features of the distribution remains the same. Most populations start mixed, with x_0 between 0.1 and 0.5. When at all present, populations with all producers or no producers are very rare.

Table S1. Specific growth rate of *P. putida* KT2440 (WT), the non-producer (3E2), and the constitutive PVD producer (KP1) under iron-rich and iron-limiting conditions.

Growth medium	μ_{WT} (h^{-1})	μ_{3E2} **(h^{-1})**	μ_{KP1} **(h^{-1})**	μ_{3E2}/μ_{KP1}
KB[a]	0.797	0.776	0.736	1.054
KB/100 µM $FeCl_3$[a]	0.766	0.749	0.692	1.082
KB/DP[a]	0.489	0.004	0.588	0.007
KB/100 µM $FeCl_3$/DP[a]	0.657	0.030	0.610	0.049
KB/100 µM $FeCl_3$[b]	1.237	1.238	1.201	1.031
KB/100 µM $FeCl_3$[c]	n.d.	1.182	1.077	1.097

[a]The specific growth rate μ was calculated from the growth curves shown in Fig 1C. Cells were grown in shaking 96-well microtiter plates at 30°C ($N_0 = 10^7$ cells mL^{-1}). Growth was analyzed by measuring the optical density at 600 nm using a Tecan microplate reader.

[b]Cells were grown in shaking 24-well microtiter plates at 30°C ($N_0 = 10^7$ cells mL^{-1}). Every hour 50% of the culture was replaced with fresh medium. Growth was analyzed by measuring the optical density at 600 nm using a 1-mL cuvette (d=1 cm).

[c]Cells were grown in shaking 96-well microtiter plates at 30°C ($N_0 = 10^4$ cells mL^{-1}). Growth was analyzed by determination of colony forming units, *cfu*.

All growth parameters represent the mean of five to fifteen growth experiments. Deviations were <10% of the mean value.

Table S2. Oligonucleotides used in this investigation

Name	Sequence (5'...3')
Generation of *P. putida* KP1	
$P_{A1\ 04\ 03}$ bw kpn	AAATAGGGGGGTACCCGCACATTTCCC
$P_{A1\ 04\ 03}$ mod2	TTCCGCCATGCTTAATTTCTCCTCTTT
pfrI start mod2	AAATTAAGCATGGCGGAACAACTATCC
pfrI end mod2	TGCGGCGTTGGATCCGCTGCGAGTTATTGGCCG
Sequencing insert on plasmid	
mini Tn7 reverse MCS	TTGCATTACAGTTTACGAACCGAAC
Sequencing Tn7 insertion on genome	
checkdown primer trans	GTCTTATTACGTGGCCGTGC
Primer TN7R as	CCACGCCCCTCTTTAATACG
tn7left s	TTTGTCATTTTTAATTTTCG
checkup primer trans	GCAGGAGCCGATGAGACAGA

Movie S1. Temporal evolution of $\bar{x}$ in a metapopulation. The evolution of $\bar{x}$ was obtained by solving equations (4) together with the evolution of the joint distribution of sizes n_i and compositions x_i.

Part II

Combined effects of environmental and demographic noise

Chapter 3

Evolution in stochastic environments

Chapter abstract The environment in which a population lives determines much of its evolution. Changing environmental conditions can affect evolution as a selective factor—modifying which traits selection favors—but it has non-selective aspects, too. This chapter, for example, focuses on how stochastic growth conditions affect population size and growth. Consider an environment in which resources randomly switch between a state of abundance and one of scarcity. Abundant resources lead populations to grow, and reduce the relative weight of demographic noise; scarce resources, instead, make the population shrink, increasing the relative weight of fluctuations. Thus extrinsic noise from the environment becomes coupled to the intrinsic noise in the population. Analytics and simulations allow a description of how this interaction affects the steady state distribution of population size and the fixation properties of the population. The analysis focuses in particular on the survival probability of a slow-growing strain (such as a public good producer) in a pure competition case (when the public good provides no benefit), as well as in the public good case (in which the public good fosters growth). In both cases, a noise-induced transition occurs in the steady state distribution of population size. We also showed that the switching environment largely amplifies demographic fluctuations, increasing the survival probability of the slow strain. Although the public good reduces this fixation probability, there are regimes in which it leads to an overall increase in the amount of producers.

Contribution to overarching question The work presented in this chapter takes a step back from biological realism, in exchange for much finer control on the forces involved. Thereby the analysis unveils the rich intertwining of environment, growth, demographic fluctuations, and social interactions.

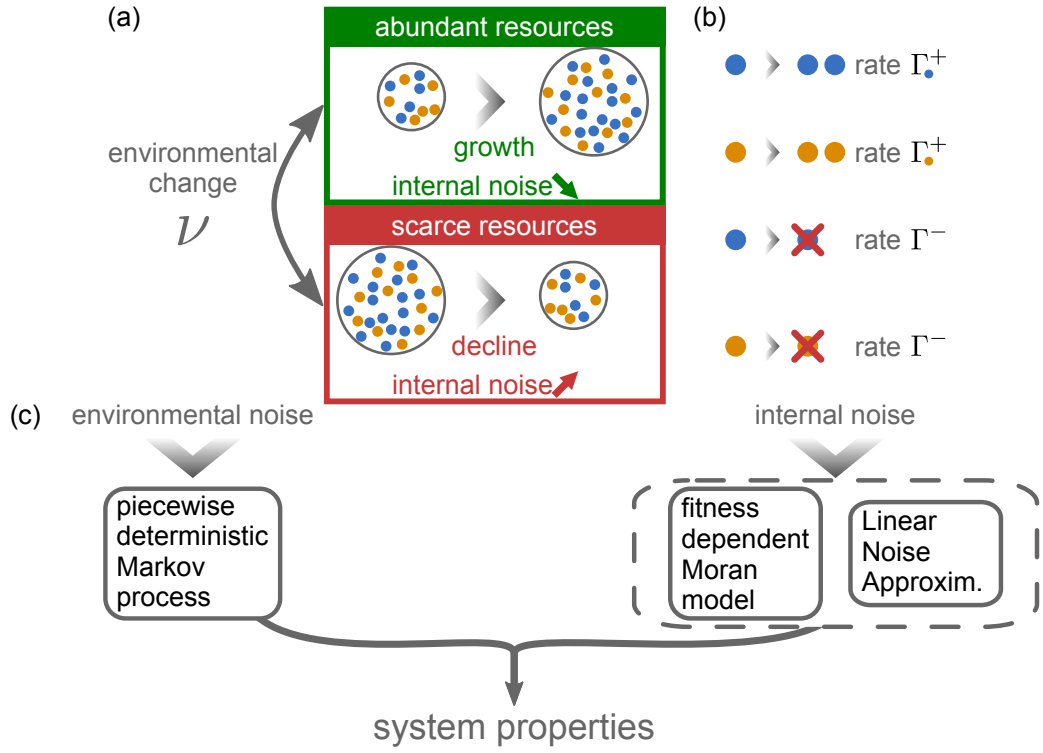

Figure 3.1: *Graphical abstract of the project.* **(a)** Cartoon of the coupled noise model. Under abundant resources (high carrying capacity), the population grows, reducing the amplitude of demographic fluctuations. Under scarce resources (low carrying capacity), the population decays, increasing the amplitude of demographic fluctuations. The environment switches stochastically between the two states at rate ν. **(b)** Internal dynamics of the population. Individuals of each strain reproduce stochastically at a strain-specific per-capita rate Γ^+. All individuals have the same per-capita death rate Γ^-. **(c)** Modeling of the noise sources. We model the effect of the changing environmental conditions (*environmental noise*) using a piecewise deterministic Markov process. To describe the effect of the stochastic birth-death dynamics, we used the Moran model or a linear noise approximation. Combining the two results, we described the overall properties of the population.

3.1 Background

3.1.1 Fitness-dependent Moran model

The fitness-dependent Moran model [57, 86], sketched in Figure 3.2, describes the evolution of a mixed population of constant size N. Individuals reproduce at a per-capita rate, depending on their fitness, creating exact copies of themselves, which replace another individual chosen at random. The Moran model then has *constant size*: to each birth corresponds a death, and the population always eventually fixates, because of genetic drift.

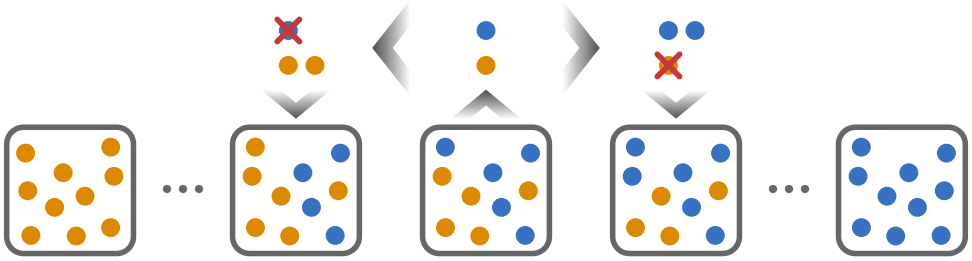

Figure 3.2: *Cartoon of the Moran model.* At each step, one individual is picked for reproduction, with a probability that depends on its fitness. Another individual is picked to die, with uniform probability. In the long run, the population always fixates to one or the other strain.

Consider a population of only two strains: N_c "cooperators" and $N_d = N - N_c$ "defectors". The selection parameter $s \ll 1$ expresses the difference of their with fitnesses: $f_c = 1 - s$ and $f_d = 1$, with average $\langle f(N_c)\rangle = N_c/N f_c + (1 - N_c/N) = 1 - sN_c/N$. The number of cooperators in the population changes with rates

$$\begin{aligned} \Gamma^+(N_c) &= \frac{1-s}{\langle f(N_c)\rangle}\left(\frac{N_c}{N}\right)\left(1-\frac{N_c}{N}\right) \\ \Gamma^-(N_c) &= \frac{1}{\langle f(N_c)\rangle}\left(\frac{N_c}{N}\right)\left(1-\frac{N_c}{N}\right) . \end{aligned} \tag{3.1}$$

$\Gamma^+(N_c)$ is the probability of picking a cooperator for reproduction and a defector for death, $\Gamma^-(N_c)$ is the opposite. The probability $P(N_c, t)$ of having N_c cooperators at time t then follows the master equation

$$\begin{aligned} \frac{d}{dt}P(N_c,t) &= \Gamma^+(N_c-1)P(N_c-1,t) + \Gamma^-(N_c+1)P(N_c+1,t) + \\ &- \left((\Gamma^+(N_c)+\Gamma^-(N_c))P(N_c,t)\right) . \end{aligned} \tag{3.2}$$

From (3.2) we can obtain a Fokker-Planck equation (through a Kramers-Moyal expansion), from which to compute the fixation probability of cooperators ϕ and the mean fixation time T (see, for example, Refs. [57, 58] for the calculation details). Specifically, calling $x_0 = N_c(t = 0)/N$ the initial fraction of cooperators in the population, we obtain

$$\phi|_N = \frac{\mathrm{e}^{-Ns(1-x_0)} - \mathrm{e}^{-Ns}}{1 - \mathrm{e}^{-Ns}} . \tag{3.3}$$

The fixation probability of cooperators $\phi|_N$ decreases exponentially with size. Indeed, because selection disfavors cooperators, the only road to fixation they have is demographic fluctuations, which decrease in intensity the larger populations are (see also Section 1.1.1). In other words, the smaller a population, the higher its demographic noise, and the less selection drives the evolution [58].

3.1.2 Linear noise approximation

While deterministic equations can describe the average development of a population, individual birth and death events cause stochastic fluctuations around it. The *linear noise approximation* (also known as *system size expansion* or *van Kampen expansion*) provides a way to describe these deviations. Refs. [87, 88] present detailed derivations.

Consider the quantity X of scale $\Omega \gg 1$. It evolves by discrete, stochastic steps $\Delta X \ll \Omega$, with transition rates $\mathcal{T}(\Delta X, X)$. The probability $P(X,t)$ of having a value X at time t thus obeys the generic master equation

$$\frac{\partial}{\partial t}P(X,t) = \int d\Delta X \left[\mathcal{T}(\Delta X, X-\Delta X)P(X-\Delta X,t) - \mathcal{T}(\Delta X, X)P(X,t)\right] . \tag{3.4}$$

Calling $\alpha(X) = \int d\Delta X \Delta X \mathcal{T}(\Delta X, X)$ and $\beta(X) = \int d\Delta X (\Delta X)^2 \mathcal{T}(\Delta X, X)$, a simple Kramers-Moyal expansion transforms the master equation (3.4) into the Fokker-Planck equation

$$\frac{\partial}{\partial t}P(X,t) = -\frac{\partial}{\partial X}\left[\alpha(X)P(X,t)\right] + \frac{1}{2}\frac{\partial^2}{\partial X^2}\left[\beta(X)P(X,t)\right] . \tag{3.5}$$

The central assumption of the linear noise approximation is that X, on average, follows some deterministic trajectory, on top of which the discrete evolution steps cause stochastic fluctuations of order $\sqrt{\Omega}$. Therefore, we make the Ansatz $X(t) = \Omega\psi(t) + \sqrt{\Omega}\xi$. $\psi(t)$ describes the deterministic trajectory of X, whereas the random variable ξ expresses the intrinsic noise, causing the stochastic fluctuations, and is associated with the probability distribution $\pi(\xi,t) = P(\Omega\psi + \sqrt{\Omega}\xi, t)$.

Defining $\bar{\alpha}(\psi) = \frac{\alpha(\Omega\psi)}{\Omega}$ (and analogously $\bar{\beta}(\psi)$), we get $\dot{\psi} = \bar{\alpha}(\psi)$, which is the known deterministic part of the development of X. To describe the fluctuations distribution $\pi(\xi,t)$, apply the chain rule to the left hand side of eq. (3.5) and use $\frac{\partial}{\partial X} = \frac{1}{\sqrt{\Omega}}\frac{\partial}{\partial \xi}$ to get

$$\frac{\partial}{\partial t}\pi(\xi,t) = -\frac{\partial}{\partial \xi}\left[\sqrt{\Omega}\left(\bar{\alpha}(\psi + \frac{\xi}{\sqrt{\Omega}}) - \bar{\alpha}(\psi)\right)\pi(\xi,t)\right] + \frac{1}{2}\frac{\partial^2}{\partial \xi^2}\left[\bar{\beta}(\psi + \frac{\xi}{\sqrt{\Omega}})\pi(\xi,t)\right] . \tag{3.6}$$

Finally, since $\xi \ll \sqrt{\Omega}$, a Taylor expansion of $\bar{\alpha}$ and $\bar{\beta}$ gives the following Fokker-Planck equation for the fluctuations distribution $\pi(\xi,t)$:

$$\frac{\partial}{\partial t}\pi(\xi,t) = -\bar{\alpha}'(\psi)\frac{\partial}{\partial \xi}\left[\xi\pi(\xi,t)\right] + \frac{1}{2}\bar{\beta}(\psi)\frac{\partial^2}{\partial \xi^2}\left[\pi(\xi,t)\right] . \tag{3.7}$$

Solving this equation, we can determine the distribution of X around its deterministically expected behavior.

3.1.3 Dichotomous Markov Noise

As the name might suggest, the Dichotomous Markov Noise $\xi(t)$ is a two-valued, stochastic, Markov process. Specifically, ξ instantaneously switches from a value A_+ to A_- at a constant rate ν_+ and back to A_+ at rate ν_-. Thus, the probability $P_\pm(t)$ that, at time t, ξ is at $A_\pm$ obeys the master equation

$$\frac{d}{dt}P_\pm(t) = \nu_\mp P_\mp(t) - \nu_\pm P_\pm(t) , \tag{3.8}$$

with stationary solution $P_\pm = \nu_\mp/(\nu_+ + \nu_-)$.

Consider, in particular, the symmetric version of the process: $\nu_+ = \nu_- =: \nu$, $A_+ = -A_-$. In this case, the stationary average is $\langle\xi(t)\rangle = 0$ and the autocorrelation function is

$$\langle\xi(t)\xi(t')\rangle \propto e^{-2\nu|t-t'|} . \tag{3.9}$$

The finite autocorrelation time $\tau_c = 1/(2\nu)$ means that such noise is *colored*, and thus adds a fundamental time scale to the system.

The Dichotomous Markov Noise is a relatively simple process, but it often suffices to study the effects of finite noise correlations. Moreover, the Dichotomous Markov Noise can be treated analytically (see Refs. [89, 90] and also references therein); while its homogeneous rates, finite support, and discrete state space make for a simple implementation. At the same time, the associated dynamics, and the interactions between time scales can create interesting effects, such as noise induced transitions (see following section).

3.1.4 Solving dichotomous flows and noise-induced transitions

Introducing noise source in a system can bring about macroscopically observable states that are not present in the noiseless system. The appearance of these new states is called a *noise-induced transition* [90].

Consider for example a quantity $y(t)$ which obeys the following *dichotomous flow* [89]:

$$\dot{y}(t) = f\left(y(t)\right) + h\left(y(t)\right)\xi(t)\,, \tag{3.10}$$

where $f(y)$ and $h(y)$ are deterministic functions, and $\xi(t)$ is some Dichotomous Markov Noise with states $A_\pm$ and transition rates $\nu_\pm$. This is also called a piecewise deterministic Markov process, since y evolves deterministically between the stochastic switches of ξ. The probability $P_\pm(y,t)$ of a value y and $\xi = A_\pm$ at time t can be proven to follow the master equation [90]

$$\frac{\partial}{\partial t}P_\pm(y,t) = -\frac{\partial}{\partial y}\left[(f(y) + A_\pm h(y))P_\pm(y,t)\right] + \nu_\mp P_\mp(y,t) - \nu_\pm P_\pm(y,t)\,. \tag{3.11}$$

In the case that $\xi(t)$ is symmetric ($\nu_+ = \nu_- = \nu$), with $A_+ = -A_- = 1$, we can then derive the following equations for $p(y,t) := P_+(y,t) + P_-(y,t)$ and $q(y,t) = P_+(y,t) - P_-(y,t)$:

$$\frac{\partial}{\partial t}p(y,t) = -\frac{\partial}{\partial y}\left[f(y)p(y,t) + h(y)q(y,t)\right] \tag{3.12}$$

$$\frac{\partial}{\partial t}q(y,t) = -\frac{\partial}{\partial y}\left[f(y)q(y,t) + h(y)p(y,t)\right] - 2\nu q(y,t)\,. \tag{3.13}$$

Using these equations, one can find the stationary distribution $p^*(y,t)$ of values of y (averaged over ξ) (see Ref.[90] for details):

$$p^*(y,t) \propto \frac{h(y)}{h^2(y) - f^2(y)} \exp\left[2\nu \int^y dy' \frac{f(y')}{h^2(y') - f^2(y')}\right]\,. \tag{3.14}$$

This distribution has a finite support, with boundaries $y_\pm$ given by the solutions of $f(y_\pm) = \pm h(y_\pm)$ [90].

The peaks of p^* are in general independent of the fixed points of the deterministic dynamics. As a result, the system may end up spending long times in the vicinity of points that are not deterministic fixed points. The stochastic switching, in this case, produces a macroscopic behavior that would not be observable otherwise, and a noise-induced transition occurs.

3.2 Coupled fluctuations shape the evolution of populations

Unpredictable environments are an important part of many natural settings, especially for bacteria. This project focused on the coupled effect of this noise source and demographic fluctuations. Specifically, we let the abundance of resources in the environment fluctuate, thus affecting the population size, which tunes the amplitude of demographic noise.

Research question: ***How do environmental and demographic fluctuations intertwine to determine the development of population?***

The effects we consider span several distinct time scales: environmental change, population growth (and decay), and internal fixation. By leveraging the separation between these time scales, we were able to analyze the effects of the different noise sources separately, then combine them. As reported in the publication reprinted in Section 3.3, and in the manuscript in Section 3.4, this allowed us to conclude that

Fluctuating environments shape population size distributions and promote the survival of slow-growing strains.

3.2.1 The coupled noise model

We consider a population of fluctuating size $N(t)$, composed of N_F individuals of a strain F, and N_S of a slower-growing strain S, corresponding to a fraction $x(t) = N_S(t)/N(t)$.

We assume F-individuals have fitness $f_F = 1$, and S-individuals have a lower $f_S = (1-s)$. $s \ll 1$ represents the selective disadvantage of the slower strain—for example the metabolic cost of public good production (see Section 2.2.3). The average fitness is $\langle f\rangle = xf_S + (1-x)f_F = 1 - sx$. Moreover, a global fitness $g(x)$ acts on the population as a whole [53–56], taking into account the effect on growth of the internal social interaction.

Both strains compete for limited resources, encoded in a finite carrying capacity K, which regulates the death rate. Altogether, birth and death events for strain $\alpha \in \{S, F\}$ occur stochastically, with per-capita rates

$$\begin{aligned} \Gamma_\alpha^+ &= g(x)\frac{f_\alpha}{\langle f \rangle}\,, \\ \Gamma_\alpha^- &= \frac{N(t)}{K}\,. \end{aligned} \tag{3.15}$$

In our research we focused on two main scenarios for the social dynamics inside the population:

1. A *pure competition scenario*: $g(x) = 1$. In this case, individuals have no real interaction, instead they simply compete for limited resources. The global growth rate is independent of the relative abundance of strains;

2. A *public good scenario*, for which $g(x) = 1 + bx$. In this case, the slow strain provides a public good that accelerates growth. A parameter b defines the benefit from the public good. The more S-individuals in the population, the faster the global growth rate.

In the deterministic limit (with neither environmental nor demographic noise), this dynamics is reflected by the equations

$$\begin{aligned} \dot{N} &= N\left(g(x) - \frac{N}{K}\right)\,, \\ \dot{x} &= -sg(x)\frac{x(1-x)}{1-sx}\,. \end{aligned} \tag{3.16}$$

When $g = 1$ (pure competition case), the deterministic dynamics of N and x are decoupled. The time scales of the two variables are actually sharply separated: N typically changes in times of order 1, while x moves at a much slower $1/s$. Indeed, the distribution of N equilibrates much faster than that of x. This time scale separation will become very useful for our analysis.

The environmental noise acts by changing the abundance of resources in time: $K = K(t)$. Specifically, resources switch abruptly between a state of scarcity $K = K_- \gg 1$ and one of abundance $K = K_+ > K_-$, following a Dichotomous Markov Noise $\xi(t) \in \{-1, 1\}$ with $\nu_+ = \nu_- = \nu$. Therefore we can write

$$K(t) = \frac{K_+ + K_-}{2} + \xi(t)\frac{K_+ - K_-}{2}\,. \tag{3.17}$$

With a little algebra, we can see that the effect of this *environmental noise* is to make the population obey a piecewise deterministic Markov process defined through:

$$\begin{aligned} \dot{x} &= -sg(x)\frac{x(1-x)}{1-sx}\,, \\ \dot{N} &= N\left(g(x) - \frac{N}{\mathcal{K}} + \xi\frac{N(K_+ - \mathcal{K})}{\mathcal{K}K_+}\right)\,, \end{aligned} \tag{3.18}$$

where $\mathcal{K} = 2K_+K_-/(K_+ + K_-)$ is the harmonic mean of K_+ and K_-. In other words—if we only consider the effect of environmental noise—K switches between the values $K_\pm$, and between switching events, N grows or decays deterministically following the appropriate logistic growth.

When considering also demographic fluctuations (internal noise), their magnitude will be coupled to the environmental noise: The environmental switching drives the change in population size, which in turn tunes the amplitude of demographic fluctuations.

3.2.2 Stationary distribution of population size

In the pure competition scenario ($b = 0$), or after fixation ($x \in \{0, 1\}$), N and x dynamics decouple. Using the properties of dichotomous flows (see Section 3.1.4 and Refs. [90, 91]), we can describe the effect of environmental noise on the population size in this situation. The probability $p(N, \xi; t)$ of the size being N while the environment is in the state $\xi = \pm 1$ at time t obeys the master equation

$$\frac{\partial}{\partial t}p(N,\xi,t) = -\frac{\partial}{\partial N}\left[N\left(1 + q - \frac{N}{\mathcal{K}}\right)p(N,\xi,t)\right] - \nu\left[p(N,\xi,t) - p(N,-\xi,t)\right]\,, \tag{3.19}$$

where q is either equal to b (when $x = 1$ in the public good scenario) or equal to 0 (in the pure competition case or when fixation to $x = 0$). From eq. (3.19), we obtained the joint distribution $p^*_{\nu,q}(N, \xi)$ (see manuscript in Section 3.4), as well as the stationary distribution of the population size

$$p^*_{\nu,q}(N) = \frac{\mathcal{Z}_{\nu,q}}{N^2}\left[\frac{(K_+(1+q)-N)\,(N-K_-(1+q))}{N^2}\right]^{\frac{\nu}{1+q}-1}, \tag{3.20}$$

where $\mathcal{Z}_{\nu,q}$ is a normalization constant. Dashed blue lines in Figure 3.3 represent the predictions of this equation for several values of ν in the pure competition case. They capture well the main features of the distributions measured in simulations (green shaded areas).

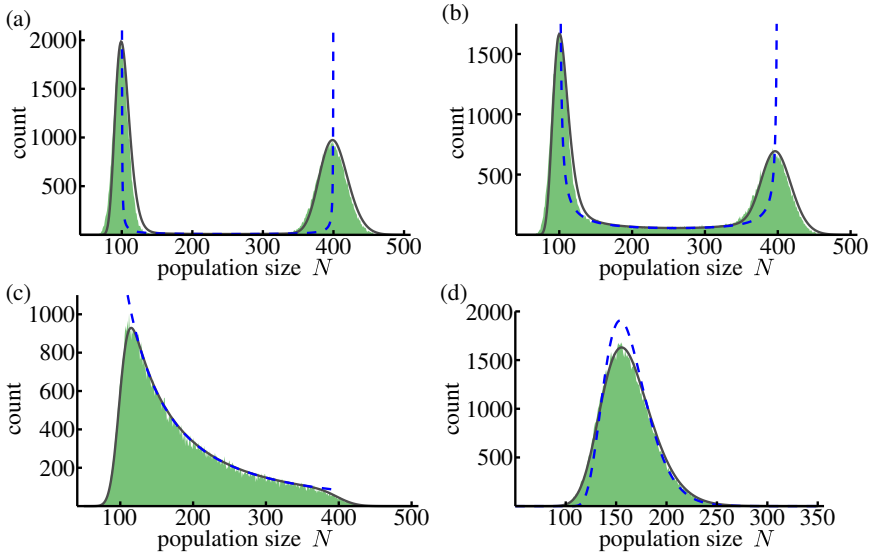

Figure 3.3: *Distribution of population sizes at different switching rates* ($\nu = 0.01$ in panel (a), $\nu = 0.1$ in panel (b), $\nu = 1$ in panel (c), $\nu = 10$ in panel (d), $K_\pm = (100, 400)$ in all). Green shaded areas denote the results of simulations. Only considering the environmental noise (eq. (3.20), blue dashed lines) allows to capture the main features of the distribution, such as number and position of peaks, identifying the noise-induced transition. For a complete description of the distribution, we need to include demographic fluctuations with a linear noise approximation of eq. (3.22, gray solid lines).

By its very construction, however, eq. (3.20) only accounts for the effect of environmental noise, so it cannot be expected to fully predict the size distribution. For example, while the support of $p^*_{\nu,q}$ is only the interval $(K_-(1+q), K_+(1+q))$, demographic fluctuations take real populations above or below those values. As a result, size distributions in simulations are smoother and have broader peaks than predicted using dichotomous flows (see shaded areas in Figure 3.3). To describe these fluctuations, we use a linear noise approximation [87, 88, 92] (see Section 3.1.2, and also the manuscript in Section 3.4). Call $n(t)$ the deterministic term of N and $\eta(t)$ the fluctuating part, scaled by a large parameter Ω (for example, $\Omega \sim 1/2(K_+ + K_-)$). Notice that, differently from the traditional linear noise approximation, in this case the "deterministic part" is actually driven by the environmental noise.

Combining the results from the linear noise approximation and the dichotomous flow, we obtain the equation of motion for the joint distribution $\pi(n, \eta, \xi; t)$ [92]:

$$\begin{aligned}\frac{\partial}{\partial t}\pi(n,\eta,\xi;t) \;=\; & -\frac{\partial}{\partial \eta}\left[\eta\left(1+q-2\frac{n}{k_\pm}\right)\pi(n,\eta,\xi;t)\right] + \frac{n}{2}\left(1+q+\frac{n}{k_\pm}\right)\frac{\partial^2}{\partial \eta^2}\pi(n,\eta,\xi;t) + \\ & -\frac{\partial}{\partial n}\left[n\left(1+q-\frac{n}{k_\pm}\right)\pi(n,\eta,\xi;t)\right] - \nu\left[\pi(n,\eta,\xi;t) - \pi(n,\eta,-\xi;t)\right].\end{aligned} \tag{3.21}$$

The first two terms correspond to the traditional Fokker-Planck equation for the fluctuations in the linear noise approximation, while the last two describe the dichotomous flow. We also write $\pi^*(n, \eta, \xi) = \pi^*(\eta|n, \xi)p^*_{\nu,q}(n, \xi)$

and assume that, given a value for n, fluctuations are independent of the environmental state [92]: $\pi^*(\eta|n,\xi=1)=\pi^*(\eta|n,\xi=-1)=:\pi^*(\eta|n)$. Thereby we can determine that a Gaussian distribution of mean 0 and variance n is a solution of eq.(3.21). With this we can compute the full distribution of population sizes $P^*_{\nu,q}(N)$. In essence, the probability of having a size N is given by the sum of the probabilities of getting to N through all possible combinations of deterministic behaviors and demographic fluctuations, summed over all possible environmental states:

$$P^*_{\nu,q}(N)=\mathcal{Z}\sum_{\xi=\pm1}\int\int dnd\eta\,\pi^*(\eta|n)p^*_{\nu,q}(n,\xi)\delta\left(N-\Omega n-\sqrt{\Omega}\eta\right), \tag{3.22}$$

where $\mathcal{Z}$ is the normalization constant. As Figure 3.3 shows, eq. (3.22) predicts almost exactly the distribution of population sizes measured in simulations.

The same approach applies to obtain the stationary distributions for $b>0$. From eq. (3.22) we can obtain the size distributions conditioned on fixation to S (taking $q=b$) and on fixation to F (taking $b=0$). Measuring the fixation probability of the slow strain (or using the effective theory presented in Section 3.2.5), we can combine the two conditional distributions to obtain the marginal P^*_ν, see Figure 3.5(c,d) (see also Manuscript in Section 3.4).

3.2.3 Noise-induced transition in population size distributions

Equation (3.20) highlights an important consequence of the environmental noise: if the exponent is negative, the distribution is bimodal, U-shaped, with singularities at $K=K_\pm(1+q)$; when the exponent is positive, the distribution becomes unimodal, with a single peak around $\mathcal{K}(1+q)$. So in each social scenario different distribution shapes arise.

Pure competition scenario: two regimes In the pure competition scenario, the transition point is $\nu\simeq1$ and the regimes can be intuitively interpreted by looking at equation (3.18):

(1) *One peak* for $\nu>1$ (see Figure 3.3 (d)). In this case, the environment changes faster than the typical population growth timescale. For $\nu\gg1$, in particular, the noise term in equation (3.18) self-averages to $\langle\xi\rangle=0$. This transforms the dynamics to a new logistic growth with carrying capacity $\mathcal{K}$. As a result, populations fluctuate around $\mathcal{K}$ and produce a *unimodal distribution*.

(2) *Two peaks* for $\nu<1$ (see Figure 3.3 (a,b)). In this case, the environmental switching is infrequent, so N has time to reach the appropriate carrying capacity following each change. Most likely, then, the population size fluctuates around the current carrying capacity, producing the observed *bimodal distribution*.

It is important to note that, without noise, the dynamics only has stable fixed points at $N=K_\pm$; the fixed point at $N=\mathcal{K}$ appearing for high ν is only present with noise. The transition we observe at $\nu\sim1$, therefore, is a veritable noise-induced transition.

Public good case: three regimes In the public good case, after fixation, we observe a more articulate dynamics. In fact, now we must set $q=0$ if the population fixates to strain F and $q=b$ if it fixates to S. So the transition point is different depending on the surviving strain: following a fixation to F, then, the regime changes at $\nu\simeq1$, while for an S-fixation, it changes around $\nu\simeq1/(1+b)$. As a result, the overall (marginal) size distribution has three regimes:

(1) *Two peaks* for $\nu>1+b$, when both conditional distributions (conditioned to S- and F-fixation) are unimodal.

(2) *Three peaks* for $1<\nu<1+b$, when the S-conditional distribution is bimodal and the F-conditional one is unimodal.

(3) *Four peaks* for $\nu<1$ when both conditional distributions are bimodal.

3.2.4 Fixation properties in the pure competition scenario

Without demographic fluctuations, fixations are impossible. So, to study the fixation properties of the population, we must combine environmental and internal noise. In this case, we account for demographic fluctuations using the fitness-dependent Moran model [57, 86] (see Section 3.1.1). Having constant size, this model is completely unaffected by the type of environmental change we consider, but maintains all the internal stochasticity.

We began by considering the pure competition scenario ($b = 0$, and $g(x) \equiv 1$), in which the deterministic dynamics of N and x are decoupled. Moreover, different noise sources drive their dynamics: N responds to environmental noise, x to internal fluctuations. Fixations also typically occur after a time of order $1/s$; by then, not only N has reached its equilibrium distribution but it also has sampled much of it. We can then compute the fixation probability ϕ of the slow strain by averaging the result from the Moran model over the equilibrium size distribution. Thus we combine the two noise sources.

Accounting for the environmental noise, however, requires an additional step. Consider, for example the case $s \ll \nu < 1$: the population size switches between carrying capacities $\nu/s \gg 1$ times (on average) before fixation. As a result, the fixation properties "feel" the effect of both conditions, as if the environmental noise self-averaged. When considering fixations, then, whether an environment changes "frequently" or "infrequently" depends on the relation between its autocorrelation time scale $1/\nu$ and the fixation time scale $1/s$. We estimate the fixation probability for the slow strain by averaging the fixed-size value $\phi|_N$ over an equilibrium distribution of N with the rescaling $\nu \to \nu/s$:

$$\phi(\nu) \simeq \int_{K_-}^{K_+} dN p^*_{\nu/s}(N)\phi|_N \,. \tag{3.23}$$

This accounts for the average number of environmental changes experienced by the population before fixation, and relates the environmental time scale directly to the one of fixations. In the limits $\nu \to 0$ and $\nu \to \infty$, the system reduces to a logistic growth and eq. (3.23) yields the correct results: $\phi(0) = 1/2(\phi|_{K_-} + \phi|_{K_+})$ and $\phi(\nu \to \infty) \to \phi|_{\mathcal{K}}$. As Figure 3.4 shows, the formula in eq. (3.23) also correctly predicts the nontrivial dependence of fixation probabilities on the environmental switching rate across a vast range of ν and s. In fact, the predicted values (solid lines) follow the smooth transition between the "slow environment" ($\nu \ll s$) and "fast environment" regimes ($\nu \gg s$).

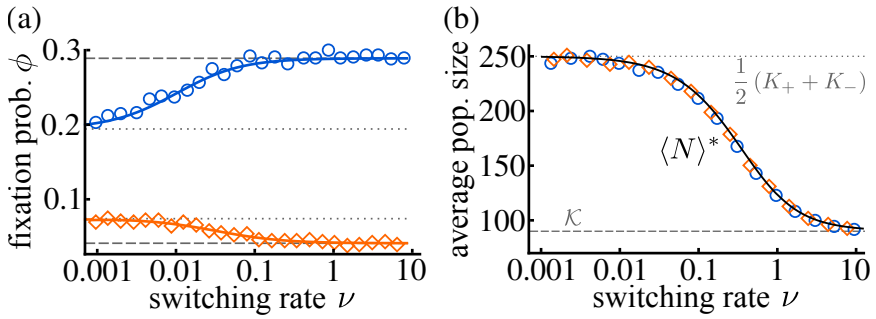

Figure 3.4: *Fixation probability and average population size as function of the switching rate* ν, for $s = 0.02$ ($\circ$, blue) and $s = 0.07$ ($\diamond$, orange), solid lines denote the predictions of eq. (3.23), symbols the results of simulations (other parameters: $K_+ = 450$, $K_- = 50$, $x_0 = 0.5$). **(a)** The fixation probability ϕ of the slow strain may increase or decrease with ν, depending on the strength of selection. **(b)** The average population sizes collapse on the curve (solid line) obtained by averaging N over eq. (3.20). Although the average population size always decreases in ν, this does not automatically translate into an increased fixation probability. Reprinted from Ref. [93].

Interestingly, one would expect smaller average populations to be related to larger fluctuations and thus yield higher probability for the slow strain to fixate. However, Figure 3.4 shows this is not always the case: while the average size $\langle N \rangle^*$ is monotonically decreasing in ν (and independent of s), the fixation probability does not always increase correspondingly. In fact, $\phi(\nu)$ is increasing for low s and decreasing for high s. This suggests more complex effects at play than what can be captured only considering average population sizes (see Section 2.2 of the publication's Supplemental Material for details). Finally, note that for all values of ν, $\phi(\nu) > \phi|_{\langle K \rangle}$: the slow strain has a much higher probability of fixating than it would in a constant environment with the same average carrying capacity.

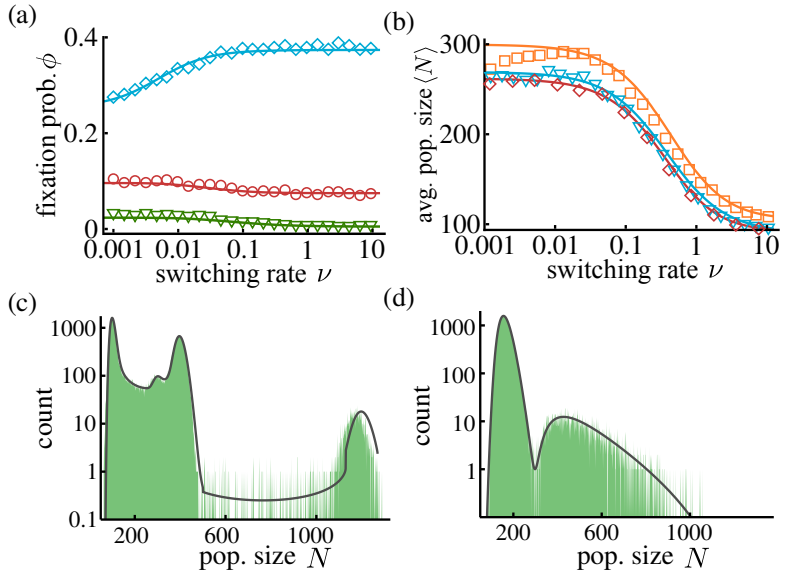

Figure 3.5: *Results of the effective approach* **(a)** $\phi(\nu)$, for $b = 0.2$, $s = 0.01$ ($\diamond$, blue); $b = 0.2$, $s = 0.05$ ($\circ$, red); $b = 2$, $s = 0.05$ (0.05,2)(∇ green), solid lines are predictions from eq. (3.24). Both increasing b and increasing s reduce the probability for the slow strain to fixate. **(b)** Average population size $\langle N \rangle$ as function of ν for $(s, b) = (0.025, 2)$ ($\square$, orange), $(0.05, 2)$ (∇, blue), $(0.025, 8)$ ($\diamond$, red). Solid lines are obtained averaging N over the appropriate versions eq. (3.20), then combining these conditional results via eq. (3.24). **(c),(d)** Size distributions for $\nu = 0.1$ (panel c), $\nu = 20$ (panel d). Theoretical predictions (gray lines) are obtained combining the results of eq. (3.22) using the fixation probability from eq. (3.24). In all panels $(K_+, K_-, x_0) = (450, 50, 0.5)$.

3.2.5 An effective approach to fixations in the public good scenario

In the public good scenario ($b > 0$), even the deterministic dynamics of N and x are coupled. This clearly breaks the time scale separation we relied upon to calculate the fixation properties in the pure competition case.

So, to calculate an approximate fixation probability, we adopted an effective approach. We know that, after fixation, the equilibrium distribution of N is given by eq. (3.20), with an appropriate choice of q ($q = 0$ if the fast strain F survived, $q = b$ if the slow strain S did). Before fixation occurs, the population size necessarily behaves in an intermediate way between being fully S and fully F. We chose to summarize this behavior as interpolating between the two extremes, and used the corresponding distribution to compute a parametrized fixation probability, analogous to that of eq. (3.23):

$$\phi_{q_{\text{eff}}}(\nu) = \int_{K_-(1+q_{\text{eff}})}^{K_+(1+q_{\text{eff}})} dN p_{\nu/s, q_{\text{eff}}}(N) \phi|_N \,. \tag{3.24}$$

To determine the appropriate value of q_{eff}, we fit the result of this equation to the fixation probability in simulations for $\nu \gg 1 + b$. With this choice, the environmental noise is in the self-averaging regime, further reducing the complexity.

With this heuristic procedure, we obtained a value of q_{eff}, which we then used to predict the fixation probability of the slow strain for all values of ν. This approach accurately predicted ϕ across a vast range of environmental switching rates and for several values of s and b, see Figure 3.5. The fixation probability of eq. (3.24), combined with the known conditional stationary size distributions, allows us to predict the average size $\langle N \rangle$ and the full marginal distribution of N, see Figure 3.5. Eq. (3.24) thus effectively summarizes the complicated intertwining of environmental noise, demographic fluctuations, and social interactions.

3.2.6 Duplicitous role of the public good

The public good accelerates growth and increases the carrying capacity. This also implies that the more benefit it provides (i.e., higher b), the larger the population becomes. As the Moran model suggests, this reduces the

probability that the slow strain fixates. Figure 3.6(a) shows that the fixation probability ϕ actually decreases exponentially in b. So, while the public good is beneficial for the population as a whole, it represents an additional burden to the survival of cooperators.

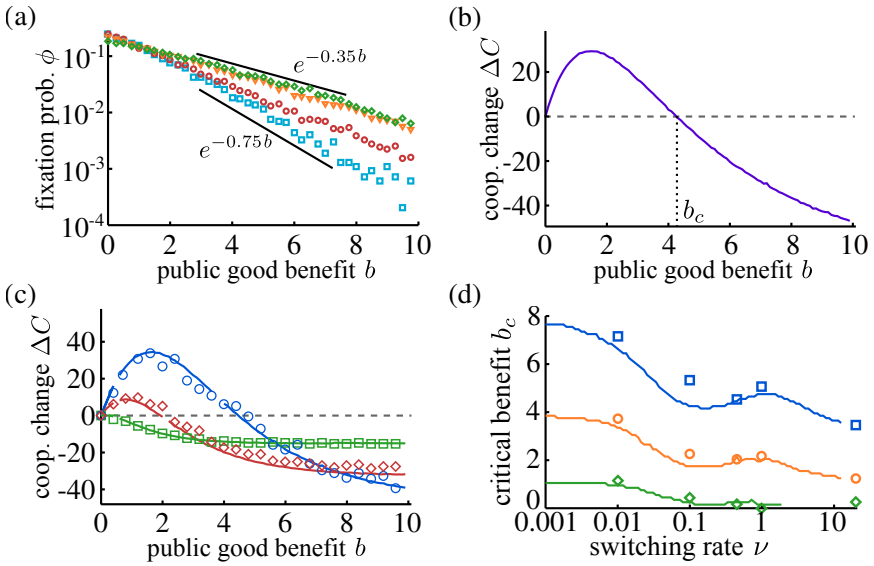

Figure 3.6: *Public good benefit and expected increase in cooperators* (a) The fixation probability of cooperators ϕ decays exponentially with b, because of the larger population size. Parameter values: $s = 0.025$, $\nu = 0.002$ ($\diamond$, green); 0.02 (∇, orange); 0.2 ($\circ$, red); 2 ($\square$, blue). (b) Larger b yields to lower fixation probability, but also larger benefit when cooperators do survive. Therefore the expected number of cooperators increases, compared to the $b = 0$ case ($\Delta C > 0$), as long as b is less than a critical value b_c. (c) For constant ν (here, $\nu \sim 0.44$), $\Delta C(b)$ increases less for higher s. Lines denote the prediction of ΔC obtained using the effective approach of Section 3.2.5. Parameter values: $s = 0.02$ ($\circ$, blue), $s = 0.03$ ($\diamond$, red), $s = 0.05$ ($\square$, green). (d) Critical value of the benefit b_c as function of the switching rate ν. Simulations (symbols) and prediction from the effective theory agree reasonably well. Parameter values: $s = 0.02$ ($\circ$, blue), $s = 0.03$ ($\diamond$, red), $s = 0.05$ ($\square$, green).

However, the higher the benefit, the larger the size difference between the few populations that fixate to S and the others. In other words, b decreases the probability that cooperators survive, but increases the reward when they do. Therefore, the fixation probability may not be the best metric for the success of the slow strain.

We considered how b affects the average number of cooperators in the population. Specifically, we looked for values leading to an increase in the expected number of slow individuals $\Delta C(b) = \langle N|x = 1\rangle|_b - \langle N|x = 1\rangle|_{b=0}$. As Figure 3.6(b,c) show, if b is lower than some value b_c, then $\Delta C > 0$: on average, there are more cooperators in the population than there would be without benefit. Increasing b beyond this threshold value, however, makes the probability that the slow strain fixates overwhelmingly small. The value of b_c depends on the other parameters of the model. As Figure 3.6(d) shows, combining our results on the stationary size distribution (Section 3.2.2) and the effective approach (Section 3.2.5) we can get a numerical prediction of how it changes with, for example, ν.

3.2.7 Consequences and outlook

Our results point to very rich interplay between environmental noise and demographic fluctuations. Because bacterial population were the primary inspiration for the model, an interesting prospect would be to see an experimental realization of the system. Microbial populations, from soil bacteria to the human microbiome, live in constantly changing conditions and variable resources. Experimental realizations of our model could validate our results or expose mechanisms bacteria use to counteract the effects of the variable environment.

3.3 Publication reprint

Evolution of a Fluctuating Population in a Randomly Switching Environment

by

K. Wienand,[1] E. Frey,[1] and M. Mobilia[2]

[1]Department of Physics, Arnold Sommerfeld Center for Theoretical Physics and Center for NanoScience, Ludwig-Maximilians-Universität München, Theresienstraße 37, 80333 München, Germany,
[2] Department of Applied Mathematics, School of Mathematics, University of Leeds, Leeds LS2 9JT, United Kingdom

reprinted from

***Phys. Rev. Lett.* 119, 158301 (2017),**
doi:10.1103/PhysRevLett.119.158301.

Evolution of a Fluctuating Population in a Randomly Switching Environment

Karl Wienand,[1] Erwin Frey,[1] and Mauro Mobilia[2,*]

[1]*Arnold Sommerfeld Center for Theoretical Physics, Department of Physics, Ludwig-Maximilians-Universität München, Theresienstrasse 37, 80333 München, Germany*

[2]*Department of Applied Mathematics, School of Mathematics, University of Leeds, Leeds LS2 9JT, United Kingdom*

(Received 16 June 2017; revised manuscript received 1 August 2017; published 11 October 2017)

Environment plays a fundamental role in the competition for resources, and hence in the evolution of populations. Here, we study a well-mixed, finite population consisting of two strains competing for the limited resources provided by an environment that randomly switches between states of abundance and scarcity. Assuming that one strain grows slightly faster than the other, we consider two scenarios—one of pure resource competition, and one in which one strain provides a public good—and investigate how environmental randomness (external noise) *coupled* to demographic (internal) noise determines the population's fixation properties and size distribution. By analytical means and simulations, we show that these coupled sources of noise can significantly enhance the fixation probability of the slower-growing species. We also show that the population size distribution can be unimodal, bimodal, or multimodal and undergoes noise-induced transitions between these regimes when the rate of switching matches the population's growth rate.

DOI: 10.1103/PhysRevLett.119.158301

Natural populations face ever-changing environmental conditions, which influence their evolutionary fate. For instance, the abundance of nutrients, the presence of toxins, or external factors like temperature and *p*H often influence the evolution of species [1,2]. Several mechanisms have been suggested for a population to cope with fluctuating environments, such as phenotypic heterogeneity, bet hedging, and storing the gains realized during good periods [3–7]. The impact of random environmental changes (external noise) on fitness variability has been studied in population genetics, predator-prey systems, as well as in game-theoretic and related models [8–19]. Demographic fluctuations (internal noise), arising in finite populations, are responsible for fixation—when one species takes over the population [20,21], and determine the population's internal composition. Internal noise is stronger in small populations and becomes negligible in large ones. The dynamics of the population composition is often coupled with the evolution of its size [22–26]. This may result in a coupling of environmental and internal noise, with external randomness affecting the population size, which in turn modulates demographic fluctuations. The interdependence of external and internal noise is especially relevant to microbial communities, which can experience sudden, extreme environmental changes [27–31]. These may lead to population bottlenecks: new colonies or biofilms formed from only few individuals, thus prone to fluctuations. This mechanism leads to feedback loops between social interactions and environment, and to population dynamics of great evolutionary relevance [27–29]. For instance, recent experiments on *Pseudomonas fluorescens* showed that the formation and sudden collapse of biofilms promotes the evolution of cooperative behaviors [30,31].

Most studies, however, treat environmental and internal noise independently [8–19]. Moreover, environmental randomness is often modeled with white noise [8,9,16], although the correlation time is finite in realistic settings. Here, we develop an approach to study the coupled effect of environmental and internal noise on the evolution of a two-species population in a stochastic environment: We assume that the carrying capacity randomly switches between two values, following a dichotomous noise [32,33]. A distinctive feature of this model is the coupling of internal and environmental noise (Fig. 1): Demographic fluctuations depend on the population size that varies following the switching environment. We first consider a scenario with pure resource competition, in which the dynamics of the population composition and its size are only linked by demographic fluctuations. Then, we investigate a public good scenario in which interspecies social interactions

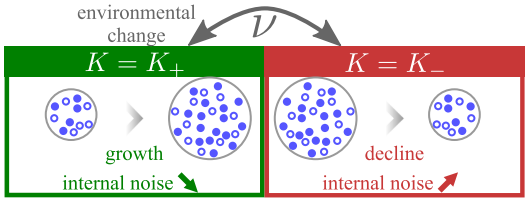

FIG. 1. Cartoon of the model: Coupled evolution of the population size and its composition, consisting of strains S (open circle) and F (filled circle), subject to a stochastically switching carrying capacity $K(t) \in \{K_-, K_+\}$; see Eq. (3). K switches with rate ν from K_- to K_+, leading to population growth and decreasing demographic fluctuations (internal noise). When K switches (with rate ν) from K_+ to K_-, the population size declines and demographic fluctuations increase.

explicitly couple the composition and ecological (size) dynamics. Using analytical and computational means, we show how environmental and internal noise can significantly influence the population's fixation properties. Moreover, we show that external noise induces a transition between different regimes of the population size distribution.

We consider a well-mixed population of finite and time-fluctuating size $N(t) = N_S(t) + N_F(t)$ consisting of two strains. At time t, $N_S(t)$ individuals are of a slow-growing strain S, corresponding to a fraction $x = N_S/N$ of the population, and N_F are of a fast-growing species F. Individuals of strain $\alpha \in \{S, F\}$ reproduce with a per-capita rate $T_\alpha^+ = f_\alpha/\bar{f}$ [23,24], where f_α is the fitness of strain α and $\bar{f} = xf_S + (1-x)f_F$ is the average fitness. Here $f_F = 1$ and $f_S = 1 - s$, where $0 < s \ll 1$ denotes the weak selection intensity that disadvantages the strain S [20]. The population size growth often depends on its composition; e.g., one strain may produce a public good. This is accounted for by multiplying the birth rates T_α^+ by a "global fitness" $g(x)$ [22–24]. Here, we focus on two important cases: (i) pure resource competition: $g(x) = 1$, in this setting x and N are only coupled by fluctuations; and (ii) public good: $g(x) = 1 + bx$, corresponding to an explicit coupling of x and N, where x represents the fraction of "cooperators" producing a public good and enhances the population growth rate through the benefit $0 < b \sim \mathcal{O}(1)$. Both strains compete for limited resources which constrains the population size as encoded by the death rate $T_\alpha^- = N/K$. We consider that in the presence of environmental randomness, K fluctuates stochastically. The population thus follows a multivariate birth-death process [34,35] in which, at each time increment, an individual at random reproduces [with per-capita rate $g(x)T_\alpha^+$], or dies (with per-capita rate T_α^-), or the carrying capacity changes state (with rate ν). The ensuing master equation fully describes the stochastic population dynamics, whose main features are the distribution of N and the probability that S or F fixates by taking over the population, but is difficult to solve [35]. Upon ignoring any form of noise, the population size N and composition x evolve deterministically according to [23,24,36]

$$\dot{N} = N\left(g(x) - \frac{N}{K}\right), \tag{1}$$

$$\dot{x} = -sg(x)\frac{x(1-x)}{1-sx}, \tag{2}$$

where the dot signifies the time derivative. Here, we study the population dynamics subject to a randomly switching carrying capacity (environmental noise) and to stochastic birth and death events (internal noise). We therefore have to account for these sources of noise.

To model environmental randomness, we let the carrying capacity $K(t)$ switch stochastically between a state of abundant resources ($K = K_+$) and one of scarcity ($K = K_- < K_+$). Figure 1 illustrates this stochastic environment and its impact on the population. We consider that environmental switching occurs continuously at rate ν, according to a dichotomous Markov noise $\xi(t) \in \{-1, +1\}$ with zero-mean, $\langle \xi(t) \rangle = 0$ ($\langle \cdot \rangle$ denotes the ensemble average), and autocorrelations $\langle \xi(t)\xi(t') \rangle = \exp(-2\nu|t-t'|)$, where $1/(2\nu)$ is the finite correlation time [32,33]. Hence, the carrying capacity obeys

$$K(t) = \frac{1}{2}[(K_+ + K_-) + \xi(t)(K_+ - K_-)], \tag{3}$$

with average $\langle K \rangle = (K_+ + K_-)/2$. If this is the sole source of noise (no internal noise), the evolution obeys a piecewise deterministic Markov process (PDMP) [18,19,39,40], defined by Eq. (2) and

$$\dot{N} = N\left(g(x) - \frac{N}{\mathcal{K}} + \xi\frac{N(K_+ - \mathcal{K})}{\mathcal{K}K_+}\right), \tag{4}$$

where $\mathcal{K} = 2K_+K_-/(K_+ + K_-)$ is the harmonic mean of K_+ and K_-. Equation (4) is obtained from Eqs. (1) and (3) as shown in the Supplemental Material [36]. Hence, environmental randomness alone yields a multiplicative noise $\propto \xi(K_+ - K_-)N^2$ in Eq. (4). Demographic fluctuations being ignored, x obeys Eq. (2), which is decoupled from N, and evolves on a time scale $\sim 1/s$; see supporting videos [37] and Supplemental Material [36].

Internal noise arises in finite populations when birth and death events occur randomly, and is responsible for fixation. If demographic fluctuations are the only source of noise (say K is constant), the fixation probability ϕ of the strain S can be computed from a fitness-dependent Moran process [20,21,41,42] with the same strain-specific fitnesses as in our model, and constant size $N = K$ [43]. Given an initial fraction x_0 of S individuals, this probability in a population of constant size N is $\phi(x_0)|_N = (e^{-Ns(1-x_0)} - e^{-Ns})/(1 - e^{-Ns})$ [44,45]. Hence, the fixation probability of the slow strain is exponentially small in large size populations. Since the fixation probability clearly depends on x_0, for notational simplicity we henceforth write $\phi \equiv \phi(x_0)$ and $\phi|_N \equiv \phi(x_0)|_N$.

Below, we investigate the *joint* effect of environmental and internal noise on the population dynamics. In particular, since extreme environmental changes can occur more or less rapidly in microbial communities [27–31], we study the influence of the switching rate ν on the species fixation probability and the distribution of N.

(i) The pure resource competition scenario.—When $g = 1$, both species simply compete for limited resources. By the competitive exclusion principle [46], F always prevails in the deterministic limit. In this case, the rate equations (1), (2) are decoupled. However, demographic fluctuations, which drive to fixation, scale with the population size: the *stochastic dynamics* of x is thus coupled with that of N; see Fig. 1. While x relaxes on a slow time scale

$t \sim 1/s$, N reaches a quasistationary state in a time $t = \mathcal{O}(1)$, see supporting videos [37] and Supplemental Material [36]. Equation (4) is associated with a PDMP whose marginal (unconditioned of $\xi = \pm 1$) stationary probability density function (PDF) is [32,36]

$$p_\nu^*(N) = \frac{\mathcal{Z}_\nu}{N^2}\left[\frac{(K_+ - N)(N - K_-)}{N^2}\right]^{\nu-1}, \qquad (5)$$

where $\mathcal{Z}_\nu$ is the normalization constant and the PDF has support $[K_-, K_+]$. Although this PDF only accounts for environmental noise, it captures the main features of the quasistationary distribution of the population size (N-QSD) of the full model when $K_- \gg 1$ [47]. Since x and N evolve on different time scales, the PDF (5) can be combined with $\phi|_N$ to determine the fixation probability. For this, we rescale the switching rate, $\nu \to \nu/s$, to map environmental changes onto the internal dynamics' relaxation time scale, where ν/s is the average number of switches occurring while x relaxes. Indeed, when $\nu \gg s$ (fast switching), many switches occur prior to fixation and the environmental noise self-averages, whereas when $\nu \ll s$ (slow switching) the population is likely to experience solely the carrying capacity K_+ or K_- before one species fixates. The fitness-dependent Moran process gives the fixation probability in those limits. When $\nu \to \infty$, there is self-averaging with $\xi \to \langle\xi\rangle = 0$ in (4) that becomes the logistic equation (1) with $K = \mathcal{K}$, yielding $\phi = \phi|_{\mathcal{K}}$. When $\nu \to 0$, K is equally likely to remain at K_+ or K_- until fixation occurs, yielding $\phi = (\phi|_{K_+} + \phi|_{K_-})/2$. Based on these physical considerations, fully detailed in the Supplemental Material [36], we propose to assume the following expression for the S fixation probability when $0 < s \ll 1$ and $K_- \gg 1$:

$$\phi \simeq \int_{K_-}^{K_+}\left(\frac{e^{-Ns(1-x_0)} - e^{-Ns}}{1 - e^{-Ns}}\right) p_{\nu/s}^*(N)dN. \qquad (6)$$

By averaging the effect of internal noise, given by $\phi|_N$, over the external-noise-induced PDF $p_{\nu/s}^*$, Eq. (6) accounts for the fact that N evolves much faster than x relaxes. The expression (6) reproduces the expected results in the two limiting regimes $\nu \gg s$ and $0 < \nu \ll s$. Moreover, Eq. (6) accurately predicts the stochastic simulation results over a broad range of ν values, capturing the nontrivial ν dependence of ϕ, see Fig. 2(a). We find that ϕ can increase or decrease with ν [36] and, importantly, environmental noise can significantly enhance the S fixation probability in *all* regimes: ϕ is always greater than $\phi|_{\langle K\rangle}$ obtained in a nonrandom environment with $N = \langle K\rangle$ [36].

We have verified that the mean fixation time scales as $\mathcal{O}(1/s)$ [36]. Hence, after a time $t \gtrsim 1/s$, either species likely fixated and, while the population then only consists of S or F, its size keeps fluctuating, see supporting videos [37] and Supplemental Material [36]. Since demographic fluctuations have a marginal influence on the N-QSD when $K_- \gg 1$, the PDF p_ν^* captures its main long-time features;

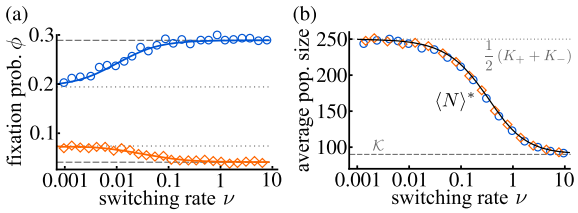

FIG. 2. (a) ϕ vs ν for $(K_+, K_-, x_0) = (450, 50, 1/2)$, with $s = 0.02$ (open circle, blue/black) and $s = 0.07$ (diamond, orange/gray). Symbols are from simulations (10^4 runs). Solid lines are from Eq. (6); dashed and dotted lines show ϕ when $\nu/s \to \infty$ (dashed) and 0, see text. (b) $\langle N\rangle^*$ vs ν. Symbols are from simulations (10^4 runs) with $s = 0.02$ (open circle) and $s = 0.07$ (diamond); they collapse on the curve (solid line) obtained by averaging N over (5); see text.

see Fig. 3. For example, the long-time average population size $\langle N\rangle^*$ is well described by the average over Eq. (5): $\langle N\rangle^* \simeq \int_{K_-}^{K_+} N p_\nu^*(N)dN$, which is independent of s and x_0; see Fig. 2(b). The histograms of Fig. 3 show that the environmental noise causes a *noise-induced* transition of the N-QSD at about $\nu = 1$ [32]. The transition, predicted by p_ν^*, separates regimes in which environmental change is faster or slower than the population's growth rate. For $\nu > 1$, fast switching results in a unimodal N-QSD, see Figs. 3(a), 3(b), whereas for $\nu < 1$, the environment changes slowly and the N-QSD is bimodal, see Figs. 3(c), 3(d) and Ref. [36]. The fast decay and slower growth of N, characteristic of a logistic dynamics, lead the population size to dwell longer about K_- than about K_+. As captured by p_ν^*, this results in right-tailed distributions in Fig. 3. Since Eq. (5) only accounts for external noise, it cannot reproduce some features caused by demographic fluctuations, such as the N-QSD not being strictly confined within the support of p_ν^*

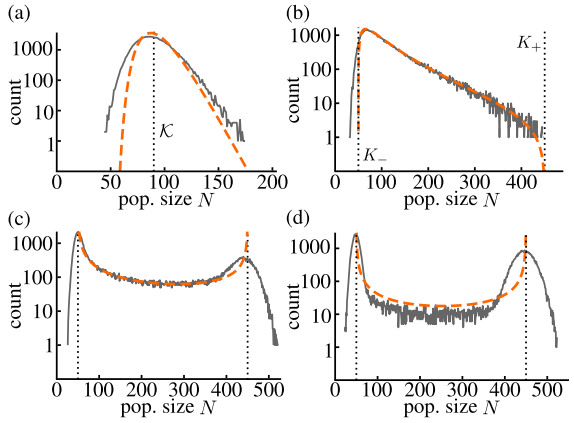

FIG. 3. Histograms of population size (N-QSD) and from p_ν^*, for $\nu = 20$ (a), $\nu = 2$ (b), $\nu = 0.2$ (c), and $\nu = 0.02$. (d) Solid lines result from simulations (10^5 samples, after $t \gtrsim 1/s$). Dashed lines are the corresponding histograms from Eq. (5). Dotted lines show $N = \mathcal{K}$ in (a), and $N = K_\pm$ in (b)–(d). Parameters are $(K_+, K_-, s, x_0) = (450, 50, 0.02, 0.5)$.

[35,36]. However, as Fig. 2 shows, these deviations only marginally affect $\langle N\rangle^*$ and ϕ.

(ii) The public good scenario.—The above approach can be generalized to cover cases where internal and ecological dynamics are explicitly coupled. As an application, we consider a public good scenario in which S is a "cooperative" strain benefiting the population by enhancing the global fitness $g(x) = 1 + bx$ ($b > 0$) and the carrying capacities, see below. The dynamics of x and N are now coupled, breaking the time scale separation: N becomes a fast variable, enslaved to the slowly varying x, see videos 6 and 7 in Ref. [37] and Supplemental Material [36]. After fixation, $x \in \{0, 1\}$ and the N-QSD can be obtained as for $b = 0$. When F fixates ($x = 0$), the N distribution is described by p^*_ν (5). If S fixates ($x = 1$), the population size distribution is captured by $p^*_{\nu,b}$, obtained by substituting $K_\pm \to (1 + b)K_\pm$ and $\nu \to \nu/(1 + b)$ in Eq. (5). Hence, p^*_ν and $p^*_{\nu,b}$ are the PDFs conditioned to fixation of F and S (but unconditioned of ξ), respectively. To address the dynamics before fixation, we approximately account for the correlations between N and x by introducing an effective (constant) parameter $0 \le q \le b$. We then set $g(x) = 1 + q$ in Eq. (4), resulting in a PDMP, decoupled from x, for the size of an effective population whose marginal PDF, $p^*_{\nu,q}$ (see Eq. (S2) in [36]), interpolates between p^*_ν and $p^*_{\nu,b}$. As for $b = 0$, when $0 < s \ll 1$ and $K_- \gg 1$, the S fixation probability in this effective population is [36]

$$\phi_q = \int_{(1+q)K_-}^{(1+q)K_+} \left(\frac{e^{-Ns(1-x_0)} - e^{-Ns}}{1 - e^{-Ns}}\right) p^*_{\nu/s,q}(N)dN. \quad (7)$$

To determine the effective value of q for given $(K_\pm, s, b)$, we consider the limit $\nu \gg 1$, where the environmental noise self-averages, and match the prediction of Eq. (7) with the fixation probability obtained in simulations [36]. As Fig. 4(a) shows, with suitable q, Eq. (7) reproduces the simulation results $\phi_q \simeq \phi$ for a broad range of ν and different values of b.

After $t \gtrsim 1/s$, fixation has typically occurred and the population size distributions (when $K_- \gg 1$) are well described by $p^*_{\nu,b}$ (S fixation) and p^*_ν (F fixation). With these conditional PDFs and ϕ_q, the long-time average population size reads

$$\langle N\rangle^* \simeq \phi_q \int_{(1+b)K_-}^{(1+b)K_+} N p^*_{\nu,b}(N)dN + \tilde{\phi}_q \int_{K_-}^{K_+} N p^*_\nu(N)dN, \quad (8)$$

with $\tilde{\phi}_q = 1 - \phi_q$. Figure 4(b) shows that Eq. (8) agrees well with simulation results, but cannot capture the behavior at very low ν (ϕ_q being inferred at $\nu \gg 1$). The conditional N-QSD and conditional PDFs p^*_ν and $p^*_{\nu,b}$ present unimodal and bimodal regimes. Specifically, after S fixation, N's growth rate is $1 + b$ and the associated PDF $p^*_{\nu,b}$ undergoes a noise-induced transition at $\nu = 1 + b$.

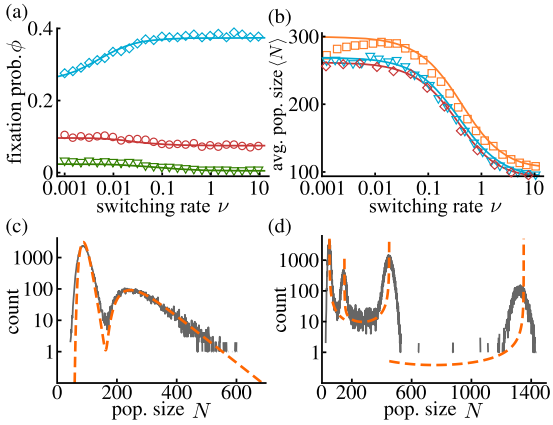

FIG. 4. (a) ϕ vs ν for $(s, b) = (0.01, 0.2)$ (diamond, blue/gray), (0.05,0.2)(open circle, red/black), (0.05,2)(downward triangle, green/dark gray). Solid lines are from Eq. (7). In all panels $(K_+, K_-, x_0) = (450, 50, 0.5)$. (b) $\langle N\rangle^*$ vs ν for $(s, b) = (0.025, 2)$ (square, orange/gray), (0.05,2) (downward triangle, blue/dark gray), (0.025,8) (diamond, red/black). Solid lines are from Eq. (8). (c),(d) Size distributions for $\nu = 20$ (c) and $\nu = 0.02$ (d), with $b = 2$ and $s = 0.02$. Solid and dashed lines are, respectively, histograms from simulations (10^5 replicas, after 99% fixation [36]) and obtained from $p^*_{\nu,b}$ and p^*_ν weighted by ϕ_q, see text.

Similarly, the N's growth rate when F fixates is 1, and p^*_ν undergoes a transition at $\nu = 1$. Since the marginal size distribution is the sum of the conditional distributions weighted by the fixation probability, it is characterized by several regimes and transitions. These properties are well captured by combining $p^*_{\nu,b}$ and p^*_ν weighted by ϕ_q, as shown in Fig. 4. When $\nu > 1 + b$, the switching rate exceeds the population's growth rate, and both conditional PDFs are unimodal with different peaks, yielding a bimodal marginal distribution; see Fig. 4(c). For $1 < \nu < 1 + b$, $p^*_{\nu,b}$ is bimodal and p^*_ν is unimodal. When ν is below the population's growth rate ($\nu < 1$), both conditional PDFs are bimodal. As a result, the marginal size distribution has three peaks when $1 < \nu < 1 + b$ and four peaks when $\nu < 1$; see Fig. 4(d). As for $b = 0$, the influence of demographic fluctuations on the N-QSD is to cause slight deviations from the PDF predictions, particularly at low ν [36].

Motivated by the evolution of microbial communities in volatile environments, we have analyzed the dynamics of a two-species population subject to a randomly switching carrying capacity (dichotomous noise). A distinctive feature of our model is the coupling of the environmental and internal noise: demographic fluctuations depend on the population size, which in turn changes with the varying carrying capacity (environmental noise). By analytical and computational means, we have studied the coupled effect of environmental and internal noise on the population's ecological and fixation properties. Our analytical approach is based on a time scale separation, arising under weak

selection, between the ecological and internal dynamics. We have also combined the properties of suitable stochastic processes governed solely by internal fluctuations on one hand, and only by environmental noise on the other hand. In the case of pure resource competition (no explicit coupling between internal and ecological dynamics), we have determined the population size distribution, characterized by various regimes, and found that the average size decreases with the switching rate. Assuming a suitable expression for the fixation probability and using stochastic simulations, we have investigated how environmental randomness affects the strains' fixation properties and found that it can significantly enhance the fixation probability of the disadvantaged strain. As an application, we have considered a public good scenario in which internal and ecological dynamics are explicitly coupled. We have thus devised an effective theory that has allowed us to probe the effects of environmental switching and public good benefit on the fixation probability and population composition. We have characterized the population size distribution and the noise-induced transitions between their unimodal (fast switching), bimodal, and multimodal forms, arising when the switching rate matches that of the population growth. Our findings show that coupled environmental and demographic noise can significantly influence the population dynamics by greatly affecting its fixation properties and therefore its composition. This is particularly relevant to microbial communities, which often feature connected internal and ecological evolution.

E. F. acknowledges funding by the Deutsche Forschungsgemeinschaft, Priority Programme 1617 "Phenotypic heterogeneity and sociobiology of bacterial populations," Grant No. FR 850/11-1,2, and the German Excellence Initiative via the program "Nanosystems Initiative Munich" (NIM). M. M. is grateful for the support of the Alexander von Humboldt Foundation, Grant No. GBR/1119205 STP, and for the hospitality of the University of Munich.

*M.Mobilia@leeds.ac.uk

[1] C. R. Morley, J. A. Trofymow, D. C. Coleman, and C. Cambardella, Microbiol. Ecol. **9**, 329 (1983).
[2] C. A. Fux, J. W. Costerton, P. S. Stewart, and P. Stoodley, Trends Microbiol. **13**, 34 (2005).
[3] P. L. Chesson and R. R. Warner, Am. Nat. **117**, 923 (1981).
[4] E. Kussell, R. Kishony, N. Q. Balaban, and S. Leibler, Genetics **169**, 1807 (2005).
[5] M. Acer, J. Mettetal, and A. van Oudenaarden, Nat. Genet. **40**, 471 (2008).
[6] H. Beaumont, J. Gallie, C. Kost, G. Ferguson, and P. Rainey, Nature (London) **462**, 90 (2009).
[7] P. Visco, R. J. Allen, S. N. Majumdar, and M. R. Evans, Biophys. J. **98**, 1099 (2010).
[8] R. M. May, *Stability and Complexity in Model Ecosystems* (Princeton University Press, Princeton, NJ, 1973).
[9] S. Karlin and B. Levikson, Theor. Popul. Biol. **6**, 383 (1974).
[10] E. Kussell and S. Leibler, Science **309**, 2075 (2005).
[11] M. Assaf, E. Roberts, Z. Luthey-Schulten, and N. Goldenfeld, Phys. Rev. Lett. **111**, 058102 (2013).
[12] Q. He, M.Mobilia, and U. C. Täuber, Phys. Rev. E **82**, 051909 (2010).
[13] U. Dobramysl and U. C. Täuber, Phys. Rev. Lett. **110**, 048105 (2013).
[14] M. Assaf, M. Mobilia, and E. Roberts, Phys. Rev. Lett. **111**, 238101 (2013).
[15] P. Ashcroft, P. M. Altrock, and T. Galla, J. R. Soc. Interface **11**, 20140663 (2014).
[16] A. Melbinger and M. Vergassola, Sci. Rep. **5**, 15211 (2015).
[17] M. Danino, N. M. Shnerb, S. Azaele, W. E. Kunin, and D. A. Kessler, J. Theor. Biol. **409**, 155 (2016).
[18] P. G. Hufton, Y. T. Lin, T. Galla, and A. J. McKane, Phys. Rev. E **93**, 052119 (2016).
[19] J. Hidalgo, S. Suweis, and A. Maritan, J. Theor. Biol. **413**, 1 (2017).
[20] J. F. Crow and M. Kimura, *An Introduction to Population Genetics Theory* (Blackburn Press, New Jersey, 2009).
[21] W. J. Ewens, *Mathematical Population Genetics* (Springer, New York, 2004).
[22] J. Roughgarden, *Theory of Population Genetics and Evolutionary Ecology: An Introduction* (Macmillan, New York, 1979).
[23] A. Melbinger, J. Cremer, and E. Frey, Phys. Rev. Lett. **105**, 178101 (2010).
[24] J. Cremer, A. Melbinger, and E. Frey, Phys. Rev. E **84**, 051921 (2011).
[25] A. Melbinger, J. Cremer, and E. Frey, J. R. Soc. Interface **12**, 20150171 (2015).
[26] J. S. Chuang, O. Rivoire, and S. Leibler, Science **323**, 272 (2009).
[27] L. M. Wahl, P. J. Gerrish, and I. Saika-Voivod, Genetics **162**, 961 (2002).
[28] K. Wienand, M. Lechner, F. Becker, H. Jung, and E. Frey, PLoS One **10**, e0134300 (2015).
[29] Z. Patwas and L. M. Wahl, Evolution **64**, 1166 (2009).
[30] M. A. Brockhurst, A. Buckling, and A. Gardner, Curr. Biol. **17**, 761 (2007).
[31] M. A. Brockhurst, PLoS One **2**, e634 (2007).
[32] W. Horsthemke and R. Lefever, *Noise-Induced Transitions* (Springer, Berlin, 2006).
[33] I. Bena, Int. J. Mod. Phys. B **20**, 2825 (2006).
[34] C. W. Gardiner, *Handbook of Stochastic Methods* (Springer, New York, 2002).
[35] K. Wienand, E. Frey, and M. Mobilia (to be published).
[36] See Supplemental Material at http://link.aps.org/supplemental/10.1103/PhysRevLett.119.158301 for the derivation of Eqs. (1), (2), (4), (6), and (7), mean fixation time results, complements to Figs. 3 and 4, and for the description of the supporting videos of Ref. [37]. The Supplemental Material includes Ref. [38].
[37] K. Wienand, E. Frey, and M. Mobilia, figshare. Supporting videos are electronically available at the following URL: https://doi.org/10.6084/m9.figshare.5082712.
[38] D. T. Gillespie, J. Comput. Phys. **22**, 403 (1976).
[39] K. Kitahara, W. Horsthemke, and R. Lefever, Phys. Lett. **70A**, 377 (1979).

[40] M. H. A. Davis, J. R. Stat. Soc. Ser. B **46**, 353 (1984).
[41] P. A. P. Moran, *The Statistical Processes of Evolutionary Theory* (Clarendon, Oxford, 1962).
[42] T. Antal and I. Scheuring, Bull. Math. Biol. **68**, 1923 (2006).
[43] S. P. Otto and M. C. Whitlock, Genetics **146**, 723 (1997).
[44] R. A. Blythe and A. J. McKane, J. Stat. Mech. (2007) P07018.
[45] J. Cremer, T. Reichenbach, and E. Frey, New J. Phys. **11**, 093029 (2009).
[46] G. Hardin, Science **131**, 1292 (1960).
[47] A finite population unavoidably collapses into $(N,x)=(0,0)$. This phenomenon, unobservable when $K_- \gg 1$, occurs after lingering in a quasistationary state well described by the N-QSD and p_ν^*.

Supplemental Material for

Evolution of a Fluctuating Population in a Randomly Switching Environment

Karl Wienand*, Erwin Frey*, and Mauro Mobilia†

In this Supplemental Material, we provide some technical details and supplementary information in support of the results discussed in the main text, as well as additional ones concerning the population's mean fixation time and its long-time distribution. We also comment the content of electronically available Videos [1] that illustrate the population dynamics in the pure resource competition and public good scenarios. In what follows, unless otherwise stated, the notation is the same as in the main text and the equations and figures refer to those therein. (As in the main text, unless stated otherwise, below we tacitly assume $x_0 = 1/2$.)

1 Derivation of Equations (1,2) and (4)

As explained in the main text, the population dynamics is governed by multivariate birth-death process in which at each time increment an individual of species $\alpha \in \{S, F\}$ is picked for reproduction, $N_\alpha \to N_\alpha + 1$, with transition rate $\mathcal{T}_\alpha^+ = T_\alpha^+ N_\alpha = g(x) f_\alpha N_\alpha / \bar{f}$ or death, $N_\alpha \to N_\alpha - 1$, with transition rate $\mathcal{T}_\alpha^- = T_\alpha^- N_\alpha = (N/K) N_\alpha$, or the carrying capacity is switched, $K_+ \leftrightarrow K_-$, with rate ν. When internal noise is neglected, N and x evolve according to the mean-field rate equations

$$\begin{aligned} \dot{N} &= \sum_{\alpha=S,F} (\mathcal{T}_\alpha^+ - \mathcal{T}_\alpha^-) = N\left(g(x) - \frac{N}{K}\right), \\ \dot{x} &= \frac{\mathcal{T}_S^+ - \mathcal{T}_S^-}{N} - x\frac{\dot{N}}{N} = -s g(x)\, \frac{x(1-x)}{1-sx}, \end{aligned}$$

where we have used $f_F = 1$, $f_S = 1 - s$ and $\bar{f} = 1 - sx$. These equations coincide with (1) and (2) and, when the carrying capacity K is constant, they provide a suitable description of the ecological and evolutionary (composition). The deterministic description of the population dynamics in terms of (1) and (2) is valid only in the absence of internal and external noise.

When the carrying capacity randomly switches according to $K(t) = \frac{1}{2}\left[(K_+ + K_-) + \xi(t)(K_+ - K_-)\right]$, where $\xi \in \{-1, +1\}$ is the dichotomous noise defined in the main text, the equation for N becomes the following stochastic differential equation obtained by substituting $K(t)$ into (1) and using $\xi^2 = 1$:

$$\begin{aligned} \dot{N} &= N\left(g(x) - \frac{2N}{K_+ + K_- + \xi(t)(K_+ - K_-)}\right) = N\left(g(x) - \frac{N}{2K_+K_-}[K_+ + K_- - \xi(t)(K_+ - K_-)]\right) \\ &= N\left(g(x) - \frac{N}{\mathcal{K}} + \xi N\left\{\frac{K_+ + K_-}{2K_+K_-} - \frac{2K_-}{2K_+K_-}\right\}\right) = N\left(g(x) - \frac{N}{\mathcal{K}} + \xi\frac{N(K_+ - \mathcal{K})}{\mathcal{K}K_+}\right), \end{aligned}$$

where $\mathcal{K} = 2K_+K_-/(K_+ + K_-)$. This stochastic differential equation coincides with (4) and, together with (2), defines a piecewise deterministic Markov process (PDMP) [2, 3, 4] describing the population dynamics when the sole form of randomness is the random switching of the carrying capacity (internal noise is neglected).

2 Fixation probability under random switching: Arguments underpinning formula (6) and (7) and their properties

We have studied the fixation probability ϕ that, starting with a fraction x_0 of individuals of the slow type S, the entire population eventually consists of $N(t)$ individuals of species S. The fixation of species F occurs with the complementary probability $\widetilde{\phi} = 1 - \phi$. We have investigated the joint effect of external (dichotomous) and internal

*Arnold Sommerfeld Center for Theoretical Physics, Department of Physics, Ludwig-Maximilians-Universität München, Theresienstrasse 37, 80333 München, Germany. *Email: karl.wienand@physik.lmu.de, Frey@lmu.de*

† Department of Applied Mathematics, School of Mathematics, University of Leeds, Leeds LS2 9JT, U.K. *Email: M.Mobilia@leeds.ac.uk*

(demographic) noise on these fixation probabilities with help of Eqs. (6) and (7) when $K_- \gg 1, 0 < s \ll 1$ and $\nu > 0$, and by comparing the predictions of these formula with the results of stochastic simulations carried out using the Gillespie algorithm [5] which *exactly* simulates the master equation.

2.1 Physical arguments underpinning formula (6) and (7) and their corroboration

Formula (6) and (7) are assumed forms for the fixation probability ϕ of the slow species S when $0 < s \ll 1$ and $K_- \gg 1$. These expressions are based on a series of physical considerations that are fully corroborated by stochastic simulations of the underlying individual-based population dynamics. At its core, the rationale behind (6) is rooted in the timescale separation between N and x and on scaling arguments. For the sake of concreteness, here we first focus on the case of pure resource competition ($b = 0$) and present the physical arguments underpinning Eq. (6):

- The condition $0 < s \ll 1$ ensures that there is a timescale separation between the evolutionary and ecological dynamics. In fact, as shown in the Videos 1-3 [1], x evolves on a much slower timescale than N when $0 < s \ll 1$: x relaxes in a time of order $1/s$ while N is at quasi-stationarity after a time of order 1. The condition $K_- \gg 1$ ensures that the evolution of the population size is chiefly driven by random switching and is well described by the PDMP (4) that neglects the effects of demographic noise that are marginal when $K_- \gg 1$ (see also Sec. 3 below).

- Due to the timescale separation, when fixation occurs, typically after a time of order $1/s$ (see Fig. S3), N can be considered to be in the stationary state of the PDMP (4) whose probability density function (PDF) has support $[K_-, K_+]$.

- The evolution of x is much slower than the dynamics of N. The population size is therefore able to span much of its quasi-stationary distribution before fixation. This suggests to (approximately) compute ϕ by averaging $\phi|_N$, which is the S fixation probability in a fitness-dependent Moran model of constant population size N (see main text), over the stationary PDF of the underlying PDMP that captures the main features of long-time dynamics of N.

- Since x evolves on a timescale $1/s$ times slower than N, when $1/\nu$ (mean time between two switches) is much shorter than x's relaxation time, the population composition changes by $1/N$ while N has already typically experienced many switches. Hence, when $\nu \gg s$, the external noise self averages on the timescale of the relaxation of x even if N experiences large excursions (*e.g.*, from $N \approx K_\pm$ to $N \approx K_\mp$ as in the case of Fig. 3(c)): Hence, x changes by $1/N$ while the population size N appears to fluctuate about a characteristic value. It is therefore necessary to rescale the switching rate $\nu \to \nu/s$ in averaging $\phi|_N$ over the stationary PDF of Eq. (4) in order to compute the fixation probability ϕ. The rescaling $\nu \to \nu/s$ reflects the fact that $K(t)$ experiences on average ν/s switches prior to fixation (while x relaxes). In other words, this means that in this context the extent to which the environmental noise self-averages relative to the typical relaxation time of x determines whether the environment changes "fast" or "slowly".

- With this rescaling, we obtain Eq. (6): $\phi \simeq \int_{K_-}^{K_+} \phi|_N \, p^*_{\nu/s}(N) dN$, where the integral over N spans $[K_-, K_+]$ which is the support of $p^*_{\nu/s}(N)$ given by Eq. (5). In Eq. (6), $\phi|_N$ accounts for internal noise in a population of size N while $p^*_{\nu/s}(N)$ captures the effect of the environmental noise on the (quasi-)stationarity distribution of N in terms of the PDMP (4).

- In the fast and slow switching regimes, the fixation probability ϕ can be computed directly from the properties of the fitness-dependent Moran model. In fact, when $\nu \to \infty$ (very fast switching), the dichotomous noise self-averages ($\xi \to \langle \xi \rangle = 0$ in Eq. (4)) and the population readily attains the the effective size $N \simeq \mathcal{K} \gg 1$. The internal evolution thus mirrors that of a population of constant size $\mathcal{K}$ obeying a fitness-dependent Moran process [6, 7, 8]. In this case, if the initial fraction of S individuals is x_0, we have $\phi \xrightarrow{\nu \to \infty} \phi^{(\infty)} = \phi|_{\mathcal{K}} = (e^{-\mathcal{K}s(1-x_0)} - e^{-\mathcal{K}s})/(1 - e^{-\mathcal{K}s})$ [7], see main text. Similarly, when $\nu \to 0$ (very slow switching), the population is equally likely to be locked in either of the environmental state $\xi = -1$ (where $N = K_-$) or $\xi = +1$ (where $N = K_+$) and from the properties of the fitness-dependent Moran model in this case the fixation probability is $\phi \xrightarrow{\nu \to 0} \phi^{(0)} = (\phi|_{K_-} + \phi|_{K_+})/2$.

- The stationary PDF $p^*_{\nu/s}(N)$ in Eq. (6) accounts for the fact that when $\nu > s$ there are typically many switches prior to fixation, and environmental noise essentially self-averages when $\nu \gg s$ and a large number of switches occur. In fact, Eq. (6) correctly reproduces the fixation probability under fast and slow switching: it predicts $\phi \simeq \phi^{(\infty)}$ when $\nu/s \gg 1$ and $\phi \simeq \phi^{(0)}$ when $\nu/s \ll 1$, see Figs. 2(a) and S1.

- The stationary PDF $p^*_{\nu/s}(N)$ is unimodal with a peak at $N \approx \mathcal{K}$ when $\nu > s$, and is bimodal with peaks about $N = K_\pm$ when $\nu < s$, see Fig. 3 and Videos 4 and 5. This suggests that in the regime of intermediate switching rate, shown as shaded areas in Fig. S1, the fixation probability interpolates between $\phi^{(0)}$ and $\phi^{(\infty)}$, and we expect that$\phi \approx \phi^{(\infty)}$ over a broad range of values of ν since $s \ll 1$ and $\nu/s \gg 1$ is always satisfied when ν is of order 1.

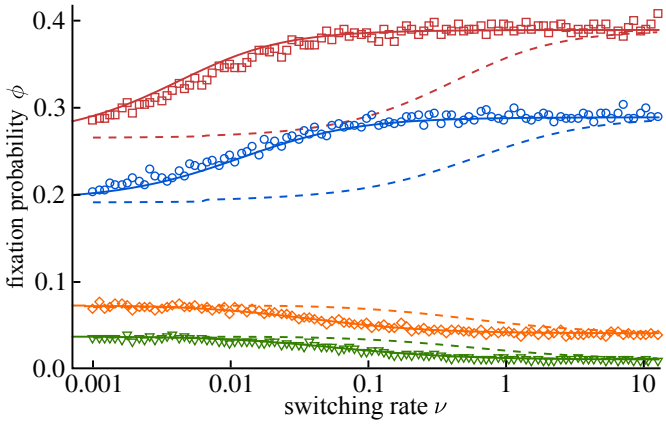

Figure S1: *(Color online)*. Fixation probability ϕ as function of ν for different values of s in the pure competition case ($b = 0$). Here, $(K_+, K_-) = (450, 50)$. Symbols denote the results of stochastic simulations for different values of s: $s = 0.01$ ($\square$, red/ dark gray), $s = 0.02$ ($\circ$, blue/black), $s = 0.07$ ($\diamond$, orange/gray) and $s = 0.1$ ($\triangledown$, green/light gray), from top to bottom. Solid lines denote the corresponding predictions of Eq. (6) and dashed lines represent the predictions of $\int_{K_-}^{K_+} \phi|_N \, p^*_\nu(N) dN$, obtained by averaging $\phi|_N$ over (5) *without* rescaling the switching rate ν, see text. The rescaling of the switching rate into ν/s in Eq. (6) reveals that ϕ is a scaling function of ν/s. In fact, without rescaling the switching rate, the predictions (dashed lines) agree with stochastic simulations only in the regimes of very large ν (fast switching) or very low ν (slow switching); whereas the predictions of Eq. (6) agree with simulations over four orders of magnitude. Hence, Eq. (6) with the average over the PDF (5) with rescaled switching rate $\nu \to \nu/s$ provides accurate predictions in the intermediate switching regime that separates the slow ($\nu/s \ll 1$) and fast ($\nu/s \gg 1$) switching regimes, see text.

At this point, it is worth emphasizing that the assumed form Eq.(6) has been proposed *without making any use of fitting parameters and does not rely on any input from stochastic simulations*, but only on the basis of the above physical considerations. Stochastic simulations have been used to validate the form of (6) by corroborating its predictions. In fact, a pragmatic and efficient way to assess the validity/accuracy of (6) is to systematically compare its predictions with results of extensive stochastic simulations of system's dynamics based on the Gillespie algorithm (typically sampling over 10^4 to 10^5 realizations). The form of Eq. (6) and the above considerations are thus supported by the following evidence:

- As shown in the supporting Videos 1-3 [1], stochastic simulations fully confirm that x always evolves much slower than N when $s \ll 1$, and that a timescale separation occurs when $b = 0$. Figs 2-4, as well as the supporting Videos 4-5 also confirm that about the time of fixation (and after fixation has occurred), the evolution of N is well described by the underlying PDMP when $K_- \gg 1$. In fact, except for the population collapse arising after an enormous, unobservable time, demographic noise has only a marginal effect on the (quasi-)stationary distribution of N.

- Stochastic simulations mirroring the predictions of the system's master equation fully confirm that Eq. (6) correctly predicts the expected behavior at fast and slow switching rate, with $\phi \simeq \phi^{(\infty)}$ when $\nu/s \gg 1$ and

$\phi \simeq \phi^{(0)}$ when $\nu/s \ll 1$. Furthermore, stochastic simulations show that the predictions of Eq. (6) correctly reproduces the nontrivial ν-dependence of ϕ, see Figs. 2(a) and S1, and agree remarkably well with simulation results also in the regime of intermediate switching rate.

The remarkable agreement between the predictions of Eq.(6) and stochastic simulations results has been confirmed for different values of s (namely $s = 0.01, 0.02, 0.07, 0.1$), and in all cases we have found an agreement within a few percent. More specifically, by a systematic comparison with simulations, we have estimated the mean square displacement of the predictions of Eq. (6) from the simulation results to be within 1.5% to 9% for the results of Fig. S1, with an accuracy that increases when s is lowered: In the tested datasets, the mean error ranges from about 1.5% when $s = 0.01$ to about 9% when $s = 0.1$ and $(K_-, K_+) = (50, 450)$ [11]. The fact that the accuracy of (6) improves when s is lowered stems from the fact that Eq. (6) is built on assuming a timescale separation between N and x, which is the more pronounced the lower s.

- Gillespie stochastic simulations confirm that rescaling $\nu \to \nu/s$ is necessary to correctly predict the fixation probability on a broad spectrum of ν/s values. This is illustrated in Fig. S1. When we compare the predictions of Eq. (6), obtained by averaging over the PDF (5) with the rescaled switching rate ν/s, against stochastic simulations for different values of s we find an excellent agreement over the entire range of ν values (spanning four orders of magnitude, from $\nu \sim 10^{-3}$ to $\nu \sim 10$) On the other hand, the predictions of $\int_{K_-}^{K_+} \phi|_N \, p^*_\nu(N)dN$, in which the switching rate has not been rescaled, are shown to be at odds with the results of stochastic simulations when $0.01 \lesssim \nu \lesssim 1$ which includes intermediate switching regime (the agreement is restricted to a limited range of very large/small values of ν/s corresponding to the very fast/slow switching regimes).

In summary, the results reported in Figs. 2(a) and S1 show that the predictions of Eq. (6) are in excellent agreement with the outcome of the system's Gillespie simulations (mirroring the dynamics described by the master equation) over a broad range of values of ν/s values. This confirms that Eq. (6) is indeed a good assumed expression (or, by a slight abuse of language, a suitable "Ansatz") for the actual fixation probability. The difference between the predictions of (6) and the corresponding simulation results can be estimated numerically, but for the purpose of our discussion here, it suffices to notice that an agreement within a few percent is found over the broad range of ν/s values tested. Further technical details about the accuracy of (6) will be investigated elsewhere [11].

The physical considerations leading to Eq. (6) when $b = 0$ also lead to Eq. (7) in the public good scenario with $b > 0$. However, since Eqs. (2) and (4) for N and x are coupled in this case, we use a constant effective parameter $q \geq 0$ in our analysis. As explained in the main text (see also below), this parameter is determined by matching simulation results. In fact, when $b > 0$, the effective parameter q is introduced by considering the auxiliary stochastic differential equation obtained by substituting $g = 1 + q$ in Eq. (4), see Sec. 1, which yields

$$\frac{\dot{N}}{N} = 1 + q - \frac{N}{K} = 1 + q - \frac{N}{\mathcal{K}} + \xi \frac{N(K_+ - \mathcal{K})}{\mathcal{K}K_+}. \tag{S1}$$

This equation is decoupled from the rate equation (2) for x and corresponds to a PDMP [2, 4], describing how the size of an *effective* population evolves under the sole effect of the environmental noise. This PDMP is characterized by a probability $p^{\pm}_{\nu,q}(N,t) = p_{\nu,q}(N, \xi = \pm 1, t)$ to be in state $\{N, \xi\}$ at time t for q given, where

$$\frac{\partial}{\partial t} p^{\pm}_{\nu,q}(N,t) = -\frac{\partial}{\partial N}\left[N\left(1 + q - \frac{N}{\mathcal{K}}\right) p^{\pm}_{\nu,q}(N,t)\right] - \nu[p^{\mp}_{\nu,q}(N,t) - p^{\pm}_{\nu,q}(N,t)].$$

By assuming that the probability current is zero at $N = (1+q)K_\pm$ (natural boundary conditions [4]) and $\nu > 0$, the stationary marginal probability density function $p^*_{\nu,q}(N) = \lim_{t\to\infty}(p^+_{\nu,q}(N,t) + p^-_{\nu,q}(N,t))$ of (S1) is given by [2, 4, 9]

$$p^*_{\nu,q}(N) = \frac{\mathcal{Z}_{\nu,q}}{N^2}\left[\frac{\{(1+q)K_+ - N\}\{N - (1+q)K_-\}}{N^2}\right]^{\frac{\nu}{1+q}-1}, \tag{S2}$$

where $\mathcal{Z}_{\nu,q}$ is the normalization constant, $(1+q)K_\pm$ are the effective carrying capacities, whose harmonic mean is $(1+q)\mathcal{K}$, and $[(1+q)K_-, (1+q)K_+]$ is the support of $p^*_{\nu,q}$.
To determine the parameter $0 \leq q \leq b$, we consider the limit $\nu \to \infty$. In such a regime, the environmental noise switches very rapidly and self-averages, and Eq. (S1) is thus characterized by an effective population size $N =$

$(1+q)\mathcal{K}$. The corresponding fixation probability of species S is thus $\phi|_{(1+q)\mathcal{K}}$. We then vary q in order to match $\phi|_{(1+q)\mathcal{K}}$ with the fixation probability obtained in our simulations for $\nu \gg 1$ [10].
In the realm of this effective theory, we can use this q to determine $p^*_{\nu,q}(N)$ given by (S2). Then, as we did to obtain Eq.(6), an expression ϕ_q fixation probability of S is obtained by averaging $\phi|_N$ over (S2) with a rescaled switching rate $\nu \to \nu/s$. This yields Eq. (7) for ϕ_q whose expression has been used in Figs. 4(b)-4(d) in lieu of ϕ, see also Sec. 4 below. It is worth noting that in the realm of this effective theory, the parameter q accounts for the correlations of the dynamics of x and N.
By setting $q = b > 0$ in (S2), we can obtain the (marginal) PDF $p^*_{\nu,b}(N)$ conditioned to the fixation of species S (but unconditioned of whether $\xi = \pm 1$) in the public good scenario. Similarly, by setting $q = 0$ in (S2), we obtain $p^*_{\nu,0}(N) = p^*_\nu(N)$ which coincides with (5) and is the marginal PDF conditioned to the fixation of F (but unconditioned of $\xi = \pm 1$) in the public good scenario and the marginal PDF in the pure resource scenario. In the latter case, $p^*_\nu(N)$ is used to obtain the expression (6) for the fixation probability ϕ.

2.2 Properties of formula (6) and (7)

It is worth noting that formula (6) and (7) explicitly reflect the coupling between internal and external noise.

As discussed above, Eq. (6) provides an excellent approximation of the fixation probability of S for all the values of $\nu > 0$, when $K_- \gg 1$. Moreover, it captures the fact that external and internal noise can jointly significantly enhance the fixation probability of the slow type with the respect to its counterpart in a population of constant size $\langle K\rangle = (K_+ + K_-)/2 \gg 1$ subject to non-random environment, where this probability is exponentially small ($\phi|_{\langle K\rangle} \approx e^{-\langle K\rangle s/2}$ when $x_0 = 1/2$ and $\langle K\rangle s \gg 1$). This is also true in the limit $\nu \to 0$ where the population is as likely to be subject to a carrying capacity smaller or larger than $\langle K\rangle$, which generally greatly increases the fixation probability of S with respect to the case where $N = \langle K\rangle$ even if there may be no switches prior to fixation. For instance, in Fig. 2(a) we find that $\phi \approx 0.20 - 0.30$ when $s = 0.02$ while $\phi|_{\langle K\rangle=250} \approx 0.08$, and for $s = 0.07$ we have obtained $\phi \approx 0.05 - 0.07$ while $\phi|_{\langle K\rangle=250} \approx 0.002$.

Fig. 4(a) shows that expression (7) of ϕ_q is very close to ϕ when $\nu/s \gg 1$ (high switching rate) and $K_- \gg 1$, but slightly deviates from it when $\nu/s \ll 1$. This stems from the fact that the effective theory underpinning (7) builds on the value of q inferred at high switching rate.

Remarkably, both (6) and (7) are able to capture the nontrivial dependence of ϕ on the switching rate ν, see Figs. 2(a), S1 and 4(a): ϕ increases with ν when $\phi^{(\infty)} > \phi^{(0)}$ and decreases when $\phi^{(\infty)} < \phi^{(0)}$. The former situation arises under sufficiently low selection pressure, whereas the latter scenario occurs above a certain selection intensity. The intuitive explanation for this is that $\nu \approx 0$ corresponds to a high-volatility-high-reward setting, in which S is equally likely to end up in an environment with relatively high demographic noise ($K = K_-$), where its fixation probability is high, or in one ($K = K_+$) with low noise and lower fixation probability. When $\nu \gg 1$, on the other hand, the species S is in a low-volatility-low-reward setting: it faces an almost constant population size ($N \approx \mathcal{K}$). When the selection intensity s is increased, it becomes increasingly less favorable for S to be in the low-volatility-low-reward setting, and thus $\phi^{(\infty)} < \phi^{(0)}$ and thus ϕ decreases with ν. In the case of Fig. 2(a), we can explicitly determine the critical selection pressure s_c below which $\phi^{(\infty)} > \phi^{(0)}$. When $K_+ \gg K_- \gg 1$, we have $\mathcal{K} = 2K_-(1 + \mathcal{O}(K_-/K_+))$ and therefore $\phi^{(\infty)} \simeq (e^{-K_- s} - e^{-2K_- s})/(1 - e^{-2K_- s})$ while $\phi^{(0)} \simeq (e^{-K_- s/2} - e^{-K_- s})/[2(1 - e^{-K_- s})]$. Hence, the condition $\phi^{(\infty)} > \phi^{(0)}$ for ϕ to increase with ν leads to $2y^2/(1 + y^2) > y/(1 + y)$, where $y = e^{-K_- s/2}$. Therefore, ϕ is an increasing function of ν/s when $y^2 + 2y - 1 > 0$, i.e. if $y = e^{-K_- s/2} > \sqrt{2} - 1$, while ϕ decreases with ν if $e^{-K_- s/2} < \sqrt{2} - 1$. The critical selection pressure is thus defined by $e^{-K_- s_c/2} = \sqrt{2} - 1$. For $(K_+, K_-, s) = (450, 50, 0.02)$, we find $s_c \approx 0.035$. Hence, $s = 0.02 < s_c$ and $s = 0.07 > s_c$. Therefore, ϕ increases with ν when $s = 0.02$, and it decreases with ν when $s = 0.07$, as reported in Figs. 2(a) and S1.

Finally, we note that while (7) is useful to obtain an approximation of ϕ and its dependence on ν and s, it is unable to capture its dependence on the public good parameter $b > 0$. However, we know that the typical population size increases with b when $x \approx 1$ and S is close to fixation, and therefore the intensity of the demographic fluctuations is reduced by increasing b. Based on the properties of the Moran process, we thus expect ϕ to decay exponentially with b [11], which is confirmed by Fig. S2.

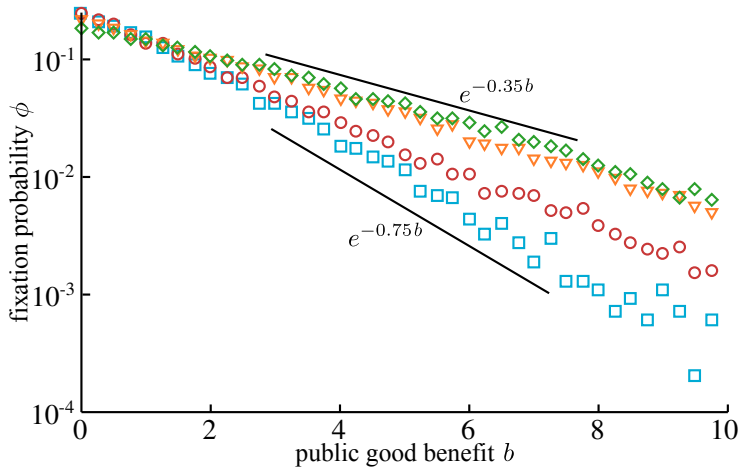

Figure S2: *(Color online).* ϕ as function of b for $\nu = (0.002, 0.02, 0.2, 2)$ (top to bottom) and $(s, K_+, K_-) = (0.025, 450, 50)$ in log scale. Straight lines show $0.3e^{-0.35b}$ and $0.175e^{-0.75b}$ as eyeguides.

3 Mean fixation time

We have also investigated the mean fixation time $T(x_0)$, which is the unconditional mean time until the fixation of either species S or F starting from a initial fraction x_0 of individuals of type S in the population.

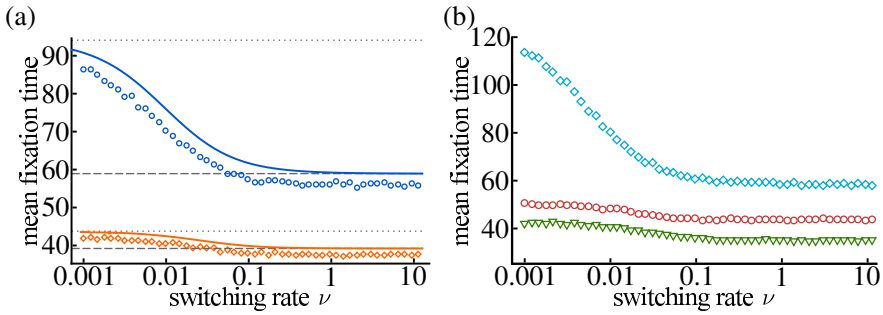

Figure S3: *(Color online).* (a) $T(x_0) = T$ vs. ν in the pure competition case $b = 0$ with $s = 0.02$ ($\circ$, blue/black) and $s = 0.07$ ($\diamond$, orange/gray). Symbols are simulation results for T, solid lines are from (S3), dashed and dotted lines show $T|_{\mathcal{K}}$ and $(T|_{K_-} + T|_{K_+})/2$, respectively. (b) T vs. ν in the public good scenario with $b = 0.2$ ($\diamond$, blue/gray for $s = 0.01$; $\circ$, red/black for $s = 0.05$) and $b = 2$, $s = 0.05$ ($\triangledown$, green/dark gray). $(K_+, K_-, x_0) = (450, 50, 1/2)$ in both panels.

3.1 Mean fixation time when $b = 0$

In the case $b = 0$, N evolves independently of which species has fixated the population, see Videos 1-3 [1]. This allows us to proceed just as we did with (6) for the fixation probability, and estimate the mean fixation time by $T_{\nu/s}$. This quantity is obtained by averaging the unconditional mean fixation time $T(x_0)|_N$ [7, 8] obtained in a Moran process for a population of constant size N over $p^*_{\nu/s}(N)$ given by (5) with a rescaled switching rate $\nu \to \nu/s$. This yields

$$T_{\nu/s} = \int_{K_-}^{K_+} T(x_0)|_N \, p^*_{\nu/s}(N) \, dN \,, \tag{S3}$$

where $T(x_0)|_N \sim \mathcal{O}(1/s)$ when $e^{1/s} \gg K_-$. As Figure S3(a) shows, this expression agrees well with the leading contribution $T(x_0) \simeq T_{\nu/s} \sim \mathcal{O}(1/s)$ when x_0 is well separated from the absorbing boundaries. The scaling of the mean fixation time in the presence of EN is therefore the same as $T(x_0)|_N = T|_N$ [7, 8]. The main effect of the EN is to affect the subleading prefactor of T [11]: as shown in Fig. S3 (a) and captured by (S3), the mean fixation time decreases when ν increases. This stems from the fact that $\langle N \rangle^*$ decreases with ν, see Fig. 2(b). In the case of pure resource competition, our theory is therefore able to correctly predict that the mean fixation time always scales as $1/s$ but is shortened when the switching rate is increased.

3.2 Mean fixation time when $b > 0$

In the public good scenario ($b > 0$), the mean fixation time still scales as $T(x_0) \sim \mathcal{O}(1/s)$ and decreases with the environmental switching rate ν, as shown in S3(b). This is because the average population size also decreases with ν (see Fig. 3). In this case, however the fixation of the S type happens in larger populations (and, hence, after longer times) than the fixation of F, see Videos 6-7 [1]. As a result, to accurately compute $T(x_0)$, it is necessary to determine the two conditional mean fixation times (which are equal only when $b = 0$) [11]. Clearly, this cannot be achieved by assuming a timescale separation between N and x, and is beyond the reach of our effective theory.

4 Population size quasi-stationary distribution: additional discussion and results

In this section, we provide additional discussion and results about the population size distribution after the occurrence of fixation. An important common feature of the $b = 0$ and $b > 0$ scenarios is that long-time population size distribution is well described by p^*_ν (5) when $b = 0$, and by combining the conditional PDFs p^*_ν and $p^*_{\nu,b}$ (S2) with ϕ when $b > 0$, as explained in the main text.

4.1 Noise-induced transitions

The quasi-stationary population size distributions are thus characterized by different regimes in which they are unimodal, bimodal, or even multimodal, see Figs. 3, 4 and S4. The transitions between these various regimes are called "noise-induced transitions" because they are solely caused by the environmental noise [4, 9]. In fact, if the carrying capacity in (S1) was oscillating periodically (deterministically), the corresponding PDF would *always* be bimodal: the transition to the unimodal regime is only possible for randomly fluctuating K [9].

4.2 Simulation and prediction of the population size steady state distribution

To assess the theoretical predictions for the long-time population size distribution inferred from (5) and (S2), we have generated 10^5 replicas that we let run until 99% of them reached fixation. The outcome has then been binned to generate the histograms shown as solid lines in Figs. 3, 4(c,d) and in Fig.S4.
In the pure competition case ($b = 0$), see Fig. 3, these simulation results are compared with $p^*_\nu(N)$ (5) multiplied by the number of replicas. (In this case, N evolves independently of x, therefore it is not necessary to wait until 99% of fixation has occurred, see Videos 4-5 [1]. We have proceeded in this way for consistency with the case $b > 0$).
In the public good scenario ($b > 0$), see Figs. 4(c,d) and S4, we have waited until fixation had occurred in almost all replicas (99% of them) to collect the data to build the histograms that correctly reflect the quasi-stationary state distributions of the population size (now depending on x), see Videos 8-10 [1]. Via our effective theory, we have computed the fixation probability of the strain S and F. Multiplying these values by 10^5 (number of samples), we have obtained the expected number of replicas to fixate to S and to F. By multiplying these numbers by p^*_ν (5) and $p^*_{\nu,b}$ (S2) we obtain the histograms associated with the conditional probability distributions (unconditioned of $\xi = \pm 1$). These are shown by dotted lines in Fig. S4 and their sum gives the histogram of the marginal distribution (orange dashed lines in Fig S4), which can be directly compared with the histogram from the simulations.

4.3 Long-time population size distribution in the public good scenario ($b > 0$)

To understand the properties of the quasi-stationary marginal population size distribution when $b > 0$, it is useful to notice that when S fixates ($x = 1$), the relevant conditional PDF (unconditioned of $\xi = \pm 1$) is $p^*_{\nu,b}$ which is unimodal and peaked at $N = (1+b)\mathcal{K}$ when $\nu > 1+b$, while it is bimodal with peaks at $N = (1+b)K_\pm$ if $\nu < 1+b$. Similarly, p^*_ν is the PDF conditioned to fixation of F (but unconditioned of $\xi = \pm 1$): it is unimodal and peaked at $N \approx \mathcal{K}$ if

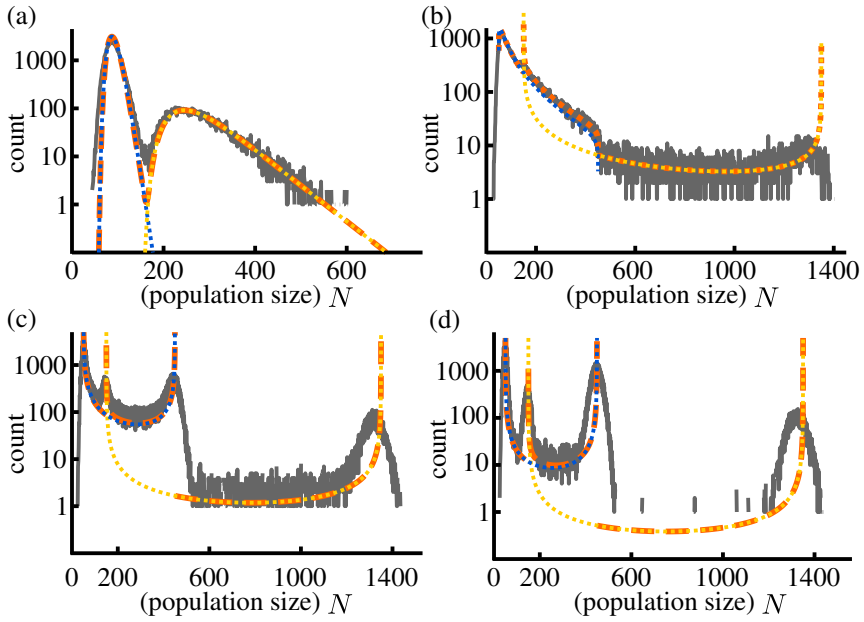

Figure S4: *(Color online).* Long-time population size distributions for $\nu = 20$ (a), $\nu = 1.2$ (b), $\nu = 0.2$ (c), and $\nu = 0.02$ (d) with $(K_+, K_-, x_0, s, b) = (450, 50, 0.5, 0.02, 2)$ similar to Fig. 4(c,d) but now showing also the results obtained from the S-conditional (dotted, yellow/light gray) and F-conditional (dotted, blue/dark gray) PDFs. The histogram of the marginal PDF (dashed) is the sum of the S/F-conditional histograms weighted by ϕ_q (7), see text.

$\nu > 1$, whereas it is bimodal with peaks at $N \approx K_\pm$ when $\nu < 1$. The sum of the conditional PDFs weighted by ϕ_q yields the marginal PDF (unconditioned of $\xi = \pm 1$ and of whether S or F fixates) that, depending on ν and b, is either bimodal or multimodal. Therefore, as shown in Figs. 4(c,d) and S4 as well as in Videos 8-10 [1], the marginal quasi-stationary population size distribution is characterized by

- two peaks at about $N = \mathcal{K}$ and $N = (1+b)\mathcal{K}$ when $\nu > 1 + p$, see Video 8.
- three peaks located about $N = \mathcal{K}$ and $N = (1+b)K_\pm$ when $1 < \nu < 1 + p$, see Video 9.
- four peaks located around $N = (1+b)K_\pm$ and $N = K_\pm$ when $\nu < 1$, see Video 10.

The peaks at $N = (1+b)K_\pm$ and $N = (1+b)\mathcal{K}$ stem from the fixation of S and thus are less marked than those at $N \approx K_\pm$ and $N \approx \mathcal{K}$ which result from the more likely fixation of F.

4.4 Figure 4(c, d) revisited

In Fig. 4(c,d), we report the histograms of the stationary marginal population distribution at $\nu = 20$ and $\nu = 0.02$ with $b = 2$. For the sake of completeness, in Fig. S4 we also consider the intermediate switching rates $\nu = 1.2$ and $\nu = 0.2$, and show the conditional PDFs p^*_ν and $p^*_{\nu,b}$. The marginal PDF is obtained as the sum of p^*_ν and $p^*_{\nu,b}$ weighted by ϕ_q and $1 - \phi_q$ given by (7).

4.5 Deviations from the PDF predictions

We have seen that coupled internal and environmental noise greatly influences the population fixation probability (aptly described by Eqs.(6) and (7)), and therefore significantly influences the population internal composition (evolutionary dynamics), and in turn also its ecological dynamics when $b > 0$ (internal and ecological dynamics being then explicitly coupled). We have also seen that once fixation has occurred, the population size quasi-stationary distribution is well described by the stationary (conditional) PDFs (5) and (S2) of underlying PDMP that are able to predict when the long-time population size distributions are unimodal, bimodal or multimodal and the location of the peaks, as shown

by Figs. 3, 4 and S4.
However, Eqs. (5) and (S2) ignore the effects of demographic fluctuations on the population size distribution. In fact, demographic fluctuations are responsible for the population size quasi-stationary distributions obtained from the simulations not to be strictly confined within the support of the PDFs (5) and (S2), especially at low ν, as can be seen in Figs. 3, 4 and S4. As clearly visible in the supporting Videos [1], these deviations appear because, due to demographic noise, the population fluctuates around the fixed points $N = K_{\pm}$ and $N = (1 + b)K_{\pm}$, see Video 10. The small deviations from the PDMP predictions have limited influence on quantity such as the average population size $\langle N \rangle^*$, see main text, and their intensity depends on the values of $K_{\pm}$ (high values of $K_{\pm}$ typically yield broader peaks) [11].

5 Supporting videos

The dynamics of the models and our findings are illustrated by a series of videos available electronically [1].

5.1 Videos 1-5: $b = 0$

Videos 1-5 illustrate the population dynamics in the pure resource competition scenario for the parameters $(s, K_+, K_-, x_0) = (0.02, 450, 50, 0.5)$ and different switching rates.

- Video 1 shows the sample paths $N(t)$ (left) and $x(t)$ (right) of five replicas for $\nu = 20$. We clearly notice a timescale separation: the population size quickly starts to endlessly fluctuate about $N \approx \mathcal{K} = 90$ while $x(t)$ evolves much more slowly, with fixation occurring in time $t \sim \mathcal{O}(1/s)$.

- Video 2 shows similar paths for $\nu = 0.01$ (and a sped-up animation). We again see the timescale separation between $N(t)$ and $x(t)$. However, in the long run $N(t)$ endlessly jumps between $N \approx K_-$ and $N \approx K_+$. Moreover, the video shows how the behavior of the population size is unaffected by changes in x: N relaxes at a faster timescale and maintains the same behavior also after fixation (of either species).

- Video 3: $N(t)$ and $x(t)$ sample paths as in Videos 1 and 2 but for very slow switching rate $\nu = 0.0001 \ll s = 0.02$. In all but one replicas, the population evolves subject to the carrying capacity K_- or K_+, randomly allocated initially with same probability, without experiencing any switches and $N(t)$ fluctuates about K_+ or K_- In only one realization, after a long time (at $t \approx 750$), the carrying capacity switches and the population jumps from K_+ to K_-. The video also illustrates that S fixation is more likely when the population is subject to $K = K_-$ than to $K = K_+$: both the purple and pink samples ending at $x = 1$ correspond to a population of size $N(t) \approx K_-$.

- Video 4 shows the histograms of the population size (left) and of the fraction of S individuals (right) for a slow-switching environment ($\nu = 0.2$). We notice that the population size distribution readily attains a right-tailed, bimodal shape with peaks about $N = K_{\pm}$, and is independent of the distribution of x (internal dynamics). On the other hand, the histogram of x evolves slowly and is eventually characterized by asymmetric peaks at $x = 0$ and $x = 1$ corresponding to the fixation probability of F and S, respectively.

- Video 5: as in Video 3, but for a fast-switching environment ($\nu = 20$). The population size histogram rapidly becomes bell-shaped and centered about $N = \mathcal{K}$. It reaches this form much before fixation typically occurs, and is independent of the distribution of x (internal dynamics). The histogram of x has the same properties as in Video 3.

5.2 Videos 6-10: $b > 0$

Movies 6-8 illustrate the internal and ecological dynamics in the public good scenario, $b > 0$, for the parameters $(s, K_+, K_-, b, x_0) = (0.02, 450, 50, 2, 0.5)$ and different switching rates. In this scenario, the fast N dynamics is enslaved to the slower evolution of x. The population size distribution is characterized by peaks that slowly emerge as occurrences of S and F fixation accumulate (right panels).

- Video 6 shows sample paths of N and x for five realizations with $\nu = 20$, as in Video 1. The population size and composition are correlated: the population size attains large values when x dwells about 1, while N is

much smaller when $x \ll 1$ (for example, the green replica is almost always larger than the purple one). As the species fixate, the sample paths for N separate into two distinct sets: those associated with the fixation of S ($x = 1$) fluctuate about $N \approx \mathcal{K} = 90$, while the paths associated to $x = 0$ (fixation of F) fluctuate around $N \approx (1 + b)\mathcal{K} = 270$.

- Video 7 shows similar sample paths for $\nu = 2$. In addition to showing the correlation between N and x, the video illustrates how populations with a high fraction of S ($x \approx 1$) experience random switching with an effectively reduced switching rate. For example, in the purple sample paths, which readily attains $x \approx 1$, N evolves by large abrupt jumps, in agreement with the properties of the S-conditional PDF $p^*_{\nu,2}$, see (S2).

- Video 8 shows the histograms of N and x for fast switching ($\nu = 20$). The histogram of the population size (left) has first a right-tailed bell shape. As fixation occurrences build up, the distribution gradually splits into asymmetric peaks about $\mathcal{K} = 90$ and $(1+b)\mathcal{K} = 270$. The histogram of x is characterized by slowly-developing asymmetric peaks at $x = 0$ and $x = 1$.

- Video 9 shows the histograms of N and x for intermediate switching ($\nu = 1.2$). Similarly to Video 7, the histogram of N changes from having first a right-tailed bell shape to its eventual quasi-stationary form. In this case, the quasi-stationary state is characterized by three asymmetric peaks, located at about $\mathcal{K} = 90$ and $(1 + b)K_- = 150$, and about $(1 + b)K_+ = 1350$, that slowly develop as fixation occurrences pile up (right panel).

- Video 10 shows the histograms of N and x for slow switching $\nu = 0.2$. Initially, the histogram of N develops as in Videos 7 and 8, but now the quasi-stationary state is characterized by four slowly-developing asymmetric peaks, located at about $K_- = 50$, $(1 + b)K_- = 150$, and about $K_+ = 450$ and $(1 + b)K_+ = 1350$.

References

[1] K. Wienand, E. Frey, and M. Mobilia, figshare, doi:10.6084/m9.figshare.5082712
Videos are electronically available at https://doi.org/10.6084/m9.figshare.5082712.

[2] K. Kitahara, W. Horsthemke, and R. Lefever, Phys. Lett. **70A**, 377 (1979).

[3] M. H. A. Davis, J. R. Stat. Soc. Ser. B **46**, 353 (1984).

[4] W. Horsthemke and R. Lefever, *Noise-Induced Transitions* (Springer, Berlin, 2006).

[5] D. T. Gillespie, J. Comput. Phys. **22**, 403 (1976).

[6] P. A. P. Moran, *The statistical processes of evolutionary theory* (Clarendon, Oxford, 1962).

[7] W. J. Ewens, *Mathematical Population Genetics* (Springer, New York, 2004).

[8] J. Cremer, T. Reichenbach, and E. Frey, New J. Phys. **11**, 093029 (2009).

[9] I. Bena, Int. J. Mod. Phys. B **20**, 2825 (2006).

[10] For instance, for $(K_+, K_-, s, b, x_0) = (450, 50, 0.025, 2, 0.5)$ we have found $q = 1.1543$.

[11] K. Wienand, E. Frey, and M. Mobilia, *in preparation*.

3.4 Publication manuscript

Eco-Evolutionary Dynamics of a Population with Randomly Switching Carrying Capacity

by

K. Wienand,[1] E. Frey,[1] and M. Mobilia[2]

[1]Department of Physics, Arnold Sommerfeld Center for Theoretical Physics and Center for NanoScience, Ludwig-Maximilians-Universität München, Theresienstraße 37, 80333 München, Germany,
[2] Department of Applied Mathematics, School of Mathematics, University of Leeds, Leeds LS2 9JT, United Kingdom

Eco-Evolutionary Dynamics of a Population with Randomly Switching Carrying Capacity

Karl Wienand,[1] Erwin Frey,[1] and Mauro Mobilia[2,*]

[1]*Arnold Sommerfeld Center for Theoretical Physics, Department of Physics, Ludwig-Maximilians-Universität München, Theresienstrasse 37, 80333 München, Germany*
[2]*Department of Applied Mathematics, School of Mathematics, University of Leeds, Leeds LS2 9JT, U.K.*

Environmental variability greatly influences the eco-evolutionary dynamics of a population, i.e. it affects how its size and composition evolve. Here, we study a well-mixed population of finite and fluctuating size whose growth is limited by a randomly switching carrying capacity. This models the environmental fluctuations between states of resources abundance and scarcity. The population consists of two strains, one slightly faster than the other, competing under two scenarios: one in which competition is solely for resources, and one in which the slow ("cooperating") strain produces a public good. We investigate how the coupling of demographic and environmental (external) noise affects the population's eco-evolutionary dynamics. By analytical and computational means, we study the correlations between the population size and its composition, and discuss the cooperation dilemma arising in the "eco-evolutionary game" of public good production in a fluctuating environment. We determine in which conditions it is best to cooperate and produce a public good; when cooperating is beneficial but outcompeted by the non-producing strain, and when the public good production is detrimental for cooperators. By generalizing the linear noise approximation to populations of varying size, we also analyze the coupled effects of demographic and environmental noise on the size distribution.

Keywords: population dynamics, evolution, ecology, fluctuations, cooperation dilemma, public goods

I. INTRODUCTION

The fate of populations is affected by a number of endlessly changing environmental conditions such as the presence of toxins, resources abundance, temperature, light, etc. [1, 2]. In the absence of detailed knowledge of how external factors vary, they are modeled as external noise (EN) shaping the randomly changing environment in which species evolve. The impact of fluctuating environments on population dynamics has been studied in a number of systems [3–14], and several evolutionary responses to exogenous changes have been studied [15–20]. In finite populations, internal noise is another important form of randomness, yielding demographic fluctuations of stronger intensity in small populations than in large ones. Internal noise (IN) is responsible for fixation [21, 22] (when one species takes over and others are wiped out) and thus plays an important role in the evolution of a population's composition. Ecological and evolutionary dynamics are often coupled, through an interdependent evolution of the population size and composition [23–25, 27–29]. As a consequence, environmental variability may affect the population size and hence the demographic fluctuations intensity, thus coupling EN and IN. The interdependence of environmental noise and demographic fluctuations is particularly relevant for microbial communities, whose properties greatly depend on the population size and the environment [1, 2]. These populations often experience sudden, extreme environmental changes, leading to *population bottlenecks*, which shrink colony size and make it more prone to fluctuations [30–33]. The coupling between the different forms of randomness therefore generates feedback loops between socio-biological interactions and the environment [30, 31, 34], which results in fascinating eco-evolutionary phenomena such as cooperative behavior. For instance, experiments on *Pseudomonas fluorescens* showed that the formation and sudden collapse of biofilms promotes the evolution of cooperation [32, 33, 35]. In most studies, however, EN and IN are treated as uncoupled [4–14].

Recently, we studied a fluctuating population—consisting of a fast strain competing with a slow (cooperating) species, that can produce a public good—evolving under a randomly switching carrying capacity [36]. In this model, demographic fluctuations are coupled to EN, resulting in a significant influence on the species fixation probability and leads to noise-induced transitions of the population size. Here, we study in detail the eco-evolutionary dynamics of the model of Ref. [36], and introduce new theoretical concepts to characterize the emergence of cooperation in populations of varying size in a fluctuating environment. We indeed show that the population size and its composition are correlated. A social dilemma of sorts arises: the public good production increases the overall expected population size, and lowers the survival probability of cooperators. We measure the evolutionary success of a species in terms of its expected long-term number of individuals, and determine the circumstances under which public good production is detrimental or beneficial to cooperators, and find the conditions in which it is best to cooperate. We also generalize the linear noise approximation to populations of fluctuating size and analyze the joint effect of coupled demographic and environmental noise on the population size distribution.

The next two sections establish our approach: In Section II, we introduce our stochastic model; in Section III, we outline the properties of the fitness-dependent Moran model and piecewise deterministic Markov processes associated with the model, and review how to combine these to compute the species fixation probability. In the following two sections, we present our main results: Section IV is dedicated to the correlations between the population size and its composition, and to the discussion of the emergence of cooperative behavior along with an "eco-evolutionary game" in a population of

*Electronic address: m.mobilia@leeds.ac.uk

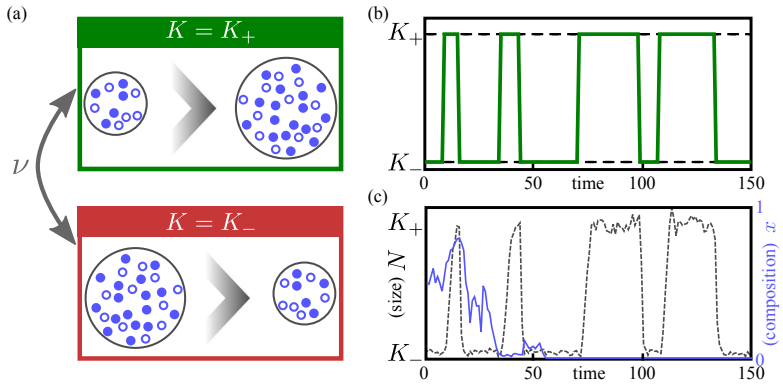

FIG. 1: (a) Cartoon of the eco-evolutionary dynamics of the model: the population consists of strains S (○) and F (●), subject to $K(t) \in \{K_-, K_+\}$ that randomly switches, see (4). After each switch, N and x change: following a K_- to K_+ switch, N increases and the intensity of the IN decreases; the opposite occurs following a K_+ to K_- switch. (b) Typical random switching of $K(t)$ according to (4). (c) Sample path of $N(t)$ (gray, dashed line)and $x(t)$ (blue, solid line), corresponding to the switching portrayed in (b). We notice that x evolves much slower than N, see text. Parameters are $(s, \nu, K_+, K_-, b) = (0.02, 0.1, 450, 50, 0)$.

fluctuation size; in Section V, we study the population size distribution within a linear noise approximation. Our conclusions are presented in Sec. VI. Additional information is provided in the Supplementary Material (SM) below and in [37].

II. MODEL

Following our recent work [36], we consider a well-mixed population of fluctuating size $N(t) = N_S(t) + N_F(t)$, consisting of N_S individuals of species S and N_F of species, or strain, F [38]. The fast-growing strain F has fitness $f_F = 1$, whereas the slow-growing strain S has a slightly lower fitness $f_S = 1 - s$, with $0 < s \ll 1$. Therefore, at time t the fraction of S individuals in the population is $x(t) = N_S(t)/N(t)$ and the average population fitness is $\bar{f} = xf_S + (1-x)f_F = 1 - sx = 1 + \mathcal{O}(1)$. Here, the evolution of the population size $N(t)$ is coupled to the internal composition $x(t)$ by a global growth rate $g(x)$, and its growth is limited by a logistic death rate $N/K(t)$ [23–25, 36]. The carrying capacity $K(t)$ is a measure of the population size that can be supported, and is assumed to vary in time. We specifically focus on two important forms of global growth rates: (i) the *pure resource competition* scenario $g(x) = 1$, in which x and N are coupled only through fluctuations; and (ii) the *public good scenario* in which $g(x) = 1 + bx$, corresponding to a situation where S individuals are "cooperators" [23–26] producing a public good (PG) that enhances the population growth rate through the benefit parameter $0 < b = \mathcal{O}(1)$. In this case, N and x are coupled, leading to explicit "eco-evolutionary dynamics" [27].

The population size and composition therefore change according to the continuous-time birth-death process [23, 36, 37]

$$N_{S/F} \xrightarrow{T^+_{S/F}} N_{S/F} + 1 \quad \text{and} \quad N_{S/F} \xrightarrow{T^-_{S/F}} N_{S/F} - 1, \quad (1)$$

with transition rates

$$T^+_{S/F} = g(x)\frac{f_{S/F}}{\bar{f}} N_{S/F} \quad \text{and} \quad T^-_{S/F} = \frac{N}{K(t)} N_{S/F}. \quad (2)$$

We model environmental randomness by letting the carrying capacity $K(t)$ randomly switch between K_+ (abundant resources) and $K_- < K_+$ (scarce resources), see figure 1(a,b). We assume that K switches at rate ν, according to a time-continuous dichotomous Markov noise (DMN) [39–41] $\xi(t) \in \{-1, +1\}$ (or *random telegraph noise*):

$$\xi \xrightarrow{\nu} -\xi\,, \quad (3)$$

with zero-mean $\langle \xi(t) \rangle = 0$ and autocorrelation $\langle \xi(t)\xi(t') \rangle = \exp(-2\nu|t - t'|)$ ($\langle \cdot \rangle$ denotes the ensemble average over the environmental noise). This is a *colored noise* with a finite correlation time $1/(2\nu)$ [39–44], see Sec. 1 in SM [37]. As a result, the fluctuating carrying capacity reads

$$K(t) = \frac{1}{2}\left[(K_+ + K_-) + \xi(t)(K_+ - K_-)\right], \quad (4)$$

and endlessly switches between K_+ and K_- with constant average $\langle K \rangle = (K_+ + K_-)/2$.

The population evolves according to the multivariate stochastic process defined by equation (1)-(4), which obeys the master equation

$$\begin{aligned} \frac{dP(\vec{N}, \xi, t)}{dt} &= (\mathbb{E}_S^- - 1)[T_S^+ P(\vec{N}, \xi, t)] \\ &+ (\mathbb{E}_F^- - 1)[T_F^+ P(\vec{N}, \xi, t)] \\ &+ (\mathbb{E}_S^+ - 1)[T_S^- P(\vec{N}, \xi, t)]] \\ &+ (\mathbb{E}_F^+ - 1)[T_F^- P(\vec{N}, \xi, t)] \\ &+ \nu[P(\vec{N}, -\xi, t) - P(\vec{N}, \xi, t)], \end{aligned} \quad (5)$$

where $\vec{N} = (N_S, N_F)$, $\mathbb{E}^\pm_{S/F}$ are shift operators such that $\mathbb{E}^\pm_S G(N_S, N_F, \xi, t) = G(N_S \pm 1, N_F, \xi, t)$ for any $G(N_S, N_F, \xi, t)$, and similarly for $\mathbb{E}^\pm_F$.

Equation (5) fully describes the stochastic eco-evolutionary dynamics of the population, and can be simulated exactly (see Sec. 2 in SM [37]). Simulation results, see figure 1(c) and Ref. [45], reveal that generally $N(t)$ evolves much faster than the population composition. We consider $K_+ > K_- \gg 1$ to ensure that, after a transient, $N(t)$ is at quasi-stationarity where it is characterized by its quasi-stationary distribution (N-QSD). The latter eventually collapses after a time that diverges with the system size [46, 47], a phenomenon that can be disregarded for our purposes. Below we study the eco-evolutionary dynamics in terms of the random variables N and x, focusing on the fixation properties of the population and its quasi-stationary distribution.

It is useful to start our analysis by considering the mean-field approximation which ignores *all noise* (say $K = \langle K \rangle$). In this case, the population size N and composition x evolve deterministically according to [23, 24, 36, 48]

$$\dot{N} = \sum_{\alpha=S,F} T_\alpha^+ - T_\alpha^- = N\left(g(x) - \frac{N}{K}\right), \tag{6}$$

$$\dot{x} = \sum_{\alpha=S,F} \frac{T_\alpha^+ - T_\alpha^-}{N} - x\frac{\dot{N}}{N} = -sg(x)\frac{x(1-x)}{1-sx}, \tag{7}$$

where the dot signifies the time derivative. Equation (7) predicts that x relaxes on a timescale $t \sim 1/s \gg 1$ and eventually vanishes while, according to equation (6), $N(t)$ equilibrates to $N(t) = \mathcal{O}(K)$ in a time $t = \mathcal{O}(1)$.

III. PIECEWISE-DETERMINISTIC MARKOV PROCESS, MORAN MODEL & FIXATION PROBABILITIES

In this section, we review the effects of environmental and demographic noise separately, and compound them to find the fixation probabilities that characterize the population composition.

A. Environmental noise & Piecewise-deterministic Markov process

If the population is only subject to external noise (EN), it follows the *bivariate* piecewise-deterministic Markov process (PDMP), see, *e.g*, Refs. [12, 13, 49], defined by (7) and

$$\dot{N} = N\left\{g(x) - \frac{N}{\mathcal{K}} + \xi N\left(\frac{1}{\mathcal{K}} - \frac{1}{K_+}\right)\right\}, \tag{8}$$

where $\mathcal{K} = 2K_+K_-/(K_+ + K_-)$ is the harmonic mean of K_+ and K_- [36]. Equation (8) is a stochastic differential equation with multiplicative DMN ξ of amplitude $N^2(K_+ - K_-)/(2K_+K_-)$ [37]; it reduces to the deterministic limit (6) when the EN is removed (i.e. $K_+ = K_-$).

Although the process is only subject to EN, the global growth rate $g(x)$ couples the evolutionary and ecological dynamics. To simplify the analysis, we introduce an effective parameter $q \geq 0$ (see Section III C 2) and assume a constant $g \equiv 1 + q$ [36], obtaining the single-variate effective PDMP

$$\dot{N} = \mathcal{F}(N,\xi) = \begin{cases} \mathcal{F}_+(N) & \text{if } \xi = 1 \\ \mathcal{F}_-(N) & \text{if } \xi = -1, \end{cases} \tag{9}$$

$$\text{with} \quad \mathcal{F}_\pm(N) \equiv N\left[1 + q - \frac{N}{K_\pm}\right], \tag{10}$$

describing the evolution of a population of size $N(t)$ subject only to EN. According to (9) and (10), each environmental state ξ has a fixed point

$$N^*(\xi) = \begin{cases} N_+^* = (1+q)K_+ & \text{if } \xi = 1 \\ N_-^* = (1+q)K_- & \text{if } \xi = -1, \end{cases} \tag{11}$$

After $t = \mathcal{O}(1)$, the PDMP is at stationarity, characterized by a stationary probability function (PDF) $p^*_{\nu,q}(N,\xi)$ (derived in the SM [37]). Central for our purposes are the features of the marginal stationary PDF $p^*_{\nu,q}(N) = p^*_{\nu,q}(N,\xi) + p^*_{\nu,q}(N,-\xi)$, giving the probability density of N regardless of the environmental state ξ:

$$p^*_{\nu,q}(N) = \frac{\mathcal{Z}_\nu}{N^2}\left[\frac{(N_+^* - N)(N - N_-^*)}{N^2}\right]^{\frac{\nu}{1+q}-1}, \tag{12}$$

with normalization constant $\mathcal{Z}_\nu$. Depending on the sign of the exponent, the distribution may be unimodal or bimodal [36], but has always support $[N_-^*, N_+^*]$, on which $\mathcal{F}_+ \geq 0$ and $\mathcal{F}_- \leq 0$.

B. Internal noise & Fitness-dependent Moran process

Internal noise stems from the inherent stochasticity of individual birth and death events in the population; it ultimately causes fixation (one strain takes over the whole population), and hence determines the long-term population composition. When internal and ecological dynamics are coupled, which strain fixates has consequences on the population size, making fixations particularly important.

If internal noise is the only source of randomness (constant K), we can study its effects using the fitness-dependent Moran model [21, 22, 26, 50, 51], with constant size $N \equiv K$ [52]. To keep the population size constant, at each birth corresponds a death. Therefore, x increases by $1/N$ if an S individual is born and an F dies ($SF \to SS$ at rate $\widetilde{T}_S^+ = T_S^+T_F^-/N$), and decreases by $1/N$ if an F individual is born, replacing a dead S ($SF \to FF$ at rate $\widetilde{T}_S^- = T_S^-T_F^+/N$), with

$$\widetilde{T}_S^+ = \frac{1-s}{1-sx}g(x)(1-x)xN, \quad \widetilde{T}_S^- = \frac{1}{1-sx}g(x)(1-x)xN,$$

whose mean-field equation is (7). For an initial fraction x_0 of S individuals, in the framework of the Fokker-Planck equation, the fixation probability of S is [21, 22, 26] (see also Section XI.A in SM [37])

$$\phi(x_0)|_N = \frac{e^{-Ns(1-x_0)} - e^{-Ns}}{1 - e^{-Ns}}. \tag{13}$$

The fixation probability of S, thus becomes exponentially smaller the larger the population (of constant) size and the selection s; and, notably is independent of g. In the following we assume $x_0 = 1/2$ and drop the initial condition for notational simplicity: $\phi|_N \equiv \phi(x_0)|_N$ and $\phi \equiv \phi(x_0)$. Clearly, the fixation probability of F is $\widetilde{\phi}|_N = 1 - \phi|_N$.

C. Fixation under switching carrying capacity

The strain S unavoidably goes extinct in the deterministic limit, see equation (7), but has an exponentially vanishing survival probability when K is constant, see equation (13). However, when the carrying capacity switches, the population undergoes "bottlenecks" that can enhance this probability [36] and alter the long-term average population size.

1. *Fixation probabilities in the pure competition scenario ($b = 0$)*

When $b = 0$, both species compete for the same finite resources, with a slight selective advantage to F. Therefore, N and x are solely coupled by demographic fluctuations. After a time $t = \mathcal{O}(1)$, N attains its quasi-stationarity where it is distributed according to its N-QSD [45], that is well described by the PDF of equation (12) with $q = 0$. Instead, x relaxes on a slower timescale $t \sim 1/s \gg 1$, meanwhile experiencing an average of $\mathcal{O}(\nu/s)$ environmental switches. We can thus exploit this timescale separation and compute ϕ by averaging $\phi|_N$ over the PDF $p^*_{\nu/s} \equiv p^*_{\nu/s,0}$, with the rescaled switching rate $\nu \to \nu/s$ [36]:

$$\phi \simeq \int_{K_-}^{K_+} \phi|_N \, p^*_{\nu/s}(N)\, dN. \tag{14}$$

When $\nu \gg s$, $p^*_{\nu/s}$ is sharply peaked at $N \simeq \mathcal{K}$, and has two sharp peaks at $N \simeq K_\pm$ when $\nu \ll s$. Equation (14) captures the limiting behavior $\phi \xrightarrow{\nu\to\infty} \phi|_{\mathcal{K}}$ resulting from the self-average of the EN (since $\xi(t) \xrightarrow{\nu\to\infty} \langle \xi(t) \rangle = 0$), as well as $\phi \xrightarrow{\nu\to 0} (\phi|_{K_-} + \phi|_{K_+})/2$ in the regime of rare switching ($\nu \to 0$) when the environment almost never changes prior to fixation [36]. As shown in figure 2 and detailed in Section X of the SM [37], equation (14) reproduces the simulation result for the fixation probability of S within a few percent over a broad range of ν values. While S remains less likely to fixate than F, its fixation probability is much higher than in a constant environment ($\phi \gg \phi|_{\langle K \rangle}$): environmental variability considerably offsets the evolutionary bias favoring F.

2. *Fixation in the public good scenario, $b > 0$*

In the public good scenario, $g(x) = 1 + bx$ with $0 < b = \mathcal{O}(1)$, S individuals act as public good producers (cooperators). The higher x, in fact, the higher the reproduction rate of both strains, see equations (2). However, since S bears alone the metabolic cost for cooperating, it grows slower than F and, deterministically, x decreases.

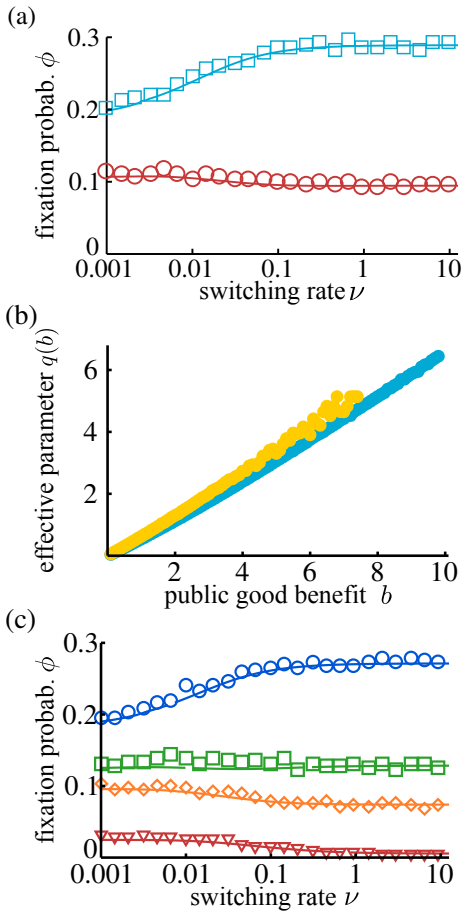

FIG. 2: (a) ϕ vs. ν in the case $b = 0$: for $s = 0.02$ (□, cyan) and $s = 0.05$ (○, red). (b) $q(b)$ vs. b for $s = 0.02$ (cyan) and $s = 0.05$ (yellow), see text. (c) ϕ vs. ν in the case $b > 0$: for $(s, b) = (0.02, 0.2)$ (blue, ○), $(0.02, 2)$ (green, □), $(0.05, 0.2)$ (orange, ◇), $(0.05, 2)$ (red, ▽). Symbols are ϕ from simulations (10^4 runs) and solid lines show ϕ_q from equation (15). In all panels, other parameters are $(K_+, K_-, x_0) = (450, 50, 0.5)$.

When $b > 0$, N and x are explicitly coupled, and they do not evolve on separate timescales: N is a fast variable, enslaved to the slow-varying x [45]. To determine the fixation probability, in Ref. [36] we devised an effective approach, based on suitably choosing the parameter q ($0 \le q \le b$) and setting $g(x) \equiv 1 + q$ in equation (8). This decouples N and x in an effective population whose size distribution, at quasi-stationarity and for any ν, is well described by the PDF (12). Within this effective theory approach, the fixation probability of S is thus determined similarly to the case $b = 0$:

$$\phi_q = \int_{N^*_-}^{N^*_+} \phi|_N \, p^*_{\nu/s,q}(N)\, dN\,. \tag{15}$$

As above, this expression simplifies in the limiting regimes $\nu \to \infty, 0$. When $\nu \gg 1$, $\phi_q \xrightarrow{\nu\to\infty} \phi_q^{(\infty)} = \phi|_{(1+q)\mathcal{K}}$

and $\phi_q \xrightarrow{\nu\to 0} \phi_q^{(0)} = (\phi|_{N_-^*} + \phi|_{N_+^*})/2$. We determined the effective parameter $q = q(b)$ for given $(K_\pm, s, b)$ by matching the prediction of $\phi_q^{(\infty)}$ with the results of simulations (see [36] and SM [37]). Figure 2(b) shows that $q(b)$ increases almost linearly with b, and depends weakly on s. Clearly, $q(0) = 0$ when $b = 0$, and equation (15) thus reverts to (14).

Figure 2(c) shows that the effective approach captures the effects of the coupling between N and x for several choices of b and s, over a broad range of ν. As detailed in the SM [37], the predictions of equation (15) agree within a few percent with simulation results when $s \ll 1$, while the accuracy deteriorates as s and b increase, therefore lowering ϕ. In fact, increasing b yields higher $q(b)$, which results in effectively increasing the carrying capacity $K_\pm \to (1 + q(b))K_\pm$. In the $\nu \to \infty, 0$ limits, this is equivalent to rescaling the selection intensity as $s \to (1 + q(b))s$, as inferred from $\phi_q^{(\infty,0)}$ and equation (13). Therefore ϕ decays (approximately) exponentially with b, as shown by figure 3(a).

IV. CORRELATIONS & COOPERATION IN THE ECO-EVOLUTIONARY GAME

When the slow strain S produces a public good (PG), the long-time eco-evolutionary dynamics is characterized by correlations between the population size and its composition. In this section, we analyze these long-term effects by characterizing the correlations first, then considering the ensuing "eco-evolutionary game".

To this end, it is useful to consider the average population size $\langle N\rangle^*_{\nu,b}$ for given ν and b, after a time $t \gg 1/s$, when the population is at quasi-stationarity and consists of only S or F individuals, see Section XI.B in SM [37]. Within the PDMP approximation—that is, approximating the evolution of N by the PDMP (9), see Section XII.A of SM [37]—we can compute the quasi-stationary average of N using $p^*_{\nu,q}$ given by eq. (12) to (see also Sec. V A):

$$\langle N\rangle^*_{\nu,b} = (1+b)\phi_b \langle N\rangle^*_{\frac{\nu}{1+b},0} + \widetilde{\phi}_b \langle N\rangle^*_{\nu,0} > \langle N\rangle^*_{\nu,0}, \qquad (16)$$

where $\langle N\rangle^*_{\nu,0}$ is the population long-time average in the absence of PG production, ϕ_b denotes the fixation probability of S for a public good parameter b, and $\widetilde{\phi}_b = 1 - \phi_b$. As figure 3(b) shows, equation (16) predicts that the long-term population size increases with b, and decreases with ν (keeping other parameters constant), in agreement with simulation results.

A. Correlations between ecological & evolutionary dynamics

Equation (16) also highlights how fixation probabilities affect the long-term average population size. When $b > 0$, there are nontrivial correlations between population size and composition. Prior to fixation, these are accounted by our effective approach $q(b)$ (see section III C 2). Here, we investigate their effect after fixation using the rescaled connected correlation

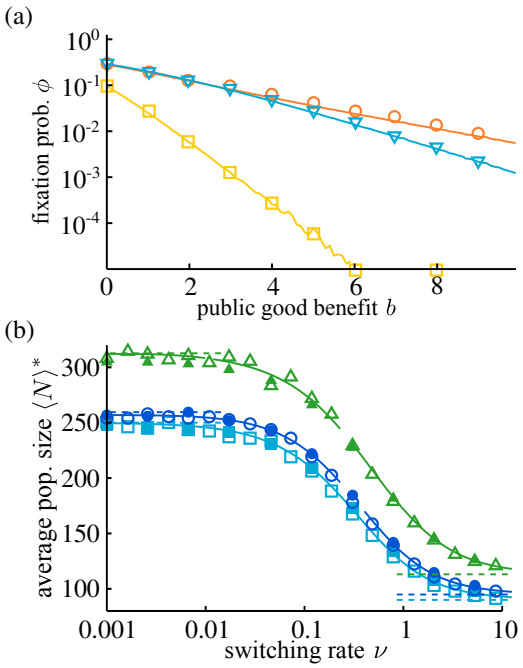

FIG. 3: (a) ϕ_q vs b in lin-log scale for $s = 0.02$, $\nu = 0.1$ (orange, $\circ$) and $\nu = 10$ (cyan, ∇); $s = 0.05$, $\nu = 10$ (yellow, $\square$). Lines are from (15) and markers are from simulations. (b) $\langle N\rangle^*_{\nu,b}$ vs. ν for $b = 0$ (cyan, squares), $b = 0.2$ (blue, circles) and $b = 2$ (green, triangles) and $s = 0.02$. Solid lines are from (16); empty symbols are from simulations; filled symbols are from (27) within the linear noise approximation. Dashed lines indicate the predictions of (15) in the regimes $\nu \to \infty, 0$, see [37]. Parameters are $(K_+, K_-, x_0) = (450, 50, 0.5)$.

function

$$\mathcal{C}_{\nu,b}(t) = \frac{\langle (N(t) - \langle N(t)\rangle)\,(x(t) - \langle x(t)\rangle)\rangle}{\langle N(t)\rangle\langle x(t)\rangle}. \qquad (17)$$

When $\langle N(t)x(t)\rangle = \langle N(t)\rangle\langle x(t)\rangle$, i.e. in absence of correlations, $\mathcal{C}_{\nu,b}(t)$ vanishes. At quasi-stationary, $\langle N(t)\rangle \to \langle N\rangle^*_{\nu,b}$ and $\langle x(t)\rangle \to \phi_b$. Within the PDMP approximation, using eq. (16) and $\phi_b \simeq \phi_q$, equation (17) becomes

$$\mathcal{C}^*_{\nu,b} = \frac{\langle Nx\rangle^*_{\nu,b}}{\langle N\rangle^*_{\nu,b}\phi_b} - 1 \simeq \frac{\widetilde{\phi}_q\left[(1+b)\langle N\rangle^*_{\frac{\nu}{1+b},0} - \langle N\rangle^*_{\nu,0}\right]}{(1+b)\phi_q\langle N\rangle^*_{\frac{\nu}{1+b},0} + \widetilde{\phi}_q\langle N\rangle^*_{\nu,0}}. \qquad (18)$$

Since $\langle N\rangle^*_{\nu,0}$ is decreasing in ν (see figure 3(a)), this long-term correlation is always positive for $b \geq 0$, and vanishes only for $b = 0$.

As shown in figure 4, $\mathcal{C}^*_{\nu,b}$ grows approximately linearly with b and is non-monotonic in ν with a maximum for $\nu = \mathcal{O}(1)$; all features that equation (18) captures well. The ν-dependence of $\mathcal{C}^*_{\nu,b}$ stems from the fact that ϕ_b increases or decreases with ν, depending on the value of s, see figure 2(c) [36]. In the limiting regimes $\nu \to \infty, 0$, equation (18) simplifies and yields $\mathcal{C}^*_{\nu,b} \simeq b[1 - (1+b)\phi^{(\infty,0)}_{q(b)}]$ [37]. Therefore,

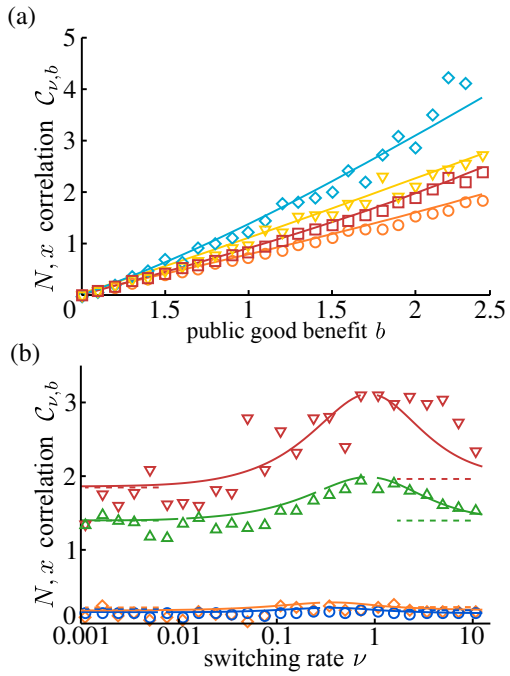

FIG. 4: (a) $\mathcal{C}^*_{\nu,b}$ vs b for $s = 0.05$ and $\nu \simeq 1$ (cyan, $\diamond$), $\nu = 0.1$ (yellow, ∇); $s = 0.02$ and $\nu = 1$ (red, $\square$), and $\nu = 0.1$ (orange, $\circ$). (b) $\mathcal{C}^*_{\nu,b}$ vs ν for $b = 2$ and $s = 0.05$ (red, ∇), $s = 0.02$ (green, $\triangle$); $b = 0.2$ and $s = 0.05$ (orange, $\diamond$), $s = 0.02$ (blue, $\circ$). In all panels, the parameters are $(K_+, K_-, x_0) = (450, 50, 0.5)$. Symbols are results from simulations and solid lines are from equation (18); dashed lines in panel (b) denote the analytical predictions of $\mathcal{C}_{\nu,b}$ in the limits $\nu \ll s$ and $\nu \gg 1$, see text.

in these the limiting regimes $\mathcal{C}^*_{\nu,b}$ increases in s, and scales as $\mathcal{O}(b)$, as shown by figure 4(b).

These results show that, when species S provides a PG, there are long-term correlations between ecological and evolutionary variables: the population size is shaped by its composition. The correlations between N and x are maximal in the intermediate switching regime where $\nu = \mathcal{O}(1)$ is comparable to the growth rate of N, and are weaker in the limiting switching regimes, on which we devised the effective theory of section III C 2.

B. When is cooperation beneficial? In which conditions is it best to cooperate?

In the long run, the PG provides a benefit to the whole population, as the overall average size increases. On the other hand, producing a PG burdens S in the short term by exponentially reducing its fixation probability, as figure 3(b) shows. This eco-evolutionary game resembles a "social dilemma" [26]: cooperators pay a cost in terms of reduced fixation probability to provide a benefit to the entire population whose long-term average size increases, see equation (16). Here, we measure the success of each strain in terms of the expected population size after fixation. We thus use the PDMP approximations and simulations to investigate the relative abundance of each species at quasi-stationarity (see also SM [37]).

The average number of F individuals at quasi-stationarity, given a switching rate ν and PG parameter b is

$$\langle N_F\rangle^*_{\nu,b} = \langle N|x=0\rangle^*_{\nu,b} = (1-\phi_b)\langle N\rangle^*_{\nu,0},$$

i.e. the average population size conditioned to F fixation. Similarly, the average number of cooperators S at quasi-stationarity is

$$\langle N_S\rangle^*_{\nu,b} = \langle N|x=1\rangle^*_{\nu,b} = (1+b)\phi_b\langle N\rangle^*_{\nu/(1+b),0}.$$

We measure the expected payoff provided by the PG as *the difference between the expected number of individuals of a strain at quasi-stationarity when $b > 0$ relative to the case $b = 0$*. Hence, the expected payoff to F is

$$\Delta F_{\nu,b} \equiv \langle N_F\rangle^*_{\nu,b} - \langle N_F\rangle^*_{\nu,0} = (\phi_0 - \phi_b)\langle N\rangle^*_{\nu,0} > 0. \quad (19)$$

Since $\phi_0 > \phi_b$, see figure 3(b), this quantity is positive and increases with b. This means that, as in the classical cooperation dilemma, the "freeriding" strain F benefits more the higher the level of cooperation. However, this does not rule out the possibility that, in certain circumstances, the PG production can be either beneficial or detrimental to S, and even permits S to be better off than F. In fact, the expected payoff for cooperators reads

$$\begin{aligned}\Delta S_{\nu,b} &\equiv \langle N_S\rangle^*_{\nu,b} - \langle N_S\rangle^*_{\nu,0} \\ &= (1+b)\phi_b\langle N\rangle^*_{\frac{\nu}{1+b},0} - \phi_0\langle N\rangle^*_{\nu,0}, \end{aligned} \quad (20)$$

and clearly varies nontrivially with ν and b. Unless $\Delta S_{\nu,b} > 0$, the PG is actually detrimental for cooperators: the expected number of S individuals is lower than it would be without PG. The PG benefits cooperators only if the increase in the average population size offsets the decrease in fixation probability, i.e. if

$$(1+b)\frac{\langle N\rangle^*_{\frac{\nu}{1+b},0}}{\langle N\rangle^*_{\nu,0}} > \frac{\phi_0}{\phi_b}$$

In figure 5, we show that $\Delta S_{\nu,b}$ is non-monotonic in b, generating a maximum at an *optimal value* $b^*(\nu, s)$, which defines the conditions where PG production is the most rewarding for cooperators. Moreover, we observe a definite *critical threshold* $b_c(\nu, s)$, below which producing a PG benefits cooperators.

Using our effective theory, $\phi \simeq \phi_{q(b)}$, and the PDMP approximation, the expected payoff of S (S21) reads

$$\begin{aligned}\Delta S_{\nu,b} &= (1+b)\phi_{q(b)}\int_{K_-}^{K_+} Np^*_{\frac{\nu}{1+b}}(N)\,dN \\ &- \phi_0\int_{K_-}^{K_+} Np^*_\nu(N)\,dN\,. \end{aligned} \quad (21)$$

Results in figure 5 show that equation (21) approximates well the simulation results over a broad range of parameters. The

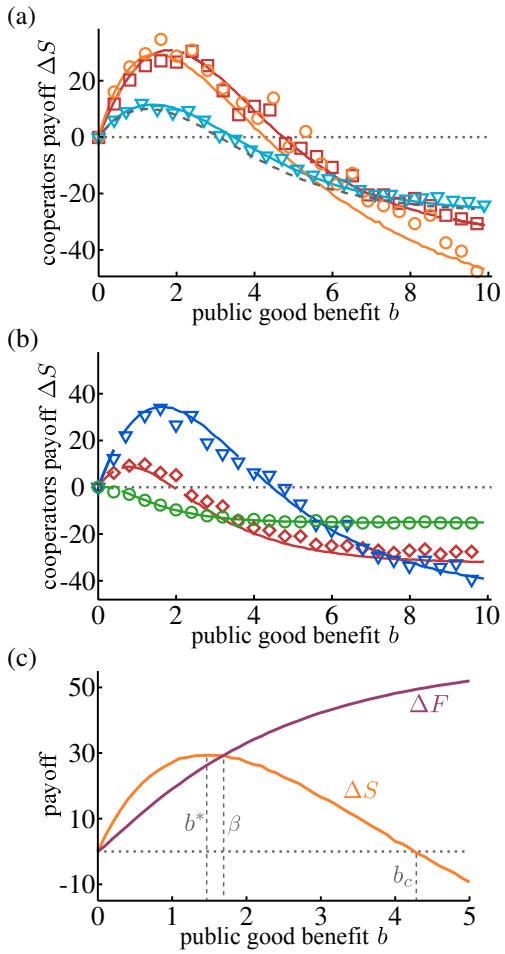

FIG. 5: (a) $\Delta S_{b,\nu}$ vs. b for $s = 0.02$ and switching rates $\nu = 10$ (cyan, ∇), $\nu = 1$ (red, $\square$), $\nu = 0.1$ (orange, $\circ$). Predictions from equation (21) (solid) are compared to simulation results (symbols). We find $\Delta S_{\nu,b} > 0$ when $0 < b < b_c(\nu, s)$ with an optimal payoff for S when $b = b^*(\nu, s)$, e.g. $(b_c, b^*) \approx (4.9, 2.1)$ at $\nu = 1$. (b) $\Delta S_{b,\nu}$ vs. b with $\nu \simeq 0.44$, for $s = 0.02$ (blue, ∇), $s = 0.03$ (red, $\diamond$), and $s = 0.05$ (green, $\circ$). Solid lines are from equation (21) and symbols are simulation results (see SM [37]). (c) Expected payoffs $\Delta S_{b,\nu}$ and $\Delta F_{b,\nu}$ vs. b obtained from equation (21). Dashed lines show the values of b^*, β and b_c. In all panels, the parameters are $(K_+, K_-, x_0) = (450, 50, 0.5)$.

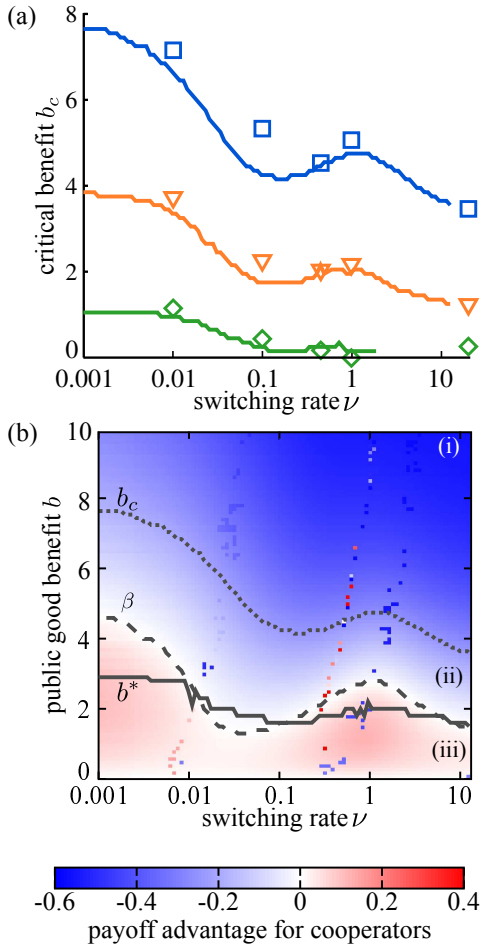

FIG. 6: (a) b_c vs ν. Symbols are results from simulations and solid lines are from equation (21) for $s = 0.02$ (blue), $s = 0.03$ (orange), and $s = 0.05$ (green). (b) Heatmap of $(\Delta S_{\nu,b} - \Delta F_{\nu,b})/\langle N\rangle^*_{\nu,0}$, from equation (21) for $s = 0.02$. The gray dotted line shows $b = b_c(\nu, s)$, the dashed line $b = \beta(\nu, s)$ and the solid line $b = b^*(\nu, s)$. In the blue area (phases (i) and (ii)), $b > \beta$ and F is better off than S ($\Delta F_{\nu,b} > \Delta S_{\nu,b}$). PG production is detrimental for S in phase (i) where $b > b_c$ and $\Delta S_{\nu,b} < 0$; beneficial for S ($\Delta S_{\nu,b} > 0$) in phase (ii) where $\beta < b < b_c$, but more beneficial for F (higher expected payoff). In the red/pink area of region (iii), $b < \beta$ and S is better off than F ($\Delta S_{\nu,b} > \Delta F_{\nu,b}$). Colored dots correspond to "gaps" in the numerical data (see [37]). Parameters are $(K_+, K_-, x_0) = (450, 50, 0.5)$.

root and the maximum of equation (21) provides (approximate) predictions for b_c and b^*, see figures 6 and S6(a) [37]. These figures reveal that b_c and b^* depend non-monotonically on ν and vary greatly with s, both behaviors well-captured by the theory. Figures 5 and S6(b) [37] also show that the maximal payoff for S can be significantly higher than that of F, especially when the selection s is low.

In order to discuss the eco-evolutionary game, it is useful to determine the value $b = \beta(\nu, s)$ of equal expected payoff, i.e. such that which $\Delta S_{\nu,\beta} = \Delta F_{\nu,\beta}$, see figure 5(c). From equations (S22)-(21), we find that when $\beta(\nu, s)$ is the solution of

$$\frac{1}{1+\beta}\left(\frac{2\phi_0}{\phi_{q(\beta)}} - 1\right) = \frac{\langle N\rangle^*_{\frac{\nu}{1+\beta},0}}{\langle N\rangle^*_{\nu,0}} = \frac{\int_{K_-}^{K_+} N p^*_{\frac{\nu}{1+\beta}}\, dN}{\int_{K_-}^{K_+} N p^*_{\nu}\, dN}. \quad (22)$$

So β is a nontrivial function of ν and s, as as shown in figure 6(b).

The eco-evolutionary game is characterized by three phases:

(i) When $b > b_c$, the PG production is detrimental for S. The cost of cooperation outweighs its benefits and the

expected payoff for S is negative ($\Delta S_{\nu,b} < 0$). The PG thus benefits only F.

(ii) When $\beta < b < b_c$, the PG production benefits S, but benefits F more ($0 < \Delta S_{\nu,b} < \Delta F_{\nu,b}$).

(iii) When $0 < b < \beta$, S reaps a higher expected payoff than F ($\Delta S_{\nu,b} > \Delta F_{\nu,b} > 0$). In this case, the benefit of the PG outweigh its cost, and its production is *favored*.

Therefore, species F effectively exploits S in phases (i) and (ii), but is at a disadvantage in phase (iii). Since the expected payoff to S is positive in regions (ii) and (iii), we say that *cooperation to produce a public good with benefit parameter b is beneficial when $0 < b < b_c(\nu, s)$, and advantageous for $0 < b < \beta(\nu, s)$*. Given a set of parameters (b, ν, s), PG production is the best strategy if two conditions are met: (a) the expected payoff of S is higher than that of F, which is satisfied in phase (iii); (b) b yields the maximum possible payoff for S, i.e., $b = b^*$. Hence, *In an environment switching at rate ν and under a selection intensity s, the best conditions to cooperate for the public good production is when the PG benefit parameter satisfies $b = b^*(\nu, s) < \beta(\nu, s)$*, represented by the solid gray line in phase (iii) of figure 6(b).

This eco-evolutionary game thus provides a way out of the cooperation dilemma arising prior to fixation. Furthermore, it exemplifies the evolutionary role of the fluctuating environment. In fact, although freeriders have a constant growth-rate advantage over cooperators, this selective bias can be efficiently balanced by environmental variability, allowing even cooperators to possibly be more successful than freeriders [37]

V. LINEAR-NOISE AND PDMP APPROXIMATIONS TO THE POPULATION QSD

After $t \gg 1/s$, one strain likely fixated, so the population is at quasi-stationarity, with its composition fixed [36]. Yet, the population size still fluctuates and $N(t)$ is distributed according to its quasi-stationary distribution. When $K_- \gg 1$, the population size is always large and, in the first instance, demographic fluctuations are negligible compared to environmental noise, and eq. (9) characterizes well the long-term behavior of $N(t)$.

A. Linear-noise approximation about the PDMP predictions

Throughout this work (and in [36]), we have shown that the PDMP approximation $p^*_{\rm PDMP}(N) = \phi p^*_{\nu,b}(N) + \widetilde{\phi} p^*_{\nu}(N)$ reproduces many characteristics of the quasi-stationary size distribution (N-QSD). However, as p^*_ν and $p^*_{\nu,b}$ only account for the external noise (EN), they cannot reproduce the complete N-QSD, which is also subject to internal noise (IN). Here, we use the linear noise approximation (LNA) about the PDMP predictions to account for the *joint effect* of the two noise sources, IN and EN, on the N-QSD.

The LNA is widely employed to quantify the effect of weak demographic fluctuations in the absence of external noise, and has recently been used to study the joint effect of decoupled internal and external noise [12]. Here, we show how to generalize the LNA to the case where the population size fluctuates and demographic fluctuations are coupled to the external noise.

For our analysis, we assume that $K_+ \gtrsim K_- \gg 1$, so that $\langle K \rangle$ is large and of the same order as $K_\pm$ (see Section XIII in SM [37] for details). It is convenient to work with the continuous random variable $n = N/\Omega$, where $\Omega = \langle K \rangle \gg 1$ is the system's "large parameter". The auxiliary Markovian process $\{n(t), \xi(t)\}$ that we consider for the LNA is defined by $n \xrightarrow{\mathcal{T}^+} n + \Omega^{-1}$, $n \xrightarrow{\mathcal{T}^-} n - \Omega^{-1}$ and $\xi \xrightarrow{\nu} -\xi$, where the transition rates $\mathcal{T}^\pm$ are given by equations (S26) in the SM [37]. We also introduce $\psi = \lim_{\Omega\to\infty} N/\Omega = \mathcal{O}(1)$, which obeys a PDMP defined by equation (S29) [37], and the random variable $\eta(t)$, capturing the fluctuations of n about ψ, according to

$$n(t) = \psi(t) + \frac{\eta(t)}{\sqrt{\Omega}}, \tag{23}$$

We are interested in the (quasi-)stationary joint probability density $\pi^*_{\nu,q}(\eta, \psi, \xi)$ of the process $\{n(t), \xi(t)\}$. This probability can be decomposed into $\pi^*_{\nu,q}(\eta, \psi, \xi) = \pi^*(\eta|\psi, \xi)\pi^*_{\nu,q}(\psi, \xi)$, where $\pi^*_{\nu,q}(\psi, \xi) = \Omega p^*_{\nu,q}(\Omega\psi, \xi)$ is the stationary joint PDF of the PDMP governing ψ's dynamics and is readily obtained from the PDF of equation (9). The probability density $\pi^*(\eta|\psi, \xi)$ accounts for the demographic fluctuations about ψ in the environmental state ξ. Following Ref. [12], we assume that the demographic fluctuations are approximately the same in both environmental states, i.e. $\pi^*_{\nu,q}(\eta|\psi, \xi) \simeq \pi^*_{\nu,q}(\eta|\psi, -\xi)$, and simply denote $\pi^*_{\nu,q}(\eta|\psi) \equiv \pi^*_{\nu,q}(\eta|\psi, \xi)$. This assumption is reasonable when K_+ and K_- are of the same order, and yields

$$\pi^*_{\nu,q}(\eta, \psi, \xi) \simeq \pi^*(\eta|\psi)\pi^*_{\nu,q}(\psi, \xi). \tag{24}$$

With this approximation, the quasi-stationary marginal LNA probability density of $\{n(t)\}$ is

$$\begin{aligned} \pi^*_{\nu,q}(n) \;&=\; \sum_{\xi=\pm1} \int\int d\psi d\eta\; \pi^*(\eta|\psi) \\ &\times\; \pi^*_{\nu,q}(\psi, \xi)\; \delta\left(n - \psi - \frac{\eta}{\sqrt{\Omega}}\right), \end{aligned} \tag{25}$$

where $\pi^*(\eta|\psi) = \exp\{-\eta^2/(2\psi)\}/\sqrt{2\pi\psi}$ (see SM [37] for details), and the Dirac delta ensures that (23) is satisfied. Calling $p^*_{\rm LNA,\nu,0}(N) = \pi^*_{\nu,0}(n)/\Omega$ and $p^*_{\rm LNA,\nu,b}(N) = \pi^*_{\nu,b}(n)/\Omega$, explicitly given by eqs. (S35) and (S36) in SM [37], the LNA quasi-stationary probability density reads

$$p^*_{\rm LNA}(N) \;=\; \phi p^*_{\rm LNA,\nu,b}(N) + \widetilde{\phi} p^*_{\rm LNA,\nu,0}(N). \tag{26}$$

Within the LNA, the quasi-stationary average population size is obtained by averaging N over $p^*_{\rm LNA}(N)$:

$$\langle N \rangle^*_{\rm LNA,\nu,b} = \int_0^\infty N p^*_{\rm LNA}(N)\, dN\,, \tag{27}$$

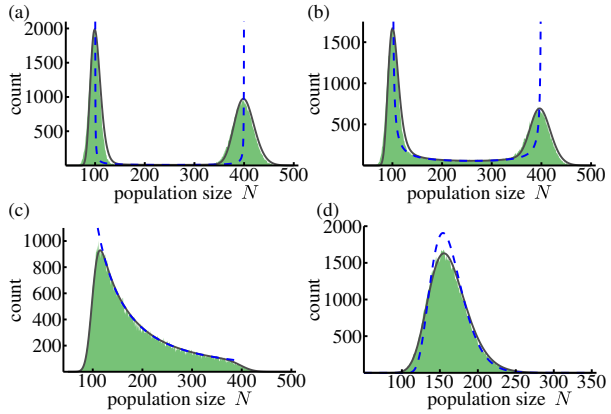

FIG. 7: Histograms of the population size distribution (N-QSD) when $b = 0$ (shaded area) compared with the predictions of the LNA (solid), from equation (S35) of the SM [37], and with the PDMP predictions (dashed), from $p^*_{\nu,0}$, for different switching rates: (a) $\nu = 0.01$, (b) $\nu = 0.1$, (c) $\nu = 1$, (d) $\nu = 10$, see text. Parameters are $(K_+, K_-, s, x_0) = (400, 100, 0.02, 0.5)$. Here, $\mathcal{K} = 160$.

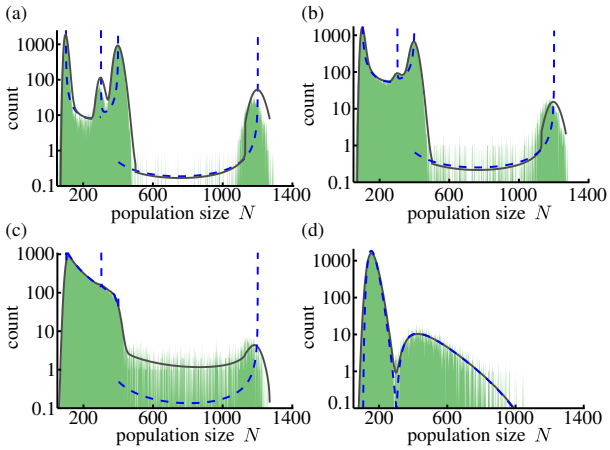

FIG. 8: Histograms of the population size distribution (N-QSD) when $b = 2$ (shaded area) compared with the predictions of the LNA (solid), from eq. (26) and equations (S35) and (S36) in SM [37], and with the PDMP predictions (dashed) based on eq. (12), with $q = b$ (when $x = 1$) and $q = 0$ (when $x = 0$), for different switching rates: (a) $\nu = 0.01$, (b) $\nu = 0.1$, (c) $\nu = 1$, (d) $\nu = 10$. Parameters are $(K_+, K_-, s, b, x_0) = (400, 100, 0.02, 2, 0.5)$. For the analytical results, we have used the expression (15) for $\phi(b) \simeq \phi_{q(b)}$.

where, it is worth noting, the integral is no longer restricted to a finite support. As figure 3(b) shows, $\langle N\rangle^*_{\mathrm{LNA},\nu,b}$ is as good an approximation of simulation results as its PDMP counterpart $\langle N\rangle^*_{\nu,b}$ from equation (16). As done in Section IV, it is thus convenient to compute the averages of N using the PDMP approximation, i.e. by averaging over $p^*_{\mathrm{PDMP}}(N)$ as in eq. (16). However, as elaborated below, equation (26) gives an excellent characterization of the full N-QSD, well beyond the scope of the PDMP approximation.

B. LNA, N-QSD, and noise-induced transitions

1. *Pure resource competition scenario, $b = 0$*

In the pure resource competition scenario ($b = 0$), $p^*_{\mathrm{LNA},0}(N) = \pi^*_0(n)/\Omega$ provides an excellent approximation of the N-QSD in all switching regimes, as shown in figure 7. In particular, $p^*_{\mathrm{LNA},0}$ captures the noise-induced transition arising about $\nu = 1$ [36, 39, 40]: When $\nu < 1$, the switching rate is lower than the population growth rate, and the N-QSD and $p^*_{\mathrm{LNA},0}$ are both bimodal, with peaks at $N \approx K_\pm$, see figure 7 (a,b). When $\nu > 1$, the switching rate exceeds the population growth rate, and the N-QSD and $p^*_{\mathrm{LNA},0}$ are thus unimodal, with a peak at $N \approx \mathcal{K}$, see Figure 7(c,d).

Figure 7 also shows that $p^*_{\mathrm{LNA},0}(N)$ accurately predicts the peaks, their width and intensity, and the skewness of the N-QSD, whereas the PDMP predictions from equation (12) only captures the position of the peaks. This demonstrates how demographic fluctuations, aptly accounted for by the LNA, cause the discrepancies between the N-QSD and p^*_ν.

2. *Public-good scenario, $b > 0$*

The LNA expression (26) also provides an excellent approximation of the N-QSD in all switching regimes for the public good scenario ($b > 0$), see figure 8. In particular, p^*_{LNA} captures the noise-induced transitions arising about $\nu = 1$ and $\nu = 1 + b$ [36]: When $\nu < 1$, both conditional population distributions (for fixations to S or F) are bimodal, with different peaks. N-QSD and p^*_{LNA} thus have four peaks at $N \approx K_\pm$ and $N \approx (1 + b)K_\pm$, see figure 8(a,b). When $1 < \nu < 1 + b$, the S-conditional distribution is bimodal, whereas the F-conditional distribution is unimodal. The N-QSD and p^*_{LNA} thus have three peaks at $N \approx (1 + b)K_\pm$ and $N \approx \mathcal{K}$, see figure 8(c). Finally, when $\nu > 1 + b$, both conditional distributions are unimodal, but with different peaks. Hence, the N-QSD and p^*_{LNA} are bimodal with peaks at $N \approx \mathcal{K}$ and $N \approx (1 + b)\mathcal{K}$, see figure 8(d)

As figure 8 shows, $p^*_{\mathrm{LNA}}(N)$ provides a faithful characterization of the N-QSD also when $b > 0$. This reiterates that the discrepancies with the PDMP approximation stem from demographic fluctuations. We also notice that the accuracy of the LNA slightly deteriorates near the lower-intensity peaks at high N and low ν (see figure 8(a)). These correspond to rare events, usually beyond the scope of the LNA. Moreover, in those regimes, some assumptions made in the derivation—*e.g.* equation (24)— reach the limit of their validity, see SM [37].

VI. CONCLUSION

We have studied the eco-evolutionary dynamics of a population subject to a randomly switching carrying capacity in which one strain has a slight selective advantage over another. In a model inspired by microbial communities evolving in fluctuating environments, we have considered two scenarios—one of pure resource competition (no interaction between strains) and one in which the slow (cooperating) strain produces a public good—and investigated the *coupled* effect of demographic and environmental noise.

We have developed an analytical procedure to determine the fixation probabilities, exploiting a time scale separation and an effective theory. Fixation probabilities characterize the population composition, which is correlated with evolution of the population size. As a result, the production of public goods gives rise to an *eco-evolutionary game*: On the one hand, producing the public good lowers the survival/fixation probability of cooperators; on the other hand, it also increases their population size. A social dilemma of sorts therefore ensues and, in a fluctuating environment, it is a priori not intuitively clear whether there are circumstances under which it is beneficial to produce a public good and what these conditions may be. Since we consider the eco-evolutionary game in a population whose composition is fixed but whose size fluctuates, we have proposed to measure the evolutionary benefit of the public good in terms of the long-term expected number of individuals of each strain. We have thus determined, both analytically and with simulations, the circumstances under which cooperation is beneficial or detrimental to public good producers, as well as the conditions under which it is the optimal strategy. The analysis of the "eco-evolutionary game" shows that in a fluctuating population the evolutionary success of a strain goes beyond having a growth-rate advantage and a higher fixation probability. In fact, the rate of switching, along with the selection intensity, also determine when one species is more successful than another and, in some circumstances, this allows a slow/cooperating strain to outcompete a fast/freeriding strain.

We have also improved on the characterization of the population size distribution by generalizing the linear noise approximation to populations of fluctuating size, thus accounting for demographic fluctuations about the predictions of the underlying piecewise deterministic Markov process. While we have found that the linear noise and the piecewise-deterministic Markov process approximations describe the average population size equally well, only the former fully characterizes the population size distribution. In fact, the linear noise approach accounts for the joint effect of environmental and demographic noise and has allowed us to capture the width and skewness of the population size distribution.

This study shows that coupled environmental and demographic noise can greatly influence how the composition and size of a population evolve. In particular, social interactions between strains—such as public good production—can lead to intricate eco-evolutionary dynamics, which potentially support cooperation. This sheds light on phenomena that are particularly relevant to microbial communities, which often feature coupled internal and ecological evolution.

Acknowledgments

KW is grateful to the University of Leeds for the hospitality during the final stage of this work. EF and KW acknowledge funding by the Deutsche Forschungsgemeinschaft, Priority Programme 1617 "Phenotypic heterogeneity and sociobiology of bacterial populations", grant FR 850/11-1,2, and the German Excellence Initiative via the program "Nanosystems Initiative Munich" (NIM). MM is grateful for the support of the Alexander von Humboldt Foundation (Grant No. GBR/1119205 STP) and for the hospitality of the University of Munich during the initial phase of this collaboration.

[1] Morley C R, Trofymow J A, Coleman D C, Cambardella C. 1983 Effects of freeze-thaw stress on bacterial populations in soil microcosms. *Microbiol. Ecol.* **9**, 329-340. (doi: 10.1007/BF02019022)

[2] Fux C A, Costerton J W, Stewart P S, Stoodley P. 2005 Survival strategies of infectious biofilms. *Trends Microbiol.* **13**, 34-40. (doi: 10.1016/j.tim.2004.11.010)

[3] May R M.1973 *Stability and complexity in model ecosystems*. Princeton, USA: Princeton University Press.

[4] Karlin S, Levikson B. 1974 Temporal fluctuations in selection intensities: Case of small population size *T. Pop. Biol.* **74**, 383-412. (doi: 10.1016/0040-5809(74)90017-3)

[5] Kussell E, Leibler S. 2005 Phenotypic Diversity, Population Growth, and Information in Fluctuating Environments *Science* **309**, 2075-2078. (doi: 10.1126/science.1114383)

[6] Assaf M, Roberts E, Luthey-Schulten Z, Goldenfeld N. 2013 Extrinsic Noise Driven Phenotype Switching in a Self-Regulating Gene. *Phys. Rev. Lett.* **111**, 058102 (2013). (doi: 10.1103/PhysRevLett.111.058102)

[7] He Q, Mobilia M, Täuber U C. 2010 Spatial rock-paper-scissors models with inhomogeneous reaction rates. *Phys. Rev. E* **82**, 051909. (doi: 10.1103/PhysRevE.82.051909)

[8] Dobramysl U, Täuber U C. 2013 Environmental Versus Demographic Variability in Two-Species Predator-Prey Models. *Phys. Rev. Lett.* **110**, 048105. (doi: 10.1103/PhysRevLett.110.048105)

[9] Assaf M, Mobilia M, Roberts E. 2013 Cooperation Dilemma in Finite Populations under Fluctuating Environments. *Phys. Rev. Lett.* **111**, 238101. (doi: 10.1103/PhysRevLett.111.238101)

[10] Ashcroft P, Altrock P M, Galla T. 2014 Fixation in finite populations evolving in fluctuating environments. *J. R. Soc. Interface* **11**, 20140663. (doi: 10.1098/rsif.2014.0663)

[11] Melbinger A, Vergassola M. 2015 The Impact of Environmental Fluctuations on Evolutionary Fitness Functions *Scientific Reports* **5**, 15211. (doi: 10.1038/srep15211)

[12] Hufton P G, Lin Y T, Galla T, McKane A J. 2016 Intrinsic noise in systems with switching environments. *Phys. Rev. E* **93**,

052119. (doi: 10.1103/PhysRevE.93.052119)
[13] Hidalgo J, Suweis S, Maritan A. 2017 Species coexistence in a neutral dynamics with environmental noise. *J. Theor. Biol.* **413**, 1-10. (doi: 10.1016/j.jtbi.2016.11.002)
[14] Danino M, Shnerb N M. 2017 Fixation and absorption in a fluctuating environment. *e-print: https://arxiv.org/abs/1710.08807*
[15] Chesson P L, Warner R R. 1981 Environmental Variability Promotes Coexistence in Lottery Competitive Systems. *American Naturalist* **117**, 923-943. (doi: 10.1086/283778)
[16] Kussell E, Kishony R, Balaban N Q, Leibler S. 2005 Bacterial Persistence: A Model of Survival in Changing Environments. *Genetics* **169**, 1807-1814. (doi: 10.1534/genetics.104.035352)
[17] Acer M, Mettetal J, van Oudenaarden A. 2008 Stochastic switching as a survival strategy in fluctuating environments. *Nature Genetics* **40**, 471-475. (doi: 10.1038/ng.110)
[18] Beaumont H, Gallie J, Kost C, Ferguson G, Rainey P. 2009 Experimental evolution of bet hedging Nature **462**, 90-93. (doi: 10.1038/nature08504)
[19] Visco P, Allen R J, Majumdar S N, Evans M R. 2010 Switching and Growth for Microbial Populations in Catastrophic Responsive Environments. *Biophys. J.* **98**, 1099-1108. (doi: 10.1016/j.bpj.2009.11.049)
[20] Xue B, Leibler S. 2017 Bet-hedging against demographic fluctuations *Phys. Rev. Lett.* **119**, 108113 (2017). (doi: 10.1103/PhysRevLett.111.058102)
[21] Crow J F, Kimura M, 2009 *An Introduction to Population Genetics Theory*. New Jersey, USA: Blackburn Press
[22] Blythe R A, McKane A J. 2007 Stochastic models of evolution in genetics, ecology and linguistics *J. Stat. Mech.* **P07018** (doi:10.1088/17442-5468/2007/07/P07018)
[23] Melbinger A, Cremer J, Frey E. 2010 Evolutionary Game Theory in Growing Populations. *Phys. Rev. Lett.* **105**, 178101. (doi:10.1103/PhysRevLett.105.178101)
[24] Cremer J, Melbinger A, Frey E. 2011 Evolutionary and population dynamics: A coupled approach. *Phys. Rev. E* **84**, 051921. (doi: 10.1103/PhysRevE.84.051921)
[25] Cremer J, Melbinger A, Frey E. 2012 Growth dynamics and the evolution of cooperation in microbial populations. *Sci. Rep.* **2**, 281 (doi: 10.1038/srep00281)
[26] Cremer J, Reichenbach T, Frey E. 2009 The edge of neutral evolution in social dilemmas *New J. Phys.* **11**, 093029. (doi: 10.1088/1367-2630/11/9/093029)
[27] Pelletier F, Garant D, Hendry H P. 2009 Eco-evolutionary dynamics. *Phil. Trans. R. Soc. B* **364** 1483-1489. (doi:10.1098/rstb.2009.0027)
[28] Melbinger A, Cremer J, Frey E. 2015 The emergence of cooperation from a single mutant during microbial life cycles. J. R. Soc. Interface **12**, 20150171. (doi: 10.1098/rsif.2015.0171)
[29] Chuang J S, Rivoire O, Leibler S. 2009 Simpson's Paradox in a Synthetic Microbial System. *Science* **323**, 272-275. (doi: 10.1126/science.1166739)
[30] Wahl L M, Gerrish P J, Saika-Voivod I. 2002 Evaluating the impact of population bottlenecks in experimental evolution. *Genetics* **162**, 961-971. (url: http://www.genetics.org/content/162/2/961)
[31] Patwas Z, Wahl L M. 2009 Adaptation rates of lytic viruses depend critically on whether host cells survive the bottleneck. *Evolution* **64**, 1166-1172. (doi: 10.1111/j.1558-5646.2009.00887.x)
[32] Brockhurst M A, Buckling A, Gardner A. 2007 Cooperation Peaks at Intermediate Disturbance. *Curr. Biol.* **17**, 761-765. (doi: 10.1016/j.cub.2007.02.057)
[33] Brockhurst M A. 2007 Population Bottlenecks Promote Cooperation in Bacterial Biofilms. PLoS One **7**, e634. (doi: 10.1371/journal.pone.0000634)
[34] Wienand K, Lechner M, Becker F, Jung H, Frey E. 2015 Non-Selective Evolution of Growing Populations. PloS one, **10(8)**, e0134300. (doi: 10.1371/journal.pone.0134300)
[35] Rainey P B, Rainey K. 2003 Evolution of cooperation and conflict in experimental bacterial populations *Nature* **425**, 72. (doi: 10.1038/nature01906)
[36] Wienand K, Frey E, Mobilia M. 2017 Evolution of a Fluctuating Population in a Randomly Switching Environment. *Phys. Rev. Lett.* **119**, 158301. (doi:10.1103/PhysRevLett.119.158301)
[37] Wienand K, Frey E, Mobilia M. 2017 The *supplementary material*, along with accopanying files, is also available electronically: *fighshare https://doi.org/10.6084/m9.figshare.5683762.v1*. (doi:10.6084/m9.figshare.5683762)
[38] Here, in reference to microbial communities, we use interchangeably use the terms "species" and "strain".
[39] Horsthemke W, Lefever R. 2006 *Noise-Induced Transitions*. Berlin, Germany: Springer
[40] Bena I. 2006 Dichotomous Markov noise: Exact results for out-of-equilibrium systems. A review. *Int. J. Mod. Phys. B* **20**, 2825-2889. (doi: 10.1142/S0217979206034881)
[41] Kitahara K, Horsthemke W, Lefever R. 1979 Coloured-noise-induced transitions: exact results for external dichotomous Markovian noise. *Phys. Lett.* **70A**, 377-380. (doi: 10.1016/0375-9601(79)90336-0)
[42] Hänggi P, Talkner P. 1981 Non-Markov processes: The problem of the mean first passage time. *Z. Phys. B* **45**, 79-83. (doi: 10.1007/BF01294279)
[43] Van den Broek C, Hänggi P. 1984 Activation rates for nonlinear stochastic flows driven by non-Gaussian noise. *Phys. Rev. A* **30**, 2730-2736. (doi: 10.1103/PhysRevA.30.2730)
[44] Sancho J M. 1985 External dichotomous noise: The problem of the mean-first-passage time. *Phys. Rev. A* **31**, 3523(R)-3526(R). (doi: 10.1103/PhysRevA.31.3523)
[45] Wienand K, Frey E, Mobilia M. 2017 *fighshare https://doi.org/10.6084/m9.figshare.5082712*. (doi:10.6084/m9.figshare.5082712.v5)
[46] Spalding C, Doering C R, Flierl G R. 2017 Resonant activation of population extinctions *e-print: https://arxiv.org/abs/1710.06274*
[47] A finite population unavoidably collapses into $(N, x) = (0, 0)$ where it is extinct [46]. This phenomenon is practically unobservable when $K_- \gg 1$ and occurs after lingering in the system's quasi-stationary state (where N is distributed according to its N-QSD) and much after the fixation of one species.
[48] Wienand K, Frey E, Mobilia M. 2017 *http://link.aps.org/supplemental/10.1103/PhysRevLett.119.158301*. (doi: 10.1103/PhysRevLett.119.158301)
[49] Davis M H A. 1984 Piecewise–deterministic Markov processes: a general class of nondiffusion stochastic models *J. R. Stat. Soc. B* **46**, 353-388. (Retrieved from http://www.jstor.org/stable/2345677)
[50] Moran P A P. 1962 *The statistical processes of evolutionary theory*. Oxford, UK: Clarendon
[51] Antal I, Scheuring I. 2006 Fixation of Strategies for an Evolutionary Game in Finite Populations *Bull. Math. Biol.* **68**, 1923-1944. (doi: 10.1007/s11538-006-9061-4)
[52] Otto S P, Whitlock M C. 1997 The Probability of Fixation in Populations of Changing Size. *Genetics* **146**, 723-733. (url: http://www.genetics.org/content/146/2/723)
[53] Wolfram Research. 2010 Mathematica, Version 10.0 *Wolfram Research Inc*

[54] Gillespie D T. 1976 A general method for numerically simulating the stochastic time evolution of coupled chemical reactions. *J. Comput. Phys.* **22**, 403. (doi: 10.1016/0021-9991(76)90041-3)
[55] Ewens E W, 2004 *Mathematical Population Genetics*. New York, USA: Springer.
[56] Gardiner C W. 2002 *Handbook of Stochastic Methods* New York, USA: Springer
[57] van Kampen N G. 2003 *Stochastic Processes in Physics and Chemistry* Amsterdam, The Netherlands: North-Holland Publishing
[58] Nowak M A, 2006 *Evolutionary Dynamics*. Cambridge, USA: Belknap Press
[59] Broom M, Rychtář J. 2013. *Game-Theoretical Models in Biology*. Boca Raton, USA: CRC Press
[60] With eq. (12), in the realm of the PDMP approximation, we find that $(1+b\phi_b)\langle N\rangle^*_{0,\nu} \leq \langle N\rangle^*_{b,\nu} \leq (1+b\phi_b)\langle K\rangle$.
[61] Since $K_\pm$ are here assumed to be of the same order, with $K_+ \gtrsim K_- \gg 1$ with $\Omega = \langle K\rangle$ [61], we could also define $\Omega = K_+$ or $\Omega = K_-$ and proceed similarly.

Supplementary Material for

Eco-Evolutionary Dynamics of a Population with Randomly Switching Carrying Capacity

In this Supplementary Material, we provide comments concerning the dichotomous noise, notes on the methodology and data avalability, the derivation of the probability densities of the piecewise-deterministic Markov process (PDMP), complementary results about the mean fixation times, as well as additional discussions about the PDMP approximation and the emergence of cooperation in the eco-evolutionary game, and additional technical details concerning the stationary properties of the underlying piecewise-deterministic Markov processes, and the linear noise approximation to the population size's quasi-stationary distribution.

In what follows, unless stated otherwise, the notation is the same as in the main text and the equations and figures refer to those therein. (As in the main text, unless explicitly mentioned otherwise, below we tacitly assume $x_0 = 1/2$.)

VII. RELATIONSHIP BETWEEN DICHOTOMOUS MARKOV NOISE AND OTHER FORMS OF ENVIRONMENTAL NOISE

It is worth outlining some of the similarities and differences between the dichotomous Markov Noise (DMN) and the Ornstein-Uhlenbeck process (OUP) that is also commonly used to model environmental noise, see *e.g.* [9]. Both are *colored noise* with exponential auto-correlation functions, see Sec. II in the main text and Refs. [39, 40]. However, while the Ornstein-Uhlenbeck Process is a Gaussian and unbounded process, the DMN is, in general, *neither*. In fact, the piecewise-deterministic Markov process (PDMP) [49]

$$\dot{N} = N\left(1+q-\frac{N}{\mathcal{K}}\right) + \Delta\xi, \tag{S1}$$

with the DMN ξ, becomes a diffusive process with Gaussian white noise and diffusion constant $D = \Delta^2/\nu$ only in the limit of $\Delta \to \infty, \nu \to \infty$ and $0 < D < \infty$, see, *e.g.*, Refs. [39–41]. The PDMP that we consider in this work has the form:

$$\dot{N} = \mathcal{F}(N,\xi) = \begin{cases} \mathcal{F}_+(N) & \text{if } \xi = 1 \\ \mathcal{F}_-(N) & \text{if } \xi = -1 \end{cases} \quad \text{with} \quad \mathcal{F}_\pm(N) \equiv N\left[1+q-\frac{N}{K_\pm}\right],$$

which corresponds to equation (S1) with $\Delta = (K_+ - K_-)/(2K_+K_-)$. Since $K_+ > K_- \gg 1$, the Gaussian white noise limit is unphysical, and the PDMP that we consider in this work is therefore *never diffusive*.

It is also worth noting that, being bounded, the DMN has the great advantage of guaranteeing that the fluctuating carrying capacity $K(t) = [(K_+ + K_-) + \xi(t)(K_+ - K_-)]/2$ remains always finite and positive, which would not be the case if $\xi(t)$ was given by an OUP. Furthermore, the DMN can be considered a discrete-step approximation [39, 40] of the OUP, but is more mathematically tractable and easier to simulate.

VIII. NOTES ON METHODOLOGY & DATA AVAILABILITY

Source code for all simulations, resulting data and the *Mathematica* notebook [53] used for calculations and figures are available electronically [37].

A. Stochastic simulations

Using Gillespie's stochastic simulation algorithm (SSA) [54], we have simulated exactly the dynamics described by the master equation (5). To efficiently ensure that quasi-stationarity was reached [47], we have run individual-based simulations until fixation occurred in 99% of the realizations (for $\nu \gtrsim s$), or until time reaches $t = 10/\nu$ (when $\nu \ll s$). We have simulated ensembles of 10^4 realizations of the system, except to determine the various population size distributions (for which we used a larger sample of 10^5 realizations) and when using "high values" of s (i.e. for $s = \mathcal{O}(1)$ as in figure S2). In this case, an even larger sample of 10^6 realizations was needed to accurately estimate the fixation probability of S.

B. Numerical limitations on effective parameter $q(b)$ approach

To obtain the parameter $q(b)$ used in the formula (15) for ϕ_q, we first recorded the fixation probability from SSA results with constant $K = \mathcal{K}$, $b \in \{0.1k : \, k \in \mathbb{N}, \, k \leq 100\}$, and $s \in \{0.02, 0.05\}$ (10^6 runs each). For each combination of parameters, we computed $q(b)$ by matching the fixation probability $\phi|_{(1+q)\mathcal{K}}$ of the fitness-dependent Moran model, see equation (13), with the corresponding fixation probability obtained in the SSA result.

The values of $q(b)$ have then been used to compute ϕ_q according to equation (15) for several values of ν, as shown in figure 3(b). Due to numerical instabilities in the evaluation of stationary distribution $p^*_{\nu,q}$ in Mathematica [53], numerical evaluations of ϕ_q occasionally "failed" or produced outliers. Data corresponding to these occasional issues were omitted (without statistical consequences) from our dataset. This has sometimes led to some gaps in the lines of the analytical predictions (see *e.g.* the green curve in figure 3 (b)). Furthermore, $q(b)$ has only been determined for a discrete set of b values, which limits the resolution in determining b_c and b^*. Specifically, since the spacing between the values used for b was 0.1, neither b^* nor b_c has been determined with an accuracy higher than 0.1. The combination of limited resolution and outliers causes the jaggedness observed in figure S6(a) for the graph of b^* obtained by looking for the maximum of equation (21).

C. Data availability: Mathematica notebook & Linear noise approximation figures 7 and 8

The direct numerical evaluation of equations (S35) and (S36), used to generate the figures 7 and 8, is commented in the accompanying Mathematica notebook [37].

IX. JOINT AND MARGINAL STATIONARY PDFS OF THE AUXILIARY PDMP (9)

In the main text, we have frequently used of the marginal stationary probability density function (PDF) of the single-variate PDMP (9) that reads

$$p^*_{\nu,q}(N) = \frac{\mathcal{Z}_\nu}{N^2} \left[\frac{(N^*_+ - N)(N - N^*_-)}{N^2} \right]^{\frac{\nu}{1+q}-1},$$

given by eq. (12) in the main text.

In this section, we outline the derivation of this PDF, as well as that of the joint stationary probability density $p^*_{\nu,q}(N, \xi)$ of N and ξ. For notational simplicity, in the remainder of this section, we write $p_{\nu,q} = p$ and $p^*_{\nu,q} = p^*$. It follows from the Chapman-Kolmogorov equation, that $p(N, \xi)$ obeys the master-like equation [39]

$$\partial_t p(N, \xi, t) = -\partial_N \left[\mathcal{F}(N, \xi) p(N, \xi, t) \right] - \nu \left[p(N, \xi, t) - p(N, -\xi, t) \right], \tag{S2}$$

which can conveniently be rewritten as $\partial_t p(N, \xi, t) = -\partial_N J(N, \xi, t)$ in terms of the probability current [12]

$$J(N, \xi, t) = \mathcal{F}(N, \xi) p(N, \xi, t) \; + \; \nu \int_{N^*_-}^{N} dN' \left[p(N', \xi, t) - p(N', -\xi, t) \right]. \tag{S3}$$

The first term on the right-hand-side (RHS) of (S3) accounts for the probability flowing outside $[N^*_-, N]$ (Liouvillian flow), whereas the second accounts for the random switching. At stationarity, $\lim_{t\to\infty} p(N, \xi, t) = p^*(N, \xi)$ and $\lim_{t\to\infty} J(N, \xi, t) = J^*(N, \xi)$, with $\partial_t p^*(N, \xi) = -\partial_N J^*(N, \xi) = 0$, which implies $\partial_N (J^*(N, \xi) + J^*(N, -\xi)) = 0$. With the (natural) zero-current boundary conditions at $N^*_\pm$ [39], i.e. $J^*(N, \xi) = 0$, we find a simple relationship between the PDFs in each of the environmental states:

$$p^*(N, \xi) = -\left(\frac{\mathcal{F}(N, -\xi)}{\mathcal{F}(N, \xi)} \right) p^*(N, -\xi). \tag{S4}$$

With this relation, $\partial_N J^*(N,-\xi)=0$ gives

$$0=\partial_N\left[\mathcal{F}(N,-\xi)p^*(N,-\xi)\right]+\nu\left[\frac{1}{\mathcal{F}(N,-\xi)}+\frac{1}{\mathcal{F}(N,\xi)}\right]\left(\mathcal{F}(N,-\xi)p^*(N,-\xi)\right).$$

Combined with equation (S4), this readily yields $p^*(N,\xi)\propto\pm\mathfrak{g}(N)/\mathcal{F}(N,\xi)$, where

$$\mathfrak{g}(N)=\exp\left[-\nu\int^N dm\left\{\frac{1}{\mathcal{F}_-(m)}+\frac{1}{\mathcal{F}_+(m)}\right\}\right]=\left[\frac{(N_+^*-N)(N-N_-^*)}{N^2}\right]^{\frac{\nu}{1+q}}, \tag{S5}$$

and $\mathcal{F}_\pm$ are defined by eq. (10). The *joint stationary PDF* giving the probability density of N in each environmental state is thus explicitly given by

$$p^*(N,\xi)=\frac{\mathcal{Z}}{\xi\mathcal{F}(N,\xi)}\,\mathfrak{g}(N)=\frac{\mathcal{Z}}{\xi\mathcal{F}(N,\xi)}\left[\frac{(N_+^*-N)(N-N_-^*)}{N^2}\right]^{\frac{\nu}{1+q}}, \tag{S6}$$

where $\mathcal{Z}$ is the normalization constant. In figure S1, we compare the predictions of the joint PDF $p^*(N,\xi)$ with the histograms of the population size obtained from SSA results, verifying that the PDMP description aptly reproduces the location and number of peaks that characterize the quasi-stationary distribution of N (see also [36, 48]).

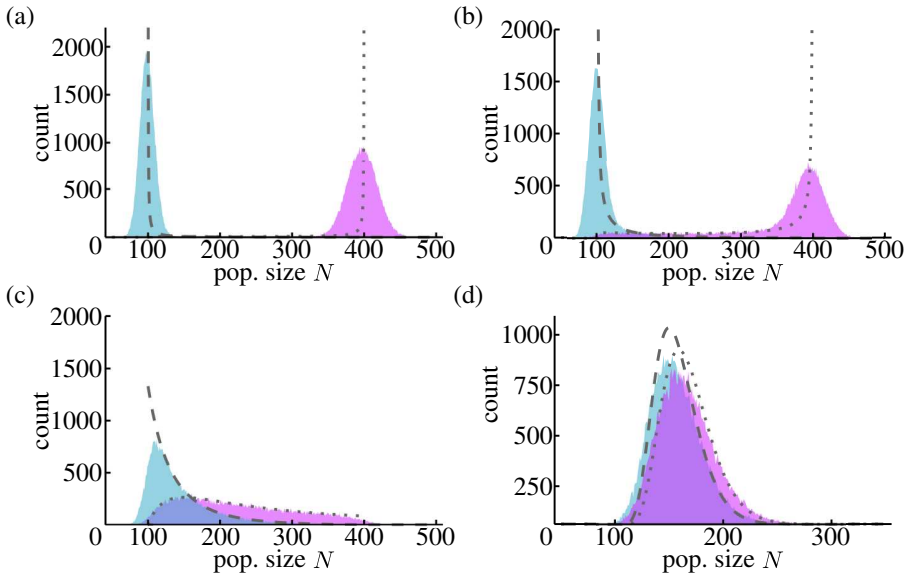

FIG. S1: Histograms of population size (N-QSD) and from the joint PDMP PDF (S6) when $b=0$, for (a) $\nu=0.01$, (b) $\nu=0.1$, (c) $\nu=1$, and (d) $\nu=10$. Shaded areas correspond to SSA results for $\xi=+1$ (purple) and $\xi=-1$ (cyan); dashed and dotted lines are from (S6) with $\xi=+1$ and $\xi=-1$, respectively. Parameters are $(K_+,K_-,s,x_0,b)=(400,100,0.02,0.5,0)$

The marginal stationary PDF $p^*(N)=p^*(N,\xi)+p^*(N,-\xi)$ is thus $p^*(N)\propto\left[(1/\mathcal{F}_+(N))-(1/\mathcal{F}_-(N))\right]\mathfrak{g}(N)$, which yields the explicit expression (12).

It is also useful to notice that, at stationarity, the probability that the PDMP (9) is in the environmental state ξ, given a population size N is given by [12]

$$p^*(\xi|N)=\frac{-\xi\mathcal{F}(-\xi,N)}{\sum_{\xi=\pm1}\xi\mathcal{F}(\xi,N)}. \tag{S7}$$

X. ASSESSMENT OF ACCURACY OF FORMULAS FOR THE FIXATION PROBABILITY

A central point of our analysis is the formula to compute the fixation probability of S (see section III.C.1), ϕ, with the formula (14) which reads [36]

$$\phi \simeq \int_{K_-}^{K_+} \left(\frac{e^{-Ns(1-x_0)} - e^{-Ns}}{1 - e^{-Ns}} \right) p^*_{\nu/s}(N)\, dN, \quad \text{when } b = 0 \ \text{ (no public good production).} \tag{S8}$$

When $s = \mathcal{O}(1)$, the assumption of a timescale separation between N and x that underpins the derivation of equation (S8) is no longer valid. As a consequence, the relative deviations between the predictions of eq. (14) and the SSA results for ϕ increase with s, as shown in figure S2. To quantify the accuracy of equation (S8), we have compared its predictions with the simulation results of 10^6 realizations obtained for different values of ν and s spanning between 0 and 0.25, recording the SSA fixation probability ϕ_{sim}. For each combination of parameters (different colors in Figure S2), we determined the theoretical prediction ϕ_{th} from eq. (S8) and the percentage deviation between it and the simulation result $\Delta\phi = 100|\phi_{\text{th}} - \phi_{\text{sim}}|/\phi_{\text{sim}}$. As figure S2 shows, theoretical results reproduce simulations for small s, with relative deviations below 10%. Discrepancies increase more and more as the selection intensity is increased towards $s = \mathcal{O}(1)$ (when $s > 0.1$, in figure S2). The approximation underpinning (S8) is therefore valid in the regime $s \ll 1$, which is the regime of weak selection pressure on which we focus (see main text), and deteriorates as s approaches $s = \mathcal{O}(1)$.

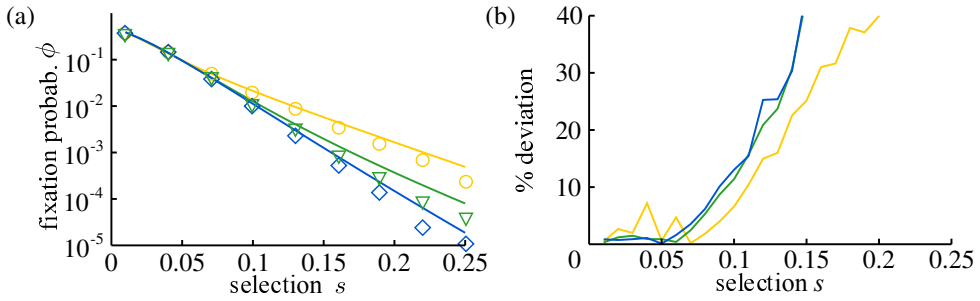

FIG. S2: (a) ϕ vs. s when $b = 0$, with $\nu = 0.1$ ($\circ$, yellow), $\nu = 1$ (∇, green), $\nu = 10$ ($\diamond$, blue). (b) Accuracy of formula as function of s with $b = 0$, measured as the relative deviations from simulation results for ϕ with the same ν as in (b), see text for details. In both panels, symbols are from simulations (10^6 runs in (a)) and solid lines are from eq. (14). Other parameters are $(K_+, K_-, x_0) = (450, 50, 0.5)$

Within the regime $s \ll 1$, we have similarly assessed the accuracy of equation (14) for different switching rates ν. We simulated 10^4 realizations of the system, for different values of s, and 100 values ν between 0.001 and 10 and computed the percentage deviation $\Delta\phi(\nu)$ as explained above. Dots in figure S3(a) are thus based on ϕ_{sim} obtained by sampling 10^4 SSA realizations; they represent the value of $\Delta\phi(\nu)$ recorded at each value of ν, with different colors signaling different values of s (red for 0.05, cyan for 0.02). The dots scatter uniformly, indicating no systematic trend in the deviation. For $s = 0.02$, we observe deviations between 0 and 8% when $s = 0.02$, with an average (solid line) of 2% and standard deviation (shaded area) $\approx 2\%$; for $s = 0.05$ (red), deviations are between 0 and 13%, with average 4% and standard deviation 2.5%.

For the case with public good production, we have used an effective approach and obtained the following expression (15) for the fixation probability of S (see section III.C.2) which, with eq. (13), reads [36]:

$$\phi_q = \int_{(1+q)K_-}^{(1+q)K_+} \left(\frac{e^{-Ns(1-x_0)} - e^{-Ns}}{1 - e^{-Ns}} \right) p^*_{\nu/s,q}(N)\, dN\,, \quad \text{when } b > 0 \ \text{ (public good production).} \tag{S9}$$

This also builds on a timescale separation between an effective population size and x. Besides the breakdown of the timescale separation when $s = \mathcal{O}(1)$, the accuracy of the approximation $\phi \simeq \phi_q$ deteriorates for higher values of b and/or s, because the fixation of S then becomes increasingly unlikely, see figure 3(a), which limits the accuracy with which $q(b)$ is determined and hence the predictions of equation (15).

Figure S3(b) shows the results for the percentage deviation of the predictions of equation (S9), using the appropriate values of the effective parameter $q(b)$ (excluding a few outliers), and ϕ_{sim} obtained from 10^4 SSA realizations. For $s = 0.02$, $b = 0.2$ (blue), $\Delta\phi$ is between 0 and 8%, with average 3% and a standard deviation of 2%. For $s = 0.05$, $b = 2$ (red), we observe larger and more scattered $\Delta\phi$ between 0 and 28%, with average 12% and standard deviation 7%. While a deterioration of the approximation when s and b are increased can explain the increase in the average $\Delta\phi$, higher values of s and b also cause lower fixation probabilities for S, see figure 3(a). The corresponding values of ϕ are small which results in noisier values of ϕ_{sim} and $\Delta\phi$, as shown by red data in figure S3.

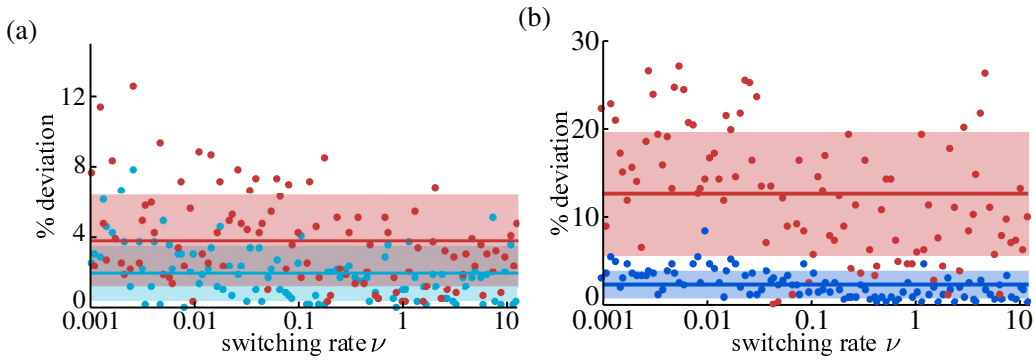

FIG. S3: (a) Percentage deviation $\Delta\phi$ between simulation and theory vs. ν, for $b = 0$ with $s = 0.02$ (cyan) and $s = 0.05$ ($\diamond$, red). Dots represent the percentage distance between prediction and simulated value for each ν, solid lines denote the average of the dots, shaded areas the standard deviation around the average. (b) Same as in panel (a) but for $(s, b) = (0.02, 0.2)$ (blue) and $(0.05, 2)$ (red). Other parameters are $(K_+, K_-, x_0) = (450, 50, 0.5)$.

Overall, the above analyis confirms that our approach is able to predict the fixation probability ϕ in the regime of weak selection intensity ($0 < s \ll 1$), both when $b = 0$ and $0 < b = \mathcal{O}(1)$, with a remarkable accuracy of a few percent over a vast range of values ν.

XI. FIXATION IN THE FITNESS-DEPENDENT MORAN PROCESS & MEAN FIXATION TIME UNDER SWITCHING CARRYING CAPACITY

A. Fixation in the fitness-dependent Moran process

To study the fixation properties of the system, we have used the properties of the fitness-dependent Moran Process (fdMP) outlined in section III.B of the main text [21, 22, 51, 55]. In a population of large but finite and constant size N, the fixation properties under weak selection of the fdMP can be inferred from the backward Fokker-Planck equation associated with the generator [21, 22, 26, 55–57]

$$\mathcal{G}(x)|_N = g(x)\,\frac{x(1-x)}{N}\left[-Ns\frac{d}{dx} + \frac{d^2}{dx^2}\right], \quad \text{where } g(x) = 1 + bx. \tag{S10}$$

For an initial fraction x_0 of S individuals, the fixation probability $\phi(x_0)|_N$ of S obeys $\mathcal{G}(x)|_N\phi(x)|_N = 0$, with $\phi(1)|_N = 1$ and $\phi(0)|_N = 0$ (absorbing boundaries at $x = 0, 1$). Yielding the result

$$\phi(x_0)|_N \;=\; \frac{e^{-Ns(1-x_0)} - e^{-Ns}}{1 - e^{-Ns}},$$

given as equation (13) in the main text.

The generator (S10) can also be used to study when fixation occurs in the fdMP in the realm of the diffusion approximation [21, 22, 26, 55]. Quantities of particular interest, are the unconditional mean fixation time (MFT)— which is the average time to reach any of the absorbing states, here either $x = 0$ or $x = 1$—as well as the conditional MFTs—the mean time to reach a specific absorbing boundary. The unconditional MFT is obtained by solving $\mathcal{G}(x_0)|_N\, T(x_0)|_N = -1$ subject to $T(0)|_N = T(1)|_N = 0$ [21, 26, 56]. The conditional MFT to reach $x = 1$ is denoted by $T^S(x_0)|_N$, while $T^F(x_0)|_N$ is the (conditional) MFT conditioned to reach $x = 0$. The MFTs and the fixation probabilities are related by $T(x)|_N = \phi T^S(x_0)|_N + (1-\phi)T^F(x_0)|_N$. Explicit, but unwieldy, expressions for the MFTs in the fdMP can be obtained [21, 26, 55, 56], *e.g.* the unconditional MFT in the case $b = 0$ reads

$$\begin{aligned} T(1/2)|_N \;=\; & \frac{1}{s}\left\{(1 - 2\phi(1/2)|_N)(\log(Ns) + \gamma) + \mathrm{e}^{-\frac{Ns}{2}}\,\mathrm{Ei}\left(\frac{Ns}{2}\right) - \mathrm{e}^{\frac{Ns}{2}}\,\mathrm{Ei}\left(-\frac{Ns}{2}\right)\right. \\ & + \left.\mathrm{e}^{Ns}\phi(1/2)|_N\mathrm{Ei}(-Ns) - \mathrm{e}^{-Ns}(1 - \phi(1/2)|_N)\mathrm{Ei}(Ns)\right\}, \end{aligned} \tag{S11}$$

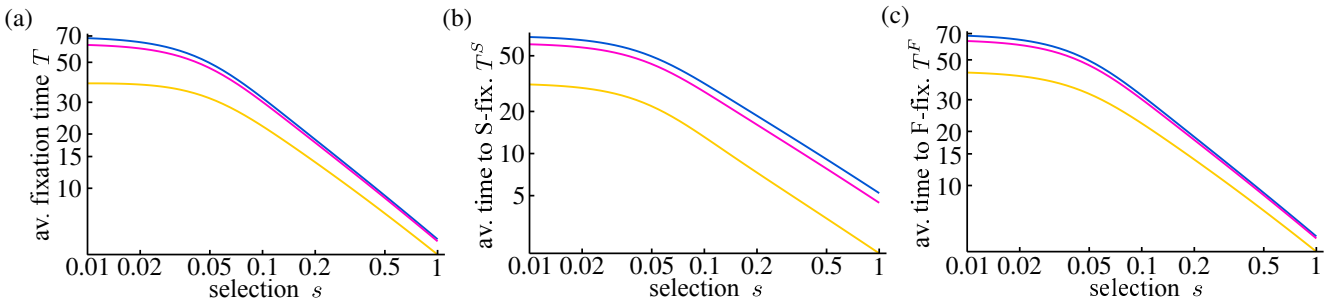

FIG. S4: (a) MFT $T|_N$ vs. s for the fdMP, given by $T|_N = \phi|_N T^S|_N + (1-\phi|_N)T^F|_N$. In the case $b = 0$ (blue), this corresponds to equation (S12). (b) $T^S|_N$ vs. s for the fdMP, from the solution of the appropriate equation associated with the generator (S10). (c) $T^F|_N$ vs. s for the fdMP, obtained as T^S. The population in the fdMP is of constant size $N = 100$ and the effect of the public good parameter b is to reduce the relaxation time of x, and thus to lower all the MFTs with respect to the case $b = 0$. However, the MFTs always scale as $\mathcal{O}(1/s)$ to leading order when $s \ll 1$. In all panels, and $b = 0$ (blue), $b = 0.2$ (pink), $b = 2$ (yellow), $x_0 = 0.5$.

where $\gamma \approx 0.577...$ is the Euler-Mascheroni constant, and $\mathrm{Ei}(z) = \int_{-z}^{\infty} dz \frac{e^{-z}}{z}$ is the exponential integral. Hence, in the regime where $s \ll 1$, with $Ns \gg 1$, and $s \ln N \ll 1$ (with x_0 is sufficiently separated from $x = 0, 1$), $T(x_0)|_N \sim (\ln N)/s$ [21, 22, 55], with a subleading prefactor $\sim \ln N$. The conditional MFTs exhibit the same behavior $T^{S/F}(x_0) \sim T(x_0) = \mathcal{O}(1/s)$ to leading order when $s \ll 1$, see figure S4. A similar behavior also holds when $b > 0$ and $s \ll 1$, with a subleading prefactor that then depends (weakly) on the public good parameter $b = \mathcal{O}(1)$, specifically $T(x_0)|_N \sim (\ln(N - \mathcal{O}(b)))/s$, as confirmed by figure S4. The public good parameter b, in fact, reduces the relaxation time of x, see equation (7), which results in a weak reduction of the unconditional and MFTs with respect to the case with $b = 0$, see also figure S4(b,c). The most relevant point for our purposes, is the fact that the unconditional MFT of the fdMP scales as $\mathcal{O}(1/s)$ to leading order when $s \ll 1$, and so do the conditional MFTs, in both cases $b = 0$ and $b > 0$.

B. Mean fixation times for switching carrying capacity

In a population subject to a randomly switching carrying capacity, with no public good production, the size and growth rate are independent of the composition. As explained in Ref. [36, 48], when $b = 0$, the conditional and unconditional MFTs admit the same scaling to leading order when $s \ll 1$, i.e. $T^{S/F}(x_0) \sim T(x_0) = \mathcal{O}(1/s)$, and we can use the approach outlined in Section III.C.1, to compute [48]

$$T(x_0) \simeq \int_{K_-}^{K_+} T(x_0)|_N p^*_{\nu/s}(N)\, dN. \tag{S12}$$

Figure S5(a) shows that the predictions of this formula (blue line) agree extremely well with SSA results ($\diamond$). This confirms that under weak selection and $b = 0$, the unconditional MFT scales as in the fdMP, i.e. $T(x_0) = \mathcal{O}(1/s)$ when $s \ll 1$. This implies that after $t \gtrsim 1/s$ fixation is likely to have occurred, and that the population size is at quasi-stationarity when $t \gg 1/s$. Quite remarkably, we also notice in figure S5(a) that even when $s = \mathcal{O}(1)$ there is a good agreement between the predictions of eq. (S12) and SSA results.

In the case $b > 0$, the evolution of the population size and its composition are coupled. As discussed in the main text, S is less likely to fixate when b is increased, and the population size at fixation depends on which species takes over (the population size is typically larger when S fixates). On the other hand, according to eq. (7), increasing b reduces the relaxation time of x. Since these two effects balance each other, we expect the effect of $b > 0$ to be even weaker in the switching environment than in the fdMP with constant population size. Having seen that b has a weak effect on the MFTs, we thus anticipate that the MFTs with a switching carrying capacity exhibit a similar behavior as those of the fdMP. To verify this picture this and figure out on which timescale fixation occurs when $b > 0$, we have considered the fixation of S and F separately by studying their conditional MFTs [48]. For this, we can attempt to generalize the approach used in the case $b = 0$ and consider the averages

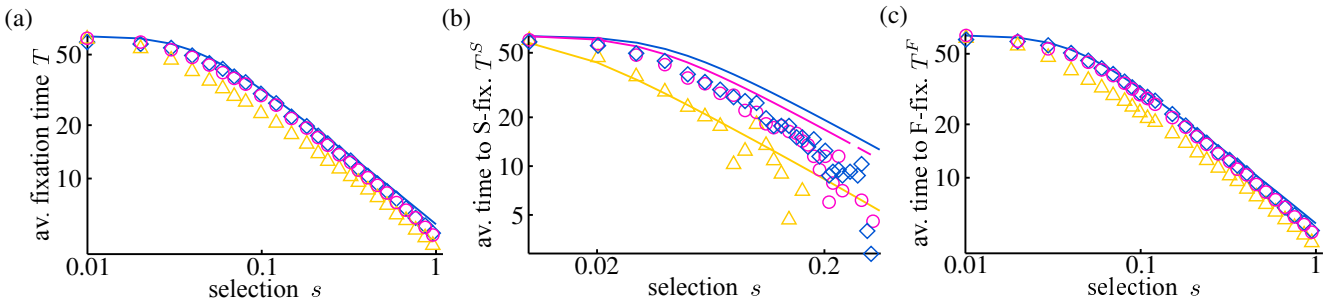

FIG. S5: (a) MFT T vs s. Symbols are from simulations (10^4 realizations) and the solid line shows $T(x_0)$ given by eq. (S12) in the case $b = 0$. (b) T^S vs s. Solid lines are the results of equation (S13) . (c) T^F vs s. The solid line is the result of equation (S14). In all panels, $\nu = 0.1$ and $b = 0$ (blue, $\diamond$), $b = 0.2$ (pink, $\circ$), $b = 2$ (yellow, $\triangle$), other parameters are $(K_-, K_+, x_0) = (50, 450, 0.5)$.

over the conditional stationary PDFs $p^*_{\nu/s,b}(N)$ and $p^*_{\nu/s}(N)$ obtained from (12) with $q = b$ and $q = 0$, i.e.

$$T^S(x_0) \simeq \int_{(1+b)K_-}^{(1+b)K_+} T^S(x_0)|_N p^*_{\nu/s,b}(N)dN\,, \tag{S13}$$

$$T^F(x_0) \simeq \int_{K_-}^{K_+} T^F(x_0)|_N p^*_{\nu/s}(N)dN\,, \tag{S14}$$

$$T(x_0) \simeq \phi_{q(b)}T^S(x_0) + (1-\phi_{q(b)})T^F(x_0)\,, \tag{S15}$$

where $T^{S/F}(x_0)|_N$ are the conditional MFTs of the fdMP with $b > 0$. A clear limitation of formula (S13) and (S14) stems from the fact that $p^*_{\nu/s,b}(N)$ and $p^*_{\nu/s}(N)$ are good approximation of the N-QSD in the quasi-stationary state that typically reached after $t \gg 1/s$, see Ref. [45], i.e. well after fixation has occurred. As a consequence, $p^*_{\nu/s,b}(N)$ and $p^*_{\nu/s}(N)$ overestimate the population size when fixation occurs, and formula (S13) and (S14) therefore overestimate the actual conditional MFTs when $b > 0$. However, since the population size and the parameter b only yield subleading contributions to the MFTs of the fdMP when $s \ll 1$, we expect that formula (S13)-(S15) are still able to capture how the MFTs scale to leading order under weak selection intensity. The comparison of SSA results for the MFTs with $b > 0$ reported in figure S5, and their comparison with those of figure (S4) confirm this picture. Since the b-dependence of the MFTs in figure (S4) is clearly subleading, we can simplify the evaluation of (S13) by setting $g \equiv 1 + b$ (and similarly $g \equiv 1$ in (S14)). As shown in figure (S5)(b), this does not affect the leading behavior of T^S.

Figures S5(b,c) show that the simplified formula (S13) and (S14) indeed correctly predict that the conditional MFTs scale as $\mathcal{O}(1/s)$ when $s \ll 1$, even if they indeed overstimate the SSA results for T^S and T^F. Hence, equation (S15) predicts that to leading order the uncoditional MFT scales as $\mathcal{O}(1/s)$, which is in good agreement with the SSA results reported in figure S5(a). As s and b increase, the fixation of S becomes less likely and thus $T(x_0) \simeq T^F(x_0)$, as shown by figures S5(a) and (c). We notice that SSA results reported in figure S5 confirm that the MFTs with randomly switching carrying capacity depend even more weakly on the public good parameter b than in the fdMP where N is constant N.

We therefore conclude that, under weak selection $s \ll 1$, and with $b = \mathcal{O}(1)$, the MFTs in the case $b > 0$ scale as $\mathcal{O}(1/s)$. This means that fixation in the public good scenario ($b > 0$) is likely to have occurred when $t \gtrsim 1/s$ and the population size is most probably at quasi-stationarity when $t \gg 1/s$, as in the case $b = 0$. These results also that, to leading order in $1/s$, the MFTs here scale as in the absence of external noise. Hence, while environmental noise has a significant effect on the fixation probability (see Section III.C in the main text), its effect on the MFTs is much less important, as captured by the formula (S13)-(S15).

XII. SUPPLEMENTARY INFORMATION ON THE PDMP APPROXIMATION AND THE "ECO-EVOLUTIONARY GAME"

A. PDMP approximation and average number of individuals

The analysis of the correlations between population size and its composition (Section IV.A), and that of the "eco-evolutionary game" (Section IV.B), relies largely on properties of the average population size at quasi-stationarity given by

$$\langle N\rangle^*_{\nu,b} = (1+b)\phi_b\langle N\rangle^*_{\nu,b} + (1-\phi_b)\langle N\rangle^*_{\nu,0}\,, \tag{S16}$$

where ϕ_b is the fixation probability of species S under a public good parameter b, within what in the main text is referred to as the "PDMP approximation". This approximation consists of averaging the population size N over the marginal PDF (12) of the PDMP (9).

To derive equation (S16), we first notice that $\langle N\rangle^*_{\nu,b}$ consists of the average population size conditioned to the fixation of F and S, i.e. $\langle N\rangle^*_{\nu,b} = \langle N_F\rangle^*_{\nu,b} + \langle N_S\rangle^*_{\nu,b}$. The fixation of F occurs with probability $\widetilde{\phi}_b = 1-\phi_b$, and results in a global growth rate $g=1$, yielding

$$\langle N_F\rangle^*_{\nu,b} = \langle N|x=0\rangle^*_{\nu,b} = \widetilde{\phi}_b\langle N\rangle^*_{\nu,0} = \widetilde{\phi}_b\int_{K_-}^{K_+} Np^*_\nu(N)dN, \tag{S17}$$

where $\langle N\rangle^*_{\nu,0}$ is the quasi-stationary average population size when $b=0$ and the integration is over $p^*_\nu \equiv p^*_{\nu,0}$ given by eq. (12). Similarly, the fixation of S occurs with probability ϕ_b, after which $g = 1+b$, yielding

$$\langle N_S\rangle^*_{\nu,b} = \langle N|x=1\rangle^*_{\nu,b} = \phi_b\langle N\rangle^*_{\nu,b} = \phi_b\int_{(1+b)K_-}^{(1+b)K_+} Np^*_{\nu,b}(N)dN = (1+b)\phi_b\langle N\rangle^*_{\frac{\nu}{1+b},0}. \tag{S18}$$

The last equality is obtained by performing the change of variable $N\to N/(1+b)$ and allows us to express $\langle N\rangle^*_{\nu,b}$ in terms of the average when $b=0$. Putting everything together, we obtain eq. (16):

$$\begin{aligned}\langle N\rangle^*_{\nu,b} &= (1+b)\phi_b\langle N\rangle^*_{\frac{\nu}{1+b},0} + (1-\phi_b)\langle N\rangle^*_{\nu,0}\\ &\simeq (1+b)\phi_{q(b)}\int_{K_-}^{K_+} Np^*_{\frac{\nu}{1+b}}(N)\,dN + (1-\phi_{q(b)})\int_{K_-}^{K_+} Np^*_\nu(N)\,dN,\end{aligned} \tag{S19}$$

where in the last line we have used the approximation $\phi_b \simeq \phi_{q(b)}$ given by equation (15). Figure 3(b) shows that predictions of $\langle N\rangle^*_{\nu,b}$ obtained with this approach are as close to simulation results as their counterparts obtained by averaging over the PDF obtained within the linear noise approximation of Section V (see also Section XIII below). It is clear from (15) that $\langle N\rangle^*_{\nu,b}$ is an increasing function of b since $\langle N\rangle^*_{\nu,0}$ is a decreasing function of ν [60].

In Section IV, we have often considered the limiting regimes of very fast/slow switching, $\nu\to\infty, 0$, in which the analytical formula greatly simplify. To obtain these simplified expressions, it suffices to notice that

$$\int_{K_-}^{K_+} Np^*_\nu(N)dN = \begin{cases}\mathcal{K} & \text{when } \nu\to\infty\\ \langle K\rangle & \text{when } \nu\to 0\end{cases}$$

Hence, when $\nu\gg 1$, we have $\langle N_F\rangle^*_{\nu,b}\to(1-\phi_b)\mathcal{K}$ and $\langle N_S\rangle^*_{\nu,b}\to(1+b)\phi_b\mathcal{K}$. Similarly, when $\nu\ll s$, we have $\langle N_F\rangle^*_{\nu,b}\to(1-\phi_b)\langle K\rangle$ and $\langle N_S\rangle^*_{\nu,b}\to(1+b)\phi_b\langle K\rangle$. Hence, from (16) and using $\phi\simeq\phi_{q(b)}$ we obtain the average population size in the limiting regimes:

$$\langle N\rangle^*_{\nu,b} = \begin{cases}(1+b\phi_{q(b)})\mathcal{K} & \text{when } \nu\to\infty\\ (1+b\phi_{q(b)})\langle K\rangle & \text{when } \nu\to 0.\end{cases} \tag{S20}$$

The limiting behavior reported as dashed lines in figures 3(b) and 4(b) can readily be obtained from equations (S20).

B. Best conditions for cooperation in the eco-evolutionary game

A finite well-mixed population of constant size is the natural setting of evolutionary game theory (EGT). The notion of evolutionary stability is central to EGT since an evolutionary stable strategy, when adopted by a population, cannot be invaded and replaced by an alternative strategy. For a population with two possible strategies, one is evolutionary stable if it satisfies the so-called invasion and replacement conditions [58, 59]. As a result, the sole fact that one strategy has a higher fitness than another does not guarantee that it is evolutionary stable since an individual of the other type may have a better chance to fixate the population.

For the model considered here, in a finite and static population, the strain F has always a higher fitness than S, and the fixation probability of S vanishes exponentially with the population size, see equation (13). In a finite and static population, F is therefore evolutionary stable, and in this sense always superior to S.

The situation is radically different in the eco-evolutionary game considered here since the population continues to evolve in a *fluctuating environment* even after fixation, and the notions of non-invadibility / non-replacement are no longer suitable to measure the species evolutionary success:

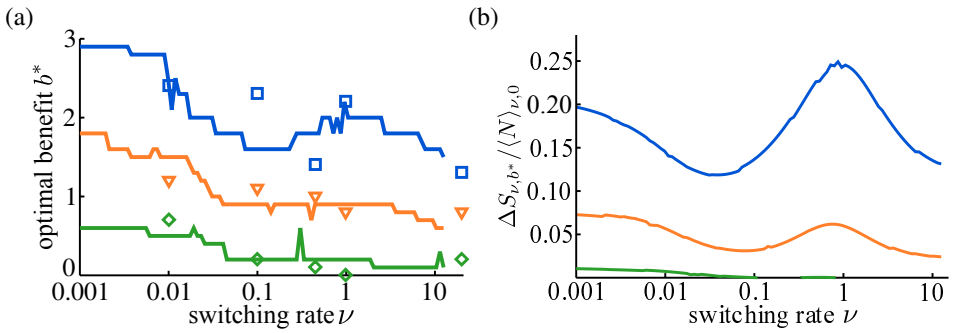

FIG. S6: (a) Optimal public good benefit parameter for the cooperating b^* vs ν for $s = 0.02$ (blue), $s = 0.03$ (orange), and $s = 0.05$ (green). Symbols are results from simulations and solid lines are from (21) (b) $\Delta S_{\nu,b^*}/\langle N\rangle^*_{\nu,0}$ vs. ν, obtained gives the highest payoff received by S by producing the public good at optimal value $b = b^*(\nu, s)$ obtained from (21) for $s = 0.02$ (blue), $s = 0.03$ (orange), $s = 0.05$ (green), see below and main text. Other parameters are $(K_+, K_-, x_0) = (450, 50, 0.5)$.

As discussed in Section IV.B of the main text, even if S has always a lower fitness and a lesser chance to fixate than F, its occasional fixation can prove very rewarding since it allows cooperators to establish a large community of S individuals (of a size that can be significantly larger than the size of an average community of F individuals). We have therefore proposed to measure the success of S and F in this eco-evolutionary game by computing the difference between the expected long-term number of individuals $\Delta S_{\nu,b}$ and $\Delta F_{\nu,b}$, compared to the $b = 0$ case. $\Delta S_{\nu,b}$ and $\Delta F_{\nu,b}$ thus serve as expected payoffs in our eco-evolutionary game. In the PDMP approximation, we can use our effective approach (see section III.C.2) and equations (S17) and (S18), to obtain

$$\Delta S_{\nu,b} = (1+b)\phi_{q(b)} \int_{K_-}^{K_+} N p^*_{\frac{\nu}{1+b}}(N)\, dN - \phi_0 \int_{K_-}^{K_+} N p^*_\nu(N)\, dN \tag{S21}$$

$$\Delta F_{\nu,b} = (\phi_0 - \phi_{q(b)}) \int_{K_-}^{K_+} N p^*_\nu(N)\, dN\,, \tag{S22}$$

Where $p^*_\nu(N)$ is given by equation (12) with $b = 0$.

As shown by figure 5, $\Delta S_{\nu,b}$ is non-monotonic in b and has a maximum for $b = b^*$. This is then the optimal value of b for the cooperating strain S (given s, ν, $K_\pm$). Figure S6(a) shows the dependence of the optimal value $b^* = b^*(\nu, s)$ on ν, for different intensities of the selection pressure s. Clearly, $b^* = b^*(\nu, s)$ exhibits a complex, non-monotonic, dependence on ν and decreases when s increases, in a similar fashion to b_c (see main text). In figure S6(a), symbols are from simulations and the lines have been obtained from evaluating the maximum of equation (S21).

Figure S6(b) shows $\Delta S_{\nu,b^*}/\langle N\rangle^*_{\nu,0}$: the optimal payoff for cooperators divided by the long-time average population at $b = 0$. In other words, it shows how much bigger is, on average, the best-performing cooperating population, compared to the average population at $b = 0$. For sufficiently low s, e.g. for $s = 0.02$ (blue), the public good can make the average number of S individuals be up to $12\% - 25\%$ larger than the average population at $b = 0$ ($\Delta S_{\nu,b^*}/\langle N\rangle^*_{\nu,0} \approx 0.12 - 0.25$ across all values of ν). Figure S6(b) corresponds to results at quasi-stationarity, i.e. after fixation has occurred (with a smaller probability for S than F) and therefore shows the actual long-term eco-evolutionary payoff for cooperation: In the optimal conditions, the S strain can gain a significant benefit from the production of a public good.

As discussed in Section IV.B of the main text, there are conditions under which S receives a higher expected payoff than F in the sense that $\Delta S_{\nu,b} > \Delta F_{\nu,b}$. When this happens, cooperating is not only beneficial but is also advantageous for S. We have considered that for given parameters (ν, s), it is best to cooperate for the production of a public good with benefit parameter b when the following two conditions are satisfied: (a) $\Delta S_{\nu,b} > \Delta F_{\nu,b}$; (b) $b = b^*(\nu, s) < \beta(\nu, s)$. These conditions ensure (a) that S receives a higher payoff than F, and (b) that S receives the maximum payoff under the switching rate ν and selection strength s. On the other hand, species F always outperforms S when $b > \beta(\nu, s)$ since it then receives a higher expected payoff than S, with $\Delta F_{\nu,b}$ that is an increasing function of b for all values of ν and s, see figure 5(c).

As shown in figure 6(b) the phases (ii), $(0 < \Delta S_{\nu,b} < \Delta F_{\nu,b})$ and (iii) $(\Delta S_{\nu,b} > \Delta F_{\nu,b})$ are separated by the value $b = \beta(\nu, s)$ at which $\Delta S_{\nu,\beta} = \Delta F_{\nu,\beta}$, defined as by the solution of

$$\frac{1}{1+\beta}\left(\frac{2\phi_0}{\phi_{q(\beta)}} - 1\right) = \frac{\int_{K_-}^{K_+} N p^*_{\frac{\nu}{1+\beta}}\, dN}{\int_{K_-}^{K_+} N p^*_\nu\, dN}\,. \tag{S23}$$

It is noteworthy that in the limiting switching regimes $\nu \gg 1$ and $\nu \ll s$, this equation greatly simplifies. In fact, using (S20), equation (S23) becomes $(1+\beta/2)\phi_\beta = \phi_0$ when $\nu \gg 1$ and $\nu \ll s$. Hence, the corresponding payoffs along $b = \beta(\nu, s)$ are $\Delta S_{\nu,\beta} = \Delta F_{\nu,\beta} = (\phi_0 - \phi_\beta)\mathcal{K} = \beta\phi_\beta\mathcal{K}/2$ when $\nu \gg 1$ and $\Delta S_{\nu,\beta} = \Delta F_{\nu,\beta} = \beta\phi_\beta\langle K\rangle/2$ when $\nu \ll s$, yielding $\Delta S_{\nu,\beta}/\langle N\rangle^*_{\nu,0} = \Delta F_{\nu,\beta}/\langle N\rangle^*_{\nu,0} = \beta\phi_\beta/2$ in both limiting regimes. It is however important to remember that $\phi_\beta \simeq \phi_{q(\beta)}$ depends nontrivially on ν and s, and can be either an increasing or decreasing function of ν, see figures 2(a) and 3(a).

While the choice made here on how to measure the success of S and F is arguably the most natural, we could have also considered other variants. For instance, we could have considered that the best conditions to cooperate for the production of the public good would be: S should receive a higher payoff than F, condition (a) as above, and, S should maximize the difference of payoffs $\Delta S_{\nu,b} - \Delta F_{\nu,b}$ (instead of condition (b)). This would lead to an optimal value of the public good benefit $\widetilde{b}$ that would generally differ from b^* especially at low switching rate (see figure 5(c)). While this alternative definition of the optimal payoff for S would lead to quantitative differences with the results reported in figure 6(b), the main qualitative features discussed here and in section IV.B would remain the same.

XIII. EFFECT OF INTERNAL AND ENVIRONMENTAL NOISE ON POPULATION SIZE DISTRIBUTION – LINEAR NOISE APPROXIMATION ABOUT THE PDMP PREDICTIONS

The PDMP approximation of the N-QSD can reproduce the number and location of its peaks, but fails to capture the width of the distribution about the peaks and its accurate skewness, see, *e.g.*, figure S1. In this section, we derive the linear noise approximation (LNA) of the N-QSD used in Section V to account for the demographic fluctuations about the PDMP predictions [12].

After the fixation of species S, $N_S = N$ and $N_F = 0$, and the transition rates of the birth-death process become $T_S^+ = (1+b)N$, $T_S^- = N^2/K(t)$, and $T_F^\pm = 0$. Similarly, after species F's fixation, $N_F = N$ and $N_S = 0$, the transition rates (3) become $T_F^+ = N$, $T_F^- = N^2/K(t)$, with $T_S^\pm = 0$. To deal simultaneously with the ecological dynamics arising after the fixation of either species, it is convenient to define the auxiliary stochastic logistic process $N \xrightarrow{T^+} N+1$ and $N \xrightarrow{T^-} N-1$, with dichotomous Markov noise $\xi \in \{-1, +1\}$ and randomly switching carrying capacity defined by equations (3) and (4). This stochastic process is defined by the transition rates:

$$T^+ = (1+q)N, \quad T^- = \frac{N^2}{K(t)} = N^2\left[\frac{1}{\mathcal{K}} - \xi\left(\frac{1}{\mathcal{K}} - \frac{1}{K_+}\right)\right], \quad \text{with} \quad q = \begin{cases} b & \text{after fixation of } S \\ 0 & \text{after fixation of } F. \end{cases} \tag{S24}$$

As explained in section V.B of the main text, it is convenient to work with the continuous Markov process $\{n(t), \xi(t)\}$ defined by

$$n \xrightarrow{\mathcal{T}^+} n + \Omega^{-1}, \quad n \xrightarrow{\mathcal{T}^-} n - \Omega^{-1}, \quad \text{with } \xi \xrightarrow{\nu} -\xi, \tag{S25}$$

and

$$\psi \equiv \lim_{\Omega\to\infty} N/\Omega, \quad \kappa \equiv \mathcal{K}/\Omega \quad \text{and} \qquad k_\xi \equiv \begin{cases} k_+ = K_+/\Omega & \text{if } \xi = 1 \\ k_- = K_-/\Omega & \text{if } \xi = -1. \end{cases}$$

We thus have

$$\mathcal{T}^+(\psi,\xi) = (1+q)\psi \quad \text{and} \quad \mathcal{T}^-(\psi,\xi) = \psi^2\left\{\kappa^{-1} - \xi(\kappa^{-1} - k_+^{-1})\right\}. \tag{S26}$$

It is also useful to define v_ξ, associated with the deterministic flows of $\{n(t), \xi(t)\}$, and u_ξ associated with the diffusive flows:

$$v_\xi(\psi) \equiv \mathcal{T}^+ - \mathcal{T}^- = \frac{\mathcal{F}(\Omega\psi,\xi)}{\Omega} = \frac{\psi}{k_\xi}\left(\psi_\xi^* - \psi\right), \quad \text{and} \quad u_\xi(\psi) \equiv \mathcal{T}^+ + \mathcal{T}^- = \frac{\psi}{k_\xi}\left(\psi_\xi^* + \psi\right), \tag{S27}$$

with $\psi_\xi^* = (1+q)k_\xi$. It is worth noting that $v_\xi(\psi) > 0$ when $\xi = +1$ and $v_\xi(\psi) < 0$ when $\xi = -1$.

When the environment is static ($K_\pm = K$), with $k_\xi = k$, $v_\xi = v$ and $u_\xi = u$, the LNA consists of performing a van Kampen system size expansion of the underlying master equation, which yields the Fokker-Planck equation (FPE) for the probability density $\pi(\eta, t)$ [56, 57]:

$$\partial_t\pi(\eta,t) = -\partial_\eta\left[\eta v'(\psi)\pi(\eta,t)\right] + \frac{u}{2}\partial_\eta^2\pi(\eta,t), \tag{S28}$$

where $v' = dv/d\psi$ and $\pi(\eta, t)$ is the PDF of the fluctuations $\{\eta(t)\}$ about the mean-field trajectory $\dot{\psi} = v(\psi)$.

Here, the environment varies stochastically: it randomly switches between two states. The process $\{n(t), \xi(t)\}$ is thus analyzed in terms of a "pseudo-Fokker-Planck equation" which consists of an FPE, accounting for the internal noise, supplemented by terms arising from environmental stochasticity via the PDMP

$$\dot{\psi} = v_\xi(\psi)\,, \tag{S29}$$

that is equivalent to (9) and whose joint PDF is readily obtained from (S6): $\pi^*_{\nu,q}(\psi,\xi) = \Omega p^*(\Omega\psi,\xi)$. Within the LNA, to account for the weak fluctuations about ψ up to linear order in η, we obtain the following pseudo-FPE for the joint PDF $\pi_{\nu,q}(\psi,\eta,\xi,t) \equiv \pi(\psi,\eta,\xi)$ of the process (S1) [12, 39]:

$$\begin{aligned}\partial_t \pi(\psi,\eta,\xi) &= -\partial_\eta\left[\eta v'_\xi(\psi)\pi(\phi,\eta,\xi)\right] + \frac{u_\xi}{2}\partial^2_\eta \pi(\psi,\eta,\xi) \\ &- \partial_\psi\left[v_\xi(\psi)\pi(\psi,\eta,\xi)\right] - \nu\left[\pi(\psi,\eta,\xi) - \pi(\psi,\eta,-\xi)\right], \end{aligned}\tag{S30}$$

where, for notational simplicity, in this section we drop the time dependence and the ν, q subscripts in the PDFs by writing $\pi(\eta,\xi)$ and $\pi(\psi,\eta,\xi)$ instead of $\pi_{\nu,q}(\eta,\xi,t)$ and $\pi_q(\psi,\eta,\xi,t)$, etc. On the RHS of eq. (S30), the first line corresponds to a usual FPE with a drift term $-\partial_\eta[\dots]$ and a diffusion coefficient u_ξ, while in the second line one recognizes the Liouvillian contribution $-\partial_\psi\left[v_\xi(\psi)\pi(\psi,\eta,\xi)\right]$ and terms from random switching.

To determine the Gaussian probability density $\pi^*(\eta|\psi,\xi)$ characterizing the demographic fluctuations η about $\psi(t)$, we notice that $\pi(\psi,\eta,\xi) = \pi(\eta|\psi,\xi)\pi(\psi,\xi)$. As explained in the main text, we then assume that demographic fluctuations about ψ are the same in each environmental state $\xi = \pm 1$, and write $\pi(\eta|\psi,\xi) = \pi(\eta|\psi)$ [12]. With this assumption, we can set set $\partial_t(\pi^*(\eta,\psi,\xi) + \pi^*(\eta,\psi,-\xi)) = 0$ and use equation (S30) to obtain

$$0 = -\left[\pi^*(\xi|\psi)v'_\xi(\psi) + \pi^*(-\xi|\psi)v'_{-\xi}(\psi)\right]\partial_\eta\left[\eta\pi^*(\eta|\psi)\right] + \frac{1}{2}\left[\pi^*(\xi|\psi)u_\xi(\psi) + \pi^*(-\xi|\psi)u_{-\xi}(\psi)\right]\partial^2_\eta\pi^*(\eta|\psi), \tag{S31}$$

where we have also used $\pi^*(\psi,\xi) = \pi^*(\psi)\pi^*(\xi|\psi)$ and the zero-current boundary condition $\sum_\xi v_\xi \pi^*(\psi,\xi) = 0$. At the PDMP level, equation (S7) expresses the probability of being in the environmental state ξ given that the populationhas size N. Hence, upon substituting $\pi^*(\xi|\psi) = -\xi v_{-\xi}/(\sum_{\xi=\pm1}\xi v_\xi)$, equation (S31) yields the stationary probability density $\pi^*(\eta|\psi)$ of an Ornstein-Uhlenbeck process [56, 57]. In other words, $\pi^*(\eta|\psi)$ is a Gaussian with zero mean and variance

$$\frac{u_-(\psi)v_+(\psi) - u_+(\psi)v_-(\psi)}{v_-(\psi)v'_+(\psi) - v_+(\psi)v'_-(\psi)} = \psi, \tag{S32}$$

where we have used (S27), and the subscripts $\pm$ refer to $\xi = \pm 1$. With eq. (S32), we find the Gaussian probability density of the fluctuations about ψ:

$$\pi^*(\eta|\psi) = \frac{e^{-\frac{\eta^2}{2\psi}}}{\sqrt{2\pi\psi}}. \tag{S33}$$

Within the LNA, see eq. (25), the marginal quasi-stationary PDF of the process $\{N(t),\xi(t)\}$ defined by (S24) therefore is

$$p^*_{\mathrm{LNA},q}(N) = \frac{\pi^*(n)}{\Omega} = \sum_{\xi=\pm1}\int\!\!\int d\psi d\eta\; \pi^*(\eta|\psi)\pi^*(\psi,\xi)\;\delta\left(n - \psi - \frac{\eta}{\sqrt{\Omega}}\right). \tag{S34}$$

Upon substituting (S33) and $\pi^*(\psi,\xi) = \Omega p^*_{\nu,q}(\Omega\psi,\xi)$ obtained from (S6), into (S34), we obtain the LNA-PDF of the process $\{N(t),\xi(t)\}$. When $b = 0$, the marginal LNA-PDF $p^*_{\mathrm{LNA},0}(N)$ in the case of the pure resource competition is obtained from $\pi^*(n)$ with $q = 0$ and reads

$$\begin{aligned} p^*_{\mathrm{LNA},0}(N) \;\propto\; &\int \frac{d\eta\, e^{-\eta^2/[2(n-\eta/\sqrt{\Omega})]}}{\left(n-\frac{\eta}{\sqrt{\Omega}}\right)^{3/2}\left(k_+ - \left(n-\frac{\eta}{\sqrt{\Omega}}\right)\right)}\left[\frac{\left\{k_+ - \left(n-\frac{\eta}{\sqrt{\Omega}}\right)\right\}\left\{\left(n-\frac{\eta}{\sqrt{\Omega}}\right) - k_-\right\}}{\left(n-\frac{\eta}{\sqrt{\Omega}}\right)^2}\right]^\nu \\ &+ \int \frac{d\eta\, e^{-\eta^2/[2(n-\eta/\sqrt{\Omega})]}}{\left(n-\frac{\eta}{\sqrt{\Omega}}\right)^{3/2}\left(\left(n-\frac{\eta}{\sqrt{\Omega}}\right) - k_-\right)}\left[\frac{\left\{k_+ - \left(n-\frac{\eta}{\sqrt{\Omega}}\right)\right\}\left\{\left(n-\frac{\eta}{\sqrt{\Omega}}\right) - k_-\right\}}{\left(n-\frac{\eta}{\sqrt{\Omega}}\right)^2}\right]^\nu, \end{aligned}\tag{S35}$$

where $n = N/\Omega$, $k_\pm = K_\pm/\Omega$ and the proportional factor is the normalization constant. In the public good scenario, $b > 0$, the F-conditional LNA-PDF is $p^*_{\mathrm{LNA},0}(N)$ while PDF conditioned on fixation of species S (but unconditioned on ξ) is proportional

to $\pi^*(n)$ with $q = b$, i.e. it is given by

$$p^*_{\mathrm{LNA},b}(N) \propto \int \frac{d\eta\, e^{-\eta^2/[2(n-\eta/\sqrt{\Omega})]}}{\left(n-\frac{\eta}{\sqrt{\Omega}}\right)^{3/2}\left(\psi^*_+ - \left(n-\frac{\eta}{\sqrt{\Omega}}\right)\right)} \left[\frac{\left\{\psi^*_+ - \left(n-\frac{\eta}{\sqrt{\Omega}}\right)\right\}\left\{\left(n-\frac{\eta}{\sqrt{\Omega}}\right) - \psi^*_-\right\}}{\left(n-\frac{\eta}{\sqrt{\Omega}}\right)^2}\right]^{\frac{\nu}{1+b}}$$
$$+ \int \frac{d\eta\, e^{-\eta^2/[2(n-\eta/\sqrt{\Omega})]}}{\left(n-\frac{\eta}{\sqrt{\Omega}}\right)^{3/2}\left(\left(n-\frac{\eta}{\sqrt{\Omega}}\right) - \psi^*_-\right)} \left[\frac{\left\{\psi^*_+ - \left(n-\frac{\eta}{\sqrt{\Omega}}\right)\right\}\left\{\left(n-\frac{\eta}{\sqrt{\Omega}}\right) - \psi^*_-\right\}}{\left(n-\frac{\eta}{\sqrt{\Omega}}\right)^2}\right]^{\frac{\nu}{1+b}}, \tag{S36}$$

where $\psi^*_+ = (1+b)k_+$ and $\psi^*_- = (1+b)k_-$.

The comparison between the LNA-PDFs and the $N-$QSD is shown in figure 7 and 8, where a remarkable agreement is found when $b = 0$ and $b > 0$. However, as mentioned in the main text, some small deviations are observed in figure 8(a), at low switching rate, near the peak of small intensity when $b > 0$. The possible reasons for these small deviations are multiple: When $\nu \ll 1$, the population near the peaks of weak intensity is of size $N \approx (1+b)K_\pm$, and the assumption $\pi(\eta|\psi,\xi) \simeq \pi(\eta|\psi,-\xi)$ on which our LNA analysis is based may not be necessary valid since the fluctuations in the state $\xi = -1$ (with $N \approx (1+b)K_-$ and $b = 2$) may be noticeably stronger than those in the state $\xi = +1$ (where $N \approx (1+b)K_+$). Furthermore, the peak in question is associated with the fixation of species S for $b = 2$ in a population of rather large size $\approx (1+b)K_+$, an event which occurs with a small probability that may be beyond the reach of the LNA. Moreover, the effective theory yielding the approximation $\phi \simeq \phi_q$ is based on the behavior at high switching rate and may be less accurate when $\nu \ll 1$ than in the regimes of intermediate and fast switching.

Conclusions

My thesis aimed at investigating the role of stochastic effects, social interaction, and growth in bacterial populations. The results show that these factors have deep and complex effects on the evolution of the population, and interplay intricately with each other. Population growth dampens the impact of demographic fluctuations, and the way social interactions, such as the exchange of public goods, tweak the environmental conditions, thus changing population growth. Stochastic aspects, meanwhile, hover around all facets of the problem. Unpredictable environments, for example, drive or stunt growth; demographic fluctuations change the internal composition of the population; and compositional variability coupled with public good dynamics affects population-level competition.

The first part—*Stochasticity and social interactions in bacterial growth*—brings to the fore the extreme complexity of bacterial systems. Plenty of theoretical models capture some aspect of the evolution of bacteria, but often take biological details for granted. As my research shows, these details do matter when it comes to describing specific bacterial systems. Their rigorous, quantitative modeling, although challenging, is possible, and reveals otherwise inaccessible aspects of the dynamics. The second part—*Combined effects of environmental and demographic noise*—highlights the diverse roles the environment plays in evolution. Environmental conditions do more than just directing the arrow of natural selection, and their effects run deeper than simply tuning of the relative weight of fluctuations. My results show how we can mathematically untangle these manifold effects.

More broadly, this work taught me a few lessons about theoretical modeling and biological systems. Ore is just how many forces are at work in evolution—in this specific case, the evolution of cooperation. My thesis shows rich interactions, despite only investigating the role of demographic fluctuations and competition between populations. The question of the emergence of cooperation is often treated by packing all complexity into few parameters or simplified two-player games. Although these approaches can give great insight into the broad principles of the problem, they have limitations that need to be reckoned with when it comes to real bacterial systems. The most glaring example my work presents is the study of a specific public good interaction. The traditional ways to phrase the problem—inclusive fitness and the prisoner's dilemma—completely neglect the intrinsic many-player nature of the interaction, as well as the potential accumulation of the public good. As I show, relevant details must be identified, quantified, and included in a model of an actual bacterial system, especially when aiming at quantitative results.

Perhaps the most important lesson concerns the fundamental difficulty of using bacteria as model systems. Thanks to their fast reproduction, relative simplicity, and almost "programmability", bacteria represent the best option to model the evolution of cooperation and similar problems. Yet, they are not automatons. They will try and take any action to survive whenever they are tasked with anything less than advantageous. Bacteria do not do what they are told: they do what they can to survive. A theoretical framework may therefore describe a social interaction in one bacterial species and not in an other, and specific adaptations need to be addressed when extrapolating to general principles.

Including more biological details is also the most interesting possible development to this part of my work. Particularly in Chapter 2, we considered a simplified interaction, involving a mutant constitutive producer (which always synthesizes the public good). Wild-type *Pseudomonas*, however, evolved complex regulatory networks whereby the public good abundance influences further production, as well as the cell's metabolism. This certainly affects the growth dynamics of individuals and of the population as a whole. As for the second, more theoretical part of my research, its natural continuation involves experimentally testing the effects of unpredictable environmental conditions. It would be interesting to investigate the effect of changing different aspects of the environment (for example, resources abundance, temperature, or presence of antibiotics). Would cells develop mechanisms to actively cope with the changing environment? How would the conditions affect their social interactions?

In a broader context (and at much larger scale), my research represents a small step in a larger journey

to understand the inner workings of bacterial colonies, as well as their relation to their environment. Studies in this field will eventually trace paths in some at the most important frontiers of modern biomedicine. For example, the study of the microbiome, whose increasingly recognized importance led it to be considered akin to an additional organ. This new "organ" can only be studied once we understand the complex social structures at its foundations. Manipulating bacterial societies can also help in the search for alternatives to antibiotics. Acting to unravel the social fabric of a population could prove more effective (and less prone to the evolution of resistance) than showering microbes with drugs. My work highlights how powerful the combination of biology and physics can be in solving these extremely complex, but vital, puzzles.

Bibliography

[1] Hamilton WD. The genetical evolution of social behaviour. I+II. Journal of Theoretical Biology. 1964 Jul;7(1). Available from: http://www.sciencedirect.com/science/article/pii/0022519364900384.

[2] Maynard-Smith J, Price R. The logic of animal conflict. Nature. 1973;.

[3] Maynard-Smith J. Evolution and the Theory of Games. Cambridge University Press; 1982.

[4] Hofbauer J, Sigmund K. Evolutionary Games and Population Dynamics. Cambridge; 1998.

[5] Nowak MA. Five rules for the evolution of cooperation. Science. 2006;314(5805):1560–3.

[6] Wilson EO. Sociobiology. Harvard University Press; 2000.

[7] Rainey PB, Rainey K. Evolution of co-operation and conflict in experimental bacterial populations. Nature. 2003;425:72–74.

[8] Gore J, Youk H, van Oudenaarden A. Snowdrift game dynamics and facultative cheating in yeast. Nature. 2009 May;459(7244):253–256. Available from: http://www.nature.com/nature/journal/v459/n7244/abs/nature07921.html.

[9] Artemova T, Gerardin Y, Dudley C, Vega NM, Gore J. Isolated cell behavior drives the evolution of antibiotic resistance. Molecular Systems Biology. 2015 Jul;11(7):822. Available from: http://msb.embopress.org/content/11/7/822.

[10] Cornelis P, Matthijs S, Van Oeffelen L. Iron uptake regulation in Pseudomonas aeruginosa. Biometals. 2009;22(1):15–22.

[11] Griffin AS, West SA, Buckling A. Cooperation and competition in pathogenic bacteria. Nature. 2004;430:1024.

[12] Matthijs S, Laus G, Meyer JM, Abbaspour-Tehrani K, Schäfer M, Budzikiewicz H, et al. Siderophore-mediated iron acquisition in the entomopathogenic bacterium Pseudomonas entomophila L48 and its close relative Pseudomonas putida KT2440. Biometals. 2009 Dec;22(6):951–964. Available from: http://link.springer.com/article/10.1007/s10534-009-9247-y.

[13] Zhang XX, Rainey PB. Exploring the Sociobiology of Pyoverdin-Producing Pseudomonas. Evolution. 2013;67(11):3161–3174. Available from: http://onlinelibrary.wiley.com/doi/10.1111/evo.12183/abstract.

[14] Kümmerli R, Ross-Gillespie A. Explaining the Sociobiology of Pyoverdin Producing Pseudomonas: A Comment on Zhang and Rainey (2013). Evolution. 2013;p. n/a–n/a. Available from: http://onlinelibrary.wiley.com/doi/10.1111/evo.12311/abstract.

[15] Buckling A, Harrison F, Vos M, Brockhurst MA, Gardner A, West SA, et al. Siderophore-mediated cooperation and virulence in Pseudomonas aeruginosa. FEMS Microbiol Ecol. 2007;62(2):135–41.

[16] Archetti M, Scheuring I. Review: Game theory of public goods in one-shot social dilemmas without assortment. Journal of Theoretical Biology. 2012 Apr;299(0):9–20. Available from: http://www.sciencedirect.com/science/article/pii/S0022519311003171.

[17] Bach LA, Helvik T, Christiansen FB. The evolution of n-player cooperation—threshold games and ESS bifurcations. Journal of Theoretical Biology. 2006 Jan;238(2):426–434. Available from: http://www.sciencedirect.com/science/article/pii/S0022519305002419.

[18] Frey E. Evolutionary Game Theory: Theoretical Concepts and Applications to Microbial Communities. Physica A. 2010;389:4265–4298.

[19] Boza G, Számadó S. Beneficial laggards: multilevel selection, cooperative polymorphism and division of labour in threshold public good games. BMC Evolutionary Biology. 2010 Nov;10(1):336. Available from: http://www.biomedcentral.com/1471-2148/10/336/abstract.

[20] Kümmerli R, Gardner A, West SA, Griffin AS. Limited dispersal, budding dispersal, and cooperation: an experimental study. Evolution. 2009;63(4):939–49.

[21] Hammerschmidt K, Rose CJ, Kerr B, Rainey PB. Life cycles, fitness decoupling and the evolution of multicellularity. Nature. 2014 Nov;515(7525):75–79. Available from: http://www.nature.com/nature/journal/v515/n7525/abs/nature13884.html.

[22] Axelrod R, Hamilton WD. The evolution of cooperation. Science. 1981 Mar;211(4489):1390–1396. Available from: http://www.sciencemag.org/content/211/4489/1390.

[23] Taylor PD. Altruism in viscous populations — an inclusive fitness model. Evol Ecol. 1992 Jul;6(4):352–356. Available from: https://link-springer-com.emedien.ub.uni-muenchen.de/article/10.1007/BF02270971.

[24] Julou T, Mora T, Guillon L, Croquette V, Schalk IJ, Bensimon D, et al. Cell–cell contacts confine public goods diffusion inside Pseudomonas aeruginosa clonal microcolonies. PNAS. 2013 Jul;110(31):12577–12582. Available from: http://www.pnas.org/content/110/31/12577.

[25] Traulsen A, Schuster HG. Minimal model for tag-based cooperation. Phys Rev E. 2003 Oct;68(4):046129. Available from: http://link.aps.org/doi/10.1103/PhysRevE.68.046129.

[26] Hauert C, Traulsen A, Brandt H, Nowak MA, Sigmund K. Via Freedom to Coercion: The Emergence of Costly Punishment. Science. 2007 Jun;316(5833):1905–1907. Available from: http://www.sciencemag.org/content/316/5833/1905.

[27] Fux CA, Costerton JW, Stewart PS, Stoodley P. Survival strategies of infectious biofilms. Trends Microbiol. 2005;13(1):34–40.

[28] Morley CR, Trofymow JA, Coleman DC, Cambardella C. Effects of Freeze-Thaw Stress on Bacterial Populations in Soil Microcosms. Microb Ecol. 1983;9:329–340.

[29] Melbinger A, Vergassola M. The Impact of Environmental Fluctuations on Evolutionary Fitness Functions. Scientific Reports. 2015 Oct;5:15211. ArXiv: 1510.05664. Available from: http://arxiv.org/abs/1510.05664.

[30] Fisher CK, Mehta P. The transition between the niche and neutral regimes in ecology. PNAS. 2014 Sep;111(36):13111–13116. Available from: http://www.pnas.org/content/111/36/13111.

[31] Hidalgo J, Suweis S, Maritan A. Species coexistence in a neutral dynamics with environmental noise. Journal of Theoretical Biology. 2017 Jan;413:1–10. Available from: http://www.sciencedirect.com/science/article/pii/S0022519316303617.

[32] Ashcroft P, Altrock PM, Galla T. Fixation in finite populations evolving in fluctuating environments. Journal of The Royal Society Interface. 2014 Nov;11(100):20140663. Available from: http://rsif.royalsocietypublishing.org/content/11/100/20140663.

[33] Assaf M, Mobilia, Mauro, Roberts, Elijah. Cooperation Dilemma in Finite Populations under Fluctuating Environments. Phys Rev Lett. 2013;111(23).

[34] Assaf M, Kamenev A, Meerson B. Population extinction in a time-modulated environment. Phys Rev E. 2008 Oct;78(4):041123. Available from: http://link.aps.org/doi/10.1103/PhysRevE.78.041123.

[35] Kussel E, Leibler S. Phenotypic diversity, population growth and information in fluctuating environments. Science. 2005;309:2075.

[36] Lambert G, Kussell E. Quantifying Selective Pressures Driving Bacterial Evolution Using Lineage Analysis. Phys Rev X. 2015 Feb;5(1):011016. Available from: http://link.aps.org/doi/10.1103/PhysRevX.5.011016.

[37] Brockhurst MA. Population bottlenecks promote cooperation in bacterial biofilms. PLoS ONE. 2007 Jan;2(7). Available from: http://www.plosone.org/article/info%253Adoi%252F10.1371%252Fjournal.pone.0000634.

[38] Campos PRA, Wahl LM. The effects of population bottlenecks on clonal interference, and the adaptation effective population size. Evolution. 2008;63:950–958.

[39] Campos PRA, Wahl LM. The adaptation rate of asexuals: Deleterious mutations, clonal interference and population bottlenecks. Evolution. 2010;64(7):1973–1983.

[40] Heffernan JM, Wahl LM. The effects of genetic drift in experimental evolution. Theoretical Population Biology. 2002 Dec;62(4):349–356. Available from: http://www.sciencedirect.com/science/article/pii/S0040580902000023.

[41] Nei M, Maruyama T, Chakraborty R. The Bottleneck Effect and Genetic Variability in Populations. Evolution. 1975 Mar;29(1):1–10. Available from: http://www.jstor.org/stable/2407137.

[42] Patwas Z, Wahl LM. Adaptation rates of lytic viruses critically depend on whether host cells survive the bottleneck. Evolution. 2009;64(4):1166–1172.

[43] Wahl LM, Gerrish PJ, Saika-Voivod I. Evaluating the impact of population bottlenecks in experimental evolution. Genetics. 2002;162:961–971.

[44] Okasha S. Multi-Level Selection, Covariance and Contextual Analysis. Br J Philos Sci. 2004 Sep;55(3):481–504. Available from: http://bjps.oxfordjournals.org/content/55/3/481.

[45] Okasha S. Evolution and the Levels of Selection. vol. 16. Clarendon Press Oxford; 2006.

[46] Michod RE. Cooperation and Conflict in the Evolution of Individuality. I. Multilevel Selection of the Organism. The American Naturalist. 1997 Apr;149(4):607–645. Available from: http://www.jstor.org/stable/2463541.

[47] Sober E, Wilson DS. Adaptation and Natural Selection revisited. Journal of Evolutionary Biology. 2011 Feb;24(2):462–468. Available from: http://onlinelibrary.wiley.com/doi/10.1111/j.1420-9101.2010.02162.x/abstract.

[48] Cooper B, Wallace C. Group selection and the evolution of altruism. Oxf Econ Pap. 2004 Apr;56(2):307–330. Available from: http://oep.oxfordjournals.org/content/56/2/307.

[49] Friedman J, Gore J. Ecological systems biology: The dynamics of interacting populations. Current Opinion in Systems Biology. 2017 Feb;1:114–121. Available from: http://www.sciencedirect.com/science/article/pii/S2452310016300208.

[50] Parsons TL, Quince C, Plotkin JB. Some Consequences of Demographic Stochasticity in Population Genetics. Genetics. 2010;185:1345–1354.

[51] Chuang JS, Rivoire O, Leibler S. Simpson's paradox in a synthetic microbial system. Science. 2009;323(5911):272–5.

[52] Chuang JS, Rivoire O, Leibler S. Cooperation and Hamilton's rule in a simple synthetic microbial system. Mol Syst Biol. 2010;6:398.

[53] Melbinger A, Cremer J, Frey E. Evolutionary game theory in growing populations. Phys Rev Lett. 2010;105:178101.

[54] Cremer J, Melbinger A, Frey E. Evolutionary and population dynamics: a coupled approach. Phys Rev E. 2011;84:051921.

[55] Cremer J, Melbinger A, Frey E. Growth dynamics and the evolution of cooperation in microbial populations. Sci Rep. 2012;2:281.

[56] Melbinger A, Cremer J, Frey E. The Emergence of Cooperation from a Single Mutant during Microbial Life-Cycles. arXiv:150503558 [q-bio]. 2015 May;ArXiv: 1505.03558. Available from: http://arxiv.org/abs/1505.03558.

[57] Blythe RA, McKane J. Stochastic models of evolution in genetics, ecology and linguistics. J Stat Mech. 2007;p. 07018.

[58] Cremer J, Reichenbach T, Frey E. The edge of neutral evolution in social dilemmas. New J Phys. 2009;11(93029).

[59] Kimura M. Solution of a process of random genetic drift with a continuous model. PNAS. 1955;(41).

[60] Hartl DL, Clark AG. Principles of population genetics. 2nd ed. Sinauer, Sunderland, MD, USA; 1989.

[61] Otto SP, Whitlock MC. The Probability of Fixation in Populations of Changing Size. Genetics. 1997;146:723–733.

[62] Eggenberger F, Pólya G. Über die Statistik verketteter Vorgänge. ZAMM - Journal of Applied Mathematics and Mechanics / Zeitschrift für Angewandte Mathematik und Mechanik. 1923;3(4):279–289. Available from: http://onlinelibrary.wiley.com/doi/10.1002/zamm.19230030407/abstract.

[63] Brian Arthur W, Ermoliev YM, Kaniovski YM. Path-dependent processes and the emergence of macro-structure. European Journal of Operational Research. 1987 Jun;30(3):294–303. Available from: http://www.sciencedirect.com/science/article/pii/0377221787900749.

[64] Pemantle R. A survey of random processes with reinforcement; 2006. math/0610076. Probability Surveys 2007, Vol. 4, 1-79. Available from: http://arxiv.org/abs/math/0610076.

[65] Sornette D. Why Stock Markets Crash: Critical Events in Complex Financial Systems. Princeton University Press; 2009.

[66] Athreya KB, Karlin S. Embedding of Urn Schemes into Continuous Time Markov Branching Processes and Related Limit Theorems. The Annals of Mathematical Statistics. 1968 Dec;39(6):1801–1817. ArticleType: research-article / Full publication date: Dec., 1968 / Copyright © 1968 Institute of Mathematical Statistics. Available from: http://www.jstor.org/stable/2239282.

[67] Kotz S, Mahmoud H, Robert P. On generalized Pólya urn models. Statistics & Probability Letters. 2000 Aug;49(2):163–173. Available from: http://www.sciencedirect.com/science/article/pii/S0167715200000456.

[68] Gillespie D. General method for numerically simulating stochastic time evolution of coupled chemical reactions. J Comp Phys. 1976;22:403–434.

[69] Gillespie D. Exact stochastic simulation of coupled chemical reactions. J Phys Chem. 1977;81(25):2340–2361.

[70] Wienand K, Lechner M, Becker F, Jung H, Frey E. Non-Selective Evolution of Growing Populations. PLOS ONE. 2015 Aug;10(8):e0134300. Available from: http://journals.plos.org/plosone/article?id=10.1371/journal.pone.0134300.

[71] Hallatschek O, Hersen P, Ramanathan S, Nelson DR. Genetic drift at expanding frontiers promotes gene segregation. PNAS. 2007 Dec;104(50):19926–19930. Available from: http://www.pnas.org/content/104/50/19926.

[72] Simpson EH. The Interpretation of Interaction in Contingency Tables. Journal of the Royal Statistical Society B. 1951;p. 238–241.

[73] Blyth CR. On Simpson's Paradox and the Sure-Thing Principle. Journal of the American Statistical Association. 1972 Jun;67(338):364–366. Available from: http://www.tandfonline.com/doi/abs/10.1080/01621459.1972.10482387.

[74] Bickel PJ, Hammel EA, O'Connell JW. Sex Bias in Graduate Admissions: Data from Berkeley. Science. 1975 Feb;187(4175):398–404. Available from: http://www.sciencemag.org/content/187/4175/398.

[75] Price GR. Selection and Covariance. Nature. 1970;227:520.

[76] Price GR. Extension of covariance selection mathematics. Ann Hum Genet. 1972;35:485.

[77] Ghoul M, West SA, Diggle SP, Griffin AS. An experimental test of whether cheating is context dependent. J Evol Biol. 2014 Mar;27(3):551–556. Available from: http://onlinelibrary.wiley.com/doi/10.1111/jeb.12319/abstract.

[78] West SA, Pen I, Griffin AS. Cooperation and competition between relatives. Science. 2002;296(5565):72–5.

[79] West SA, Griffin AS, Gardner A, Diggle SP. Social evolution theory of microorganisms. Nat Rev Microbiol. 2006;4:597.

[80] Becker F, Wienand K, Lechner M, Frey E, Jung H. Interactions mediated by a public good transiently increase cooperativity in growing Pseudomonas putida metapopulations. Scientific Reports. 2018 Mar;8(1):4093. Available from: https://www.nature.com/articles/s41598-018-22306-9.

[81] Hannauer M, Barda Y, Mislin GLA, Shanzer A, Schalk IJ. The Ferrichrome Uptake Pathway in Pseudomonas aeruginosa Involves an Iron Release Mechanism with Acylation of the Siderophore and Recycling of the Modified Desferrichrome. J Bacteriol. 2010 Mar;192(5):1212–1220. Available from: http://jb.asm.org/content/192/5/1212.

[82] Gasser V, Guillon L, Cunrath O, Schalk IJ. Cellular organization of siderophore biosynthesis in Pseudomonas aeruginosa: Evidence for siderosomes. Journal of Inorganic Biochemistry. 2015 Jul;148(Supplement C):27–34. Available from: http://www.sciencedirect.com/science/article/pii/S0162013415000343.

[83] Hol FJH, Galajda P, Nagy K, Woolthuis RG, Dekker C, Keymer JE. Spatial Structure Facilitates Cooperation in a Social Dilemma: Empirical Evidence from a Bacterial Community. PLoS ONE. 2013 Oct;8(10):e77042. Available from: http://dx.doi.org/10.1371/journal.pone.0077042.

[84] Ghoul M, West SA, McCorkell FA, Lee ZB, Bruce JB, Griffin AS. Pyoverdin cheats fail to invade bacterial populations in stationary phase. J Evol Biol. 2016 Sep;29(9):1728–1736. Available from: http://onlinelibrary.wiley.com.emedien.ub.uni-muenchen.de/doi/10.1111/jeb.12904/abstract.

[85] Swingle B, Thete D, Moll M, Myers CR, Schneider DJ, Cartinhour S. Characterization of the PvdS-regulated promoter motif in Pseudomonas syringae pv. tomato DC3000 reveals regulon members and insights regarding PvdS function in other pseudomonads. Molecular Microbiology. 2008 May;68(4):871–889. Available from: http://onlinelibrary.wiley.com/doi/10.1111/j.1365-2958.2008.06209.x/abstract.

[86] Moran PA. The Statistical Processes of Evolutionary Theory. Clarendon; 1964.

[87] van Kampen NG. Stochastic Processes in Physics and Chemistry. North-Holland Personal Library; 2007.

[88] Gardiner CW. Stochastic Methods. 2nd ed. Springer; 2004.

[89] Bena I. Dichotomous markov noise: exact results for out-of-equilibrium systems. Int J Mod Phys B. 2006 Aug;20(20):2825–2888. Available from: http://www.worldscientific.com/doi/abs/10.1142/S0217979206034881.

[90] Horsthemke W, Lefever R. Noise-Induced Transitions. vol. 15 of Springer Series in Synergetics. Springer Berlin Heidelberg; 2006. Available from: http://link.springer.com/10.1007/3-540-36852-3.

[91] Kitahara K, Horsthemke W, Lefever R. Coloured-noise-induced transitions: Exact results for external dichotomous Markovian noise. Physics Letters A. 1979 Apr;70(5):377–380. Available from: http://www.sciencedirect.com/science/article/pii/0375960179903360.

[92] Hufton PG, Lin YT, Galla T, McKane AJ. Intrinsic noise in systems with switching environments. Phys Rev E. 2016 May;93(5):052119. Available from: https://link.aps.org/doi/10.1103/PhysRevE.93.052119.

[93] Wienand K, Frey E, Mobilia M. Evolution of a Fluctuating Population in a Randomly Switching Environment. Phys Rev Lett. 2017 Oct;119(15):158301. Available from: https://link.aps.org/doi/10.1103/PhysRevLett.119.158301.

Acknowledgements

None of this could have been possible without the help and guidance of Erwin Frey. Thank you so much for making me discover these most interesting questions and giving me the opportunity to work on them in this fantastic group. What I've learned from you—about science and well beyond—helped me find my way and will never leave me. A huge thank you to Heinrich Jung, who led the lab that was so instrumental for this research. He also taught me pretty much all I came to know about bacteria (including that cool line about them not doing what they are told), and did so much to shape my view of my work. I also greatly appreciate the guidance and support of Mauro Mobilia. Your help and intuition got me out of a very difficult time and turned it into a great success. Thank you for that, for being a most stimulating work partner, and for graciously hosting me for two unforgettable weeks in Leeds.

Thank you to everyone at LS Frey: you all create a fun and stimulating environment, and make work so much more enjoyable. In particular, Matthias Lechner—with whom it has been a pleasure to share much of this ride—as well as Matthias Rank, Lorenz Huber, Emanuel Reithmann, and Federica Mura, who have all become much more friends than colleagues by now. Thanks also to Marianne Bauer, Johannes Knebel, Markus Weber, and Madeleine Opitz, who were always great discussion partners. A great thank you also to Silke Bergeler, Stefano Duca, Nanni Giunta, Isabella Graf, Johannes Knebel, Lorenz Huber, Matthias Lechner, Leila Mirzagholi, Federica Mura, Emanuel Reithmann, and Ulrich Wienand, who generously gave their time to proofread this thesis.

Good times, bad times, you know I've had my share, and my good friennds Alberto Vesentini, Gabriele Calabrese, Leila Mirzagholi, Michela Amicone, Nanni Giunta, Rui Coelho, and Stefano Duca supported me more than they know with their companionship and game nights and laughter (and basketball discussions). I also deeply appreciate all Cristina Pop, Anna Melbinger, and Andrea Fertl have done to help me through the roughest patches.

Finally, there simply is not enough I can say to express my gratitude to my family. To my parents, Lorenza and Ulrich, for their support and encouragement, for everything they have done to get me to this point and into the ones to come. Of course, thanks to mu wife Carmen, who believes in me beyond what's reasonable. She was always there, in good times and bad, and whenever I fell, she was there to help me get up—or carry me like a limp Frodo if I couldn't. I hope I'll be able to repay you in time, I would have never *ever* made it through without you.